From the Institute for Clinical Chemistry and Laboratory Diagnostics,
at Heinrich Heine University Düsseldorf

Regulatory Protein-Protein Interactions within the PER Complex of the Circadian Clock

Dissertation

to obtain the academic title of Doctor rerum medicarum (Dr. rer. med.) from the Faculty of Medicine at Heinrich Heine University Düsseldorf

Submitted by

Hussam Ibrahim

2024

As an inaugural dissertation printed by permission of the Faculty of Medicine at Heinrich Heine University Düsseldorf

Signed:

Dean. Prof. Dr. med Nikolaj Klöcker
Examiners:
1. Prof. Andrea Icks (Chair, member of the PhD commission)
2. Prof. Hans Reinke (1st Supervisor)
3. Prof. Björn Stork (2nd Supervisor)
4. PD Dr. Thomas Haarmann-Stemmann (additional member of the examination board)

Date of the oral examination: 03.12.2024

Dedication

To **my soul**, **the sun**, **the moon**, **the ten-constellation**, and **the little star**

List of publications

Published article, which is part of this thesis.

Ibrahim H, Reus P, Mundorf AK, Grothoff A-L, Rudenko V, Buschhaus C, Stefanski A, Berleth N, Stork B, Stühler K, Kalfalah F, Reinke H. Phosphorylation of GAPVD1 Is Regulated by the PER Complex and Linked to GAPVD1 Degradation. *International Journal of Molecular Sciences*. 2021; 22(7):3787.
https://doi.org/10.3390/ijms22073787

Published article, which is not part of this thesis.

Bolshette, N., **Ibrahim, H**., Reinke, H., & Asher, G. (2023). Circadian regulation of liver function: from molecular mechanisms to disease pathophysiology. *Nature Reviews Gastroenterology & Hepatology, 1-13.*
https://doi.org/10.1038/s41575-023-00792-1

German Summary (Zusammenfassung)

Der molekulare Mechanismus der zirkadianen Uhr wird von einer Transkriptions-Translations-Rückkopplungsschleife gesteuert, was die Interaktion zahlreicher Uhren-Gene und -Proteine einschließlich PERIODs (PERs) und CRYPTOCHROMEs (CRYs) beinhaltet. PER2 ist ein transkriptioneller Repressor, der eine entscheidende Rolle bei der Regulation der zirkadianen Uhr sowie bei einer vielfältigen Palette physiologischer Prozesse spielt, einschließlich der DNA-Schadensreaktion, des Stoffwechsels und der Immunität. Neuere Forschungen legen nahe, dass PER2 neben seiner bekannten Funktion bei der transkriptionellen Regulation der zirkadianen Uhr auch nicht-transkriptionelle Funktionen besitzt. Beispielsweise haben Studien gezeigt, dass die Herunterregulierung von PER2 die Autophagie vermindert, die im Wesentlichen durch posttranslationale Mechanismen reguliert wird und im Zytoplasma stattfindet. Darüber hinaus wurde festgestellt, dass PER2 als Gerüst dient, um die Proteine TSC complex subunit 1 (TSC1) und Mammalian Target of Rapamycin (mTOR) aneinander zu lagern und so die Aktivität von Mammalian Target of Rapamycin Complex 1 (mTORC1) in der Leber während des Fastens zu unterdrücken, was seine zytoplasmatische Rolle weiter hervorhebt. Diese Ergebnisse legen nahe, dass PER2 eine breitere Palette von Funktionen hat als die transkriptionelle Regulation der zirkadianen Uhr und betonen die Bedeutung weiterer Forschung zu seinen nicht-transkriptionellen Funktionen.

Diese Arbeit zielte darauf ab, mögliche zytoplasmatische Bindungspartner von PER2 zu identifizieren, um weitere Einblicke in dessen nicht-transkriptionelle Funktionen zu gewinnen. Zunächst wurde ein biochemisches Screening auf Interaktionsproteine durchgeführt, das unter anderem das Protein GTPase Activating Protein and VPS9 Domains 1 (GAPVD1) als einen starken Bindungspartner von PER2 identifizierte. GAPVD1 fungiert sowohl als GTPase-aktivierendes Protein (GAP) für die kleine GTPase RAS als auch als Guaninnukleotid-Austauschfaktor (GEF) für die Proteine Ras-related protein RAB5A und RAB31. GAPVD1 ist an verschiedenen biologischen Prozessen wie Endozytose, Epidermal growth factor receptor (EGFR)-Transport und -Abbau sowie der Insulinrezeptor-Internalisierung beteiligt.

Die gegenseitige funktionale Wechselwirkung zwischen PER2 und GAPVD1 wurde in meiner Dissertation eingehend untersucht. CSNK1D ist eine Kinase, die eine grundlegende Rolle für die Funktion des PER-Komplexes spielt. Die Untersuchung der Phosphorylierung von GAPVD1 deckte deren Regulation durch CSNK1D und PER-Proteine auf, wobei sieben Phosphorylierungsstellen in der zentralen Domäne kartiert wurden, was eine zytoplasmatische Rolle von PER2 bei der Modulation der Phosphorylierung interagierender Proteine hervorhebt. Darüber hinaus zeigen meine Ergebnisse, dass GAPVD1 ein rhythmisches Phosphorylierungsmuster aufweist, das zeitlich mit dessen Assoziation mit dem PER-Komplex korreliert. GAPVD1 beeinflusst auch die Bindung von PER2 an CSNK1D, was dessen Bedeutung für den CSNK1D-abhängigen PER2-Phosphoswitch innerhalb des PER-Komplexes unterstreicht. Schließlich wurden die für die Bindung von PER2 und CSNK1D verantwortlichen Domänen in GAPVD1 untersucht. Die Domänen Helix 2 und Bottom Helix (H2B), die vom Algorithmus Alphafold als klar strukturierte Domänen in GAPVD1 deklariert werden, binden an PER2 und CSNK1D. Darüber hinaus deuten die Ergebnisse an, dass GAPVD1 zusätzliche Domänen besitzt, die an PER2 und CSNK1D binden, und die sich im intrinsisch ungeordneten Bereich (IDR) befinden könnten. Schließlich decken meine Befunde auch eine im Wesentlichen inhibierende Wirkung der VPS9-Domäne von GAPVD1 bei der Regulation der Bindung von PER2 aber nicht von CSNK1D an GAPVD1 auf. Zusammengefasst verschaffen diese Ergebnisse neue Erkenntnisse über die molekularen Mechanismen, deren GAPVD1 sich bei der Regulation des PER-Komplexes innerhalb des molekularen Oszillators bedient.

Insgesamt eröffnet diese Arbeit neue Perspektiven auf die Regulation des PER-Komplexes durch GAPVD1 und damit auch potenzielle Wege für therapeutische Interventionen zur Verbesserung der Gesundheit und des Wohlbefindens im Zusammenhang mit dem zirkadianen Rhythmus.

Summary

The molecular mechanism of the circadian clock is governed by a transcription-translation feedback loop, involving the interaction of numerous clock genes and proteins including PERIODs (PERs) and CRYPTOCHROMEs (CRYs). PER2 is a transcriptional repressor that plays a critical role in regulating the circadian clock as well as in a diverse array of physiological processes, encompassing DNA damage response, metabolism, and immunity. Recent research has suggested that PER2 has non-transcriptional roles in addition to its well-known function in transcriptional regulation of the circadian clock. For instance, studies have shown that downregulation of PER2 reduces levels of autophagy, a predominantly posttranslationally regulated cytoplasmic process. Additionally, PER2 has been found to act as a scaffold for tethering Tuberous sclerosis 1 (TSC1) and Mammalian target of rapamycin (mTOR) together, thereby suppressing liver mammalian target of rapamycin complex 1 (mTORC1) activity during fasting, which further supports its cytoplasmic role. These findings suggest that PER2 has a diverse range of functions beyond its role in transcriptional regulation of the circadian clock and highlight the importance of further research into its non-transcriptional functions.

This work aimed at characterizing potential cytoplasmic PER2 binding proteins in order to shed more light on its non-transcriptional functions. First, a biochemical screen for interacting proteins was conducted, identifying among other proteins GTPase Activating Protein and VPS9 Domains 1 (GAPVD1) as a strong binding partner of PER2. GAPVD1 functions both as a GTPase-activating protein (GAP) for the small GTPase RAS and as a guanine nucleotide exchange factor (GEF) for the Ras-related proteins RAB5A and RAB31. GAPVD1 is involved in diverse biological processes such as endocytosis, epidermal growth factor receptor (EGFR) trafficking and degradation, and insulin receptor internalization.

The mutual functional relationship between PER2 and GAPVD1 has been extensively studied in my thesis. CSNK1D is a kinase that plays a fundamental role for the function of the PER complex. Investigation of GAPVD1 phosphorylation revealed its regulation by CSNK1D and PER proteins, with seven mapped phosphorylation sites in its central domain, thus highlighting a cytoplasmc role of PER2 in modulating phosphorylation levels of interacting proteins. Furthermore, my results show that GAPVD1 is rhythmically phosphorylated with a timely correlation to its association with the PER complex, and that GAPVD1 modulates PER2-CSNK1D binding, indicating its importance for the CSNK1D-dependent PER2 phosphoswitch within the PER complex. Finally, the binding domains in GAPVD1 responsible for PER2 and CSNK1D binding were investigated. The domains Helix 2 and Bottom helix (H2B), which the Alphafold algorithm predicts to be highly structured domains in GAPVD1, bind to PER2 and CSNK1D. Moreover, the results also indicate that GAPVD1 might contain additional domains that bind PER2 and CSNK1D, which might be located in the Intrinsically Disordered Region (IDR). Finally, my findings also reveal a predominantly inhibitory role of the VPS9 domain of GAPVD1 in regulating the binding of PER2 but not CSNK1D to GAPVD1. Taken together, these findings provide novel insights into the molecular mechanisms that GAPVD1 employs for regulation of PER complex function within the molecular circadian oscillator.

Overall, this thesis provides new perspectives on the regulation of the PER complex by GAPVD1 and thereby suggests potential avenues for therapeutic interventions to enhance personal health and well-being in relation to circadian rhythmicity.

Table of Contents

List of Abbreviations

ACBD3	Acyl-CoA-binding domain-containing 3
AE/AP-LC-MS	Affinity enrichment/purification-liquid chromatography-mass spectrometry
AMPK	Adenosine monophosphate-activated protein kinase
AP2A1	Adaptor Related Protein Complex 2 Subunit Alpha 1
AP2M1	adaptor related protein complex 2 subunit mu 1
ARHGEF11	Rho guanine nucleotide exchange factor 11
ARNT	Aryl hydrocarbon receptor nuclear translocator protein
BCA	Bicinchoninic acid assay
BHLHE40	Basic Helix-Loop-Helix Family Member E40
BHLHE41	Basic Helix-Loop-Helix Family Member E41
BICD2	Bicaudal D homolog 2
BMAL1	Brain and muscle ARNT-like 1
BP	Biological process
CBD	CRY-binding domain
CC	Cellular component
CCAR2	cell cycle and apoptosis regulator 2
CCGs	Clock-controlled genes
CDK1	Cyclin-dependent kinase 1
CDK5	Cyclin-dependent Kinase 5
cDNA	Complementary DNA
CHRONO	ChIP-derived repressor of network oscillator
CK2α	Casein kinase 2 Alpha
CKI	Casein Kinase 1
CLOCK	Circadian locomotor output cycles protein kaput
CNOT1	CCR4-NOT deadenylase complex
CNX	Calnexin
COPA	COP Alpha
COPB1	COP Beta 1
COPG1	COP Gamma 1
COPG2	COP Gamma 2
COPI	Coat protein complex I
CRY	Cryptochrome
CSNK1D/CK1D/ CK1δ	Casein kinase 1 isoform delta
CSNK1E/CK1E/ CK1ϵ	Casein kinase 1 isoform epsilon
CT	Circadian time
DAVID	Database for Annotation, Visualization and Integrated Discovery
DBP	D Site-Binding Protein
DDB1	damage specific DNA binding protein 1
dH2O	Distilled water
DMEM	Dulbecco's modified eagle medium
DNA	Deoxyribonucleic acid
DNA-PKcs	DNA-dependent protein kinase
DVL	dishevelled homolog

E-box	Enhancer box
E'-box	E-box-like
EDTA	Ethylenediaminetetraacetic acid
EGFR	Epidermal growth factor receptor
ER	Endoplasmic Reticulum
FASP	Familial advanced sleep phase
FBXL21	Putative F-box/LRR-repeat protein 21
FBXL3	F-box/LRR-repeat protein 3
FBXW7	F-box/WD repeat-containing protein 7
FCS	Fetal calf serum
GAP	GTPase-activating protein
GAPDH	Glyceraldehyde-3-Phosphate Dehydrogenase
GAPVD1	GTPase-activating protein and VPS9 domain-containing protein 1
GEF	Guanine nucleotide exchange factor
GFP	Green fluorescent protein
GFPT1/2	Glutamine-fructose-6-phosphate transaminase
GLUT4	Glucose transporter type 4
GO	Gene ontology
GPCR	G protein–coupled receptor
GR	glucocorticoid receptor
GSK3β	Glycogen synthase kinase-3 beta
Gsα	G-Protein α-Subunit
GTPase	Guanosine triphosphatase
H2B	Helix 2 and Bottom helix
HBx	hepatitis B virus X protein
HLH	helix-loop-helix
HNRNPD	RNA-binding protein Heterogeneous Nuclear Ribonucleoprotein D
HRP	Horseradish peroxidase
IDR	Intrinsically disordered region
IP	Immunoprecipitation
JIP4	c-Jun N-terminal kinase (JNK)-interacting protein 4
LARG	Leukemia-associated RhoGEF
lncRNA	long noncoding RNA
MAPK	Mitogen-activated protein kinase
MAPKKK	MAPK kinase kinase
MCM	MiniChromosome Maintenance
MDM2	Mouse double minute 2 homolog
miRNAs	MicroRNAs
MKK4	mitogen-activated protein kinase kinase 4
mRNA	Messenger RNA
mTOR	Mammalian target of rapamycin
mTORC1	mammalian target of rapamycin complex 1
MYCBP2	MYC binding protein 2
NFIL3	nuclear factor, interleukin 3 regulated
NPAS2	Neuronal PAS domain protein 2
NR1D1	Nuclear receptor subfamily 1 group D member 1
NR1D2	Nuclear receptor subfamily 1 group D member 2
NR3C1	Nuclear receptor subfamily 3 group C member 1
p53	Tumor protein P53
PAC	PAS-associated C-terminal motif

PAS domain	Per-Arnt-Sim domain
PBS	Phosphate-buffered saline
PCR	Polymerase chain reaction
PER	Period Circadian Regulator protein
PFKM/P/L	Phosphofructokinase
PHR	Photolyase homology region
PKCα	Ca2+-sensitive protein kinase C subunit α
PLA	proximity ligation assay
PLD1	Phospholipase D1
PPIs	Protein-protein interactions
Pura	Puratrophin-1-like
PVDF	Polyvinylidene fluoride
Pyk2	Non-receptor Tyrosine Kinase
RAB31	Ras-related protein Rab-31
RAB5	Ras-related protein Rab-5A
RACK1	Receptor for activated C kinase-1
Raptor	regulatory-associated protein of mTOR
RBPs	RNA-binding proteins
RHT	retinohypothalamic tract
RME-6	Receptor-mediated endocytosis protein 6
RNA	Ribonucleic acid
ROR	RAR-related orphan receptor
RORα	Retinoic acid receptor-related Orphan Receptor α
RORβ	Retinoic acid receptor-related Orphan Receptor β
RORγ	Retinoic acid receptor-related Orphan Receptor γ
SAR1A	auxin resistance 1 A
SAR1B	auxin resistance 1 B
SCF	Skp-Cullin-F box
SCF E3	Skp, Cullin, F-box E3 ubiquitin ligase complex
SCN	Suprachiasmatic nucleus
SDS-PAGE	Sodium dodecyl sulfate polyacrylamide gel electrophoresis
SIRT1	Sirtuin 1
SKI	Exosome-associated superkiller complex
SKIV2L	Ski2 like RNA helicase
TAE	Tris-acetate-EDTA
TAK1	TGF-β-activated kinase 1
TBS	Tris-buffered saline
TGF-β	Transforming growth factor-β
TGS	Tris-glycine-SDS
tRFP	Tag red fluorescent protein
TSC1	Tuberous sclerosis 1
TTC37	Tetratricopeptide repeat domain 37,
TTFL	Transcriptional/post-translational feedback loop
UBE3A	HECT-type E3 ligase
USP7	Ubiquitin specific peptidase 7
USP9X	Ubiquitin Specific Peptidase 9 X-Linked
VPS9	Vacuolar protein sorting associated
WDR61	WD repeat domain 61
WT	Wild type
Y2H, Y3H	Yeast two/three-hybrid

List of abbreviations

ZT	Zeitgeber
βTrCP1/2	beta-transducin repeats-containing E3 ubiquitin protein ligase 1-2

1. Introduction

1.1. Circadian rhythms and the circadian clock

Circadian rhythms are oscillating biological processes that are present in almost all organisms, and they play a crucial role in coordinating an organism's behavior and physiology with environmental changes in the 24-hour rotation period of the earth. The term "circadian" originates from Latin (circa = about, and dies = day) and was first introduced by Franz Halberg in 1959 (Kuhlman et al., 2018). Circadian rhythms are observable as the sleep/wake cycle, feeding cycle, and fluctuations in body temperature, blood pressure, hormone secretion and many other processes in the body (Farhud and Aryan, 2018).

These rhythms are generated by the circadian clock, which is a complex system that coordinates internal processes to optimize an organism's fitness and survival. The circadian clock consists of three physical parts: oscillators, input pathways and output components. Input signals are received via receptors (e.g. photoreceptors in the mammalian eye), and then delivered to a pacemaker (oscillator) that generates the circadian rhythm. Biological oscillators are genetic mechanisms by nature and are primarily governed by a group of genes that work together to generate and regulate oscillations and ultimately drive biological rhythms (output components). These oscillators are synchronized to the outside world and to each other by external timing cues known as Zeitgebers (time-givers), which can also be referred to as synchronizers or entraining agents (Golombek and Rosenstein, 2010).

The circadian clock in mammals consists of a hierarchical arrangement of oscillators operating at the cellular, tissue, and systemic levels (Figure 1). At the apex is the central clock in the suprachiasmatic nucleus (SCN), which is situated in the anterior part of the hypothalamus. It receives light cues from the eyes via the retinohypothalamic tract (RHT) (Gooley et al., 2001). This information helps the SCN to reset the clock and synchronize it with the external environment. Furthermore, the central circadian clock serves as a primary regulator conveying vital entrainment cues to independent peripheral oscillators via various neuronal pathways including parasympathetic and sympathetic innervation and hormonal pathways (Albrecht, 2012) (Figure 1).

Circadian rhythms are essential for maintaining health and well-being, as they ensure that physiological processes occur at the appropriate time. In the context of circadian rhythms, cortisol, a stress hormone, exhibits its peak release during the morning, facilitating the initiation of daily activities. Conversely, melatonin levels, crucial for sleep regulation, are elevated in the evening, thereby promoting the onset of sleep. When the circadian clock is disrupted, these processes can become misaligned, leading to decreased performance and increased health risks (Patke et al., 2020).

Recent findings indicate that circadian clock disruptions can contribute to a range of pathologic conditions, including depression, cardiovascular disease, and type 2 diabetes (Fishbein et al., 2021). In addition, exposure to artificial light and modern lifestyle factors, such as shift work and frequent travel, can disrupt the circadian clock, leading to decreased sleep quality and increased health risks. Therefore, it is important to maintain a healthy circadian rhythm by exposure to natural light, regular sleep-wake patterns, and minimizing exposure to artificial light in the evenings (Gupta, 2019).

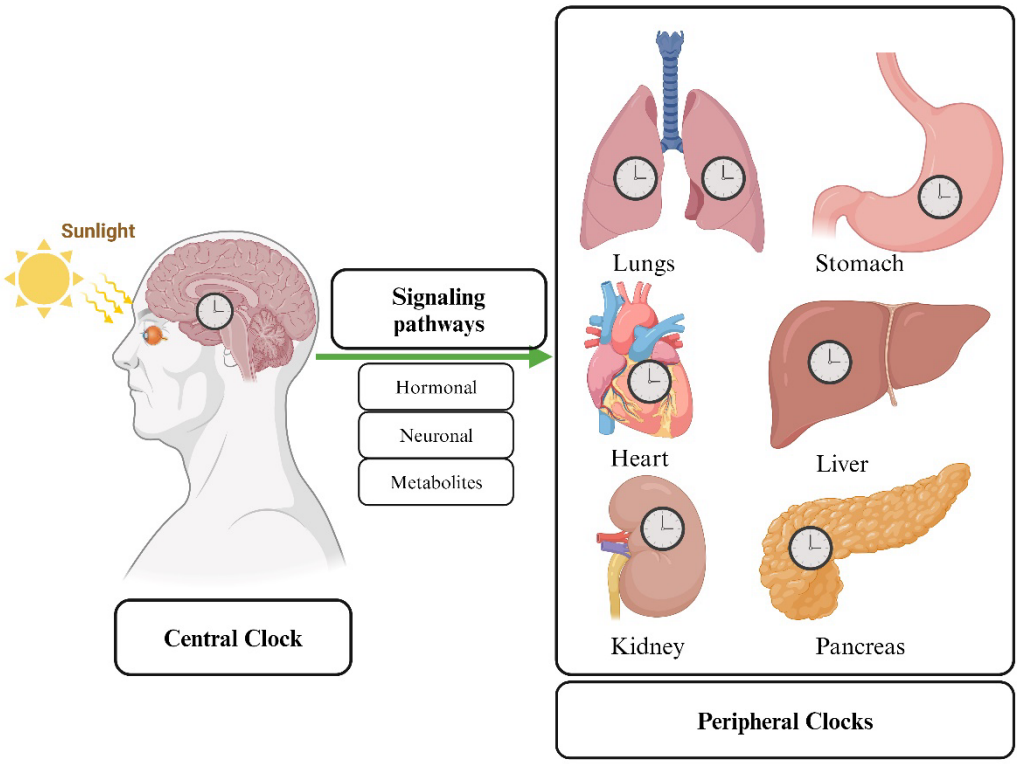

Figure 1. Hierarchical organization of the mammalian circadian system. Left side: The central clock, situated in the suprachiasmatic nucleus (SCN), acquires light/dark cues from the retina via the retinohypothalamic tract (RHT). The central clock then orchestrates peripheral clocks through periodic timing cues such as humoral and neuronal signals. Right side: The peripheral clocks are located in almost all tissues including lung, stomach, heart, liver, kidney and pancreas. Figure created with BioRender.com based on (Gonçalves and Meng, 2019).

1.2. The discovery of core clock genes

The discovery of the Period Circadian Regulator (*Per)* gene in the circadian clock was a significant breakthrough in the field of chronobiology and it was identified by examining abnormal eclosion cycles in Drosophila mutants (Reddy et al., 1984). It was observed that the *Per* gene orchestrates the accumulation of its own mRNA, leading to the concept of the feedback loop that produces approximately 24-hour long circadian rhythms (Hardin et al., 1990). *PER1* was discovered in mammals while searching for orthologs of drosophila *Per* (Sun et al., 1997). Based on that *Per2* was discovered while searching for homologous cDNA sequences to the *Per1* gene (Albrecht et al., 1997). Again in an attempt for finding homologous cDNA sequences to *Per2*, two research groups have independently cloned *Per3* (Takumi et al., 1998; Zylka et al., 1998). Studies using mouse mutants revealed that the *Per1*/*2* genes are crucial for regulating circadian rhythms, whereas the role of the *Per3* gene in the mouse clock is comparatively minor (Lee et al., 2004). Evidence has then emerged that *Per2* has a more prominent impact on the clock than *Per1* . Around the same time, the Cryptochrome 1 and 2 genes (*Cry1* and *Cry2*) were discovered (Kume et al., 1999) as well as Circadian locomotor output cycles protein kaput (*Clock*) (Gekakis et al., 1998) and Brain and muscle aryl hydrocarbon receptor nuclear translocator protein-like 1 (*Bmal1*) (Bunger et al., 2000). Together, these proteins work in collaboration and form the fundamental loop of the molecular oscillator.

1.3. Molecular components and mechanisms in the circadian clock

The core of the circadian oscillator is formed by a group of genes which together with their protein products produce the molecular oscillator through several mechanisms such as transcription, post- transcriptional regulation, translation, and post-translational regulation.

1.3.1. Transcriptional/translational feedback loops

The core clock genes and their protein products constitute the interlocking transcriptional/translational feedback loops (TTFL). These feedback loops ensure that the levels of clock proteins oscillate with a period of approximately 24 hours, which is the length of a typical circadian cycle. TTFLs involve a set of interacting clock proteins that control the expression and activity of clock genes which include transcription factors that bind to DNA activating or repressing mRNA expression, as well as enzymes that are responsible for posttranslational protein modification. The interactions between these components generate the rhythmic oscillations in gene expression and protein activity that underlie circadian rhythms. The circadian clock has four TTFLs which are described briefly below and depicted in Figure 2 (Hurley et al., 2016).

1.3.1.1. The PERIOD feedback loop

This is the main circadian feedback loop and is depicted with black arrows in Figure 2. The transcription factors CLOCK or its human paralog Neuronal PAS domain protein 2 (NPAS2) and BMAL1 form a transcriptional complex that binds to E-box (CACGTG) and E-box-like (E'-box) (CACGTT) element-containing genes (Akashi et al., 2006). CLOCK/BMAL1 binds rhythmically to E-box motifs and reaches a maximal promoter occupancy between ZT5 and ZT8 (Ripperger and Schibler, 2006) (Figure 2). Zeitgeber time (ZT) is used to define the time phase of circadian rhythms. ZT0 is the time when a Zeitgeber is applied (e.g. when the lights go on) (Vitaterna et al., 2001). CLOCK/BMAL1 also binds to E-Box elements in the promoters of their own negative regulators *Per1/2/3* (Shearman et al., 1997) and *Cry*1/2 (Takahashi, 2017). PERs and CRYs form multimers that translocate into the nucleus, where they directly interact with CLOCK/BMAL1 to repress their own gene transcription. In addition, the expression of *Per1/2/3* and *Cry1/2* mRNA is regulated by several post-transcriptional mechanisms such as deadenylation (Mohamed et al., 2022). When the negative transcriptional feedback together with post-transcriptional and post-translational regulation sufficiently decreased the nuclear PER and CRY protein levels, repression is lifted, and CLOCK/BMAL1 activates *Per/Cry* gene transcription once again, thus starting a new circadian cycle (Cox and Takahashi, 2019).

1.3.1.2. The CLOCK/BMAL1 feedback loop

In a second feedback loop, CLOCK/BMAL1 or NPAS2/BMAL1 induces the expression of nuclear receptor subfamily 1 group D member 1 and 2 (NR1D1/NR1D2), and ChIP-derived repressor of network oscillator (CHRONO) which both act as negative regulators of BMAL1 transcription (Goriki et al., 2014; Preitner et al., 2002). The expression of BMAL1 is inhibited by binding to a ROR Response Element (RRE) located in its promoter region (Lee et al., 2016). On the other hand, BMAL1 expression is regulated positively via Retinoic acid receptor-related Orphan Receptor α, β and γ (RORα/β/γ) (T. K. Sato et al., 2004). The yellow lines in Figure 2 show this feedback loop.

1.3.1.3. The RORα/β/γ feedback loop

A third feedback loop involves RORα/β/γ, which induce the transcription of genes containing RREs, including BMAL1 and Nuclear Factor Interleukin 3 Regulated (NFIL3), also known as

E4BP4 (T. K. Sato et al., 2004; Takeda et al., 2012). D-box-dependent transcription is inhibited by NFIL3, which is a REV-ERB and ROR target gene. CLOCK/BMAL1 mediates the transcription of the gene D Site-Binding Protein (*Dbp*) (Stratmann et al., 2010). DBP binds to D-box elements in target genes such as RORα/β/γ, activating their transcription and providing additional layers of regulation (Jetten, 2009). Green lines were designated to track this loop in Figure 2.

1.3.1.4. The DEC1/2 feedback loop

Lastly, another loop consists of Basic Helix-Loop-Helix Family Member E40 and 41 (BHLHE40/41) mostly known as DEC1 and DEC2, which are members of the basic helix–loop–helix (bHLH) family of transcription factors (Rossner et al., 1997). In this loop the DEC1 and DEC2 transcription factors, through direct interactions with BMAL1, inhibit CLOCK/BMAL1-induced transactivation at E-box promoter elements (F. Sato et al., 2004). Nevertheless, DEC proteins have a low affinity to the CACGTT E'-box compared to CLOCK/BMAL1, which leads to only a slight impact on transcription induced by CLOCK/BMAL1 through the E'-box (Nakashima et al., 2008). The CLOCK/BMAL1 heterodimer induces *Dec1*/*2* expression via the CACGTG E-box, however, binding of DEC1/2 to the same E-box suppresses it (Honma et al., 2002). Pink lines indicate the DEC1/2 loop in Figure 2.

All loops additionally regulate the expression of clock-controlled genes (CCGs), which facilitate circadian output. In addition to transcription, post-transcriptional mechanisms and post-translational modification also play important roles.

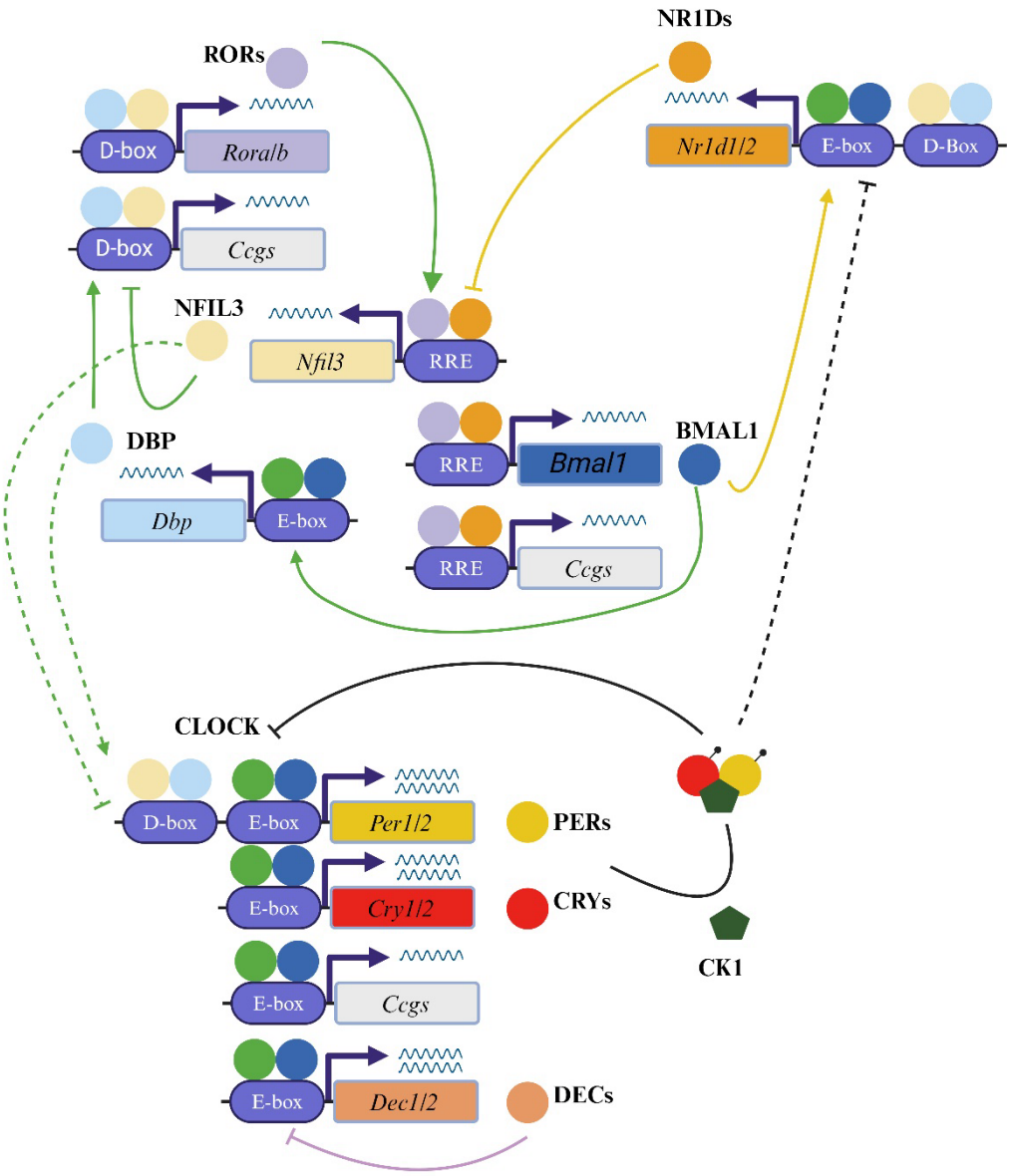

Figure 2. In the transcriptional/translational feedback loop model, the PER feedback loop (solid black line) involves CLOCK (green) and BMAL1 (blue) binding to E-box containing genes such as Per1/2 (yellow) and Cry1/2 (red) inducing their transcription. In a second loop (solid yellow line), CLOCK/BMAL1 regulates NR1D1/2 (orange), which negatively regulates BMAL1 transcription. In the third loop (solid green line), CLOCK/BMAL1 activates Dbp (light blue), which in turn activates RORs. RORs activate Nfil3 (light yellow). In the fourth loop (pink solid line) CLOCK/BMAL1 activates DEC1/2. Interlocking steps are depicted as dotted lines, and these factors regulate many other clock output genes (CCGs). Arrows indicate activation while horizontal lines indicate repression. Figure created with BioRender.com based on (Cox and Takahashi, 2019; Schibler, 2007).

1.3.2. Posttranscriptional mechanisms

One of the critical posttranscriptional mechanisms in the circadian clock is the regulation of gene expression by RNA processing, stability, and translation (Kojima et al., 2011). This process involves various regulatory molecules, including RNA-binding proteins (RBPs), microRNAs, and non-coding RNAs.

RBPs can bind to specific mRNAs and regulate their stability, translation, and localization. Several RNA-binding proteins have been discovered to participate in the posttranscriptional regulation of circadian clock genes (Green, 2018). For instance, the CCR4-NOT deadenylase

complex (CNOT1) regulates the deadenylation-dependent decay of *Per2* mRNA (Mohamed et al., 2022). Similarly, the RNA-binding protein Heterogeneous Nuclear Ribonucleoprotein D (HNRNPD) controls the turnover rate of *Cry1* mRNA (Woo et al., 2010). These RBP-mediated regulations ensure the rhythmic expression of clock genes, contributing to the accurate maintenance of the circadian clock.

MicroRNAs (miRNAs) are small non-coding RNA molecules that can bind to specific mRNAs, thereby repressing their translation or promoting their degradation. In the circadian clock, microRNAs play an essential role in regulating the expression of clock genes and controlling the amplitude and phase of the clock. For example, *mi*R-142-3p might be involved in the post-transcriptional regulation of *Bmal1* mRNA (Shende et al., 2013). Additionally, the CLOCK/BMAL1 complex targets miR-219, whereas miR-132 is stimulated by photic entrainment cues through a MAPK/CREB-dependent mechanism (Cheng et al., 2007). These miRNA-mediated regulations ensure the precise control of clock gene expression, contributing to the robust and synchronized circadian rhythm. Beyond miRNAs, non-coding RNAs, including long non-coding RNAs and circular RNAs, have also emerged as important players in circadian regulation (Mosig and Kojima, 2022). For instance, the long non coding RNA (lncRNA) TCONS_00044595 interacts with miR-182, a key regulator of *Clock* expression, modulating its regulation (Li et al., 2020). These non-coding RNAs can act as scaffolds to recruit other regulatory proteins or compete with other RNAs to bind to regulatory molecules.

In summary, posttranscriptional mechanisms, including microRNA regulation, RNA-binding protein control, and non-coding RNA action, are critical components of the circadian clock that help regulate gene expression and maintain the daily rhythm.

1.3.3. Posttranslational mechanisms

In addition to transcriptional and posttranscriptional mechanisms, posttranslational regulation is an essential component of the molecular circadian oscillator (Mehra et al., 2009). The circadian clock is controlled by a complex network of proteins that undergo various posttranslational modifications to regulate their activity, stability, and subcellular localization. These posttranslational mechanisms can be for example phosphorylation, ubiquitination, acetylation, SUMOylation, and glycosylation.

Many clock proteins, such as CLOCK, BMAL1, PERs, and CRYs, undergo phosphorylation, which can regulate their stability, localization, and interaction with other clock proteins. For example, the phosphorylation of PERs is regulated by serine/threonine kinases such as CSNK1D/E (Vanselow et al., 2006) and will be discussed in detail later in the section. Ubiquitination is a process in which poly-ubiquitin molecules are covalently attached to target proteins, leading to their degradation by the proteasome. Several clock proteins, including PER and CRY, are regulated by ubiquitination, which plays an important role in their degradation and turnover (Stojkovic et al., 2014). Phosphorylation and other PTMs can be categorized into three phases based on time-dependent regulation and hence can be classified as daytime phase (ZT0-12), early night phase (ZT12-16) and late night phase (ZT16-24). Figure 3 illustrates these three phases.

Daytime phase (ZT0-12). Cyclin-dependent Kinase 5 (CDK5)-mediated phosphorylation at Thr-451/461 promotes nuclear localization of CLOCK (Kwak et al., 2013). Meanwhile, BMAL1 is also phosphorylated by Casein kinase 2 Alpha (CK2α) on Ser-90 which leads to heterodimerization with CLOCK and nuclear translocation of the complex (Tamaru et al.,

2015). Within the nucleus, CLOCK undergoes phosphorylation at Ser-440, 441, and 446, which enhances transactivation facilitated by CLOCK/BMAL1 (Robles et al., 2017). This results in transcription of E-box containing genes including PERs and CRYs. As a consequence, PER2 protein levels start to rise at ZT 8 and peak at ZT 16 (Brenna et al., 2019; Nam et al., 2014). The Daytime phase is depicted in the upper panel of figure 3.

Early night phase (ZT12-16). CDK5 mediated phosphorylation of PER2 at Ser-394 in the cytoplasm promotes PER2/CRY2 heterodimerization and their nuclear entry (Brenna et al., 2019). CDK5 also phosphorylates CSNK1D at Thr-347, which regulates its activity towards PER2 (Eng et al., 2017). Another factor is Glycogen synthase kinase-3 beta (GSK3β) which influences accumulation of PER2 in the nucleus independently of its interaction with CRY1 (Iitaka et al., 2005; Ohsaki et al., 2008). CSNK1E phosphorylates a serine cluster of mouse PER1 from amino acid residues 902-916 which is accountable for masking its NLS motif and henceforth regulation of its nuclear translocation (Vielhaber et al., 2000).

In the nucleus, the PER/CRY complex binds to CLOCK/BMAL1. Mitogen-activated protein kinase (MAPK) phosphorylates CRY1 at Ser-247 and 588 and CRY2 at Ser-265 which promotes their association with CLOCK/BMAL1 (Sanada et al., 2004). Notably, CRY proteins promote the cyclical binding of CK2β to BMAL1, which subsequently inhibits CK2α-induced BMAL1-S90 phosphorylation (Tamaru et al., 2015). This results in the formation of BMAL1 complexes with Receptor for activated C kinase-1 (RACK1) and Ca2+-sensitive protein kinase C subunit α (PKCα), leading to the inhibition of BMAL1's transactivation activity (Robles et al., 2010). Phosphorylation of CLOCK Ser-38/42 leads to inhibition of CLOCK's transactivation activity followed by its translocation to the cytoplasm (Brenna and Albrecht, 2020; Yoshitane et al., 2009). The early night phase is depicted in the middle panel of figure 3.

Late night phase (ZT16-24). This phase is marked by the disassembly of the nuclear macromolecular complex. GSK3β phosphorylates BMAL1 at Ser-17/ Thr-21 priming it for ubiquitination through the HECT-type E3 ligase (UBE3A) (Gossan et al., 2014; Sahar et al., 2010). CLOCK Ser-431 is phosphorylated by an unknown kinase at the priming site so that phosphorylation at Ser-427 by GSK3β can take place and this step is associated with the regulation of CLOCK degradation (Spengler et al., 2009). Notably, this phosphorylation step is modulated by BMAL1 (Spengler et al., 2009). In parallel, CSNK1E phosphorylates PER2 Ser-477, which then interacts with βTrCP1/2 to direct the proteasomal degradation of PER2 through the 26S proteasome (Eide et al., 2005; Reischl et al., 2007). CK2 phosphorylates PER2 Ser-53 and that plays a role in fine-tuning circadian rhythms and regulating PER2 stability (Tsuchiya et al., 2009). CK1 and CK1 gamma2-mediated PER1 degradation is also driven by interaction with β-TRCP1/2 (Shirogane et al., 2005). FBXL3 facilitates CRY ubiquitination which leads to its proteasomal degradation (Busino et al., 2007). DNA-dependent protein kinase (DNA-PKcs) negatively regulates dephosphorylated CRY1 at serine-588 which stabilizes the interaction with FBXL3 that promotes CRY1 degradation (Gao et al., 2013). Putative F-box/LRR-repeat protein 21 (FBXL21) forms a SCF E3 complex that degrades CRYs slowly in the cytoplasm but antagonizes FBXL3-mediated degradation of CRYs in the nucleus (Yoo et al., 2013). CRY2 phosphorylation at T300 leads to CRY2 degradation via F-box/WD repeat-containing protein 7 (FBXW7)-containing SCF complex ubiquitination (Fang et al., 2015). These events close the 24 h cycle. The late night phase is depicted in the lower panel of figure 3.

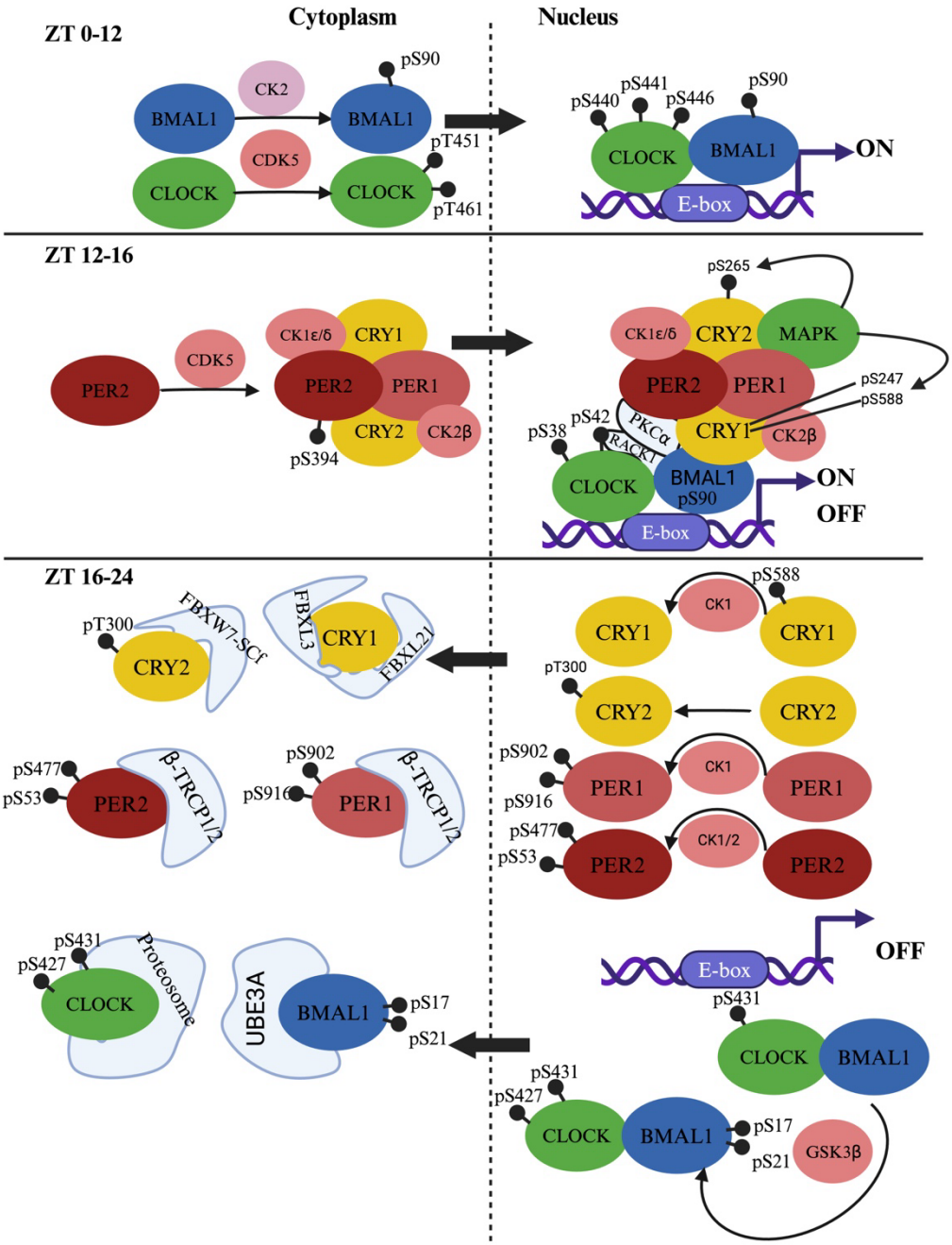

Figure 3. The phosphorylation phase of the circadian clock in a time frame of 24 hours. Upper panel: during the daytime phase (ZT 0-12), CDK5 and CK2 phosphorylate CLOCK and BMAL1, promoting their heterodimerization and nuclear translocation. CLOCK phosphorylation leads to the expression of PERs and CRYs. Middle panel: In the early night phase (ZT 12-16), CDK5 phosphorylates PER2, triggering heterodimerization with CRY1, and MAPK phosphorylates CRY1/2, leading to CLOCK transactivation shutdown. Lower panel: In the late night phase (ZT 16-24), GSK3β phosphorylates CLOCK and BMAL1, initiating their cytoplasmic shuttling and degradation. CKI phosphorylates PER1/2, promoting their degradation in the cytoplasm. CRY1 is dephosphorylated, translocated to the cytoplasm and degraded, while CRY2 is phosphorylated and degraded. Figure created with BioRender.com based on (Brenna and Albrecht, 2020).

Additional posttranslational modifications also take place, such as acetylation of CLOCK and BMAL1, which regulates their activity and interaction with other clock proteins (Hirayama et al., 2007). In addition, SUMOylation is a process in which small ubiquitin-like modifier (SUMO) proteins are covalently attached to target proteins, regulating their activity, stability, and localization. Several clock proteins, including PER and BMAL1 undergo SUMOylation, which plays an important role in their regulation and turnover (Chen et al., 2021; Lee et al.,

2015). Glycosylation is a posttranslational modification in which sugars are covalently attached to proteins, regulating their stability and activity. Other clock proteins, such as PER, undergo glycosylation, which can affect their localization and stability (Kim et al., 2012).

In summary, posttranslational mechanisms, including phosphorylation, ubiquitination, acetylation, SUMOylation, and glycosylation, are critical processes of the circadian clock, regulating the activity, stability, and localization of clock proteins and helping to maintain the daily rhythm.

1.4. Functional and structural domains of PERIOD proteins

As mentioned previously, PER2 plays a crucial role in the regulation of circadian rhythms. Structurally, the PER2 protein consists of several domains that are depicted in Figure 4. PER2 has an amino-terminal helix-loop-helix (HLH) motif, which is unlikely to bind to DNA due to the lack of basic amino acids preceding it (Albrecht et al., 2007). The Per-Arnt-Sim (PAS) A domain, located downstream of the HLH motif, consists of two imperfect repeats (PAS A and PAS B) and a PAS-associated C-terminal PAC motif. PAS domains are involved in protein-protein interaction and dimerization (Huang et al., 1993; Yildiz et al., 2005). Gsk3-β has been shown to interact with the PAS A/B domains in PER2 (Iitaka et al., 2005). PAS/PAC domains are postulated to function additionally as ligand-binding domains, such as binding to heme and functioning as oxygen sensors, and heme has been identified as a prosthetic group of the PER2 protein (Kaasik and Lee, 2004; Ponting and Aravind, 1997). PER2 has a nuclear localization domain that is responsible for its translocation to the nucleus where it acts as transcription factor (Chiou et al., 2016; Miyazaki et al., 2007).

Towards the C-terminal end of the PER2 protein there is a coiled coil structure, which typically consists of a repeated seven-amino-acid residue pattern that forms a helix. This helix can bind to the helix of another protein to form a dimer that is held together by burying their hydrophobic surfaces from the surrounding water. Previous studies have reported that the carboxy-terminal domain of PER2 can interact with CRY and the transcription factor E4BP4 (Miyazaki et al., 2001; Ohno et al., 2007). PER2 contains other structural features that enable it to interact with other proteins. Studies have pointed out that the C-terminus of PER2 currently known as CRY-binding domain (CBD) interacts with the CRY photolyase homology region (PHR) which is modulated by zinc binding and disulfide bond formation (Nangle et al., 2014; Schmalen et al., 2014). It has been proposed that PER2 attenuates the CRY1 PHR–tail interaction which regulates its association with CLOCK/BMAL1 (Parico et al., 2020; Parico and Partch, 2020). In between the PAS domain and the coiled coil domain there is a proline-rich sequence that divides the PER2 protein into two structural entities that may fold back to bind to another protein. This proline-rich sequence makes the amino acid chain less structured, meaning that PER2 could serve as a scaffold for binding different proteins in close proximity, allowing each of them to perform a specific function. This concept is not unique, as hormone receptors, their coactivators, and corepressors function in a similar manner (Stallcup et al., 2003).

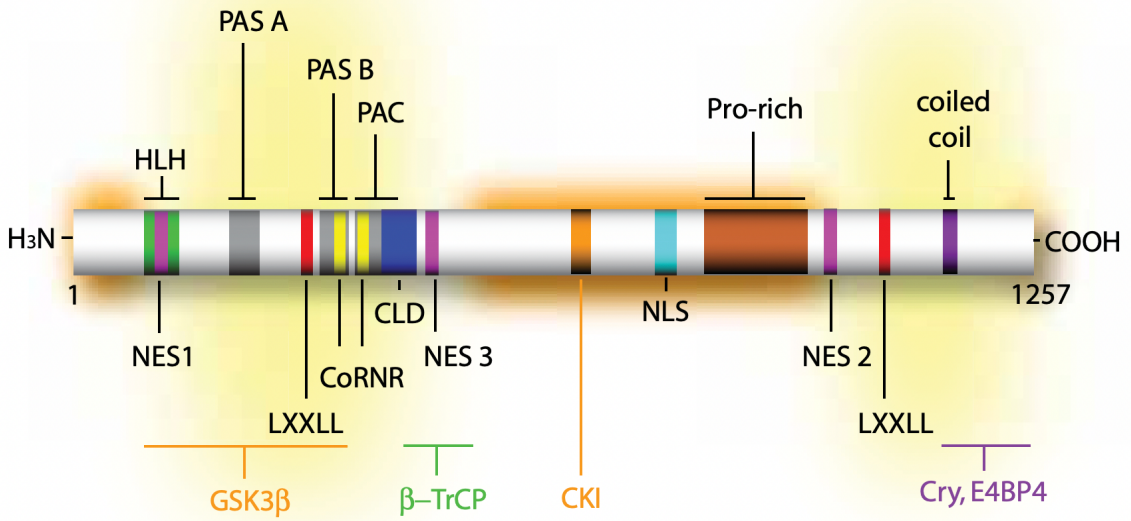

Figure 4. Domain structure of mouse PER2 protein. From N- to C- terminus: (HLH) Helix-loop-helix motif (green) with an embedded nuclear export sequence 1 (NES1); PAS domain, which consists of the PAS A, PAS B, and PAC subdomains (gray); (LXXLL) motif found in coactivators that associate with nuclear receptors (red); (CoRNR) motif found in corepressors that associate with nuclear receptors (yellow); (CLD) cytoplasmic localization domain; NES3 (pink); (NLS) nuclear localization sequence (cyan); (Pro-rich) proline rich sequence (brown); NES2 (pink); (LXXLL) (red); (coiled-coil) dimerization domain (purple). Yellow-shaded areas are potential protein-binding domains; orange shaded areas indicate localizations of protein phosphorylation and contain a (CKI) casein kinase-binding site (orange). (Permission granted) (Albrecht et al., 2007)

1.5. The CSNK1D/E-dependent phosphoswitch of PER2

One of the first clock-related mutations identified in mammals was the tau mutation in Syrian hamsters, which results in a significant shortening of circadian period from 24h to 20h (Ralph and Menaker, 1988). Further investigation using genetic mapping studies determined that the tau mutation is C178T in CSNK1E (Lowrey et al., 2000). Later it has been shown that the mutation does not impact the expression of *Per* mRNA or the accumulation of PER proteins in the nucleus. Nevertheless, it does speed up the removal of PER proteins from the nucleus, which is enough to account for the reduced circadian rhythm period of behavioural patterns (Dey et al., 2005). It has been revealed that the CSNK1E tau mutation functions as a gain-of-function mutation and operates during a distinct circadian phase to enhance the breakdown of PER proteins, thereby accelerating the circadian system in both the brain and the peripheral regions (Meng et al., 2008).

It has been shown as well that CSNK1D is the dominant form of CK1 (Etchegaray et al., 2009). Phosphorylation of PER2 by CSNK1D leads to either stabilization or degradation of PER2 in a model called the phosphoswitch as depicted in Figure 5 (Brenna and Albrecht, 2020). Phosphorylation of a region that is known as phosphodegron leads to PER2 degradation, while phosphorylation of the so-called FASP region leads to enhanced stabilization (Masuda et al., 2020; Narasimamurthy and Virshup, 2021). Studies have shown that CSNK1D-dependent Ser-478 phosphorylation at the phosphodegron recruits β-TrCP1/2, which is followed by proteasomal degradation (Eide et al., 2005; Ohsaki et al., 2008). The activity of CSNK1D on the Ser-478 phosphodegron is regulated by the other motif, the FASP region. Within this motif CSNK1D phosphorylates Ser-659, which accelerates phosphorylation of further downstream serines in the motif pS-x-x-S-x-x-S (pS: primed Serine, x: any amino aicd, S: Serine to be phosphorylated) (Figur 5). In summary, multiphosphorylation of the FASP domain stabilizes

PER2 by blocking phosphorylation of the Ser-478 phosphodegron (Narasimamurthy et al., 2018; Zhou et al., 2015).

Interestingly, the equilibrium between the two opposing phosphorylation pathways is impacted by temperature and is believed to contribute to temperature compensation in the mammalian clock. Elevated temperatures increase phosphorylation in the vicinity of Ser-659, which stabilizes PER2. Conversely, lower temperatures promote phosphorylation of the β-TrCP1 site, which results in the degradation of PER2 (Chappuis et al., 2013; Zhou et al., 2015).

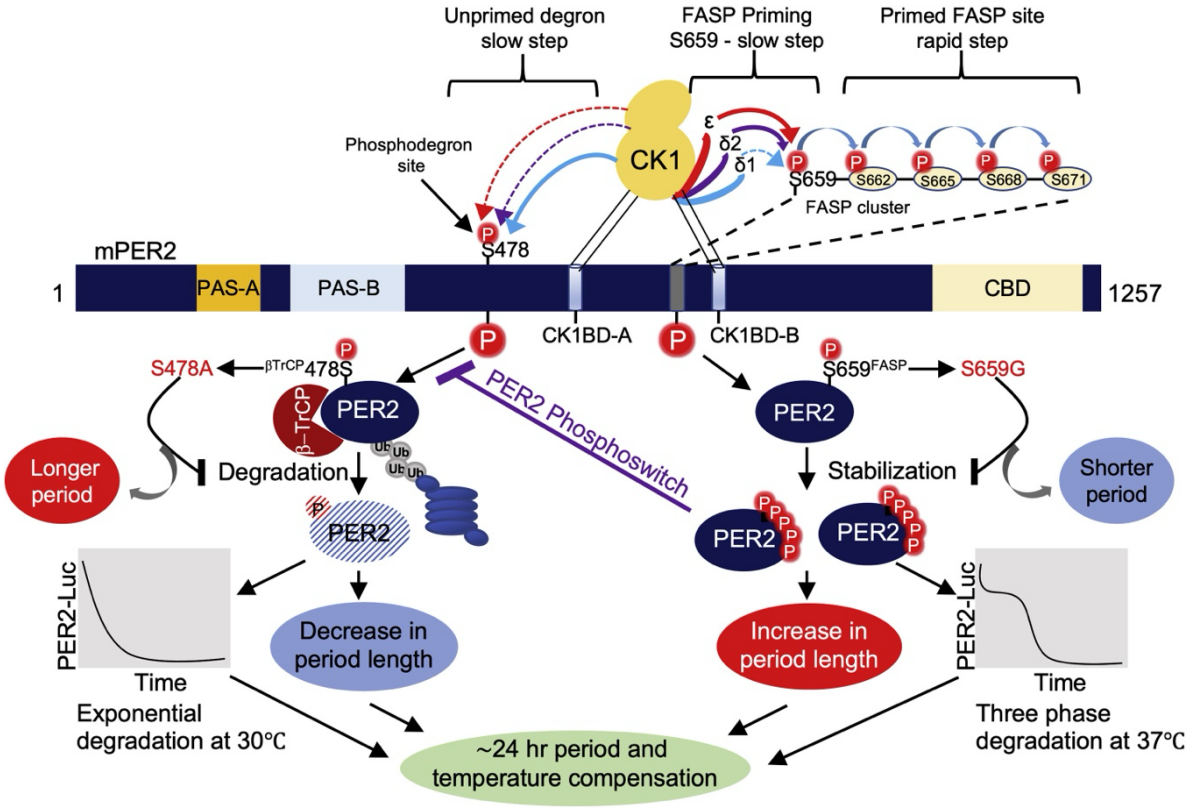

Figure 5. Phosphoswitch model. PER2 modulates the pace of the circadian clock. CSNK1D/E (CKIδ/ε) typically phosphorylates PER2 at Ser-478, triggering its eventual degradation via the proteasome. A temperature increase leads to higher PER2 phosphorylation at the FASP site (pSer-659-662-665-668-671), which increases the stability of PER2 and slows down the clock. (Permission granted) (Narasimamurthy and Virshup, 2021)

1.6. PER2: A Master Conductor in the Orchestra of Circadian Rhythms

The discovery of PER proteins has had a major impact on the field of chronobiology, as it has opened new avenues for research into the molecular mechanisms that regulate the circadian clock. Additionally, it has enhanced understanding of the link between circadian disruption and human health and has paved the way for the development of new treatments for sleep and circadian disorders.

PER2 has diverse functions in the circadian clock including the one that has been discussed earlier as transcription factor that negatively regulates E box containing genes and in addition clock resetting (Spoelstra et al., 2004). Additionally, PER2 directs other clock proteins such as CRY into the nucleus and maintains their stability (Yagita et al., 2002). In addition, PER2 regulates the temporal expression of genes associated with cell cycle regulation and tumor suppression, such as Cyclin D1, Cyclin A, E3 ubiquitin-protein ligase Mdm2, and Growth arrest and DNA-damage-inducible protein Gadd45alpha, and c-myc. Hence, it appears that PER2

plays a role in tumor suppression by regulating DNA damage responsive pathways (Fu et al., 2002). It has been demonstrated that the *Per2* gene expression rhythm improves tumor control (Iurisci et al., 2006). Besides that, PER2 overexpression appears to induce cancer cell apoptosis (Hua et al., 2006). Emerging evidence suggests that the *Per2* gene is involved in the immune system (Liu et al., 2006). PER2 expression is associated with the levels of proinflammatory cytokines such as IFN-and interleukin-1 as well as native immune cells such as natural killer cells (Liu et al., 2006; Viswambharan et al., 2007). Aortic endothelial dysfunction in mice is linked to a *Per2* gene mutation, which leads to a reduction in the production of nitric oxide (NO) and vasodilatory prostaglandins coupled with increased release of vasoconstrictors derived from cyclooxygenase-1 (COX-1). These findings suggest that the *Per2* gene plays an important role in the maintenance of normal cardiovascular functions (Viswambharan et al., 2007).

It has been demonstrated that PER2 is localized in the cytoplasm and in the nucleus (Yagita et al., 2002). Furthermore, studies showed that PER2 localization is cell specific. For example, PER2 remains mostly in the nucleus in Human Embryonic Retinoblasts (HER) while it is mostly cytoplasmic in Human Embryonic Kidney 293 cells (HEK 293) (Albrecht et al., 2007; Vielhaber et al., 2000). In connection to these observations, recent studies pointed to non-transcriptional roles of PER2. For example, the downregulation of *PER2* through siRNA reduces autophagy levels while keeping core clock oscillations unaffected (Kalfalah et al., 2016). Furthermore, it has been found that PER2 acts as a scaffold to tether Tuberous Sclerosis 1 (TSC1) and Mammalian target of rapamycin (mTOR) together and to suppress the mammalian Target of Rapamycin Complex 1 (mTORC1) activity in the liver during fasting , which likewise emphasizes its cytoplasmic role. PER2 also binds the C-terminal half of Tumor Protein p53 (p53) and forms a stable trimeric complex with p53's negative regulator E3 ubiquitin-protein ligase Mdm2 (MDM2) (Gotoh et al., 2014). The binding of PER2 to p53 prevents MDM2-mediated ubiquitination and subsequent targeting of p53 for degradation by the proteasome (Gotoh et al., 2014). In synopsis, these findings suggest a non-transcriptional role of PER2 in the cytoplasm.

1.7. Goals and aims

PER2 is a critical component of the circadian clock, a complex system that regulates physiological processes in our bodies over a 24-hour cycle. Despite our considerable knowledge regarding PER2's role as a transcription factor in maintaining circadian rhythms, emerging evidence indicates that it may also play a role in other cellular processes and possibly in a post-transcriptional role.

The aim of this dissertation is to elucidate novel cytoplasmic roles of PER2 by focusing on previously undiscovered protein interactions. In the first phase of the study, an affinity enrichment mass spectrometry analysis using stably expressed PER2-GFP as bait will be conducted to identify unknown PER2 binding proteins. Moreover, I aim to perform meta-analysis of the mass spectrometry data that should lead to the identification of functional biological pathways in which PER2 might be directly or indirectly involved. Additionaly, I aim to verify the identified interactions using western blot of the immunoprecipitated PER2-interacting proteins.

In the second phase of the study one highly interesting PER2-interacting protein will be selected for an in-depth analysis of mutual molecular functions between PER2 and the novel protein. This includes assessing whether the novel protein is influenced by PER2 itself or other clock proteins such as kinases or other enzymes, and relevant functions will be evaluated in detail. Additionally, the involvement of the novel protein in the circadian clock machinery in relation to PER2 protein function will be explored.

In the third phase, interaction domains between PER2 and its interacting partner will be characterized. This will be achieved through immunoprecipitation of expressed tagged proteins and various deletion mutants. This step should pave the way for subsequent structural analyses and further functional studies.

With these objectives I hope to contribute to a deeper understanding of the cytoplasmic role of PER2 and its interaction with proteins, thereby providing valuable insights into the regulation of the circadian clock.

2. Materials

2.1. Cell culture

Table 1: Cell lines used for experiments.

Original cell line	Description	Name	DSMZ number
HT1080	Human fibrosarcoma cell line established from the biopsy from a 35- year-old man	HT1080-WT	ACC 315
HT1080	HT1080 that stably express PER2-GFP. Puromycin-resistant	HT1080-P	
HT1080	HT1080 that stably express GFP. Hygromycin-resistant	HT1080-GFP-	
HT1080	HT1080 that stably express both CSNK1D and PER2. Puromycin - resistant	HT1080-CP	
HT1080	HT1080 that stably express GAPVD1. Puromycin-resistant.	HT1080-G	
HEK293T	The 293T cell line, originally referred as 293tsA1609neo, is a highly transfectable derivative of human embryonic kidney 293 cells and contains the SV40 T-antigen.		CRL-3216
HeLa WT	HeLa is an epithelial cell that was isolated from the cervix of a 31-year-old, Black female with adenocarcinoma.		CRM-CCL-2
HeLa GAPVD1 KO	HeLa cell line, in which GAPVD1 is knocked out by CRISPR/Cas9		
U2OS	U-2 OS is a cell line with epithelial morphology that was derived in 1964 from a moderately differentiated sarcoma of the tibia of a 15-year-old, White, female osteosarcoma patient.		ACC 785

Table 2: Solutions and Antibiotics for cell culture.

Name	Manufacturer
Dulbecco's Modified Eagle's Medium (DMEM) high glucose	Gibco/Invitrogen, Carlsbad, USA
Phosphate-buffered saline (PBS) Ca^{2+}-, Mg^{2+}- free)	Gibco/Invitrogen, Carlsbad, USA
Fetal calf serum (FCS)	Gibco/Invitrogen, Carlsbad, USA
Ethylenediaminetetraacetic acid (EDTA)	Sigma, St. Louis, USA
Penicillin (10,000 U/ml) & Streptomycin (100 µg/ml)	Gibco/Invitrogen, Carlsbad, USA
Hygromycin	Sigma, St. Louis, USA
Puromycin	Sigma, St. Louis, USA

Name	Manufacturer
Dimethyl sulfoxide (DMSO)	Sigma, St. Louis, USA

Table 3: Media used for the cultivation of cells.

Name	Composition
Growth medium	DMEM high glucose, 10% FCS, 100 U/ml penicillin, 100 µg/ml streptomycin
Growth medium I	DMEM high glucose, 10% FCS, 100 U/ml penicillin, 100 µg/ml streptomycin, 0.4 µg/ml puromycin
Growth medium II	DMEM high glucose, 10% FCS, 100 U/ml penicillin, 100 µg/ml streptomycin, 100 µg/ml hygromycin
Freezing medium	FCS containing 10% DMSO

2.2. Bacterial strains and growth conditions

Table 4: Bacterial strain.

Bacteria strain	Genotype
Escherichia coli DH5α	supE44 ΔlacU169 (Φ80lacZΔM15) hsdR17 recA1 endA1 gyrA96 thi-1 relA1

Table 5: Bacterial growth media.

Name	Composition
LB-medium	10 g Trypton, 5 g yeast extract, 10 g NaCl, adjusted to pH 7.5 by (NaOH)
LB-Agar	1g Agar in 100 ml LB-medium
TB-Medium for growth	12 g tryptone, 24 g yeast extract, 4 ml glycerol (87%) in 900 ml H_2O then autoclaved. 100 ml sterile phosphate-buffer Were added prior to use. (0.17 M KH2PO4, 0.72 M K2HPO4).

For selection 50 µg/ml ampicillin was added to the media.

2.3. Vectors and oligonucleotides

2.3.1. Expression of bicistronic vectors

The bicistronic vectors pMCC-GFP-P/HpMCC-tagRFP-P/H enable the expression of fluorescent chimeras of specific proteins in mammalian cells and are based on pMC-GFP-P vectors (Christensen et al., 2002; Mielke et al., 2000). These vectors utilize an internal ribosome entry site (IRES) element from the polio virus to simultaneously translate both the first cistron which is gene of interest (GFP/tagRFP-tagged protein) and the second cistron which is selection marker (puromycin "pyromycin-N-acetyltransferas" or hygromycin "hygromycin B phosphotransferase resistance gene") from a single mRNA molecule. Following the selection marker, the simian virus 40 (SV40) polyadenylation signal is positioned. The cytomegalovirus promoter (CMV), fused upstream with the myeloproliferative sarcomvirus MPSV LTR enhancer repeat, ensures robust transcription levels of proteins of interest in the mammalian cells. This combination of elements allows for the stable and controlled expression of fluorescent proteins and selection markers in mammalian cells, facilitating the study of protein localization, dynamics, and function (Figure 6).

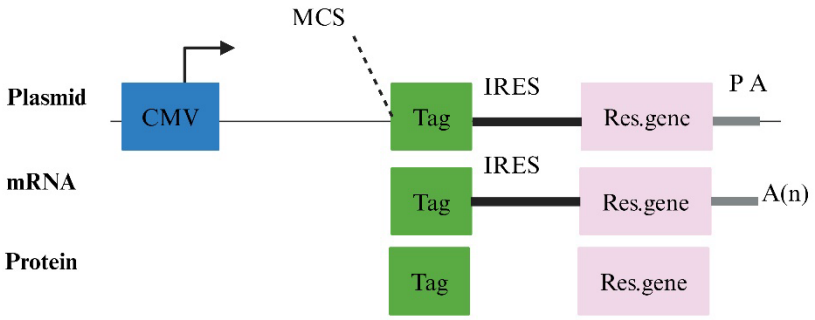

Figure 6. A schematic representation of the *bicistronic plasmid. Upper: The plasmid DNA sequence contains the CMV promotor (blue box), followed by a multiple cloning site (MCS) and a tag which can be tRFP or GFP (green box), and an IRES element (thick black bar), Resistance gene (pink box), and SV40 P(A) site (thicked grey bar). The translation of the first cistron (protein of interest and the tag) is mediated by CAP dependent translation while the translation of the second cistron (resistance gene) is cap-independent i.e IRES.*

The plasmids served as fundamental templates for cloning all proteins mentioned in this study, with the multiple cloning site positioned upstream of the fluorescent protein, either GFP or TAGRFP Bicistronic plasmids used in this thesis are listed in table 6.

Table 6: Bicistronic plasmids used in cloning and for the transfection of HT1080 and HEK293T cells. Each plasmid was given a number and stored in our lab database.

Number	Name	Description
NA	GAPex5 (GAPVD1) (NM_001282679) Human Tagged ORF Clone	#RG240160 Origene
M858	pMCC-PER2-GFP- P	
M859	pMCC-PER2-TagRFP-H	
M574	pMCC-TagRFP-H	
M572	pMCC-GFP-P	
M862	pMCC-GAPVD1-T12-tRFP-H	Human GAPVD1, transcript variant 12
M909	pMCC-GAPVD1-T1-tRFP-H	Human GAPVD1, transcript variant 1
M969	pMCC-GAPVD1-T1 ΔVPS9-tRFP-H	1-1260 Δ 1261- 1478
M968	pMCC-GAPVD1-ΔVPS9Δ H2ΔB-tRFP-H	1-1113 Δ1114-1478
M896	pMCC-GAPVD1- M1-tRFP-H	1-690 Δ 691-1478
M910	pMCC- GAPVD1- M2-tRFP-H	679-1478 Δ1-678
M913	pMCC-GAPVD1-M3-tRFP-H	1-360 + 1367-1478 Δ 361-1366
M914	pMCC- GAPVD1-M4-tRFP-H	354-1372 Δ 1-353 Δ 1374-1478
M920	pMCC- GAPVD1-M2 ΔVPS9-tRFP-H	679-1260 Δ1-678 Δ 1261- 1478
M921	pMCC- GAPVD1-M2 ΔVPS9 ΔH2-tRFP-H	679-1192 Δ1-678 Δ 1193-1478
M922	pMCC- GAPVD1-M2 ΔVPS9ΔH2ΔB -tRFP-H	679-1113 Δ1-678 Δ1114-1478
M924	pMCC-GAPVD1-M2Δ C1ΔVPS9-tRFP-H	782-1260
M923	pMCC-GAPVD1-M2ΔC2ΔVPS9-tRFP-H	977-1260

Number	Name	Description
M925	pMCC-GAPVD1-M2 ΔIDR ΔVPS9-tRFP-H	1098-1260
M919	pMCC-GAPVD1-T1 Δ H1 tRFP-H	60-1478 Δ1-59
M941	pMCC-GAPVD1- T1 ΔH1ΔH2B-tRFP-H	60-1113 + 1261-1478 Δ1-59 Δ1114-1260
M936	pMCC-GAPVD1-T1 Δ H2B tRFP-H	1-1113 + 1261-1478 Δ1114-1260
M948	pMCC-GAPVD1-T1 Δ H1 Δ B-tRFP-H	60-1113 + 1193-1478 Δ1-59 Δ1193-1260
M947	pMCC-GAPVD1-T1 ΔB-tRFP-H	1-1113 + 1193-1478 Δ1193-1260
M942	pMCC-GAPVD1- M1 Δ H1-tRFP-H	60-690
M949	pMCC-GAPVD1-M2 Δ B-tRFP-H	679- 1113 + 1193-1478
M950	pMCC-GAPVD1- M2 Δ H2B-tRFP-H	679- 1113 + 1261-1478

2.3.2. Expression of tricistronic vectors

To simultaneously express three independent genes in mammalian cells, tricistronic expression vectors were used (Mielke et al., 2000). The tricistronic plasmid incorporates two IRES elements in a three-gene element, the first cistron tagged with TagRFP, the second cistron tagged with GFP and the third cistron the resistance gene. This arrangement ensures efficient transcription of all three cistrons (coding regions) within the vector's single mRNA transcript (Figure 7).

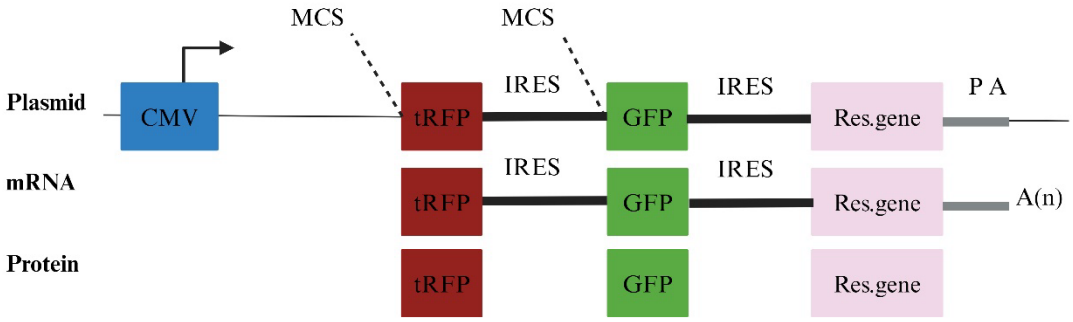

Figure 7. A schematic representation of the *tricistronic plasmid. Upper: The plasmid contains the CMV promotor (blue box), the multiple cloning site (MCS) followed by tRFP (red box), an IRES element (thick black bar), a second multiple cloning site (MCS) followed by GFP, a second IRES element (thick black bar), Resistance gene (pink box), and SV40 P(A) site (thick grey bar). The translation of the first cistron (first protein of interest and the tRFP) on the mRNA is mediated by CAP dependent translation, the translation of the second cistron (second protein of interest and the GFP) and the third cistron are cap-independent, i.e IRES.*

Table 7: Tricistronic plasmids used in cloning and for the transfection of HT1080 and HEK293T cells.

Number	Plasmid name
M873	pMCC-CSNK1d-tRFP-hPer2-EGFP-P

2.4. cDNA

GAPVD1 transcript 12 was generously provided by Professor Elizabeth Smythe (UK) and the vector with GAPVD1 transcript 1 was bought from Origene (product number RC240160#). MluI/ApaI restriction sites were inserted into GAPVD1 by means of linker PCR, facilitating its cloning in the basic construct. Starting from section 4.4 in the results, GAPVD1 transcript 1 (ENSEMBL) was used in the experiments.

2.5. DNA oligonucleotides and siRNAs

All nucleotides used for PCR amplification, oligohybridization, and DNA sequencing were obtained in HPLC grade from either Biomers (Ulm, Germany) or IBA (Göttingen, Germany).

2.5.1. For convenience, the oligonucleotides used for PCR as part of the cloning process are listed in Section 3.4.9.

Table 8: Oligonucleotides used for PCR as a part of cloning.

Name	Sequence
5’ MluI-Primer	ACGCGTCCATGGTGAAACTAGATATTCATACT
3’ Apa-Primer	GGGCCCCTTTCGGTCATCGATGGTTTTAATGAA

2.5.2. Q.PCR Primer

Table 9: Oligonucleotides used for qPCR.

Name	Sequence
CSNK1D	5’ GAAGGATTAGCGAGAAG 3’ TACGAGTAGTCAGGCCTTGT
CSNK1E	5’ ATCTACCCTGAGTGCCAAACAT 3’ GATCCCCACGCCACCCT
PER1	5’ CCCAGCACACTAAGCGTAAA 3’ TGCTGACGGCCGGATCTTT
PER2	5’ AGAGTCCAGATACCTTTAGC 3’ GACCTTCAGCTCCTTTAG T
GAPVD1	5’ GCTTGCTCTTTGCTCTGCG 3’ TCTTCTGGGTCTGTGTGGTCT
GAPDH	5’ TCCATGACAACTTTGGTATCG 3’ CAGTCTTCTGGG TGGCAGTGA
B actin	5’ CGCGAGAAGATGACCCAGATC 3’ CACAGCCTGGATAGCAACGT

2.5.3. Oligonucleotides used for siRNA transfection.

Table 10: Oligonucleotides used for siRNA transfection.

Name	Sequence
CSNK1D	(L-003478-01-0005, Dharmacon), Lafayette, CO, USA)
CSNK1E	(L-003479-00-0005, Dharmacon)
PER1	(L-003479-00-0005, Dharmacon)
PER2	(L-003479-00-0005, Dharmacon)
non-target (nt)	(D-001810-10-05, Dharmacon)

2.6. Chemicals

2.6.1. Chemicals for cell treatement

2.6.1.1. Dexamethasone

Dexamethasone (CAS No: 50-02-2) is a synthetic pregnane corticosteroid and derivative of cortisol (hydrocortisone) and well known to synchronize clocks in mammalian cells (Feillet et al., 2014). A 10 mM stock solution followed by 100 µM stock solution of Dexamethasone (D4902, Sigma) was prepared and stored at -20°C until further use.

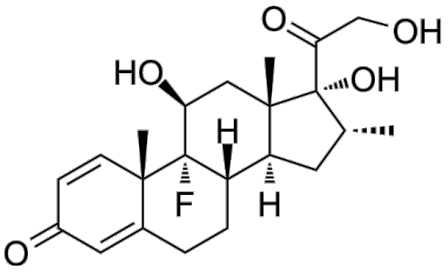

Figure 8. Chemical Structure of Dexamethasone.

2.6.1.2. PF670462

PF670462 dihydrochloride (CAS No: 950912-80-8) is a potent and selective inhibitor of CSNK1D/E, with IC50s of 7.7 nM and 14 nM, respectively (Badura et al., 2007; Janovska et al., 2018). A 4 mM stock solution of PF670462 (SML0795, Sigma) was prepared and stored at 4°C until further use.

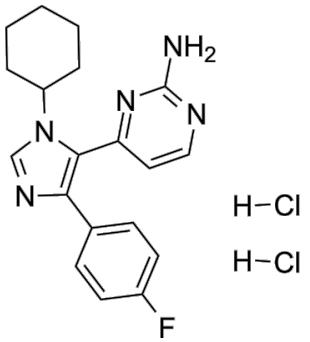

Figure 9. Chemical Structure of PF670462.

2.6.2. Other chemicals

Table 11: Chemicals used in experiments.

Name	Manufacturer
Agarose	Sigma, St. Louis, USA
Ammonium peroxodisulfate (APS)	Roth, Karlsruhe, Germany
Bromophenol blue	Merck, Darmstadt, Germany
cOmplete Tablets EDTA-free, *EASY pack* (Protease Inhibitor Cocktail Tablets)	Roche Diagnostics, Basel, Switzerland
dH2O	Merck, Darmstadt, Germany
Dithiothreitol (DTT)	Applichem, Darmstadt, Germany
Dimethyl sulfoxide (DMSO)	Sigma, St. Louis, USA
Ethanol	Merck, Darmstadt, Germany
Ethylenediaminetetraacetic acid (EDTA)	Sigma, St. Louis, USA
Glycerol	Merck, Darmstadt, Germany
Glycine	Roth, Karlsruhe, Germany
Hydrochloric acid	Merck, Darmstadt, Germany
IGEPAL® CA-630	Sigma, St. Louis, Germany
Isopropanol	Merck, Darmstadt, Germany
Methanol	Merck, Darmstadt, Germany
Midori-Green	Biozym Scientific, Hessisch Oldendorf, Germany
PhosStop EASYpack (Phosphatase Inhibitor Cocktail Tablets)	Roche Diagnostics, Basel, Switzerland
Polyacrylamide Rotiphorese® Gel 30	Roth, Karlsruhe, Germany
Sodium chloride	VWR International, West Chester, USA
Sodium dodecyl sulfate (SDS)	Roth, Karlsruhe, Germany
TEMED	Roth, Karlsruhe, Germany
Tris	Roth, Karlsruhe, Germany
Triton X-100	Sigma, St. Louis, USA
Tween20	Sigma, St. Louis, USA

2.7. Buffer and Stock Solutions

Table 12: Buffers used for experiments.

Name	Composition or Manufacturer
5x Laemmli buffer	156.25 mM Tris/HCl pH 6, 25% glycerol, 5% SDS, 50 mM DTT, bromophenol blue
1x Laemmli buffer	200 µl 5x Laemmli buffer, 100 µl 10% SDS, 10 µl DTT, 10 µl pefa, 680 µl PBS
10x TGS buffer (Tris-glycine-SDS)	0.25 M Tris, 1.92 M glycine, 1% SDS
Sensitive Coomassie staining	5% Aluminiumsulfat (Al2(SO4)3 x (H2O x, x= 14-18), 10% Ethanol, 0.02%), Coomassie Brilliant Blue G250 2.3% Phosphoric acid 85%.

Name	Composition or Manufacturer
Fixation buffer for protein on gel	30% EtoH, 2% (w/v) (Phosphoric acid 85%)
Transfer buffer for western blot A1	0.3 M TrisCl pH 10.4, 20% methanol
Transfer buffer for western blot A2	25 mM TrisCl pH 10.4, 10% methanol
Transfer buffer for western blot K	70 mM CAPS/NaOH pH 10.5
10x TBS (Tris-buffered saline)	1.5 M NaCl, 0.2 M Tris
TBS-T	100 mL 10x TBS, 899 mL H_2O, 1 mL Tween20 (0.1%)
Triton x-100 lysis buffer	150 mM NaCl, 50 mM Tris pH 8.0, 1% Triton X-100, 1x EDTA Free - PI, 1x PhosStop - PS
High salt washing buffer	500 mM NaCl, 50 mM Tris pH 8.0, 1% IGEPAL® CA-630, 1x EDTA Free - PI, 1x PhosStop - PS
Law salt washing buffer	50 mM Tris pH 8.0, 1% IGEPAL® CA-630, 1x EDTA Free - PI, 1x PhosStop - PS
Elution buffer for IP	50 mM Tris pH 6.8, 50 mM DTT, 1% SDS, 10% Glycerol, 1x EDTA Free - PI, 1x PhosStop - PS, 0.005% bromophenol blue
CHAPS lysis buffer	20 mM Tris.HCl, pH 7.5, 150 mM NaCl, mM EDTA pH 8.0, 0.03% CHAPS
CHAPS High salt washing buffer	20 mM Tris.HCl, pH 7.5, 500 mM NaCl, mM EDTA pH 8.0, 0.03% CHAPS
Elution buffer A	50 mM Tris HCl pH7.5, 0.1 mM EGTA
50x TAE buffer (Tris-acetate-EDTA)	2 M Tris-acetate, 0.05 M EDTA (pH 8.3)
6x DNA loading buffer	10 mM Tris-HCl (pH 7.6), 0.03% bromophenol blue, 0.03% xylene cyanol FF, 60% glycerol, 60 mM EDTA
Phosphate-buffer	0.17 M KH2PO4, 0.72 M K2HPO4
EB buffer	10 mM Tris-Cl pH 8.5
10x NEBuffer™ 2	New England Biolabs, Frankfurt a. M., Germany
10x NEBuffer™ 3.1	New England Biolabs, Frankfurt a. M., Germany
10x buffer Tango (DNA-restriction)	Thermo Scientific, Nürnbrecht, Germany
10x buffer Fast Digest (DNA-restriction)	Fermentas, St. Leon-Roth, Germany
2x Quick Ligase buffer	New England Biolabs, Frankfurt a. M., Germany

2.8. Antibodies

2.8.1. Primary antibodies

Table 13: Primary antibodies used for protein detection on western blot membranes.

Antibody	Antigen	Origin	Dilution for western blot	Manufacturer
Anti-CSNK1D	CSNK1D	Mouse	1:2000	#AB85320, clone #AF12G4, Abcam, UK
Anti-CSNK1D	CSNK1D	Mouse	1:1000	#CBMAB-C11246-LY, Creative biolabs, USA
Anti-JL-8	JL-8 (GFP)	Mouse	1:3000	#632381, Clontech, Mountain View, USA
Anti-PER2	PER2	Rabbit	1:500	#20359-1-AP, Proteintech, USA
Anti-RAP6	GAPVD1 /RAP6	Rabbit	1:1000	#NBP1-19156 Novus Biologicals, USA
Anti-tRFP	tagRFP	Rabbit	For IP	#AB233, Evrogen, Russia
TagRFP Polyclonal Antibody	TagRFP	Rabbit	For IP	R10367, Thermo Fisher Scientific, USA
TagRFP monoclonal Antibody	TagRFP	Mouse	1:1000	MA5-15257 Thermo Fisher Scientific, USA

2.8.2. Secondary antibodies

Table 14: Secondary antibodies used for protein detection on western blot membranes.

Antibody	Antigen	Origin	Dilution for western blot	Manufacturer
Anti-mouse HRP coupled	Mouse antibody	Sheep	1:40000	Amersham, Little Chalfont, England
Anti-rabbit HRP coupled	Rabbit antibody	Donkey	1:10000	GE Healthcare, Chalfont St. Giles, UK

2.9. Enzymes

Table 15: Enzymes used for DNA restriction in cloning.

Enzymes	Manufacturer
ApaI	Thermo Scientific, Rockford, USA
ApaI (FastDigest)	Fermentas, St. Leon-Roth, Germany
BglII (FastDigest)	Fermentas, St. Leon-Roth, Germany
EcoRI (FastDigest)	Fermentas, St. Leon-Roth, Germany
MluI	New England Biolabs, Frankfurt a. M., Germany
MluI	Thermo Scientific, Rockford, USA
MluI (FastDigest)	Fermentas, St. Leon-Roth, Germany
PciI (BsplU11I)	New England Biolabs, Frankfurt a. M., Germany

Enzymes	Manufacturer
SalI (FastDigest)	Fermentas, St. Leon-Roth, Germany
SpeI	New England Biolabs, Frankfurt a. M., Germany
SpeI (FastDigest)	Fermentas, St. Leon-Roth, Germany

2.10. Proteins

Table 16: Further proteins used for experiments.

Protein	Manufacturer
Bovine serum albumin	Sigma, St. Louis, USA
Skim milk	Roth, Karlsruhe, Germany
µMACS Protein A/G MicroBeads	Miltenyi Biotec, Bergisch Gladbach, Germany

2.11. Kits

Table 17: Kits used for experiments.

Kit	Manufacturer
Effectene Transfection Kit	Qiagen, Hilden, Germany
MyTaq™ Red DNA Polymerase	BioCat GmbH, Heidelberg, Germany
Pierce™ BCA Protein Assay Kit	Thermo Scientific, Rockford, USA
Pierce™ ECL Plus Western Blotting Substrate	Thermo Scientific, Rockford, USA
Q5® Hot Start High-Fidelity 2X Master Mix	New England Biolabs, Frankfurt a. M., Germany
QIAfilter Plasmid Maxi Kit	Qiagen, Hilden, Germany
QIAprep Spin Miniprep Kit	Qiagen, Hilden, Germany
QIAquick Gel Extraction Kit	Qiagen, Hilden, Germany
Quick Ligation Kit	New England Biolabs, Frankfurt a. M., Germany
TOPO TA Cloning Kit	Gibco/Invitrogen, Carlsbad, USA
QIAshredder	74104 Qiagen, Hilden, Germany
RNeasy Mini Kit	79656 Qiagen, Hilden, Germany
QuantiTect SYBR Green RT-PCR Kit	204243 Qiagen, Hilden, Germany
Transformation Kit & Buffer Set	Zymo research, California, USA

2.12. Other Materials

Table 18: Other Materials

Name	Manufacturer
15 mL BD Falcon Tube	BD Biosciences, Franklin Lakes, USA
50 mL BD Falcon Tube	BD Biosciences, Franklin Lakes, USA
Cell culture flask T-25	Thermo Scientific, Nürnbrecht, Germany
Cell culture flask T-75	Thermo Scientific, Nürnbrecht, Germany
Cell culture flask T-175	Thermo Scientific, Nürnbrecht, Germany
Color Prestained Protein Standard, Broad Range	New England Biolabs, Frankfurt a. M., Germany
Corning® Costar® Stripette®	Corning Incorporated, Corning, New York, USA
Invitrogen™ 1 Kb Plus DNA Ladder	Invitrogen, Carlsbad, USA
µ Columns	Miltenyi Biotec, Bergisch Gladbach, Germany
µ-slide 8 well	Ibidi, Martinsried, Germany
Novex® gel cassette	Invitrogen, Carlsbad, USA
Nunc™ MicroWell™ 96-Well Microplate	Thermo Scientific, Nürnbrecht, Germany
Parafilm	Pechiney Plastic Packaging, Chicago, USA
PVDF transfer membrane	Millipore, Bedford, USA
Tubes 5 mL, 75x13 mm, PS	Sarstedt, Nümbrecht, Germany
Whatman filter paper	GEHealthcare, Buckinghamshire, England

2.13. Equipment

Table 19: Devices

Device	Manufacturer
Autoclave VX-150	Systec, Wettenberg, Germany
Centrifuge 5417R	Eppendorf, Hamburg, Germany
Centrifuge 5418	Eppendorf, Hamburg, Germany
Centrifuge Avanti J-30I	Beckman-Coulter GmbH, Krefeld, Germany
Centrifuge Heraeus™ Fresco 17	Thermo Scientific, Nürnbrecht, Germany
Centrifuge Rotixa 50 RS	Hettich, Tuttlingen, Germany
ChemoStar PC ECL & Fluorescence Imager	INTAS Science Imaging Instruments, Göttingen, Germany
CO_2-incubator Hera Cell	Heraeus, Hanau, Germany
Countess®-Cell-Counter	Invitrogen, Carlsbad, Germany

Device	Manufacturer
Cryo 1 °C Freezing Container	Nalge Nunc, Rochester, New York, USA
Electrophoresis Power Supply EPS 301	GEHealthcare, Buckinghamshire, UK
Heating Block MBT 250	ETG, Illmenau, Germany
Heating block ThermoStat plus	Eppendorf, Hamburg, Germany
Horizon® 11-14 Horizontal Gel Electrophoresis System	Thermo Scientific, Nürnbrecht, Germany
Luminescent image analyzer LAS-4000	Fujifilm, Tokyo, Japan
Microscope Wilovert S	Hund, Wetzlar, Germany
Nutating mixer	VWR International
µMACS™ Separator	Miltenyi Biotec, Bergisch Gladbach, Germany
pH-Meter Climatic 766	Knick, Berlin, Germany
Pipetting aid pipetus®	Hirschmann Laborgeräte, Eberstadt, Germany
Precision scales AE 166	Mettler Toledo, Giessen, Germany
Rotator SB2	Cole-Parmer Stuart, Staffordshire, UK
Shaker WT16	Biometra, Göttingen, Germany
Sonotrode SH-70G	Bandelin, Berlin, Germany
Spectrophotometer Epoch	BioTek, Berlin, Germany
Trans-Blot® SD Semi-Dry Transfer Cell	Bio-Rad Laboratories, Hercules, USA
Ultrasound Homogenizer Sonopuls	Bandelin, Berlin, Germany
Vortex Genie 2	Scientific Industries, Inc., New York, USA
Water bath WB20	Medingen, Dresden, Germany
X CellSureLock™ Mini-Cell Electrophoresis System	Invitrogen, Carlsbad, Germany
Epifluorescent Inverse Microscope Axiovert 100	Carl Zeiss, Göttingen, Germany
Lightcycler® 480 II	Roche Diagnostics, Basel, Switzerland

2.14. Software

Table 20: Software used for planning and analysis

Name	Manufacturer
ApE	M. Wayne Davis
ChemoStar	INTAS Science Imaging Instruments, Göttingen, Germany
Gen5™	BioTek, Berlin, Germany
ImageJ	Wayne Rasband

Name	**Manufacturer**
LAS4000	Fujifilm, Tokyo, Japan
MS Office	Microsoft, Redmond, USA
Multi-Gauge	GE Healthcare, Chalfont St. Giles, UK
GraphPad Prism	Insight Partners, NewYork, USA
ChimeraX	University of California San Francisco, USA
Lightcycler® 480 SW 1.5	Roche Diagnostics, Basel, Switzerland

3. Methods

3.1. Cell Culture

3.1.1. Cultivation of Cell Lines

Cells were cultured as subconfluent monolayers in its suitable medium (I, II, or III) under standard conditions of 37°C and 5% CO2 in a humidified environment. Cell passage (splitting) involved a procedure where cell layers were rinsed with phosphate-buffered saline (PBS), followed by detachment using EDTA for HEK-293 cells and Trypsin-EDTA for other cell types. Subsequently, cells were reseeded after dilution with culture medium at a ratio of 1:6. Subsequent cell splitting occurred every two to three days.

3.1.2. Freezing of cells

After reaching a certain confluently cells were trypsinized and resuspended in growth medium and centrifuged at 1200 RPM for 3 mins. The cell pellet was suspended in 7 ml of freezing medium. The cell suspension was splitted in 7 cryovials, which were then incubated in isopropanol freezing boxes at -80°C for 24 hours. Cryovials were then transferred to a liquid nitrogen tank.

3.1.3. Thawing of cells

Frozen cells were thawed rapidly in a 37°C water bath, and then transferred to a falcon tube with 5 ml pre-warmed (37°C) culture medium. Cells were centrifuged at 1200 RPM for 3 mins. Following centrifugation, the supernatant was carefully aspirated, and the cells resuspended in 6 ml of suitable medium (I, II, or III) in a small cell culture flask. The flask was then incubated at 37°C in a humidified atmosphere with 5% CO2 for further growth and expansion. In the following day, the cells were examined under a microscope to assess their viability, morphology and density. Based on the results of these evaluations, further steps such as passaging or experimental treatments might have been carried out to continue the cell culture process or perform specific experiments.

3.1.4. Cell Transfection

3.1.4.1. siRNA transfection

Cells were harvested from cell culture flasks, and 10^5 cells were seeded onto 6-well plates one day prior to siRNA transfection. 100 nM for each siRNA targeting CSNK1D, CSNK1E, PER1, PER2, or a non-target (nt) control siRNA were mixed with DharmaFECT 1 Transfection Reagent following the manufacturer’s protocol. Cells were harvested for mRNA analysis by quantitative polymerase chain reaction (qPCR) after 48 hours or for protein analysis by Western blotting after 72 hours.

3.1.4.2. Plasmid transfection

Cells were harvested from a T175 cell culture flask and split at a 1:8 ratio 24 hours before transfection. Transfection was carried out using 5 µg DNA for single pasmid transfections and 10 µg DNA for double transfections using Effectene transfection reagent according to the manufacturer's instructions. The efficacy of transient expression varied between 20-90% depending on the construct used and could be estimated under the microscope after 12-24 hours

of transfection. 24 hours post-transfection, the media containing Effectene reagent was substituted with growth medium. The cells were harvested after 48 hours and frozen at -80°C for later use. For stable transfection, cells were harvested and plated onto tissue culture dishes, followed by the selection of stable cell clones using appropriate growth medium (II or III). Subsequently, the chosen clones were expanded and cultured in the respective suitable growth medium (II or III) for maintenance.

3.1.5. Cell Synchronization

(2.5 × 10^6) U2OS cells were seeded onto T175 flasks 48 hours prior to the dexamethasone shock. Cell synchronization was achieved by treating cells with 100 nM dexamethasone for 30 minutes at 37°C. Cells were then harvested at specific time points post-dexamethasone treatment, including 26, 30, 34, 38, 42, and 46 hours, for further analysis. The harvested cells pellet was kept at -80 C until further use.

3.1.6. Cell treatment with PF670462

Cells were seeded onto T175 flasks or onto 6 wells plate 24 hour prior to the PF PF670462 treatment. Cells were then treated with either control PBS (mock) or 20nM, 200nM, 2µM or 20µM of PF670462 for 18 hrs at 37°C. Cells were then harvested for further analysis. The harvested cells pellet was kept at -80 C until further use.

3.1.7. Harvesting of Cells

To harvest cells, cells were rinsed with PBS, followed by detachment using EDTA for HEK-293 cells and Trypsin-EDTA for other cell types. Subsequently, the cells were resuspended in fresh medium, transferred to a 15 mL Falcon tube, and centrifuged for 3 minutes at 1200 rpm. Following centrifugation, the supernatant was discarded, the cell pellet rinsed once with 15 ml PBS. After washing, the sample was again centrifuged for 3 minutes at 1200 rpm, and cell pellets were stored at -80 °C until further use.

Cell pellets intended for immunoprecipitation (IP) were resuspended in either 2 mL Triton X-100 lysis buffer or CHAPS lysis buffer, sonicated twice for 10 seconds at 20% power, and then placed on ice. Subsequently, the samples were stored at -20°C for later use in Western blotting or at -80°C for later use in real time PCR analysis.

Cells in cell pellets designated for western blot analysis were counted, and for every 10^6 cells, 100 µl of Laemmli buffer was added. The mixture was homogenized by ultrasound for 15 seconds at 20% power. Subsequently, the samples were stored at -20°C for later use in Western blotting.

3.2. Protein analysis

3.2.1 Quantification of total protein concentration

Initially, a standard curve was established utilizing bovine serum albumin (BSA) as the protein standard. BSA standards were prepared by diluting a 2 mg/mL BSA stock solution with water, resulting in concentrations of 2000, 1500, 1000, 750, 500, 250, 125, and 0 µg/mL. Subsequently, a working reagent was formulated by combining Pierce ™ BCA Reagent A and B at a ratio of 50:1, respectively. This working reagent was then added to each sample, BSA standard, and blank (comprising lysis buffer alone) in a 1:50 ratio. Following this, the samples underwent a 30-minute incubation at 37°C to enable the protein in the samples to reduce the copper ions within the working reagent, thus forming a purple-colored complex. Post-incubation, the absorbance of each sample was measured at 562 nm employing a spectrophotometer. Subsequently, the protein concentration of each sample was determined based on the absorbance values and the standard curve, utilizing the following formula.

$$\text{Protein concentration } (\mu g/mL) = \frac{(\text{Absorbance sample} - \text{Absorbance blank})}{(\text{Absorbance standard} - \text{Absorbance blank})} x \text{ Standard concentration}$$

The determined protein concentration of each sample was subsequently used to ensure an equal amount of proteins for subsequent applications, including immunoprecipitation (IP) or mass spectrometry analysis.

3.2.2. Immunoprecipitation

3.2.2.1. Affinity enrichment of GFP fusion protein using GFP nanobodies coupled to agarose beads

Cells were washed twice with 1X PBS and collected by centrifugation at 1300 RPM for 3 minutes. The supernatant was discarded, and the cells were frozen at -80°C. Upon thawing, the cells were lysed by adding 2 mL of freshly prepared ice-cold CHAPS lysis buffer. The lysate was incubated on ice for 30 minutes with vortexing every 10 minutes. Then, the lysate was centrifuged at maximum speed for 30 minutes, and the lysate supernatant was transferred to a new pre-cooled tube. Protein concentrations for each sample were determined using the PierceTM BCA Protein Assay Kit according to the manufacturer's instructions.

Protein purification was performed using GFP nanobodies coupled to agarose beads. First, the beads were equilibrated by resuspending 25 µL beads in 500 µL ice-cold lysis buffer and centrifuging at 1300 RPM for 2 minutes at +4°C. The supernatant was discarded, and the beads were washed two more times with 500 µL ice-cold lysis buffer. The volume of the lysate-supernatant was adjusted to 100-500 µL and incubated with the washed beads overnight at 4°C with rotation.

The next day, the beads were centrifuged at 1300 RPM for 2 minutes at +4°C. The beads were washed three times with 1 mL lysis buffer and an additional three times with 1 mL high salt buffer. Washing was performed by centrifuging at 1300 RPM for 5 minutes at +4°C, discarding the supernatant, and adding new buffer.

Subsequently, the beads were resuspended in 60 µL Laemmli sample buffer (1X), and the samples were heated for 5 minutes at 95°C. The samples were then ready for western blotting or stored at -20°C. Alternatively, the beads could be resuspended in 60 µL elution buffer A, and

a small aliquot of 5 µL was taken for western blotting (usually enough for 3 blots), while the rest (55 µL) was stored at -20°C or analysed by mass spectrometry.

3.2.2.2. Immunoprecipitation of proteins using magnetic microbeads

Cells were washed twice with 1X PBS and collected by centrifugation at 1300 RPM for 3 minutes. The supernatant was discarded, and the cells were frozen at -80°C. Upon thawing, the cells were lysed by adding 2 mL of freshly prepared ice-cold Triton X-100 lysis buffer. The lysate was incubated on ice for 30 minutes with vortexing every 10 minutes. Then, the lysate was centrifuged at maximum speed for 30 minutes, and the lysate supernatant was transferred to a new pre-cooled tube. Protein concentrations for each sample were determined using the Pierce™ BCA Protein Assay Kit according to the manufacturer's instructions.

A total of 4 mg protein was used for the immunoprecipitation of the protein of interest, and volumes were adjusted to 4 mL and incubated with either 100 µl protein A and 4 µg tRFP or GAPVD1 antibodies, or 100 µl protein G and 4 µg CSNK1D antibodies. Samples were then incubated overnight at 4°C with rotation.

The following day, immunoprecipitation was performed from the lysates with µ columns and a MACS® separator. Columns were washed 4 times with 200 µl high salt washing buffer followed by 1 time 100 µl low salt washing buffer. Samples were then incubated with 20 µl of previously heated at 95°C 1x Laemmli buffer for 5 minutes followed by elution with 70 µl of previously heated at 95°C 1x Laemmli buffer. The eluted samples were stored at -20°C until further use.

3.2.3. Protein electrophoresis and detection

3.2.3.1. Sodium Dodecyl Sulfate Polyacrylamide Gel Electrophoresis (SDS-PAGE)

SDS-PAGE is utilized to separate proteins according to their molecular weight. The amount of polyacrylamide in the separating gel was determined based on the protein of interest. Separating gels with 12%, 10%, and 10% polyacrylamide were used for CSNK1D, PER2, and GAPVD1, respectively. The gel was cast into a Novex® gel cassette, and a 4% stacking gel was layered on top after polymerization. The gel cassette was placed in the XCell SureLock Mini-Cell Electrophoresis System and filled with 1x tris-glycine-SDS (TGS) buffer. Before loading the cell lysates, the samples were heated for 5 minutes at 95°C. The Color Prestained Protein Standard, Broad Range, was also loaded as a marker. Gel electrophoresis was conducted at 60 V until the sample reached the border between the stacking and separating gel, after which the voltage was increased to 130 V.

3.2.3.2. Sensitive Coomassie Staining

The Coomassie staining method is commonly used to detect and visualize proteins in polyacrylamide gels. The Sensitive Coomassie Staining Protocol used in this study was adapted from (Kang et al., 2002). The gel was washed three times for 10 minutes each with ddH2O to remove any unpolymerized acrylamide, urea, or any other contaminants. Optionally, the proteins in the gel were fixed by incubation in fixation buffer for 30 minutes. The gel was then incubated with the Coomassie staining solution overnight on a shaker, and the stain could be seen on the gel within two hours without background. To increase contrast, the gel was washed with ddH2O. Target bands were cut using sterile scissors and handled later by the Mass

Spectrometry Facility, Molecular Proteomics Laboratory (MPL), Biologisch-Medizinisches Forschungszentrum (BMFZ) at Heinrich Heine University.

3.2.3.3. Western Blot

Proteins separated by SDS-PAGE were transferred from the gel to a polyvinylidene fluoride (PVDF) membrane through electrophoretic transfer using the semi-dry method. Membranes were first activated by equilibrating in methanol for 1 minute followed by washing in distilled water (dH2O) for 2 minutes and placed in transfer buffer. After removing the gel cassette, the gel was equilibrated in transfer buffer K as well. The anode side of the semi-dry device was layered with two 3MM paper filters soaked in A1-buffer followed by one 3MM paper filter soaked in A2-buffer. On top of that, an activated PVDF membrane soaked in A2 buffer was placed followed by the previously soaked gel in K-buffer. Finally, towards the cathode side, five 3MM paper filters soaked in K-buffer were placed. The stack was then sandwiched between two graphite plates, and the protein transfer was performed at 0.8 mA/cm2 for 1-4 hours, depending on the size of the protein. Specifically, 300 V, 100 mA, and 45 or 38 or 25 minutes were used for GAPVD1, PER2, CSNK1D, respectively.

After transfer, the PVDF membrane was incubated overnight at 4°C in 20 mL 5% skim milk in TBST for blocking nonspecific proteins. Next, the membrane was washed with TBST containing 0.05% Tween 20 and incubated for 2 hours with the primary antibody diluted in 5% BSA, followed by three washes (3 x 10 minutes). Subsequently, the membrane was incubated for 1 hour with the secondary peroxidase-conjugated antibody diluted in 5% BSA in TBST and then washed again (3 x 10 minutes) in TBST. Finally, the protein bands were visualized using the ECL Plus system through chemiluminescence. Band intensities were then analyzed with the Luminescent image analyzer LAS4000. Data were plotted on a bar graph and analyzed for significance using the computer software Prism.

3.2.3.4. Protein Detection by Chemiluminescence

The PierceTM ECL plus Western Blotting Substrate Kit was employed according to the manufacturer's guidelines. It provides the substrate for the horseradish peroxidase (HRP) linked to the secondary antibody to detect bound antibodies on the membrane. The HRP in conjunction with peroxide and the substrate generates chemiluminescence, which was captured by the ImageQuant LAS-4000 imaging system.

3.3. RNA analysis

3.3.1. Primer design

Primers for quantitative PCR were designed as instructed in (Thornton and Basu, 2011) with the Primer3 Software V.0.4.0 (Untergasser et al., 2012) and the primers were then checked for their secondary structure using Beacon Designer™ Free Edition. Amplicon secondary structure was checked using mFOLD software (Zuker, 2003). Specificity of the primers was checked using NCBI blast. Primers were then dissolved in mQ H_2O and stored in -20°C.

Primers/oligonucleotides for conventional PCR or for cloning were designed using APE software. Primers were then dissolved in mQ H_2O and stored in -20°C.

3.3.2. RNA extraction

Frozen cell pellets were disrupted in buffer RLT and homogenized with QIAshredder (Germany) which uses a unique biopolymer-shredding system in a microcentrifuge spin-column format. The total RNA was then extracted with the commercially available RNeasy Mini Kit (Germany) which ensures efficient rapid purification of high-quality RNA from varying quantities of cells through the utilization of silica membrane RNeasy spin columns. Cell pellet homogenization and RNA extraction were performed according to the manfucturer's instructions. The RNA was eluted with 50 µl of RNAease free water and the concentration was determined spectrophotometrically. The samples were first dilueted to 50 ng/µl and then to 0.5 ng/µl. Samples were then stored at -80°C until further use.

3.3.3. One step-quantitative-real time PCR

With this method cDNA reverse transcription from mRNA and quantification can be performed in a single tube. 5 ng of RNA were used for each sample with 0.5 µM primers. Reactions were prepared on ice with the QuantiTect SYBR Green RT-PCR Kit (Qiagen, Germany) in a total volume of 25 µl as stated below.

Reaction Components	µl
2x SYBRGREEN Master Mix	12,5
F Primer 100µM	0,125
R Primer 100µM	0,125
RT Mix	0,25
H20	2
RNA (5 ng)	10
Reaction Volume	25

For each sample, two technical replicates were made, and two control genes were analysed in all experiments, GAPDH and beta-actin. The experiments were carried out in 96 well plates which were loaded into the real time PCR machine (Lightcycler® 480 SW 1.5) and the following cycle conditions were used:

Step		Time	Temperature
Reverse transcription		30 min	50°C
PCR initial activation step		10 min	95°C
40 cycls	Denaturation	20 s	94°C
	Annealing	20 s	57°C with Data acquisition
	Extension	30 s	72°C
		4 min	40°C

3.3.4. Data acquisition and analysis

Abolute quantification and fit point analysis for all samples were calculated using the built in software absolute quantification/fit points for All Samples. The analysis yielded cDNA crossing points (CP) values. The ΔΔCP method (Giulietti et al., 2001) was used to calculate the average CP for each gene and then substract that from the total average CP of all control genes.

$$\Delta CP \text{ (target gene)} = \Delta CP \text{ (target gene)} - \Delta CP \text{ (house keeping genes)}$$

ΔΔCP values were then calculated using the following formula (Livak and Schmittgen, 2001).

$$(\Delta\Delta CP = 2^{(-\Delta CP)}).$$

The ΔΔCP values in the non-target siRNA (NT) control were set to 1. All other samples were then normalized to this reference value before plotting with Prism software.

3.4. Cloning

3.4.1. Polymerase chain reaction (PCR)

3.4.1.1. Primer design

Primers/oligonucleotides for conventional PCR or for cloning were designed using APE software. Primers were then dissolved in mQ H_2O and stored in -20°C.

3.4.1.2. Oligonucleotide hybdrization

Single-stranded oligonucleotides (oligos) were annealed for downstream applications. Briefly, oligos were resuspended in H_2O or TE buffer to 100 µM, mixed in equal volumes (e.g., 5 µl each at 5 pmol/µl) with additional TE buffer and 50 mM NaCl to reach the desired final volume of 100 µl. The mixture was then incubated at 72°C for 20 minutes followed by slow cooling to room temperature over at least 60 minutes. The annealed oligos were further diluted 1:250 in TE buffer (to 20 fmol/µl) and stored at -20°C.

3.4.1.3. Conventional PCR

Polymerase chain reaction (PCR) is a method used for the amplification of a specific part of a template DNA. The part of the DNA that needs to be amplified is marked by two primers that complementary bind to the 3' ends of the DNA sequence. PCR was performed using either MyTaqTM HS DNA Polymerase or Q5® Hot Start High-Fidelity 2x Master Mix. The following PCR cycle protocol was used:

Steps		tim	Temp
Initial Denaturation		2'	96°C
22 cycles	Denaturation	30''	94°C
	Anealing	30''	55°C
	Elongation	1-3	72°C
Final elongation		12'	72°C

3.4.1.4 Overlap extension PCR

The Overlap Extension method was employed in this study to create chimeric DNA constructs. The first step involved the design of primers that allowed for the amplification of the two DNA fragments to be joined. The amplification reaction was carried out using high-fidelity Taq polymerase under standard conditions (Q5® Hot Start High-Fidelity 2x Master Mix). The PCR products were then purified using the Qiaquick PCR purification Kit according to the manufacturer's protocol.

Next, the purified fragments were mixed in an equimolar ratio and subjected to a second PCR reaction, termed the "fusion PCR". This reaction utilized the purified PCR products as templates to generate a single, fused product with overlapping ends. The fusion PCR reaction was carried out using MyTaqTM HS DNA Polymerase and a specific set of primers designed to anneal to the overlapping regions of the purified PCR products. Finally, the fused product were then separated by agarose gel electrophoresis.

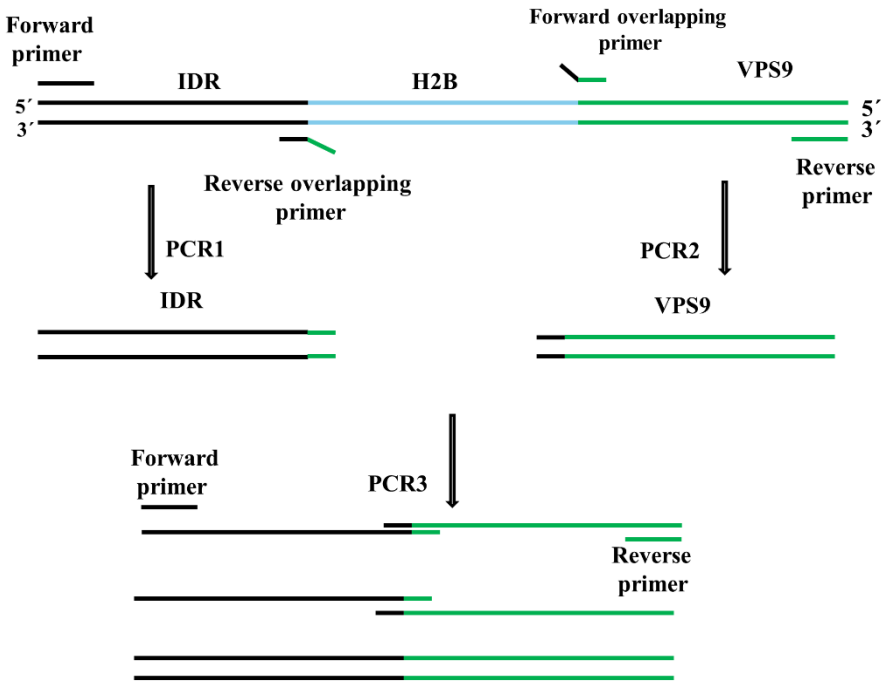

Figure 10. Overlapping PCR Primers that flank each of the functional domains of GAPVD1 (RasGAP and VPS9) were used for the first and second PCR. The products were both used as template for the third PCR with the primers flanking the whole sequence resulting in a combined product of both functional domains with deletion of the IDR

3.4.2. Restriction digestion

3.4.2.1. Preparative restriction digestion

A preparative restriction digestion technique was employed to cut DNA molecules at specific sites using restriction enzymes in order to isolate specific DNA fragments. To begin the process, 1 µg of plasmid DNA was digested with 5-10 units of a suitable restriction enzyme in the appropriate buffer at 37°C for a duration of 1 hour. The resulting DNA fragments were then separated by agarose gel electrophoresis.

3.4.2.2. Partial restriction digestion

Partial restriction digestion technique was employed to cut DNA molecules at specific sites using restriction enzymes, but with incomplete digestion, to isolate specific DNA fragments. A single cutting enzyme was used to digest 4-5 µg of plasmid DNA in a final volume of 100 µl at 37°C for 1 hour. After that, 2, 0.57, 0.163, and 0.046 units of a multi cutting enzyme were added, and the final volume was adjusted to 35 µl. The digestion process was then carried out for 15 minutes at 37°C, following which the samples were analyzed by agarose gel electrophoresis.

3.4.2.3 Analytical restriction digestion

Analytical restriction digestion technique is smiliar to a preparative restriction digestion technique, but it is used to validate the correct orientation and length of the inserted DNA fragment within the plasmid vector. For this procedure, 5µl from a plasmid DNA mini prepation (1-2 µg) was subjected to digestion with 1µL of specific FastDigest restriction enzymes (Thermoscientific) in total volume of 20 µl. A general 10X FastDigest® Green buffer was used in this reaction. Subsequently, the samples were typically incubated for 30 minutes at 37°C, and the resultant DNA fragments were analyzed by agarose gel electrophoresis.

3.4.3. Agarose Gel Electrophoresis

Agarose gel electrophoresis is a widely used technique for separating DNA fragments based on their size using an electric field. The concentration of agarose in the gel was adjusted based on the size of the DNA fragments. To prepare the gel, agarose was melted in 1x TAE buffer and cooled to 60°C, and Midrogreen was added to a final concentration of 1 µg/ml.

Prior to loading, the samples were mixed with 6x DNA loading buffer, and InvitrogenTM 1 Kb Plus DNA Ladder was used as a size marker. Gel electrophoresis was performed at 120 V for 1 hour. After the run, the separated DNA bands were visualized using either a transilluminator at 280 nm or analyzed in a ChemoStar PC ECL & Fluorescence Imager.
These techniques were reliable and effective methods for separating DNA fragments according to their size and were essential for various downstream applications, including cloning, sequencing, and genetic analysis.

3.4.4. DNA purification

The agarose gel was visualized under UV light, and the desired DNA bands were carefully excised from the gel using a disposable scalpel under 280 nm transillumination. To purify the excised DNA fragments, a gel extraction kit was used according to the manufacturer's instructions. This involved the use of a silica-based membrane and a spin column to efficiently isolate and purify the desired DNA fragments. The isolated fragments can then be used for downstream applications such as cloning, sequencing, or PCR.

3.4.5. Ligation

3.4.5.1. Ligation in PmCC vector

To facilitate the insertion of restriction fragments into vectors, the Quick Ligation kit from New England Biolabs (NEB) was employed according to the manufacturer's protocol. A molar ratio of 1 to 3 of vector to insert was utilized. During the ligation process, the restriction fragments and vector were treated with a DNA ligase enzyme to covalently join the two DNA pieces together. Typically, this reaction was performed in a final volume of 20 µl, with the reaction duration set to 10 minutes at room temperature.

Upon completion of the ligation process, the reaction mixture was transferred to ice to stop the reaction and stabilize the DNA molecules for 5 minutes. The resulting construct could then be utilized in various downstream applications, including cloning or gene expression analysis.

3.4.5.2. TA Cloning Kit with pCR2.1 Vector.

The TA Cloning Kit with pCR2.1 Vector (Figure A5) was used in this study to clone PCR products for subsequent analysis. Topo-TA cloning was carried out using the Topo® TA Cloning® Kit from Invitrogen. The kit utilizes a Taq polymerase that creates a 3’ terminal adenine overhang, which allows for direct insertion of PCR products into the pCR2.1 plasmid vector. The ligation reaction was transformed into competent DH5α *Escherichia coli* cells, and the cells were plated onto selective agar plates containing ampicillin.

3.4.6. Transformation of plasmid DNA

3.4.6.1 Generation of competent *E. coli* cells

Competent *E. coli* cells were generated according to the Mix & Go E. coli Transformation Kit & Buffer Set instruction manual (zymo research).

3.4.6.2 Transformation of E. coli

0.1 ml competent cells were combined with 5 µl of a ligation reaction mixture and kept on ice for 5 minutes. The cells were then transferred onto LB-agar plates that contained 50 µg/ml of ampicillin and incubated over night at 37°C. Resulting colonies were subjected mostly to small scale plasmid preparation.

3.4.7. Isolation of plasmid DNA

3.4.7.1. Small scale Plasmid preparation (Minipreps)

Selected colonies resulting from the transformation process were used to inoculate 2 ml TB medium containing 50 µg/ml ampicillin. This mixture was incubated at 37°C with vigorous shaking at 250 rpm for approximately 14 hours. The bacteria were pelleted by centrifugation at 10000 RPM for 30 seconds. The resulting cell pellet was subjected to Miniprep extraction according to the manfucturer's protocol and eluted with 50 µl TE buffer. Finally, 5 µl of each eluate each was used for restriction digestion assays. The DNA concentrations of correct clones were determined spectrophotometrically at 260 nm and subjected to DNA sequencing analysis.

3.4.7.2 Large scale Plasmid preparation (Maxipreps)

Single colonies of each correct clone were used to inoculate 2 ml TB medium containing 50 µg/ml of ampicillin. This pre-culture was incubated for 8 hours at 37°C with vigorous shaking at 250 rpm. The pre-culture was then used to inoculate 250 ml TB medium containing 50 µg/ml of ampicillin and incubated overnight at 37°C with vigorous shaking at 250 rpm. Subsequently, cells were harvested via centrifugation at 6000 x g and 4°C for 15 minutes. Plasmid DNA was then purified from the harvested cells using the QIAGEN Plasmid Maxi kit following the manufacturer's protocol. DNA concentrations were determined spectrophotometrically at 260 nm.

3.4.8. Sequencing of plasmids

Appropriate forward and reverse primers were designed for sequencing using the software ApE, A Plasmid Editor. Standard Sanger sequencing was performed at Biologisch-Medizinisches Forschungszentrum (BMFZ) at Heinrich-Heine-University in Düsseldorf, Germany.

3.4.9. Plasmid construction

3.4.9.1. Construction of pMCC-G- 1-1460-TagRFP-H (T1)

A. PCR

MluI/ ApaI restriction sites were inserted in GAPVD1 by means of PCR using pCDNA3-2XHAhRME-6 (a kind gift from Prof. Elizabeth Smythe (UK) as template with the following primers.

Primer	Sequence
5` MLU1 GAPVD1	ACGCGTCCATGGTGAAACTAGATATTCATACT
3' APAI GAPVD1	GGGCCCCTTTCGGTCATCGATGGTTTTAATGAA

B. Topo cloning

The resulting amplicon was then ligated to pCR™2.1-TOPO® using the topo cloning kit. The plasmid was then sequenced, and correct clones were selected to be digested with Mlul and ApaI and ligated with the Mlul and APaI digested backbone of pMCC-TagRFP-H (Figure A3).

3.4.9.2. Construction of pMCC-G- 1-690-TagRFP-H (M1)

pMC-G- 1-1460-TagRFP-H was digested by ApaI and PciI and ligated with following hybridized oligos:

Primer	**Sequence**
5` M2	CATGTTAGGCAGTTTGCTGTGCGGGCC
3` M2	CATGTTCTCTGCTGCAGCCATGGA

3.4.9.3 Construction of pMCC-G- 679-1460-TagRFP-H (M2)

pMC-G- 1-1460-TagRFP-H was digested by MluI and BspLU11I and ligated with following hybridized oligos:

Primer	**Sequence**
5` M1	CGCGTCCATGGCTGCAGCAGAGAA
3` M1	CGCACAGCAAACTGCCTAA

3.4.9.4. Construction of pMCC-G-679-1260-TagRFP-H (M2 ΔVPS9)

pMC-G- 679-1478-TagRFP-H was digested by SalI and ApaI and with following hybridized oligos:

Primer	**Sequence**
5` M2Δ VPS9	TCGACAAGGACTACAGACCACACAGGCTCACCTGGAAAGG CTATTGCAAAGAGTTTTGCGGGACAAAGAAGTGGCCAATC GATACTTTACCACTGTCTGTGTGAGATTACTGCTTGAGAGC GGGCC
3` M2 ΔVPS9	CGCTCTCAAGCAGTAATCTCACACAGACAGTGGTAAAGTA TCGATTGGCCACTTCTTTGTCCCGCAAAACTCTTTGCAATA GCCTTTCCAGGTGAGCCTGTGTGGTCTGTAGTCCTTG

3.4.9.5 Construction of pMCC-G-679-1192-TagRFP-H (M2 ΔVPS9 ΔH2)

pMC-G- 679-1478-TagRFP-H was digested by VSP1and ApaI and ligated with following hybridized oligos:

Primer	**Sequence**
5` M2ΔH2 and VPS9	TAATTTACAAGATAAGAATCTAATGGCTCAACTTCAAGAA ACAATGCGCTGTGTGTGCCGTTTTGATGGGCC
3` M2 ΔH2 and VPS9	CATCAAAACGGCACACACAGCGCATTGTTTCTTGAAGTTGA GCCATTAGATTCTTATCTTGTAAAT

3.4.9.6. Construction of pMCC-G- 679-1113-TagRFP-H (M2ΔVPS9Δ H2B)

pMC-G- 679-1478-TagRFP-H was digested by BspH1 and ApaI and ligated with following hybridized oligos:

Primer	Sequence
5` M2∆B, ∆H2 and ∆VPS9	CATGACAGAGATTTGAGTAGTAAACTTTTATATCATAGTGA TAAAGAGGTTATGGGTGATGGTGAAAGTGCACATGATTCT CCCCGTGACGAAGCACTGCAGAACATCTCGGCTGATGATCT CCCAGACTCTGCAAGCCAAGCAGCCCACCCGCAGGATTCA GGGCC
3` M2∆B, ∆H2 and ∆VPS9	CTGAATCCTGCGGGTGGGCTGCTTGGCTTGCAGAGTCTGGG AGATCATCAGCCGAGATGTTCTGCAGTGCTTCGTCACGGGG AGAATCATGTGCACTTTCACCATCACCCATAACCTCTTTAT CACTATGATATAAAAGTTTACTACTCAAATCTCTGT

3.4.9.7. Construction of pMCC-G- 782-1260-TagRFP-H (M2ΔC1ΔVPS9)

pMC-G-679-1260-TagRFP-H was digested by MluI and BGIII and ligated with following hybridized oligos:

Primer	Sequence
5` M2∆VPS9∆C1	CGCGTCCATGATTGAAGACCTGA
3` M2∆VPS9∆C1	GATCTCAGGTCTTCAATCATGGA

3.4.9.8. Construction of pMCC-G-977-1260 -TagRFP-H (M2ΔC2ΔVPS9)

pMC-G-679-1260-TagRFP-H was digested by MluI and APaI of which its insert of 1763 bp was again digested with ACII and XHOII. The result was four bands of which the 848bp band cut with ApaI and ACII was ligated with the MluI and APaI digested backbone of pMC-G-679-1260-TagRFP-H and hybridized with following hybridized oligos:

Primer	Sequence
5` M2∆C2 ∆VPS9	CGCGTCCATGTGGTGGAGAAAA
3` M2∆C2∆VPS9	CGTTTTCTCCACCACATGGA

3.4.9.9. Construction of pMCC-G- 1098-1260 -TagRFP-H (H2B)

pMC-G-679-1260-TagRFP-H was digested by MluI and aLwNI and ligated with following hybridized oligos:

Primer	Sequence
5` ∆IDR	CGCGTCCATGGATGATCTCCCAGACT
3` ∆IDR	CTGGGAGATCATCCATGGA

3.4.9.10. Construction of pMCC-G-60-1478 -TagRFP-H T1 Δ H1

pMC-G- 1-1478-TagRFP-H was digested by Mlul and BSTX1and ligated with following hybridized oligos:

Primer	Sequence
5`GAPVD1 ∆H1	CGCGTCCATGATAACCAGTGCTGAAGCTTCCCCTGCTGAATG TTGCCAACATGCCAAAATT
3`GAPVD1 ∆H1	TTGGCATGTTGGCAACATTCAGCAGGGGAAGCTTCAGCACT GGTTATCATGGA

3.4.9.11. Construction of pMCC-G- 1-1113 + 1261-1478-TagRFP-H (T1ΔH2B)

A. Overlapping PCR

Construction of pMCC-G- 1-1113 + 1261-1478-TagRFP-H (T1ΔH2B) was performed using overlap-PCR as schematically shown in figure 10. In the first steps, the sequences 679-1113 and 1261-1478 were amplified of the template plasmid pMC-G-679-1478-TagRFP-H with specifically flanking primers. The resulting DNA constructs were used as templates for a third PCR. With the primers that flank either the N- (P1) or the C-terminal end (P2) of the G- 679-1478.

Primer	**Sequence**
5` BstB1	GACTAGTTCGAAGCAGGAGCTCTGATATAG
3´ Deletion H2B	GATCTTCTTTTCTTTTGAATCCTGCGGGTG
5` Deletion H2B	CACCCGCAGGATTCAAAAGAAAAGAAGATC
3' ApaI GAPVD1	GGGCCCCTTTCGGTCATCGATGGTTTTAATGAA

B. Topo cloning

The resulting amplicon was then ligated to pCR™2.1-TOPO® using the topo cloning kit. The plasmid was then sequenced correct clones were selected to be digested with BstB1 and ApaI and ligated with the BstB1 and APaI digested backbone of pMC-1460-TagRFP-H (T1).

3.4.9.12. Construction of pMCC-G-1-1260-TagRFP-H T1 Δ VPS9

pMC-G-1-1478 -TagRFP-H T1 was digested by SalI and ApaI and ligated with following hybridized oligos:

Primer	**Sequence**
5`M2Δ VPS9	TCGACAAGGACTACAGACCACACAGGCTCACCTGGAAAGGCT ATTGCAAAGAGTTTTGCGGGACAAAGAAGTGGCCAATCGATA CTTTACCACTGTCTGTGTGAGATTACTGCTTGAGAGCGGGCC
3` M2ΔVPS9	CGCTCTCAAGCAGTAATCTCACACAGACAGTGGTAAAGTATC GATTGGCCACTTCTTTGTCCCGCAAAACTCTTTGCAATAGCCT TTCCAGGTGAGCCTGTGTGGTCTGTAGTCCTTG

3.4.9.13. Construction of pMCC-G-1-1113-TagRFP-H T1 Δ VPS9 Δ H2B

pMC-G-1-1478 -TagRFP-H T1 was digested by BspH1 and ApaI and ligated with following hybridized oligos:

Primer	**Sequence**
5` M2ΔB, ΔH2 and ΔVPS9	CATGACAGAGATTTGAGTAGTAAACTTTTATATCATAGTGA TAAAGAGGTTATGGGTGATGGTGAAAGTGCACATGATTCT CCCCGTGACGAAGCACTGCAGAACATCTCGGCTGATGATCT CCCAGACTCTGCAAGCCAAGCAGCCCACCCGCAGGATTCA GGGCC
3` M2ΔB, ΔH2 and ΔVPS9	CTGAATCCTGCGGGTGGGCTGCTTGGCTTGCAGAGTCTGGG AGATCATCAGCCGAGATGTTCTGCAGTGCTTCGTCACGGGG AGAATCATGTGCACTTTCACCATCACCCATAACCTCTTTAT CACTATGATATAAAAGTTTACTACTCAAATCTCTGT

3.4.9.14. Construction of pMCC-PER2-GFP-P

pMC-PER2-GFP-H was digested by MluI and SpeI and the insert was then ligated with the MluI and APaI digested backbone pMC-GFP-P.

3.4.9.15. Construction of pMCC-CSNK1D-TagRFP-PER2-GFP-P

pMC-PER2-GFP-P served as backbone vector and was digested with ClaI and NotI thus removing MPSV and CMV region. In parallel, pMC-CSNK1D-TagRFP-H was digested with ClaI and NotI which yields an insert that contains MPSV-CMV-CSNK1D-TagRFP-Polio-IRES 3598 bp. The insert was then ligated with the backbone of pMC-PER2-GFP-P.

3.5. Statistical analysis

Statistical analyses were performed using GraphPad Prism. For comparisons between two groups, either a Student's t-test (parametric, normally distributed data) or a Mann-Whitney U test (non-parametric, not normally distributed data) was employed. One-way ANOVA (parametric) or Kruskal-Wallis test (non-parametric) was used for comparisons between multiple groups. If multiple comparisons were conducted within an experiment, a correction method like Bonferroni correction was applied to address the issue of multiple testing. Statistical results are presented throughout the thesis as means ± standard deviation, accompanied by the corresponding p-values.

4. Results

4.1. Screening for PER2 binding proteins

PER2 is a repressor protein in the molecular circadian oscillator that inhibits transcriptional activation by CLOCK/BMAL1 at E-box elements in gene promotors (Chiou et al., 2016; Ye et al., 2014). PER2 forms a multimeric complex with PER1/3, CRY1/2 and CSNK1D/E in the cytoplasm and then translocates to the nucleus (Miyazaki et al., 2001; Smyllie et al., 2016; Vitaterna et al., 1999). Recent studies pointed towards other non-transcriptional roles of PER2. For example, PER2 has been found to promote nuclear translocation of the clock protein CRY1 (Miyazaki et al., 2001) or to suppress mTORC1 activity via recruiting TSC1 to the mTORC1 complex (Wu et al., 2019). It is therefore a fair assumption that, besides its function as a transcriptional repressor, PER2 might additionally regulate a variety of other proteins by direct protein-protein interactions.

Protein-protein interactions (PPIs) are involved in practically all cellular activities, with each particular protein often spending the bulk of its existence in complexes with other proteins. As a result, proteins do not operate as solitary, independent entities, but rather through interacting with other biological components. These various interaction patterns appear to be as essential as a protein's inherent biological activity state. The biological significance of a protein is therefore heavily dependent on the underlying PPI network, which may also exhibit significant geographical and temporal changes (Milroy et al., 2013). In order to follow up on these findings and to identify other potential roles of PER2 aside from being a transcriptional repressor, a screen for PER2-interacting proteins seemed to be a promising strategy.

Screens for PPIs can be performed in different ways and can be divided into three categories*: in silico*, *in vivo, and in vitro* approaches (Rao et al., 2014). *In silico* approaches are carried out through computer simulations and are considered to be powerful approaches; however, being only predictive and theoretical, they require assessments of their accuracy (Deane et al., 2002; Lee et al., 2008). *In vivo* procedures include operations on entire living organisms, such as the yeast two- and three-hybrid systems (Y2H, Y3H), and screens for synthetic lethality (Bender and Pringle, 1991; Ito et al., 2001; Ooi et al., 2006). However, in Y2H/Y3H a bait protein is used in combination with a random library of potential protein interaction partners, which might be incomplete. Additionally, synthetic lethality screens are based on functional rather than physical interactions. *In vitro* techniques involve procedures carried out in a controlled environment outside of a living organism. Various *in vitro* methods exist for detecting PPIs, such as affinity enrichment/purification followed by liquid chromatography mass spectrometry (AE/AP-LC-MS), protein arrays, protein fragment complementation, and phage display (Rao et al., 2014). Since *in vitro* approaches offer cell-based screens for real physical interactions with a protein of interest, an *in vitro* method was favored for the screening of PER2 interacting proteins.

4.1.1. Affinity Enrichment-Liquid Chromatography–Mass Spectrometry (AE-LC-MS) of PER2-interacting proteins

Proteomic analyses of cultured cells and mouse organs by LC-MS have been extensively used in the last three decades to characterize post-transcriptional and post-translational regulations involved in circadian biology (Busino et al., 2007; Dang et al., 2016; Lamia et al., 2009; Mauvoisin and Gachon, 2020; Robles and Mann, 2013). Additionally, LC-MS can be coupled with affinity purification or affinity enrichment of a protein of interest, for example by using

antibodies against a protein of interest to screen for potential binding partners. Alternatively, an epitope tag, e.g., GFP, FLAG, TAP or others (Li, 2010), can be added to the N- or C-terminus of a protein of interest and the protein can be expressed either heterogeneously or from its chromosomal locus in cultured cells or animals. The epitope within the protein tag is used by an antibody to enrich the tagged protein, potentially along with its interaction partners (Gingras et al., 2007; Keilhauer et al., 2015). For affinity purification usually various biochemical separation steps have to be performed in order to obtain a highly clean protein complex with the protein of interest. In this case the presence of a protein in the purified complex and its absence in a control purification indicates that it is a real interactor. On the other hand, in affinity enrichment only a significant enrichment level of a protein compared to a control purification is required to suggest that it is a bona fide interactor (Keilhauer et al., 2015). Affinity enrichment was therefore favored over affinity purification for its relative simplicity. Moreover, since the available antibodies against endogenous PER2 are not efficient for protein enrichment (Eide et al., 2005), and the use of these antibodies usually creates a high degree of unspecific binding (unpublished observation in our lab), overexpressed PER2 tagged at the C-terminus with GFP was used for affinity enrichment.

Human PER2 was tagged with GFP at its C terminus (PER2-GFP) and expressed from a vector that was stably inserted into human HT1080 fibrosarcoma cells. Affinity enrichment of PER2-GFP or GFP alone as a control was performed using ChromoTek GFP-Trap® nanobodies coupled to agarose. The eluted samples were then used for LC-MS analysis, a routine analytical technique used to identify molecules in samples based on their mass-to-charge ratio (Pitt, 2009). It is a highly sensitive and powerful quantitative technique for determining protein-protein interactions and distinguishing real interactors from background (Keilhauer et al., 2015). Since the specific LC-MS technique has a greater influence on the background contamination profile than the bait protein itself (Caesar et al., 2018), three biological replicates were made and analyzed at the mass spectrometry facility (Molecular Proteomics Laboratory (MPL), Biologisch-Medizinisches Forschungszentrum (BMFZ) at Heinrich Heine University.

The data from the mass spectrometry analysis are shown as a table that contains 1056 interacting proteins with different enrichment values, t-test p-values and t-test differences between the PER2-GFP and GFP sets. While the t-test p-value indicates the significance of the enrichment, the t-test difference shows the difference between the means of the enrichment values of a protein between the two groups. There were 364 co-purified proteins in HT1080-PER2-GFP cells relative to cells expressing GFP alone that have a p-value of ≤ 0.05 (Table A1, appendix). T-test difference of protein enrichment values was used to filter out and sort the enriched proteins in PER2-GFP purifications compared to GFP alone. There were 184 proteins, which are highlighted with green color in table A1, with a t-test difference of enrichment <0, which means that they are specifically enriched in the PER2-GFP samples. Ribosomal, proteasomal, and tubulin proteins frequently generate non-specific background signals in LC-MS experiments (Hodge et al., 2013). Therefore, these proteins were excluded from the list and are highlight in yellow in table A1.

4.1.1.1. Enrichment of PER2 interacting proteins

It is a reasonable assumption that the proteins most closely associated with PER2 should have high enrichment values and low p-values at the same time. To visualize all interacting proteins according to their enrichment and p-values, a volcano plot was generated using VolcanoR (Naumov et al., 2017). A volcano plot is a type of scatterplot that shows statistical significance as -log10*p-value versus enrichment change (fold change) of two experimental groups. Fold change is the mean of enrichment values in the PER2-GFP group divided by the corresponding

mean in the GFP group. Proteins that significantly bind PER2 are highlighted as red squares (Figure 11) and are divided into four groups based on their fold change and P values.

The volcano plot revealed that one group of proteins (dark red squares, right upper square), has enrichment characteristics very similar to PER2 (fold change > 1.3; $p < 0.0005$). This group contains PER1/2, CRY1/2, and CSNK1D which are the compoments of cytoplasmic PER complexes in mice with the exception of PER3 (Aryal et al., 2017) , indicating the high specificity for PER2 interacting proteins in this analysis. Interestingly, this group also contained GAPVD1 (GTPase Activating Protein and VPS9 Domains 1), which up to that point had not been associated with the molecular circadian clock and had only been found to be connected to CSNK1D through in vitro affinity purification experiments (Kategaya et al., 2012). GAPVD1 contains a GTPase-activating protein (GAP) and a guanine nucleotide exchange factor (GEF) domain and is known to participate in various processes related to vesicular transport such as endocytosis (Sato et al., 2005). Based on these results GAPVD1 was considered to be a potential new member of the PER complex, and a significant part of this thesis consists of experiments with the goal to unravel the mutual physical and functional interactions between the PER complex and GAPVD1. Additionally, this group also contained E3 ligase F-box and WD repeat domain-containing 11 (FBXW11/β-TrCP2), a protein that targets clock proteins for degradation (Shirogane et al., 2005).

In the second group the highest scoring interactors in the lower right square of the volcano plot are two proteins with fold change > 1.3 and $0.0005 < p < 0.05$. One is the adaptor-related protein complex 2 subunit mu 1 (AP2M1) that has a 1.36-fold fold change value closely trailing GAPVD1. However, its p-value of 0.005 just fell short of meeting the enrichment properties observed for the PER complex components. AP2M1 is part of the AP-2 complex that works at cell membranes to internalize cargo in the process of clathrin-mediated endocytosis (Faini et al., 2013). Interestingly, the role of GAPVD1 in vesicular transport is mediated at least in part by binding to the AP-2 complex and regulating AP2M1 phosphorylation (Semerdjieva et al., 2008). A second protein in this group with similar enrichment values is Acyl-CoA dehydrogenase family member 11 (ACAD11), a mitochondrial Acyl-CoA dehydrogenase which aids in fatty acid β-oxidation and exhibits protein rhythmicity in mitochondria, which is lost in PER1/2 knockout mutant mice (Neufeld-Cohen et al., 2016).

The third group, which localizes in the left upper square, contains proteins with a fold change < 1.3 and > 1 with $p < 0.0005$. This group contains among others the proteins RAF proto-oncogene serine/threonine-protein kinase (RAF1), mRNA-capping enzyme (MCE1), Cell cycle and apoptosis regulator protein 2 (CCAR2), and Long-chain-fatty-acid--CoA ligase 1 (ACSL1). RAF1 initiates a mitogen-activated protein kinase (MAPK) cascade which is an essential step in the MAPK/ERK pathway that couples the circadian clock to entrainment pathways in the SCN (Antoun et al., 2012; Molina and Adjei, 2006). MCE1 is a bifunctional mRNA-capping enzyme exhibiting RNA 5'-triphosphate monophosphatase activity and mRNA guanylyltransferase activity in the N-terminal and C-terminal parts respectively (Martins and Shuman, 2002). Although there are no data showing that the regulation of mRNA capping is under circadian control at this moment, it is has been reported that in later stages of mRNA processing BMAl1 binds to the cap-binding protein complex eIF4E allowing the process to be under circadian control (Lipton et al., 2015). CCAR2, which is an important player of the DNA damage reponse, promotes Rev-erbα protein stability and represses BMAL1 and CLOCK expression (Magni et al., 2018). ACSL1, which aids in fatty acid and cholesterol transport, has rhythmic mRNA levels, which are disrupted upon a high-fat diet in mice (Liu et al., 2024). In addition, protein acetylation is facilitated through the PER2-SIRT1 axis (Frahm et al., 2011; Wang et al., 2016).

The fourth group located in the right lower square, contains proteins with a fold change < 1.3 and > 1 and 0.0005< p < 0. 05. This group comprises most of the PER2 interacting proteins and will be discucced as a whole from different perspectives in the upcoming sections.

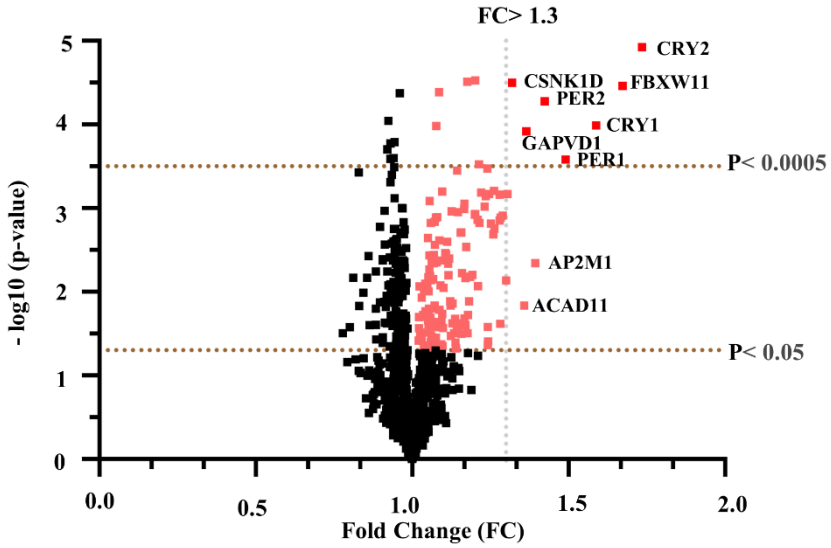

Figure 11. Volcano plot of all proteins identified by affinity liquid chromatography–mass spectrometry (LC-MS). Fold change FC, which is equal to the mean of protein enrichment in all PER2-GFP replicates compared to the corresponding value in the GFP replicates, and -log10(p-value) were plotted for each interacting protein. Broken horizontal lines demarcate p-value thresholds of 0.05 and 0.0005, respectively. A broken vertical line demarcates an FC threshold of 1.3. Proteins that meet the criteria p<0.05, FC>1 are colored in red. Proteins that meet the criteria p<0.0005, FC>1.3 are labeled and highlighted in dark red. (n=3)

To better visualize all significantly enriched proteins with the magnitude of enrichment of each replicate a heat map was generated (Figure 12). A heat map is a data visualization technique that shows the magnitude of a phenomenon, in this case protein enrichment relative to a control experiment, through a color code. In this analysis, distance of sample means to standard deviations (Z-scores) were calculated which allows comparing the relative positions of the sample means within each group. The consistency of protein colors within each group and across different samples indicates a high degree of quality control over the experiment (Figure 12). Moreover, the intensity of both blue and yellow colors, corresponding to GFP or PER2-GFP interacting proteins, reflects the strength of the interaction between GFP or PER2-GFP and the co-immunoprecipitated proteins.

Again, PER complex proteins including the potentially novel component GAPVD1 were on top of the ranking (black box in figure 12). In addition to AP2M1, Adaptor Related Protein Complex 2 Subunit Beta 1 (AP2B1) and Adaptor Related Protein Complex 2 Subunit Alpha 1 (AP2A1) were highly enriched (orange box in figure 12). Notably The AP-2 complex is a heterotetramer consisting of two large adaptins (α and β), a medium size adaptin (μ), and a small adaptin (σ) (Faini et al., 2013), of which three interact with PER2.

Proteins of the positive limb of the circadian clock (ARNTL/BMAL1 and NPAS2) were also identified. Less enriched, the core clock proteins BTRC/β-TrCP1, and CSNK1E were identified. In addition, the clock related proteins MYC binding protein 2 (MYCBP2) (Yin et al., 2010), nuclear receptor subfamily 3 group C member 1 (NR3C1) (Lamia et al., 2011), ubiquitin specific peptidase 9 X-linked (USP9X) (Zhang et al., 2018), ubiquitin specific peptidase 7 (USP7) (Papp et al., 2015), cell cycle and apoptosis regulator 2 (CCAR2) (Giguère

et al., 2016), and damage specific DNA binding protein 1 (DDB1) (Tamayo et al., 2015) were found to be associated with PER2 (Figure 12).

Furthermore, interaction of PER2 with all three components of the exosome-associated superkiller (SKI) complex, tetratricopeptide repeat domain 37, Ski2 like RNA helicase and WD repeat domain 61 (TTC37, SKIV2L and WDR61), was detected, in line with the finding that post-transcriptional mRNA regulation plays a significant role in determining the phase of rhythmic transcripts (green box in figure 12) (Maekawa et al., 2012; Zinder and Lima, 2017). The SKI complex is the cytoplasmic co-factor and regulator of the RNA-degrading exosome (Kögel et al., 2022).

With lesser enrichment four out of seven core subunits that form the coat protein complex I (COPI), COP Alpha, COP Gamma 1, COP Gamma 2, COP Beta 1(COPA, COPg1, COPg2 and COPB1) were associated with PER2 (violet box in Figure 12) (Béthune and Wieland, 2018). COPI allows the precise sorting of lipids and proteins between Golgi cisternae and their retrieval from the Golgi to the Endoplasmic Reticulum (ER) (Arakel and Schwappach, 2018). Thus, the heat map analysis (Figure 12) successfully visualized the enriched proteins interacting with PER2 providing a visual representation of the strength of interactions between PER2 and various co-immunoprecipitated proteins.

In conclusion, analysis using volcano plot and heat map revealed both known and novel interactors of PER2, including components of the PER complex, the AP-2 complex, the SKI complex, and proteins involved in vesicular transport, fatty acid metabolism, and potential novel regulatory pathways. These findings provide a deeper understanding of the molecular network surrounding PER2 and its role in the circadian rhythm. To further explore the functional roles of PER2-interacting proteins, they will be classified by gene ontology (GO) in the upcoming analysis. This will allow the identification of enriched biological processes or molecular functions associated with PER2 interactors, providing additional insights into the mechanisms by which PER2 regulates the circadian rhythm and other ceullar processes.

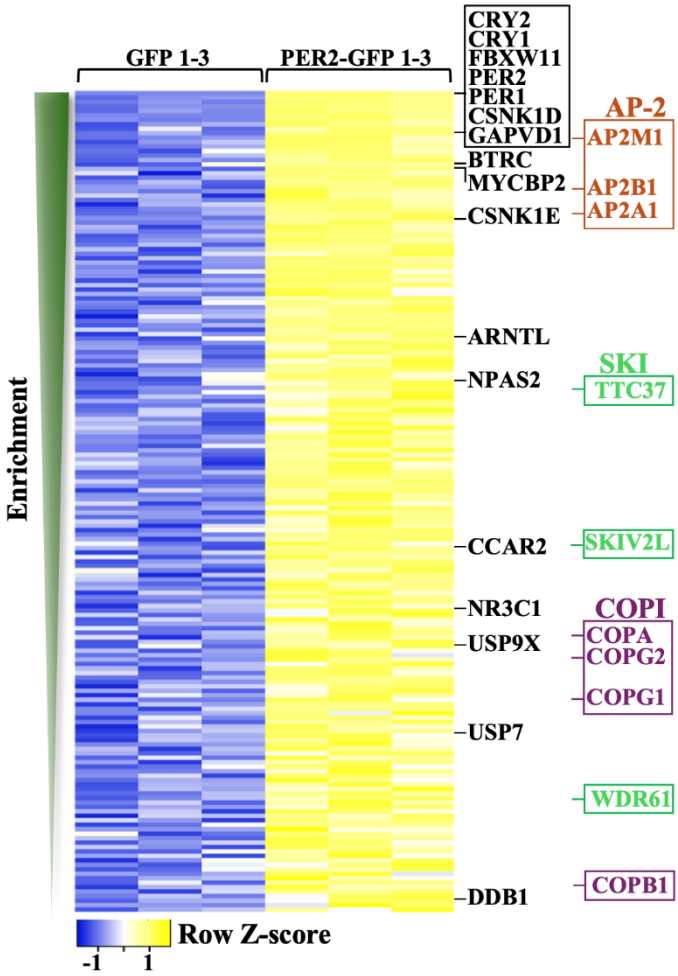

Figure 12. Heat map illustrating significantly enriched PER2-interacting proteins created with the help of http://www.heatmapper.ca (Babicki et al., 2016). The three control replicates (GFP#1–3) are shown on the left side and the bait-containing replicates (PER2-GFP#1-3) on the right side. The vertical axis represents enrichment with the highest value at the top. The color code used on the horizontal axis corresponds to the signal distance from the sample mean expressed in standard deviations (Z-score). Selected protein names are displayed on the right side of the heatmap, with boxes highlighting protein complexes.

4.1.1.2. Classification of PER2-interacting proteins by gene ontology

The mass spectrometry data provided a list of PER2-interacting proteins with their enrichment values and p-values. In order to get an overview of the functional characteristics and cellular localizations of PER2 binding proteins, Gene ontology (GO) analysis of PER2-interacting proteins was performed. GO analysis is widely used to simplify omics experiments featuring cellular localization and biological processes (Young et al., 2010). Several algorithms are currently available for GO analysis, for example, GOnet (Pomaznoy et al., 2018), g:Profiler (Raudvere et al., 2019), EasyGO (Zhou and Su, 2007), GOAT (Bada et al., 2004) and DAVID (Huang et al., 2009). Each possesses distinct advantages and disadvantages, with the optimal choice depending on the particular research inquiry and dataset. DAVID, short for Database for Annotation, Visualization, and Integrated Discovery, was favored due to its robust capability in categorizing functionally associated genes and terms into coherent biological modules, facilitating efficient interpretation of gene lists within a network context (Huang et al., 2009). Furthermore, DAVID is renowned for its user-friendly interface and extensive analysis features.

For the analysis of the identified proteins using DAVID, only proteins enriched with a significant p-value were used. DAVID was configured to produce tables for different GO terms, in which proteins can fall into two groups, biological process (BP) and cellular component (CC). BP represents specific objectives that the organism is genetically programmed to achieve, while CC represents a location such as a cellular compartment or a structure like a macromolecular machine that carries out a specific cellular function. The results from DAVID (Tabel A2) are presented as bar graphs in Figure 13.

GO classification showed for CCs that 42% of PER2-interacting proteins can be located in the nucleus, which is similar to the ratio for location in the cytoplasm (Figure 13B). Among the nuclear proteins list CRY1, CRY2, ARNTL and NPAS2. In addition, PER2 binds two out of six components, MCM2 and MCM7, of the MiniChromosome Maintenance (MCM) complex, which recruits DNA polymerases and initiates DNA synthesis (Lei, 2005). PER2 participates in various cytoplasmic process such as glucose metabolism and apoptosis (Carvas et al., 2012), and the cytosol is on top of the CC list with 58 identified proteins. Moreover, 46 of the identified proteins are confined to membranes. PER2 is involved in autophagy (Kalfalah et al., 2016) and endocytosis (Oyama et al., 2022), and its binding partners the CRY proteins modulate G protein–coupled receptor (GPCR) activity directly through interaction with the G-Protein α-Subunit (Gsα) (Zhang et al., 2010). All these processes take place in intracellular membranous organelles.

The classification based on gene ontology predictably showed that 40 proteins interacting with PER2 primarily participate in the regulation of gene expression and the circadian clock, which comprises 6 terms out of 20 (Table A2). Additionally, this classification encompasses the negative regulation of the glucocorticoid receptor (GR) signaling pathway, a pathway through which the circadian clock directly influences output functions. (Lamia et al., 2011), as well as the G2 phase to M phase (G2/M) transition of the mitotic cell cycle, which is synchronized with the circadian clock through bidirectional coupling (Yan and Goldbeter, 2019) (Figure 13A). Furthermore, GO revealed involvement of the WNT signaling pathway, which is also regulated by PER2 regulators (Ma et al., 2020) (Figure 13A).

Gene ontology (GO) enrichment analysis revealed a potential role for PER2 in long-chain fatty acid (LCFA) metabolism. Three distinct GO terms were enriched: biosynthesis of long-chain fatty-acyl-CoA, biosynthesis of long-chain fatty acid, and long-chain fatty acid metabolic process. These terms collectively suggest PER2 involvement in LCFA synthesis and utilization. Interestingly, Long-chain-fatty-acid-CoA ligase 1 (ACSL1) and Fatty acid CoA ligase 4 (ACSL3) were identified in all three enriched GO categories. ACSL1 and ACSL3 are key enzymes responsible for activating LCFAs by attaching them to CoA, a crucial step for mitochondrial import and subsequent β-oxidation for energy production (Rossi Sebastiano and Konstantinidou, 2019). Additionally, studies suggest a potential interaction between PER2 and SIRT1, a protein deacetylase known to regulate various metabolic processes (Asher et al., 2008; Wang et al., 2016). SIRT1-mediated acetylation of ACSL proteins could potentially modulate their activity and influence the LCFA metabolism axis (Frahm et al., 2011; Wang et al., 2016). These findings warrant further investigations to elucidate the precise role of PER2 in regulating LCFA homeostasis through potential interactions with SIRT1 and ACSL enzymes. Moreover, Phospholipase D1 (PLD1) was classified in the GO term phosphatidic acid biosynthesis.

The GO analysis pointed towards the term fructose 6-phosphate (F6P) metabolic process, which includes key enzymes of metabolic pathways such as ATP-dependent 6-phosphofructokinase, liver type/platelet type/muscle type (PFKL/PFKP/PFKM) or Glutamine-fructose-6-phosphate transaminase 1/2 (GFPT1/2). F6P metabolism can lead into either glycolysis or the hexosamine

pathway (Furuya et al., 1982; Paneque et al., 2023) (Figure 13A), and both pathways have been connected to the circadian clock. All three Phosphofructokinase enzymes PFKL, PFKP and PFKM were found to be PER2-interacting enzymes in this experiment. They facilitate the entry of F6P into the glycolytic pathway and are regulated by the circadian clock (Thurley et al., 2017) (Table A2). On the other hand, the hexosamine pathway provides the substrate uridine diphosphate-N-acetyl glucosamine UDP-GlcNAc used for O-linked glycosylation (Paneque et al., 2023), which posttranslationally modulates the function of clock proteins (Li et al., 2013). In this analysis, GFPT1/2, the rate-limiting enzyme in the hexosamine pathway was one of the PER2-interacting proteins (Table A2).

The GO analysis identified two terms related to golgi vesicle transport. One is intra-Golgi vesicle-mediated transport, and the other is retrograde vesicle-mediated transport. Notably, these processes involve the coat protein complex I (COPI) coatomer, of which four out of a total of seven core subunits were precipitated together with PER2 (Figure 12, 13) (Béthune and Wieland, 2018). The GO analysis sorted the three identified components of the AP2 complex into the GO terms AP-2 adaptor complex, microtubule-based movement, membrane, endolysosome membrane and cytosol (Figure 13). Finally, the interplay between the circadian clock and viral infection is well established (Borrmann et al., 2021; Zhuang et al., 2017), and the GO analysis identified a considerable number of proteins that are involved in viral processes. Among these proteins is Ribonucleic Acid Export 1 (RAE1), an mRNA export factor, which enhances the amplitude of PER2 and CRY1 expression as part of the RAE1-NUP98 complex that increases the transcription activation activity of CLOCK/BMAL1 (Zheng et al., 2019). Notably, viral proteins, for example, Orf6, an accessory protein for severe acute respiratory syndrome coronavirus 2 targets the Rae1–Nup98 Complex to Compete With mRNA Nuclear Export (Li et al., 2022).

In summary, the 184 PER2 binding proteins show versatile biological functions that are involved mostly in regulation of gene expression and negative regulation of the glucocorticoid receptor (GR) signaling pathway. In addition, pathways that have not been previously associated with PER2 such as endocytosis, retrograde vesicle-mediated transport, and post-transcriptional mRNA regulation were identified. To validate the interactors identified through my initial analyses, the upcoming section will focus on the confirmation of selected PER2-interacting proteins by co-immunoprecipitation and western blotting.

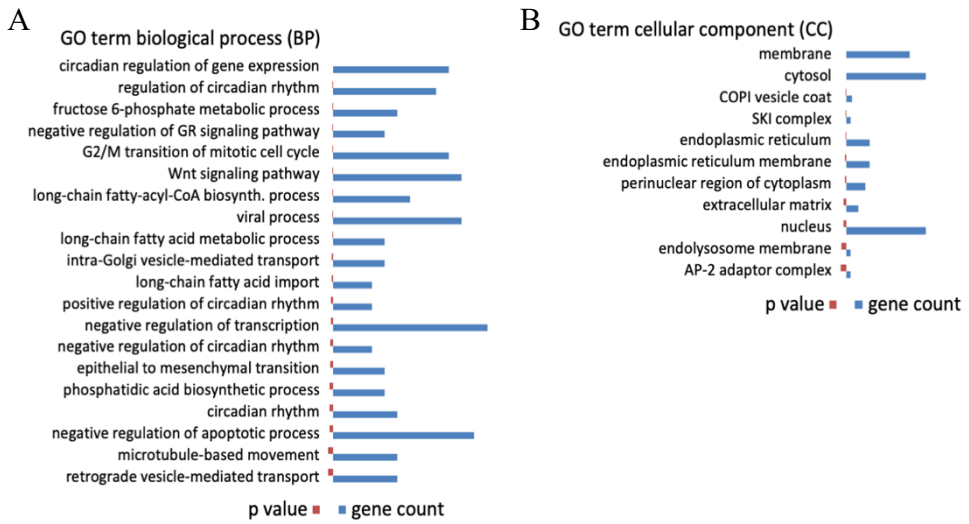

Figure 13. Gene ontology (GO) analysis of PER2-interacting proteins using DAVID. The proteins enriched with a significant p-value ($p<0.05$) were analyzed by DAVID. Listed are GO terms in two categories, namely biological process (BP) and cellular component (CC). GO terms are listed with gene count (blue bar, range: BP 3 − 12; CC 3 − 58) and p value (red bar, range: BP 1.2×10^{-8} − 0.004; CC 1.3×10^{-10} − 0.004). The lists are sorted by ascending p-value

4.1.1. Confirmation of PER2-interacting proteins by co-immunoprecipitation and western blotting

The analysis identified 184 PER2 binding partners with a t-test difference of enrichment > 0 and a p-value of ≤ 0.05. GAPVD1 took a special place in this analysis since it had enrichment values close to PER2 (fold change >1.3; $p < 0.0005$). It might therefore be considered a potential new member of the PER complex with no existing studies on its function within the PER complex. Therefore, a thorough investigation on the regulation that might take place between GAPVD1 and the PER complex will be covered in the rest of the thesis. First, western blot analysis of GAPVD1 co-immunoprecipitated with PER2-GFP was necessary for the validation of the mass spectrometry results.

To further validate the interactions between PER2 and GAPVD1 as well as some of its known binding partners, GFP was immunoprecipitated from HT1080 cells stably expressing either PER2-GFP or GFP using GFP nanobodies. Immunoprecipitated samples were subjected to Western blotting using antibodies against GFP, CSNK1D, CRY1, and GAPVD1 (Figure 14). Calnexin (CNX) served as a control. Western blot analysis with an anti-GFP antibody revealed bands of GFP at a molecular weight of approximately 27 kDa in both the whole cell extracts (Input) and immunoprecipitated (IP) samples (Figure 14). Similarly, bands of PER2-GFP were detected at a size of around 245 kDa in both the input and IP lanes. This confirms the successful immunoprecipitation of GFP. Additionally, several bands were observed at approximate positions of 90, 45, 40, and 28 kDa in the PER2-GFP IP lane, likely representing degradation products of the protein. Two bands at approximately 45 and 40 kDa were identified in both whole cell extracts, corresponding to CSNK1D protein. Notably, more CSNK1D is present in whole cell extracts from PER2-GFP compared to GFP expressing cells, implying that PER2 stabilizes CSNK1D. CSNK1D was only co-immunoprecipitated in the PER2-GFP samples, demonstrating that PER2-GFP specifically binds to CSNK1D.

Detection with an anti-CRY1 antibody yielded a band at approximately 60 kDa in the Input sample of PER2-GFP but not of GFP expressing cells. The presence of overexpressed PER2

seemed to lead to higher cellular levels of CRY1, indicating that PER2 stabilizes CRY1. Additionally, co-immunoprecipitated CRY1 was detected exclusively in the PER2-GFP samples, confirming the ability of PER2-GFP to interact with CRY1 as has been reported previously (Langmesser et al., 2008). Detection with an anti-GAPVD1 antibody revealed a protein band at around 200 kDa in the input material from both GFP and PER2-GFP cells. Only in the immunoprecipitated material from PER2-GFP extracts could GAPVD1 be detected with a slightly higher molecular weight than in the input material. This indicates that PER2 interacts with GAPVD1 and confirms the previous findings by AE-LC/MS detection. The higher position of immunoprecipitated GAPVD1 in the SDS gel may be attributed to phosphorylation or other posttranslational modifications. To assess the quality of the immunoprecipitations, calnexin antibodies were used as a control on all membranes. A signal at approximately 95 kDa was detected only in the input lanes of both GFP and PER2-GFP, corresponding to calnexin. In conjunction with the GFP control this demonstrates the sufficient specificity of the immunoprecipitation (Figure 14).

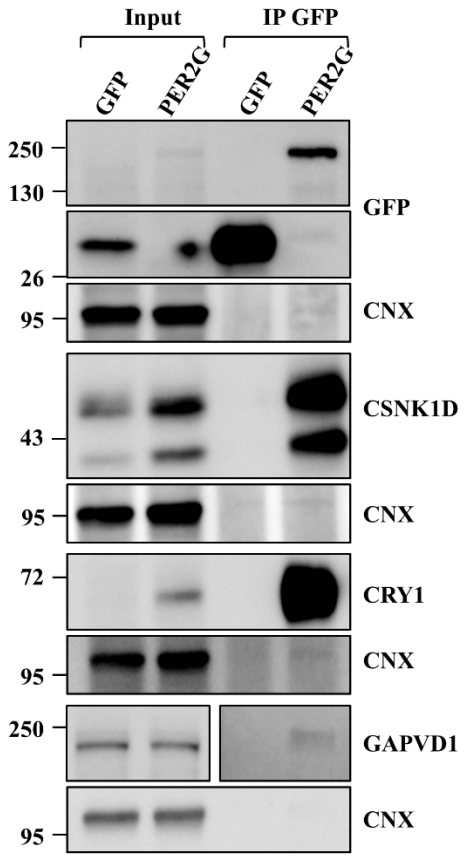

*Figure 14. Western blot analysis of the interaction of PER2 with various binding partners. Immunoprecipitation was conducted with GFP nanobodies with total cell lysate of HT1080 cells that stably express GFP (GFP) or PER2-GFP (PER2G). Western blot analysis was performed with total cell lysate (input) and immunoprecipitate (IP:GFP). A*ntibodies against GFP, CSNK1D, CRY1, GAPVD1 and CNX were used for detection. Selected bands of the protein size marker are indicated on the left side on each panel. Representative western blot image of at least three independent experiments.

In summary, this experiment investigated the interactions between PER2 and its potential new binding partner GAPVD1 as well as the known PER complex components CSNK1D and CRY1. Using co-immunoprecipitation and Western blotting, it was found that PER2-GFP specifically binds to GAPVD1 and the positive controls CSNK1D and CRY1, further strengthening the evidence that GAPVD1 is a novel component of the PER complex. Having

established a physical interaction between PER2 and GAPVD1, the next section delves deeper into the potential regulation of this interaction, specifically the phosphorylation of GAPVD1.

4.2. The PER complex is involved in the regulation of GAPVD1 phosphorylation

In the previous section, AE-LC/MS and co-immunoprecipitation experiments have demonstrated that there is physical interaction between PER2 and GAPVD1. It had been demonstrated before that PER2 and CSNK1D build stable protein complexes (Cao et al., 2023). Moreover, there is a very close association between GAPVD1 with CSNK1D and PER2 in situ as measured by proximity ligation assay (PLA), which detects protein associations with a distance of less than ~30 nm (Ibrahim et al., 2021). In addition, CSNK1D has a pivotal role in the PER complex as it phosphorylates PER and CRY proteins (Aryal et al., 2017; Lee et al., 2001; Philpott et al., 2020). Therefore, the question arose if the PER complex, and in particular the kinase CSNK1D might be involved in the regulation of GAPVD1 phosphorylation.

GAPVD1 contains a Ras GTPase-activating protein domain (Ras-GAP) and a vacuolar sorting protein 9 associated domain (VPS9), which acts as Guanine nucleotide exchange factor (GEF) domain, at its N- and C-terminal, respectively (Hunker et al., 2006; Lodhi et al., 2007). Both domains are separated by a predicted intrinsically disordered region (IDR). IDRs are generally more susceptible to phosphorylation due to their length and unstructured nature than compactly folded parts of a protein (Fealey et al., 2018; Koike et al., 2020). Phosphorylation of an IDR can have a structural impact by leading to conformational changes or promoting the formation of protein condensates (Rieloff and Skepö, 2020; Sridharan et al., 2022). Several high-throughput studies have reported that GAPVD1 is highly phosphorylated, predominantly in the IDR (Dephoure et al., 2008; Olsen et al., 2010; Zhou et al., 2013), and that most of the phosphorylation sites match the consensus motif for CSNK1D/E (Venerando et al., 2014) . A summary of the various mass spectrometry and in vitro kinase studies of GAPDV1 phosphorylation is provided by PhosphoSitePlus (http://www.phosphosite.org), an open, comprehensive, manually curated and interactive resource for studying experimentally observed post-translational modifications, primarily of human and mouse proteins (Hornbeck et al., 2012). It shows different posttranslational modifications such as phosphorylation, acetylation and ubiquitylation on specific amino acid residues of a protein. Human GAPVD1 is shown as a highly phosphorylated protein that is phosphorylated predominantly in the IDR (Figure 15). If and how the PER complex regulates GAPVD1 phosphorylation has been chosen as the first question in an effort to dissect the regulatory interplay between the PER complex proteins, in particular of PER2, CSNK1D and GAPVD1.

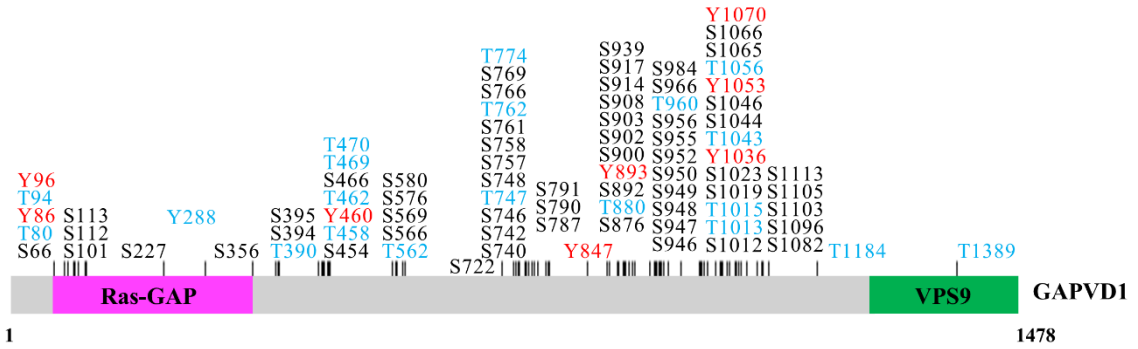

Figure 15. Linear representation of GAPVD1 structure showing phosphorylated amino aicds. Postulated amino acid phosphorylation at Serines (black color), Threonines (blue color) and Tyrosines (red color) is highlighted on top. The bars represent the extact position of each amino acid (from: https://www.phosphosite.org).

4.2.1. The CSNK1D/E-specific inhibitor PF670462 inhibits GAPVD1 phosphorylation

Numerous proteins exhibit a shift in mobility on SDS-PAGE contingent on their phosphorylation level. This phenomenon could arise from reduced SDS binding to the phosphorylated form of the protein (Lee et al., 2013). Thus, a protein may show more than one band on an SDS PAG according to its phosphorylation state. This is the case for GAPVD1 in HeLa cells, which shows two bands around 250 kDa that are readily separated and detected by western blot analysis (Guillen et al., 2020). In order to address if the appearance of these bands is due to phosphorylation of GAPVD1 and if CSNK1D regulates this potential GAPVD1 phosphorylation, treatment with the CSNK1D-specific kinase inhibitor PF670462 (Figure 9) was employed in HeLa cells, followed by analysis of GAPVD1 protein by western blot analysis (Figure 16).

CSNK1D can be inhibited *in vivo* and *in vitro* by various small molecules, thus allowing studying the consequences of its inhibition on the phosphorylation level of potential substrates. Several inhibitors for CSNK1D are available such as CK1-7, IC261, and PF670462 (Bibian et al., 2013). CK1-7 was the first competitive inhibitor for CK1 with an activity in the micromolar range. However, it lacks specificity for CK1 isoforms. Moreover, its capacity to permeate cell membranes is limited owing to its charge under physiological conditions (Chico et al., 2009). Conversely, IC261 exhibits selectivity towards CSNK1D/E within the micromolar range, potentially facilitated by its lack of charge under physiological conditions, thereby enabling significant biological activity. Nonetheless, IC261 also inhibits various other kinases at concentrations ranging from nano- to micromolar levels (Rodrigues and Silva, 2017). PF670462, on the other hand, is a potent selective inhibitor of CSNK1D and CSNK1E with IC50 values of 7.7 and 14 nM respectively (Badura et al., 2007; Janovska et al., 2018) (Figure 5). PF670462 has been shown to inhibit the nuclear translocation of PER proteins causing phase shifts in circadian rhythms with an EC50 of 290 nM (Badura et al., 2007; Jeffrey et al., 2009; Richards et al., 2012). PF670462 was used at concentrations of 20 nM, 200 nM, 2 µM and 20 µM to treat HeLa cells and in addition control cells were treated with PBS. Cells were collected after 24h of treatment for protein analysis by western blotting (Figure 16A). GAPVD1 protein levels were determined relative to the Calnexin control and subsequently the relative intensity of the lower to the upper band of GAPVD1 was calculated (Figure 16B).

The result shows that treatment of HeLa cells with 20 nM PF670462 does not affect the level of GAPVD1 phosphorylation compared to the mock (PBS) control. Interestingly, treatment with PF670462 at a concentration of 200 nM (close to its reported EC50 of 290 nM) – known to inhibit PER protein nuclear translocation and disrupt circadian rhythms (Badura et al., 2007a; Jeffrey et al., 2009; Richards et al., 2012) – resulted in a decrease in the relative abundance of the lower band of GAPVD1. Application of the inhibitor at a concentration of 20 μM further decreased the quantity of the slower migrating, phosphorylated form of GAPVD1 (Figure 16). The variation observed between the different inhibitor concentrations on GAPVD1 phosphorylation could be attributed to partial or complete inhibition of CSNK1D, as well as potential unspecific effects on other kinases.

Consequently, these results indicated that the kinase activity of CSNK1D plays a crucial role in determining the phosphorylation state of GAPVD1. Whether or not other PER complex components participate in the regulation of GAPVD1 phosphorylation remained unclear and was addressed in the following experiment.

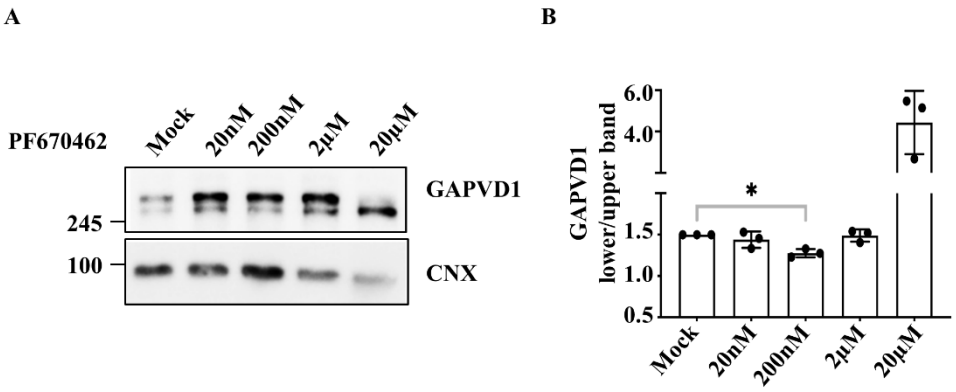

*Figure 16. Inhibition of CSNK1D/E kinase activity modulates GAPVD1 phosphorylation levels in HeLa cells. A. HeLa cells were treated with increasing concentrations of PF670462 (20 nM, 200 nM, 2 μM and 20 μM) for 18 hours. Western blots of the cell extracts with antibodies against GAPVD1 and CNX as loading control including s*elected bands of a *protein size marker are shown. Representative western blot image of* three *independent experiments (n=3). B. Quantification of the data shown in A. Band intensities for each sample were quantified and the ratios between the lower and the higher bands were calculated. Ratios were normalised to the mock-treated sample. * p < 0.05 (t-test).*

4.2.2. PER complex components regulate CSNK1D-dependent GAPVD1 phosphorylation

In the previous section, it has been demonstrated that the kinase activity of CSNK1D influences the phosphorylation status of GAPVD1. Since CSNK1D is part of the PER complex and GAPVD1 has initially been identified as a PER2-interacting protein, the involvement of other PER complex components, i.e. PER2, PER1 and CSNK1E, in the regulation of GAPVD1 phosphorylation should be addressed.

Several cases are known in which an interacting protein can modulate the activity of a kinase binding partner. For example reduced aurora B kinase activity has been noted in cells lacking the N terminus of the inner centromere protein (INCENP) or in cells expressing a mutant INCENP that cannot bind aurora B (Xu et al., 2009). Another example is heat shock protein 90 (HSP90) that can bind to the serine/threonine kinase AKT and modulate its kinase activity (Sato et al., 2000). PER2 is a CSNK1D binding partner and substrate and might therefore also affect GAPVD1 phosphorylation. In order to address the involvement of CSNK1E, PER1, and PER2 in CSNK1D-dependent GAPVD1 phosphorylation, interference with the expression of those

proteins at their mRNA levels using siRNA was utilized in HeLa cells (Figure 17), followed by analysis of GAPVD1 phosphorylation by western blot analysis (Figure 18).

In order to assess the efficiency of the siRNA treatments, RNA was purified from cells treated for 48h, and gene specific transcripts were quantified by qPCR. In the qPCR assays, *Csnk1d*, *Csnk1e*, *Per1*, *Per2* and *Gapvd1* were assessed together with the two non-clock genes Glyceraldehyde-3-Phosphate Dehydrogenase (*Gapdh*) and Actin Beta (*Actb*) as reference genes. The qPCR analyses showed for all examined genes that siRNA treatment resulted in reduced mRNA levels compared to the negative control performed with non-targeted siRNA (Figure 17).

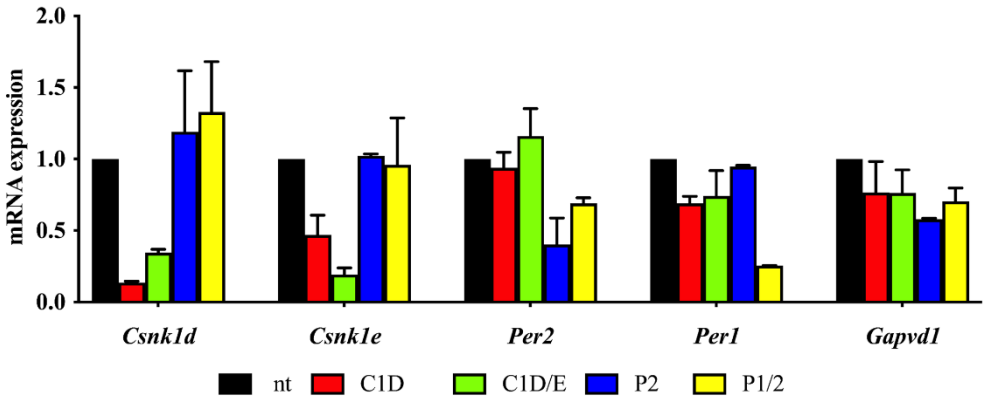

Figure 17. RT-qPCR analysis of the expression of Csnk1d, Csnk1e, Per1, Per2 and Gapvd1 in HeLa cells treated with siRNA for *Csnk1d* (C1D), *Per2* (P2), *Csnk1d/e* (C1D/E), *Per1/2* (P1/2) *or control siRNA (non-target, nt). Data were normalized to the control genes Gapdh and Actb. Bars show data ± standard deviation from two biological replicates (n=2), each with two technical replicates.*

Examination of the protein samples by western blot analysis 72h after siRNA treatment detected two bands for GAPVD1 in cells treated with nt-siRNA (Figure 18A). The intensities of the GAPVD1 and CNX protein bands were quantified, then the relative intensity of the lower band to the upper band of GAPVD1 was calculated for each individual replicate (Figure 18B). SiRNA mediated knockdown of CSNK1D strongly decreased the relative abundance of the lower band of GAPVD1, while knockdown of CSNK1D and CSNK1E marginally intensified this decrease. These findings suggest that CSNK1E may not be essential for GAPVD1 phosphorylation, as CSNK1D appears capable of largely replacing its function. Knockdown of PER2 alone had only a weak influence on GAPVD1 phosphorylation but knockdown of PER1 and PER2 together had a similar effect as knockdown of CSNK1D. The reason that PER2 alone did not affect the relative amount of the lower GAPVD1 band might be because PER1 has partially redundant roles with PER2 in the circadian clock (Akashi et al., 2014; Bae et al., 2001; Zheng et al., 2001). Nevertheless, the requirement for either PER1 or PER2 in this mechanism indicates that the CSNK1D-mediated phosphorylation of GAPVD1 is heavily mediated by the PER complex. Consequently, both CSNK1D and PER proteins appear essential for establishing the phosphorylation status of GAPVD1. After this finding it seemed obvious to ask which specific amino acid residues are susceptible to phosphorylation and whether the observed phosphorylation patterns reflect the activity of CSNK1D in isolation or the combined activities of PER2 and CSNK1D. This question was addressed in the next section.

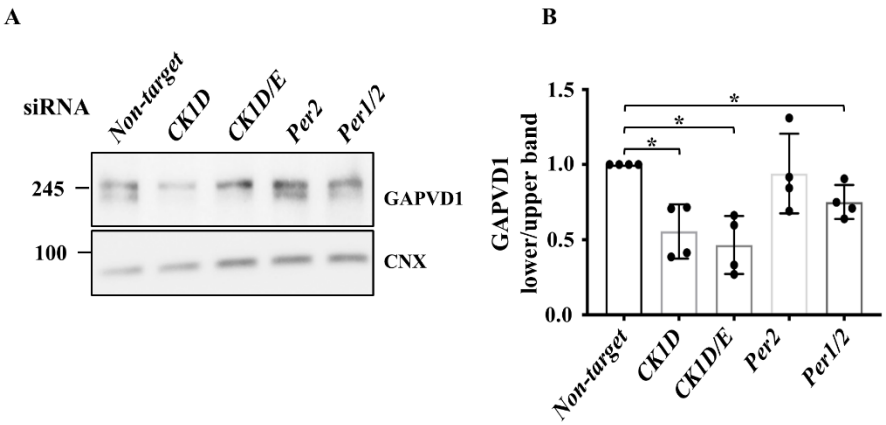

Figure 18. Downregulation of PER complex components modulates GAPVD1 phosphorylation levels in HeLa cells. A. HeLa cells were treated with siRNA for *Csnk1d* (C1D), *Per2* (P2), *Csnk1d/e* (C1D/E), *Per1/2* (P1/2) *or control siRNA (non-target). Western blots were performed* with *antibodies against GAPVD1 and CNX. Western blots of the cell extracts with antibodies against GAPVD1 and CNX as loading control including s*elected bands of a *protein size marker are shown. Representative western blot image of* four *independent experiments (n=4). B. Quantification of the data shown in A. Band intensities for each sample were quantified and the ratios between the lower and the higher bands were calculated. Ratios were normalised to the mock-treated sample. * p < 0.05 (t-test).*

4.2.3. Identification of amino acid residues in GAPVD1 phosphorylated by CSNK1D under different conditions

The previous results from the inhibition and knockdown experiments suggest that both CSNK1D and PER proteins are necessary for the establishment of normal GAPVD1 phosphorylation levels. However, on which amino acid residues CSNK1D-dependent phosphorylation takes place on GAPVD1 remained unclear. Several studies have pointed out the importance of the exact position of a phosphorylated amino acid for the biological consequences in protein function (Hosaka et al., 1999; Zhou et al., 2015). For example, within the circadian clock phosphorylation of S478 in mPER2 leads to its proteasomal degradation while phosphorylation of S659 on mPER2 leads to its stabilization (Zhou et al., 2015). Likewise, CDK5 phosphorylates PER2 at S394 in a diurnal fashion. This phosphorylation facilitates the interaction with CRY1 and nuclear entry of the PER2/CRY1 complex (Brenna et al., 2019). Therefore, mapping of CSNK1D-dependent phosphorylation sites in GAPVD1 was addressed next.

In order to identify amino acids in GAPVD1 that are phosphorylated by CSNK1D, and to analyze how PER2 affects these modifications, HT1080 cells were grown under various conditions that would potentially result in different GAPVD1 phosphorylation profiles. Firstly, untreated HT1080 wild type cells were used, which should represent the default cellular phosphorylation state of GAPVD1. Analysis of HT1080 cells treated with 20 µM PF670462 should allow conclusions about the role of the CSNK1D-kinase activity on GAPVD1 phosphorylation. In addition, HT1080 that stably express CSNK1D and PER2 (CP cells) were used (Ibrahim et al., 2021; Reus, 2020). In contrast to wild type HT1080 cells, GAPVD1 seems to be phosphorylated to a much higher level in CP cells as concluded from the appearance of a second slower migrating band in western blots of GAPVD1 (Reus, 2020).

Immunoprecipitation of GAPVD1 from these cell lines was followed by mass spectrometry analysis to determine the phosphorylated amino acid residues within the samples. Prior to the mass spectrometry analysis, immunoprecipitated proteins were analyzed by SDS PAGE followed by Coomassie staining (Figure 19). According to the Western blot experiments GAPVD1 should be present at a size of around 245 kDa. Protein bands between 180 and 250

kDa were cut from the gel and analyzed by liquid chromatography–mass spectrometry (LC-MS).

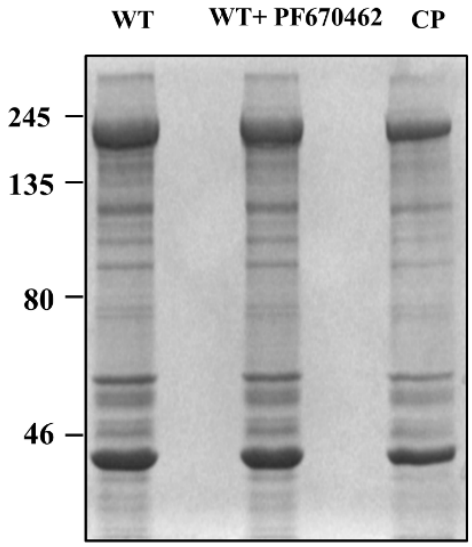

Figure 19. Gel electrophoresis and Coomassie brilliant blue staining of GAPVD1 immunoprecipitates. Immunoprecipitations of GAPVD1 were performed from HT1080 WT, HT1080 WT treated with 20 µM PF670462 and HT1080 CP cells. An empty lane was left between two samples to avoid contaminations when cutting the bands. Proteins were separated on 10% SDS PAGs and visualized using Coomassie brilliant blue staining. Selected bands of a protein size marker are indicated on the left side of the panel. Representative SDS/PAGE image of three independent experiments (n=3).

The sequenced peptides coverage was in WT 42.7 ± 7.6%; CP 41.3 ± 10.3%; WT + PF670462 38.7 ± 7.0% of the protein sequence, which makes sequence coverage quite equivalent in all samples. The analysis identified seven different phosphopeptides (Figure 20A), all of which are located in the predicted IDR region of GAPVD1. This is in alignment with several high throughput studies, which also showed that GAPVD1 is phosphorylated mainly in the IDR region (Dephoure et al., 2008; Olsen et al., 2010; Zhou et al., 2013).

The ratios of phosphorylated to unphosphorylated peptides in each sample for all identified peptides are presented as a bar graph in Figure 20B. The analysis shows that site 5 and to a lesser extent site 3 are highly phosphorylated in CP cells compared to WT cells with or without inhibitor treatment (Figure 20B). This confirms that PER2 and CSNK1D can affect the phosphorylation pattern of GAPVD1. Site 3 contains an S-x-x-S-D site, which is similar to the CSNK1D primed consensus site pS/pT-x-x-S/T-φ (pS/pT: priming phosphoserine or threonine, x: any amino acid, underline: phosphorylated residue, and φ. Hydrophobic residue) (Marin et al., 2003) and might explain its dependence on CSNK1D activity. The presence of the hydrophilic aspartic acid residue instead of a hydrophobic residue may not hinder CSNK1D activity as it has been shown that CSNK1D is able to phosphorylate a large number of non-consensus sites (Philpott et al., 2020). This might also be the case for site 5 which contains the similar motif S-x-x-S-D. In addition, the involvement of other kinases in phosphorylation of these two sites can not be excluded.

Conversely, the phosphorylation levels at all remaining sites did not demonstrate a uniform reaction to increased CSNK1D activity or to the inhibitor (Figure 20B). For example, site 1 showed similar low phosphorylation pattern while site 4 was highly phosphorylated under all conditions. However, the motif S-x-x-S-T is also present in site 4 (Figure 20A) and shows no specific response to CSNK1D activity. Overall, this phosphorylation may play a role in the regulation of GAPVD1 function, like in PER2, and possibly the regulation of PER complex

function. Indeed. it has been shown that CSNK1D-dependent phosphorylation of GAPVD1 is linked to its degradation (Ibrahim et al., 2021). Since PER complex accumulation is rhythmic (Aryal et al., 2017; Chen et al., 2009), it is fair to speculate that GAPVD1 phosphorylation may exhibit rhythmic fluctuations within a 24-hour period. Therefore, temporal phosphorylation of GAPVD1 was addressed in the next section.

A

P-Site number	Peptide sequence	Amino acid
P-site 1	387 AVETPPLSSVNLLEGLSR 404	T390
P-site 2	452 SSSLEMTPYNTPQLSPATTPANK 474	S466
P-site 3	562 TLRFSLCSDNLEGISEGPSNR 582	T562 S566 S569
P-site 4	755 EVSSRPSTPGLSVVSGISATSEDIPNK 781	S757 S758 S761 T762
P-site 5	900 SRSSDIVSSVR 910	S902 S903
P-site 6	928 ELPPAAAIGATSLVAAPHSSSSSPSK 953	S949 S950
P-site 7	1089 DEALQNISADDLPDSASQAAHPQDSAFSYR 1118	S1096 S1105

B

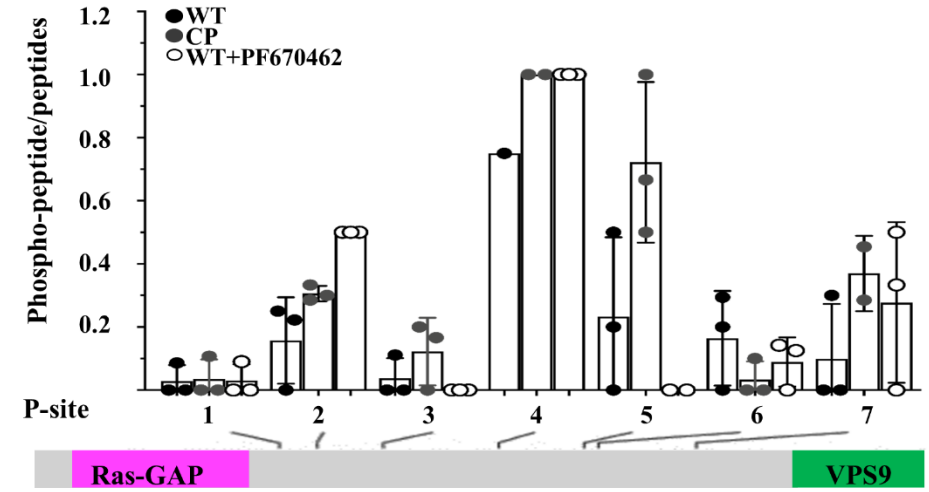

*Figure 20. Mapping of GAPVD1 phosphorylation sites. A. The identified phosphopeptides are listed and phosphorylated amino acids are highlighted in red and listed separately in the right panel. The positions of the first and last amino acid of each phosphopeptide within the GAPVD1 polypeptide are indicated. B. Bars show the ratios of phosphorylated to unphosphorylated peptides in each sample for all identified peptides. HT1080 wild type cells (black), CP cells (grey), pre-treated HT1080 wild type cells plus 20 µM PF670462 (white). The positions of the phosphopeptides within GAPVD1 are illustrated below. Single data points are shown by circles and standard deviations are represented by error bars. * $p < 0.05$ (t-test) (n=3).*

4.2.4. Temporal phosphorylation of GAPVD1 is rhythmic

I have shown previously that the PER complex regulates GAPVD1 phosphorylation. PER proteins show striking temporal circadian rhythmicity in protein abundance and exhibit circadian phosphorylation patterns which are mediated by several kinases, mainly by CSNK1D and CSNK1E (Lee et al., 2001, 2009) and by CDK5 (Brenna et al., 2019). Such phosphorylation patterns determine the pace of proteasomal degradation (Vanselow et al., 2006), turnover (Virshup et al., 2007), and nuclear translocation (Vielhaber et al., 2000). In addition, rhythmic protein phosphorylation has been detected in the first circadian phosphoproteome analysis that was performed on mouse liver tissue, which has a very robust circadian rhythmicity. Although only 10% of the transcriptome exhibits circadian oscillations in gene expression (Panda et al., 2002; Storch et al., 2002), 25% of the phosphopeptides on more than 40% of the identified phosphoproteins displayed circadian oscillations (Robles et al., 2017).

In order to reveal a potential circadian profile of GAPVD1 phosphorylation, human U2OS osteosarcoma cells were used. These cells possess a functional circadian oscillator in contrast to the previously used HT1080 and HeLa cells. U2OS cells were synchronized with dexamethasone (Figure 8), and cells were collected at different circadian time points after synchronization (CT26, 30, 34, 38, 42 and 46). GAPVD1 was immunoprecipitated from cell extracts using GAPVD1 antibodies and immunoprecipitated samples were subjected to Western blotting using antibodies against GAPVD1 (Figure 21A). The western blot detected two GAPVD1 bands at around 250 kDa. Phosphorylation levels were measured by the intensity ratio between the upper and lower GAPVD1 bands in the 24h time course and turned out to be rhythmic with a maximum at CT38 (Figure 21A).

Given the observed phosphorylation pattern, I next investigated the possibility of rhythmic CSNK1D binding to GAPVD1 as a potential mechanism. To address this question, CSNK1D was immunoprecipitated from synchronized U2OS cells and the relative amount of co-immunoprecipitated GAPVD1 and PER2 was analyzed by western blot (Figure 21B). The results showed a constant amount of immunoprecipitated CSNK1D around the day. However, the association of GAPVD1 with CSNK1D had a rhythmic profile with the least binding of GAPVD1 to CSNK1D at CT 38. Intriguingly, the strength of the CSNK1D/GAPVD1 interaction mirrored the binding of PER2 to CSNK1D, opening the possibility that association with the PER complex might confer rhythmicity to GAPVD1 phosphorylation. The rhythmic binding of GAPVD1 to CSNK1D coinciding with PER2 association raises the possibility that GAPVD1 might influence the interaction between CSNK1D and PER2. GAPVD1 could act as scaffold and induce a conformation change in CSNK1D or compete with PER2 for binding to CSNK1D. Both scenarios would allow GAPVD1 to regulate CSNK1D-PER2 interaction. To test this hypothesis, I next aimed to assess whether GAPVD1 affects the CSNK1D-PER2 complex formation.

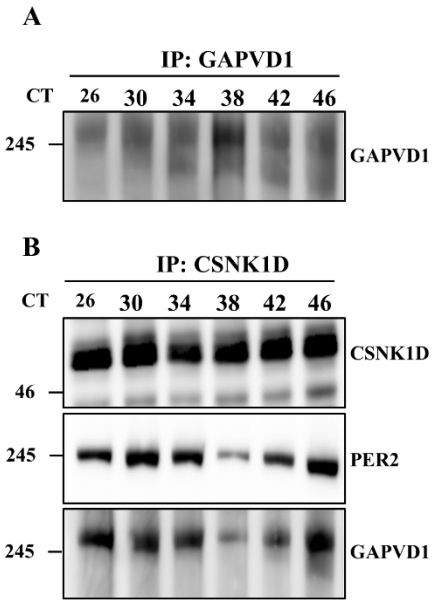

Figure 21. Phosphorylation of GAPVD1 is rhythmic in U2OS cells. U2OS cells were synchronized with Dexamethasone and cells were collected 26 h, 30 h, 34 h, 38 h, 42 h, and 46 h after synchronization. Immunoprecipitation was conducted with antibodies against GAPVD1 or CSNK1D and samples were subjected to Western blot analysis. A) For GAPVD1 immunoprecipitates, antibodies against GAPVD1 were used for detection. B) For CSNK1D immunoprecipitates, antibodies against CSNK1D, PER2 and GAPVD1 were used for detection. Selected bands of a protein size marker are indicated on the left side of each panel. Representative western blot image of at least three independent experiments (n=3).

4.3. GAPVD1 influences PER2-CSNK1D binding

PPIs perform a variety of roles in biology and vary depending on the composition, affinity, and whether the association is permanent or transient (Nooren and Thornton, 2003). PPIs in PER/CRY and CLOCK/BMAL1 complexes and the stoichiometry of their monomer components are crucial elements for proper circadian clock function. The CSNK1D-PER2 interaction is at the core of the circadian clock mechanism, as it either leads to PER2 accumulation by increasing stability, or to its degradation by the ubiquitination pathway, depending on the specific sites that are phosphorylated by CSNK1D (Narasimamurthy et al., 2018). Attenuating this process with kinase inhibitors can alter the period of the molecular clock (Chen et al., 2012; Eide et al., 2005; Isojima et al., 2009). The earlier results showed that GAPVD1 is a substrate for CSNK1D. In addition, in synchronized human U2OS cells, GAPVD1 was rhythmically associated with CSNK1D, and the strength of this interaction mirrored the binding of PER2 to CSNK1D (Figure 21). Since both GAPVD1 and PER2 bind to CSNK1D, I next wanted to test whether GAPVD1 affects the CSNK1D-PER2 interaction, which might help to explain the influence of GAPVD1 on the period length of the molecular oscillator (Aryal et al., 2017).

4.3.1 Decreased binding of PER2 to CSNK1D in GAPVD1 overexpressing cell lines

To investigate the influence of GAPVD1 on PER2-CSNK1D binding, we analyzed this interaction in two cell lines: HT1080 wild-type (WT) and a cell line stably overexpressing GAPVD1-TagRFP (abbreviated as G). This approach allowed us to assess the effect of an unphysiologically high GAPVD1 level on PER2-CSNK1D complex formation. CSNK1D was immunoprecipitated from the two cell extracts, and the immunoprecipitated proteins were analyzed by western blot (Figure 22A). As a negative control, only beads were used for immunoprecipitation in both cell lines with no added antibodies. Negative controls showed no signal for CSNK1D or any other non-specific proteins. Calnexin served as a control, verifying

both sample loading in the input and the effectiveness of the immunoprecipitation. No significant amount of Calnexin was detected in the IP of CSNK1D or in the control samples. The trace amounts of Calnexin detected on the PER2 membrane in the IP samples were treated as a blotting artifact because Calnexin was not detected in the same samples on the GAPVD1 and CSNK1D membranes. Band intensity was then analyzed for PER2 and CSNK1D, normalized to either calnexin in the input lanes or to immunoprecipitated CSNK1D in the IP lanes (Figure 22B, A6).

In the input samples, the levels of endogenous PER2 and CSNK1D were slightly but not significantly increased in GAPVD1 overexpressing cells compared to wild type cells (Figure 22A, A6). This indicates that GAPVD1 might have a subtle influence on PER2 and CSNK1D protein levels. The amount of CSNK1D in the IP samples is comparable in both cell lines. Western blot analysis revealed that the amount of PER2 bound to CSNK1D was significantly lower in GAPVD1 overexpressing cells compared to HT1080 WT cells. These findings indicate that GAPVD1 abundancy influences the amount of PER2 that binds to CSNK1D. This experiment also suggests that GAPVD1 could act as a competitor of PER2 for binding to CSNK1D, but other scenarios are possible as well such as allosteric regulation or regulation of post-translational modifications. However, the limited quantity of endogenous PER2 in this experiment could mimic a competitive binding scenario, potentially confounding the assessment of its full binding capacity to CSNK1D. To elucidate the mechanism by which GAPVD1 modulates PER2-CSNK1D binding, PER2 could be overexpressed in addition to GAPVD1. A reduction of PER2-CSNK1D binding by GAPVD1 under these conditions would argue against a simple competition model and suggest a more complex regulatory role for GAPVD1.

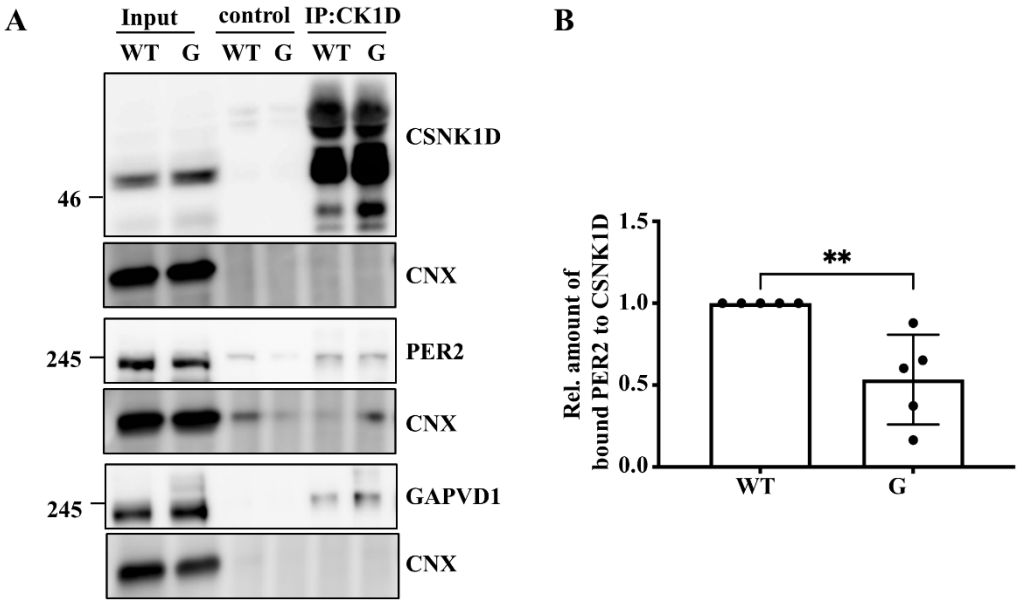

*Figure 22. Decreased binding of PER2 to CSNK1D in GAPVD1 overexpressing HT1080 cells. A. Immunoprecipitation (IP) was conducted with CSNK1D (IP:CK1D) antibodies with total cell lysate of HT1080 cells that stably overexpress GAPVD1 (G) or HT1080 wild type (WT). Beads-only samples were used as negative controls. Antibodies against CSNK1D, PER2 and GAPVD1 were used for detection. CNX served as loading control. Selected bands of a protein size marker are indicated on the left side of each panel. Representative western blot image of five independent experiments (n=5). B. Band intensities for each sample were quantified and plotted as a bar diagram. Single data points are represented by black circles and standard deviations are represented by error bars. * $p < 0.05$ (t-test).*

4.3.2. Unchanged binding of PER2 to CSNK1D in GAPVD1 and PER2 overexpressing cell lines

From previous experiments and longstanding experience in the lab we know that endogenous PER2 is expressed at very low levels in cultured cells. This low expression level could contribute to the observed weaker binding of PER2 to CSNK1D upon overexpression of GAPVD1, as the limited amount of PER2 may be sequestered by the overexpressed GAPVD1. To address this possibility and to determine if GAPVD1 can still decrease the binding of PER2 to CSNK1D when PER2 is abundant, I examined GAPVD1-dependent binding of PER2 to CSNK1D in HT1080 cells that stably overexpress PER2-GFP.

To examine the binding of PER2 to CSNK1D, different clones of HT1080-PER2-GFP cells (P cell lines) were transiently transfected with GAPVD1-TagRFP (P*G, only one clone is shown in Figure 23A). As a negative control, only beads were used for immunoprecipitation in untreated cell lines with no added antibodies. The proteins that were immunoprecipitated by the CSNK1D antibody were analyzed by western blot (Figure 23A). The negative controls were treated in the same way as described for the immunoprecipitation protocol and no signals could be detected.

The western blot detected CSNK1D, overexpressed PER2 and GAPVD1 at sizes of around 46, 245 and 250 kDa respectively. The overexpressed GAPVD1 is detected at a size above 245 kDa as indicated in the P*G Cell lines lanes both in the input and IP lanes. Additionally, calnexin served as a loading control for the analysis and quality of the IP. The intensities of the signals were then measured and analyzed for PER2, CSNK1D, and CNX in both the input and IP lanes (Figure 23B, A7).

In the input samples, PER2 and CSNK1D are present in similar amounts in P*G cells compared to P cells (Figure 23A). The quantification analysis shows that the levels of endogenous PER2 and CSNK1D were slightly but not significantly increased in P*G cell lines compared to P cells (Figure 23, A7), which is similar to the result from the previous experiment with cells that only overexpress GAPVD1. The amount of immunoprecipitated CSNK1D from both cell lines was quite similar. However, not significantly less PER2 was co-immunoprecipitated with CSNK1D in P*G compared to P cells (Figure 23). These findings indicate that the availability of PER2 contributes to the modulating activity of GAPVD1 on the binding of PER2 to CSNK1D. This could also mean that GAPVD1 might exert its effect when PER2 is at its lowest cellular concentration, for example between CT 0 and 6 (Buhr and Takahashi, 2013). In summary, these results indicate that GAPVD1 can reduce the PER2-CSNK1D interaction but only if the availability of PER2 is limiting. Next, I aimed to validate these findings in a GAPVD1-deficient cell line.

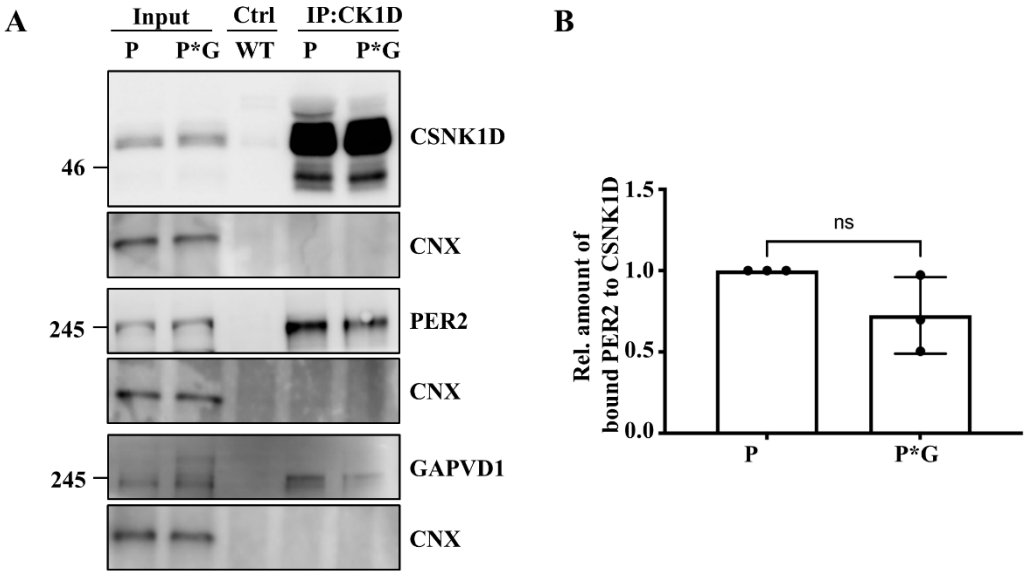

*Figure 23. Unchanged binding of PER2 to CSNK1D in a GAPVD1 overexpressing HT1080 cell line. Immunoprecipitation (IP) was conducted with CSNK1D (IP:CK) antibodies with total cell lysate of HT1080-PER2-GFP that transiently overexpress GAPVD1 (P*G) or HT1080-PER2-GFP (P) alone to investigate the interaction between PER2 and CSNK1D. A beads-only sample was used as negative control. Antibodies against CSNK1D, PER2 and GAPVD1 were used for detection. CNX served as loading control. Selected bands of a protein size marker are indicated on the left side of each panel. Representative western blot image of three independent experiments (n=3). B. Band intensities for each sample were quantified and plotted as a bar diagram. Single data points are represented by black circles and standard deviations are represented by error bars. * $p < 0.05$ (t-test).*

4.3.3. Increased binding of PER2 to CSNK1D in GAPVD1 knockout cells

My previous findings suggest that GAPVD1 affects the interaction between PER2 and CSNK1D. To corroborate these findings, I explored the PER2-CSNK1D interaction in the absence of GAPVD1. In order to further strengthen the validity of these findings, this experiment was performed in a different cell line (HeLa) to assess the generalizability of the results. Therefore, PER2-CSNK1D binding was analyzed in HeLa WT and GAPVD1 KO cells. The binding between CSNK1D and PER2 was examined by a co-immunoprecipitation experiment. CSNK1D was immunoprecipitated from the two cell extracts and the immunoprecipitated proteins were analyzed by western blot (Figure 24).

The western blot detected bands of CSNK1D, PER2 and two bands of GAPVD1 in wild type cells. The two bands arose probably due to phosphorylation, and no bands were detected in the GAPVD1 KO cell line. In the total cell lysates, the CSNK1D signal was slightly decreased in GAPVD1 KO cells compared to WT cells (Figure 24A, A8). The band intensity analysis shows that the difference was not significant (Figure A8). In contrast, PER2 protein levels were slightly but not significantly increased in GAPVD1 KO cells compared to the wild type cells. The results might therefore indicate subtle effects of GAPVD1 on CSNK1D and PER2 levels.

The comparable amounts of CSNK1D and PER2 in the whole cell extracts of both cell lines nevertheless allowed the comparison of the PER2-CSNK1D interaction between both cell lines. The amount of immunoprecipitated CSNK1D was similar in both cell lines (Figure 24). However, the amount of co-purified PER2 bound to CSNK1D was significantly higher in GAPVD1 KO cells compared to the wild type cells (Figure 24). These findings indicate that GAPVD1 negatively influences PER2-CSNK1D binding. Overall, the PER2-CSNK1D interaction is significantly affected by GAPVD1, as evidenced in cell lines that stably express

GAPVD1, as well as in GAPVD1 knockout cell lines. These findings suggest that the interaction of GAPVD1 with the PER complex might be a regulatory step, as seen in the consequence for CSNK1D-PER2 binding. However, the specific domains of GAPVD1 responsible for its interaction with PER2 and/or CSNK1D remain unknown. It is unclear whether a single domain or multiple domains of GAPVD1 bind to PER2 and CSNK1D. This will be addressed in the next section.

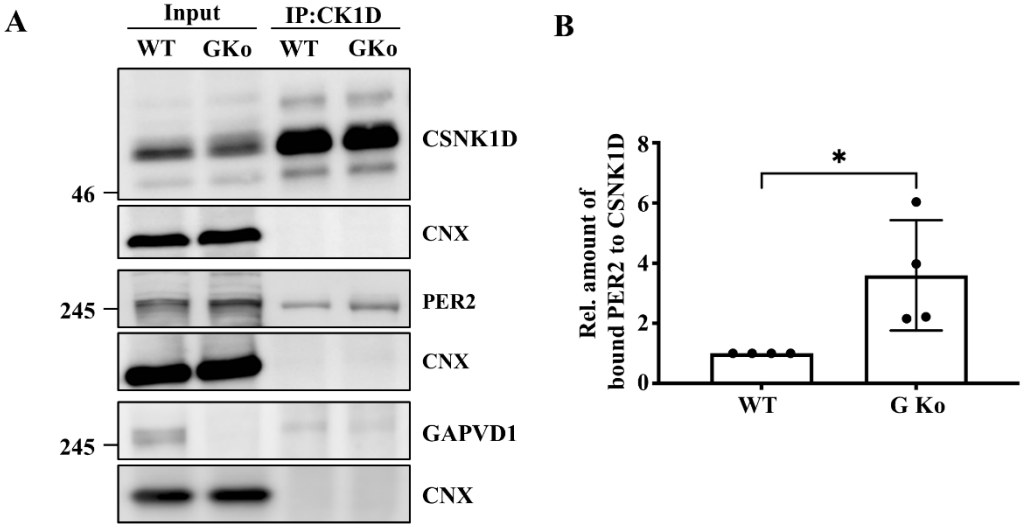

*Figure 24. Increased binding of PER2 to CSNK1D in GAPVD1 KO HeLa cells. A. Immunoprecipitation (IP) was conducted with CSNK1D (IP:CK1D) antibodies with total cell lysate of HeLa cells, in which Gapvd1 has been deleted (GKo) or wild type (WT) cells. Antibodies against CSNK1D, PER2 and GAPVD1 were used for detection. CNX served as loading control. Selected bands of a protein size marker are indicated on the left side of each panel. Representative western blot image of four independent experiments (n=4). B. Band intensities for each sample were quantified and plotted as a bar diagram. Single data points are represented by black circles and standard deviations are represented by error bars. * $p < 0.05$ (t-test).*

4.4. Mapping interaction domains of GAPVD1 with PER2 and CSNK1D

Previously I showed that binding of GAPVD1 to the PER complex proteins PER2 and CSNK1D affects the strength of the interaction between each other. Numerous biological processes are governed by protein-protein interactions and locating the binding domains on proteins can aid to understand the regulatory mechanisms within a protein complex. For instance, the amino acid Leu730 is essential for the physical interaction between PER2 and CSNK1D and is furthermore important for their roles in the circadian clock machinery (An et al., 2022). Thus, mapping protein interaction surfaces can facilitate the discovery of small molecules that block or enhance such interactions or aid in structural analysis.

The first step in mapping protein interaction domains was done by a former master student in our lab using two constructs which consist of the N- and C-terminal halfs of GAPVD1 designated M1 and M2, respectively (Figure 25).The results demonstrated that PER2 and CSNK1D exhibited strong binding affinity to M2 but exhibited negligible binding affinity to M1 (Buschhaus, 2021).

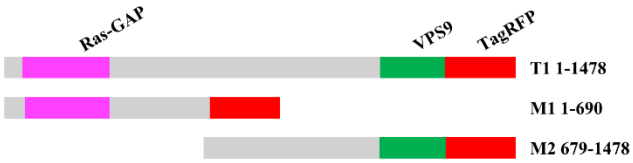

Figure 25. Schematic overview of GAPVD1 deletion mutants. T1: full length GAPVD1 (Ensembl Transcript 1) (1-1478 aa) which contains Ras-GAP (magenta), VPS9 domain (green), IDR (gray) and TagRFP (red). M1: N-terminal half of GAPVD1 (1-690), consisting of the Ras-GAP domain and the IDR. M2: C-terminal half of GAPVD1 (679-1478), consisting of a part of the IDR and the VPS9 domain. All constructs were tagged with tRFP at their C terminus enabling visualization and tracking of the proteins in subsequent experiments.

In order to further determine the specific GAPVD1 domains that are responsible for binding to PER2 and CSNK1D, first the highly accurate protein structure prediction tool Alpha Fold was employed to identify potential protein domains in GAPVD1 (Jumper et al., 2021; Varadi et al., 2022) (Figure 26). In Critical Assessment of Structure Prediction 14 (CASP14), which assesses methods of protein structure modeling since 1994, AlphaFold structures were vastly more accurate than other methods and outperformed 146 competing methods. It is scalable to very long proteins with accurate domains and domain-packing. AlphaFold's exceptional protein structure prediction capabilities are rooted in its innovative deep learning architecture, ensemble learning approach, attentive focus, extensive training data, superior contact map prediction, ability to handle novel sequences, and open access. These features have revolutionized the field of protein science, paving the way for transformative advancements in medicine, biotechnology, and materials science (Callaway, 2020).

AlphaFold produces a per-residue confidence score (pLDDT) between 0 and 100. Regions below 50 pLDDT may be unstructured in isolation. The structured parts of the proteins have confidence scores assigned between “Confident” (90 > pLDDT > 70) to “Very high” (pLDDT > 90). AlphaFold predictions suggest that some regions in GAPVD1 may not be as unstructured as previously predicted by other methods. This newfound understanding of GAPVD1 protein structure has significant implications for our comprehension of potential functions and regulation. For instance, as depicted in Figure 26, the IDR region is now limited to AA 354 to 1113 whereas before it had been predicted to reach from AA 354 to 1260. In addition, the unstructured region N-terminal of the RasGAP domain (1-60) is structured as a helix in Alphafold. Generally, GAPVD1 structure is predicted as two coiled coil helices with the RasGAP and VPS9 domain on one end of the helices. The N-terminal helix (AA 6-60) directly precedes the RasGAP domain and was named helix 1 (H1). The confidence level for H1 is Very high for residues 19-52 and Confident for residues 6-18 and 53-60. The second helix (AA 1193-1274) precedes the VPS9 domain and was named helix 2 (H2). The confidence level for H2 is very high for residues 1213-1274 and confident for the rest of the domain. In addition, there is three helices bundle on the other end of the coiled coil helices, preceding H2, which was named bottom (B). The VPS9 domain spans residues 1278-1477, and the RasGAP domain residues 61-353 (Figure 26).

For a better visualization of the GAPVD1 3D structure, the domain colors assigned by AlphaFold have been changed using UCSF ChimeraX (Meng et al., 2023).Yellow color was assigned to helix 1, magenta color to RasGAP, gray color to IDR, light blue color to bottom, blue color to helix 2 and green color to VPS9 (Figure 26).

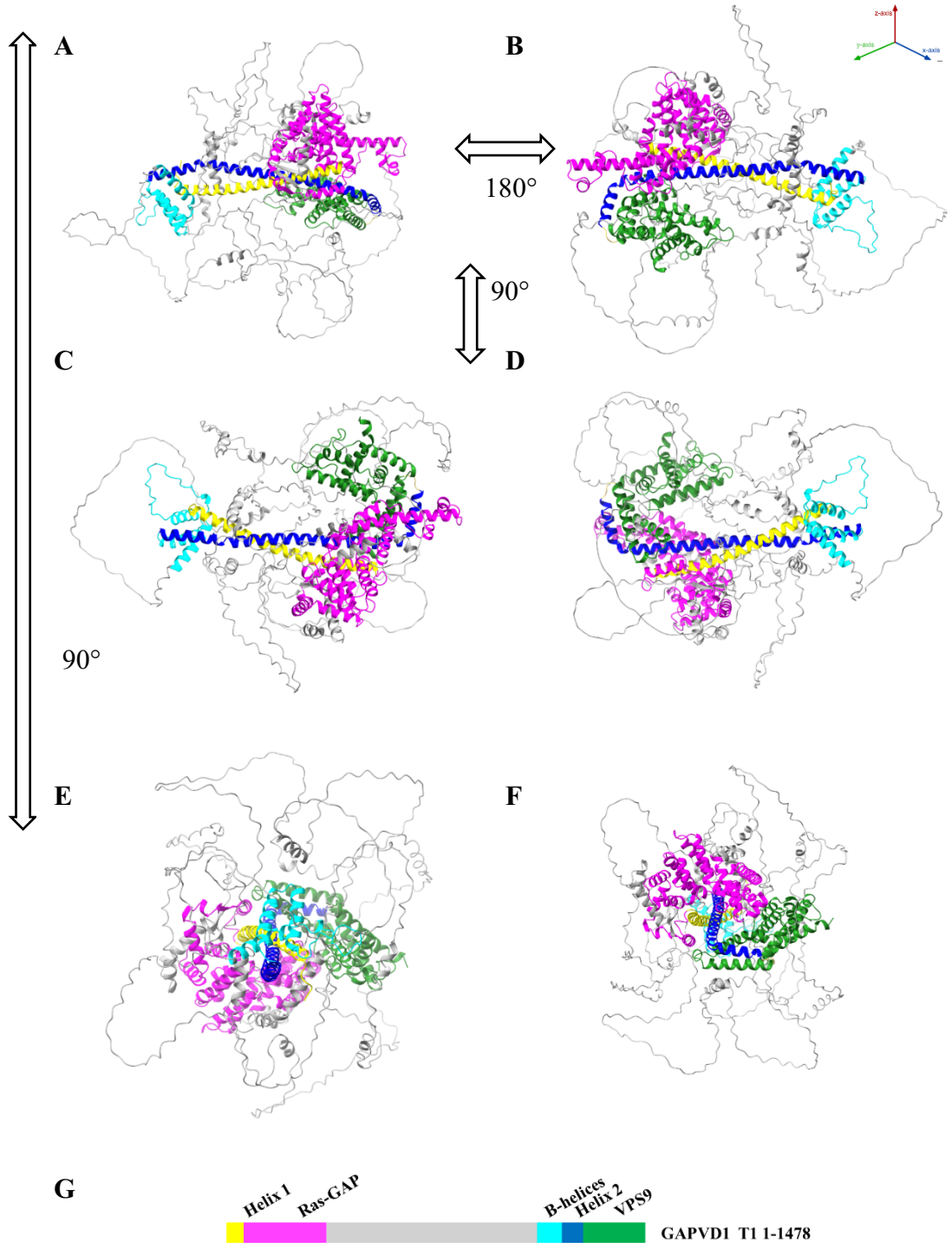

Figure 26. 3D structure of GAPVD1 and schematic overview of its domain structure. GAPVD1 T1 AA 1-1478 is shown with Helix 1 (yellow), RasGAP (magenta), IDR (gray), bottom (cyan) Helix 2 (blue) and VPS9 domain (green). A) Left View: Looking along the negative X-axis (from the left side of GAPVD1). B) Right View: Looking along the positive X-axis (from the right side of GAPVD1). C) Top View: Looking along the negative Z-axis (from above GAPVD1). D) Bottom View: Looking along the positive Z-axis (from below GAPVD1). E) Front View: Looking along the negative Y-axis (facing GAPVD1). F) Back View: Looking along the positive Y-axis (facing the backside of GAPVD1). G) Schematic overview of GAPVD1 domains.

4.4.1. Deletions of predicted GAPVD1 domains and their effects on GAPVD1-PER2 and GAPVD1-CSNK1D binding.

Different truncated mutants of GAPVD1 were constructed to allow the characterization of GAPVD1 binding to CSNK1D and PER2. As mentioned earlier the GAPVD1 variant M2 binds efficiently to PER2 and CSNK1D (Buschhaus, 2021). To further narrow down the binding domain in M2 (AA679-1478), deletions of the structured part at the C terminus of M2 were performed. The mutant proteins were designated as M2ΔVPS9 (AA679-1260) and M2ΔH2 (AA679-1192) (Figure 27). In addition, since the coiled coil structure of H1 and H2 is intriguing because it provides an apparent "spine/backbone" to the protein (Truebestein and Leonard, 2016), a full length GAPVD1 construct lacking H1 was constructed designated as T1ΔH1 (AA60-1478) in order to break up the rigidity in this part of the protein (Figure 27).

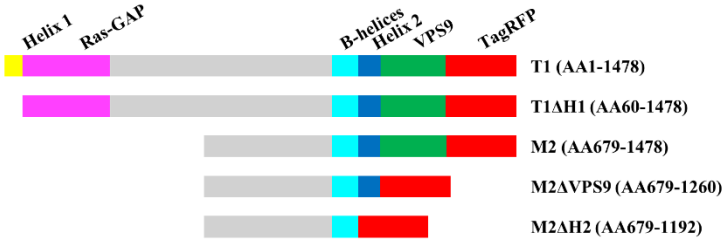

Figure 27. A schematic representation of the GAPVD1 deletion mutants. Top: full length GAPVD1 (Ensembl Transcript 1) (AA1-1478), Helix 1 (yellow), Ras-GAP (magenta), IDR (gray), B helices (cyan) Helix 2 (blue), VPS9 domain (green) and TagRFP (Red). Below T1 are T1ΔH1 (AA60-1478), M2 (AA679-1478), M2Δ VPS9 (AA679-1260), and M2ΔH2 (AA679-1192). All constructs were tagged with tRFP (red) at their C terminus enabling visualization and tracking of the proteins in subsequent experiments.

To investigate which of the GAPVD1 deletion mutants could still bind to PER2 or CSNK1D, HEK293T cells were transiently transfected with the GAPVD1 mutants shown in Figure 27. Immunoprecipitation assays were performed using tRFP antibodies and the enriched proteins were then analyzed using western blot. Figure 28 shows western blots of whole cell extracts, immunoprecipitated and co-immunoprecipitated proteins. These were probed with antibodies against tagRFP, GFP, and CSNK1D. The presence of signals corresponding to the transfected proteins in the input samples indicates successful transfection and expression of the constructs. The western blot shows that immunoprecipitation of tagRFP yielded a highly intense tagRFP signal at around 27 kDa, consistent with the expected size of the protein. The sizes of the GAPVD1 constructs appeared to be much higher than the calculated sizes. This may be due to phosphorylation or other PTMs. For example, the calculated size of T1 is 192 kDa but it was detected at a higher position than the 250 kDa protein standard band. The Western blot also revealed the presence of several protein bands in each lane, which likely represent degradation products of the proteins. TagRFP cleavage product bands were detected at nearly 27 kDa in all constructs.

M2 showed a higher binding affinity to PER2 but not to CSNK1D compared with full-length GAPVD1, which is in agreement with previous results from our lab (Buschhaus, 2021). Furthermore, the western blot analysis shows that co-immunoprecipitation of PER2 and CSNK1D is slightly increased with M2ΔVPS9 compared to M2, although M2 is expressed at a higher level (Figure 25). This suggests that the VPS9 domain might inhibit binding to PER2 and CSNK1D, potentially by making the yet unknown binding domain(s) in GAPVD1 less accessible to PER2 and CSNK1D. In addition, Western blot analysis demonstrated a slight decrease in the binding of both PER2 and CSNK1D to M2ΔH2 compared to M2 and M2ΔVPS9, suggesting that H2 might play a role in mediating the interaction between GAPVD1 and PER2

or CSNK1D. Meanwhile, the blot also revealved that PER2 or CSNK1D binding to GAPVD1 is barely affected by deletion of H1 in T1.

In summary, the results suggest that VPS9 and H2 might regulate CSNK1D and PER2 binding to GAPVD1. However, since all GAPVD1 mutants analyzed so far have at least residual binding activity towards PER2 and CSNK1D, it was necessary to further truncate the GAPVD1 protein in order to identify domains that are potentially sufficient for binding.

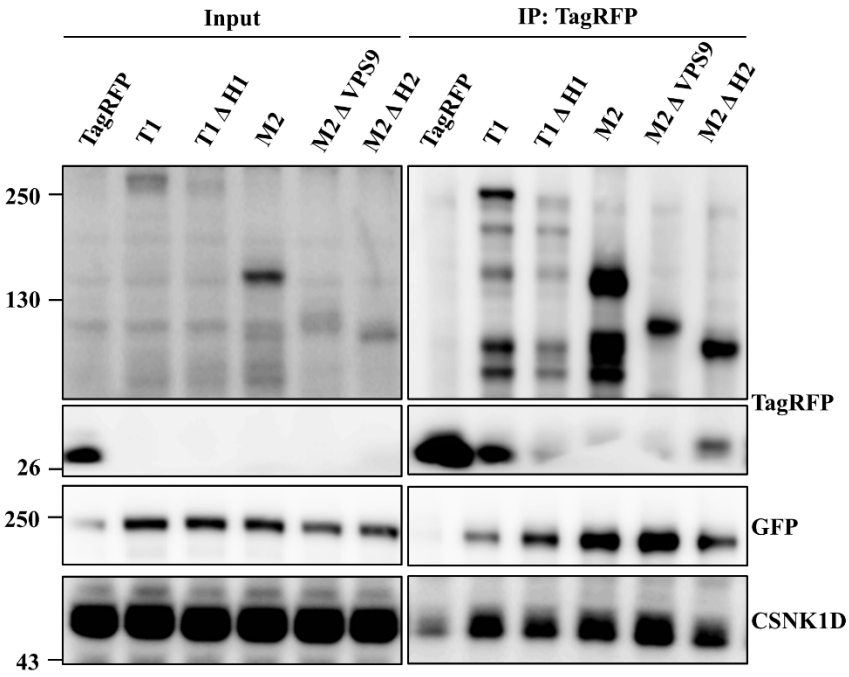

Figure 28. Analysis of the interaction of CSNK1D and PER2 with truncated GAPVD1 mutants. HEK293T cells were transiently transfected with PER2-GFP and either GAPVD1 full length (T1), T1ΔH1, M2, M2ΔVPS9, M2ΔH2 or tagRFP as a control. Immunoprecipitation (IP) was conducted with tagRFP (IP:tagRFP) antibodies and total cell lysate of the trasfected samples. Western blot analysis was performed on input and immunoprecipitates (IP:tagRFP). Antibodies against TagRFP, GFP and CSNK1D were used for detection. Selected bands of a protein size marker are indicated on the left side of each panel. Representative western blot image of three (n=3) independent experiments.

4.4.2. A predicted helical domain at position 1114-1260 of GAPVD1 is a novel binding domain for PER2

In the previous experiment the potential binding domain H2 (AA1193-1260) was discovered. To further narrow down the region in M2 responsible for the interaction with PER2 and CSNK1D, another set of truncated mutants was constructed. Since H2 was shown to affect the interaction between GAPVD1 and PER2 or CSNK1D, the adjacent Bottom domain (AA1114-1192) might also play a significant role. Thus, a deletion of M2 from the C terminus resulted in construction of M2ΔH2B (AA679-1113), which only contains a part of the unstructured region of GAPVD1 (AA1098-1260). A series of constructs was generated, employing a sequential deletion strategy from the N-terminus of M2ΔVPS9. Initially, 103 amino acids were removed, followed by a further 195 amino acids, and finally, an additional 121 amino acids were removed until only the domains H2 and B (AA1114-1260) remained (Figure 29). These three constructs were designated as M2ΔC1, M2ΔC2 and H2B respectively.

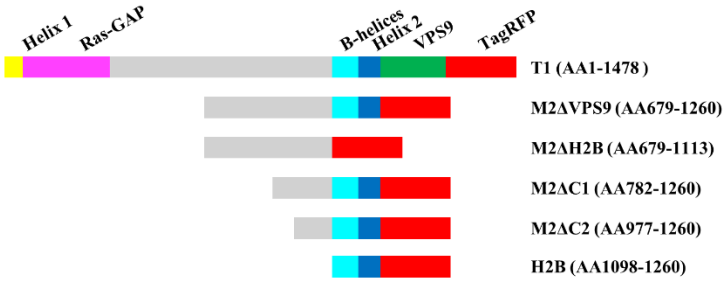

Figure 29. A schematic representation of the GAPVD1 deletion mutants. Top: T1 (AA1-1478), M2Δ VPS9 (AA679-1260), M2ΔH2B (679-1113), M2ΔC1 (782-1260), M2ΔC2 (977-1260), and H2B (1098-1260). *Helix 1 (yellow), Ras-GAP (magenta), IDR (gray), Bottom (cyan), Helix 2 (blue), VPS9 domain (green) and TagRFP (red).* All constructs were tagged with tRFP (red) at their C terminus enabling visualization and tracking of the proteins in subsequent experiments.

To investigate the binding capacity of these constructs, HEK293T cells were transiently transfected. Subsequently, tRFP immunoprecipitation was conducted and the results were analyzed by western blot. Figure 30 shows western blots of whole cell extracts, immunoprecipitated and co-immunoprecipitated proteins. These were probed with antibodies against tagRFP, GFP, and CSNK1D. M2ΔB has a calculated size of 74 kDa but the corresponding protein band was positioned around 100 kDa. This finding is consistent with previous results demonstrating that the IDR is highly phosphorylated. The same was observed for M2ΔC1, which migrated slower than expected, appearing at approximately 95 kDa instead of the expected 84 kDa. However, the M2ΔC2 and H2B constructs migrated at their expected sizes, around 59 kDa and 45 kDa, respectively.

Co-immunoprecipitation analysis demonstrated a prominent reduction in PER2 and CSNK1D binding to M2ΔB compared to T1 and M2ΔVPS9. This result suggests that the bottom domain is crucial for the interaction between GAPVD1 and PER2 or CSNK1D. PER2 and CSNK1D were co-immunoprecipitated with H2B (AA1114-1260), indicating that H2B alone is sufficient for binding to both PER2 and CSNK1D. The N-terminal portion (AA679-1113) preceding H2B does not seem to play a role in binding to PER2 or CSNK1D since there is no difference between M2ΔC1 or M2ΔC2 and M2ΔVPS9. The Bottom domain consisting of the three helical bundle together with Helix 2 is therefore a potential binding domain for PER2 and CSNK2D in GAPVD1. To validate these findings, a full-length GAPVD1 mutant lacking both the H2 and the Bottom domains was generated for further investigation.

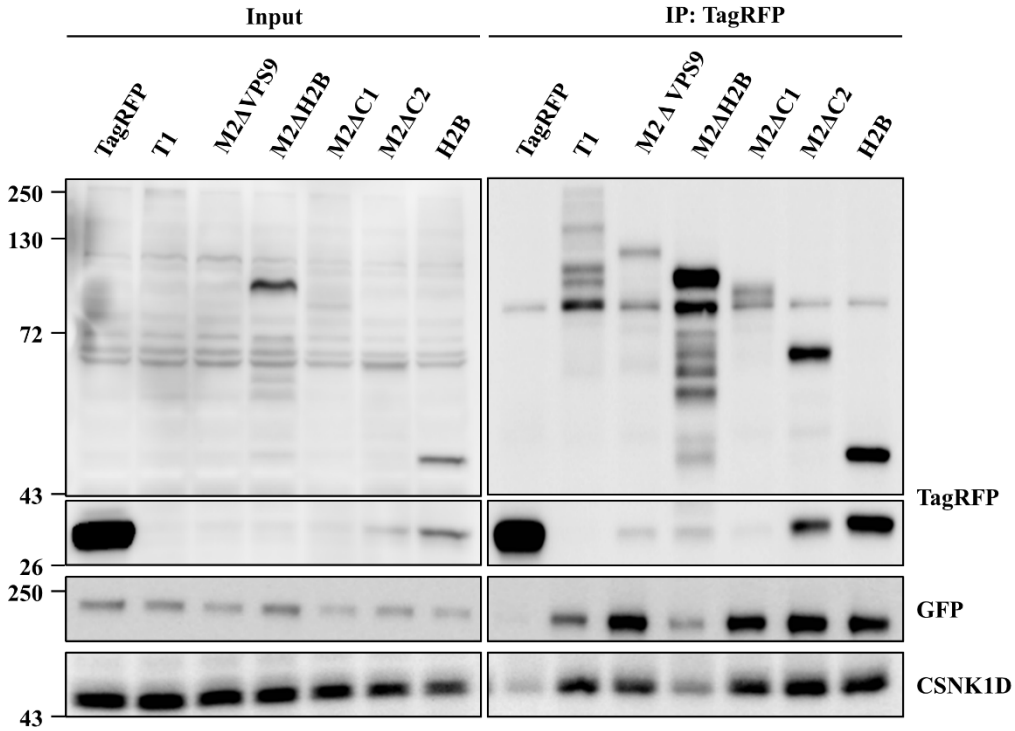

Figure 30. Analysis of the interaction of CSNK1D and PER2 with truncated GAPVD1 mutants. HEK293T cells were transiently transfected with PER2-GFP and either GAPVD1 full length (T1), M2, M2ΔVPS9, M2ΔB, M2ΔC1, M2ΔC2, H2B or tagRFP as a control. Immunoprecipitation (IP) was conducted with tagRFP (IP:tagRFP) antibodies and total cell lysate of the trasfected samples. Western blot analysis was performed on input and immunoprecipitates (IP:tagRFP). Antibodies against TagRFP, GFP and CSNK1D were used for detection. Selected bands of a protein size marker are indicated on the left side of each panel. Representative western blot image of three (n=3) independent experiments.

4.4.3. Beyond H2B: Identification of a Second Binding Site for PER2 in GAPVD1 and VPS9 is a regulatory domain in GAPVD1 that inhibits PER2 binding

The previous experiments have shown that the VPS9 domain of GAPVD1 inhibits binding of PER2 and CSNK1D since M2ΔVPS9 binds stronger to PER2 and CSNK1D than full-length GAPVD1 and all other mutants tested (Figures 25 & 27). The results have also indicated that H2B (AA1114-1260) is sufficient for binding and therefore constitutes a potential interaction surface for CSNK1D and PER2. To further validate these findings, mutant proteins that lack either H2B or VPS9 or both domains were constructed and their ability to bind to PER2 and CSNK1D was examined.

Three mutant GAPVD1 proteins were engineered, as depicted in Figure 31. One mutant lacks residues 1114-1260, resulting in a truncated GAPVD1 protein that lacks the H2B domain. Another mutant has a deletion from the C-terminal end of the full-length GAPVD1 protein removing residues 1261-1478. This deletion encompasses the VPS9 domain. The third mutant has an even more extensive deletion, removing residues 1114-1478, encompassing both the H2B and VPS9 domains.

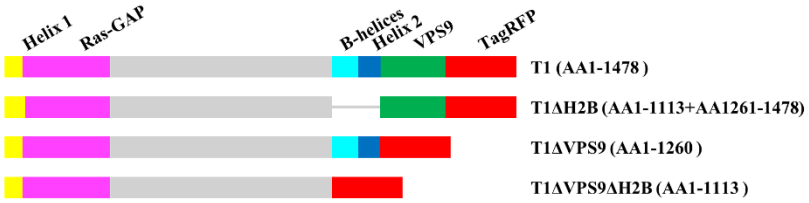

Figure 31. Schematic representation of the GAPVD1 deletion mutants. Top: full length GAPVD1 (Ensembl Transcript 1) (1-1478 aa), T1ΔH2B (1-1113) and (1261-1478) Δ1114-1260, T1ΔVPS9 1-1260 Δ 1261- 1478, and T1ΔVPS9ΔH2B 1-1113 Δ1114-1478. Helix 1 (yellow), Ras-GAP (magenta), IDR (gray), Bottom (cyan), Helix 2 (blue), VPS9 domain (green) and TagRFP (red). All constructs were tagged with tRFP (red) at their C terminus enabling visualization and tracking of the proteins in subsequent experiments.

To investigate the binding ability of these mutants, HEK293T cells were transiently transfected, TagRFP immunoprecipitation was performed, and the precipitates were analyzed using western blotting (Figure 32). The western blot showed that PER2 co-immunoprecipitated with full-length GAPVD1 (T1) and T1ΔH2B (Figure 32A). In other words, and contrary to our expectation based on the result shown in Figure 30, T1ΔH2B retained the ability to bind to PER2 and CSNK1D. Therefore, I hypothesized that GAPVD1 may have additional domains that can interact with PER2. Furthermore, PER2 also bound to T1ΔVPS9H2B, which adds further evidence to the notion that GAPVD1 might have at least two binding domains for PER2 (Figure 32B). Unlike PER2, CSNK1D seemed to bind less to T1ΔH2B and T1ΔVPS9H2B compared to full-length GAPVD1, indicating that loss of the H2B domain affects to some extent GAPVD1-CSNK1D binding (Figure 32B).

The results also showed more binding of T1ΔVPS9 to PER2 compared to full-length GAPVD1 thus highlighting the potential impact of VPS9 as inhibitory domain for PER2 or CSNK1D binding to GAPVD1 (Figure 32B). This is consistent with my previous results in which M2ΔVPS9 showed more binding to PER2 compared to M2 (Figure 28). In addition, all mutants that lack the VPS9 domain show similar effects, for example M2ΔC1, M2ΔC2 and H2B (Figure 30). The fact that PER2 binds to T1ΔVPS9H2B to a similar degree as T1ΔVPS9 and stronger than full-length GAPVD1 implies that the VPS9 domain exerts its inhibitory action not only on the H2B domain but also on a hypothetical additional binding domain for PER2 and/or CSNK1D. The VPS9 domain is known to be involved in protein sorting and vesicle trafficking (Carney et al., 2006; Sakura et al., 2016). Therefore, deletion of VPS9 could alter GAPVD1 localization, e.g. by moving it towards or away from membranous vesicles, thereby affecting its interaction with PER2. To investigate whether the VPS9 domain influences the localization of GAPVD1, I aimed to determine whether GAPVD1 lacking the VPS9 domain exhibits the same subcellular localization as full-length GAPVD1.

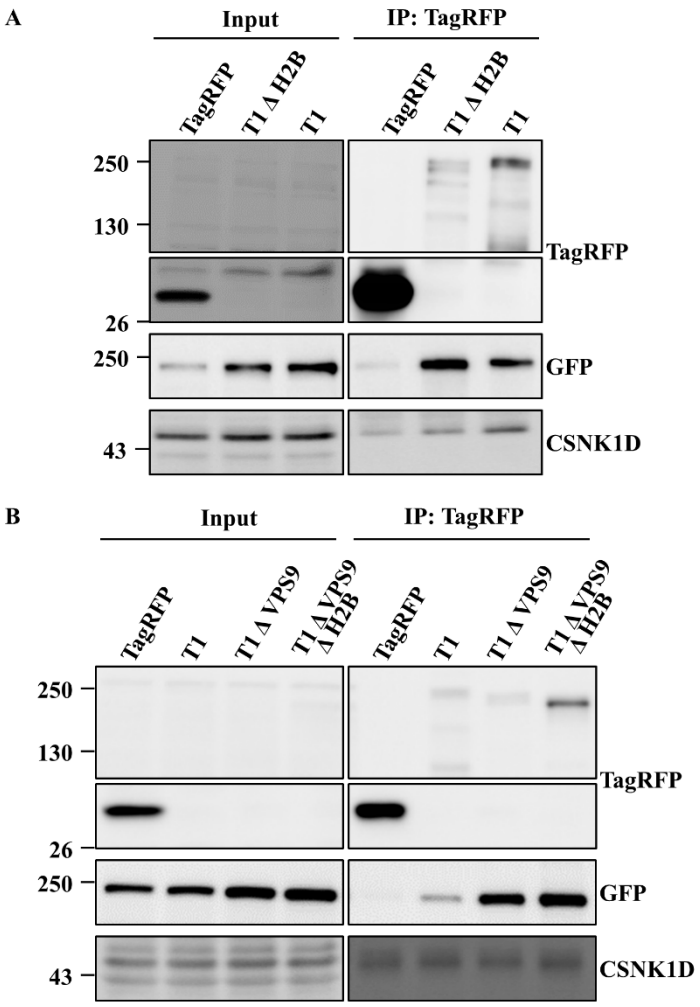

Figure 32. Analysis of the interaction of CSNK1D and PER2 with truncated GAPVD1 mutants. A: HEK293T cells were transiently transfected with PER2-GFP and either GAPVD1 full length (T1), T1ΔH2B or tagRFP as a control. B: GAPVD1 full length (T1), T1ΔVPS9, T1ΔVPS9ΔH2B, or tagRFP as a control. Immunoprecipitation (IP) was conducted with tagRFP (IP:tagRFP) antibodies and total cell lysate of the trasfected samples. Western blot analysis was performed on input and immunoprecipitates (IP:tagRFP). Antibodies against TagRFP, GFP and CSNK1D were used for detection. Selected bands of a protein size marker are indicated on the left side of each panel. Representative western blot image of three (n=3) independent experiments

4.4.4. Deletion of VPS9 does not change the gross subcellular localization of GAPVD1

The previous results indicate a regulatory function of the GAPVD1 VPS9 domain. However, one possibility is a potential mislocalization of GAPVD1 without VPS9 domain, which might result in increased PER2 binding. To eliminate the possibility that VPS9 deletion causes GAPVD1 mislocalization and thereby alters PER2 binding, localization studies were conducted. HEK293T cells were transiently transfected with four constructs. PER2-GFP was co-transfected with either TagRFP, T1-tagRFP or T1ΔVPS9-tagRFP or M2ΔVPS9-tagRFP. Fluorescence microscopy was utilized to capture live cell images 72 hours following transfection (Figure 33).

Live-cell imaging using fluorescence microscopy with tagRFP as a control demonstrated that RFP was distributed uniformly throughout the cell, while PER2 exhibited a preferential localization to the cell nucleus (Figure 33). Upon co-expression of GAPVD1 PER2 still

predominantly resided in the cell nucleus, whereas GAPVD1 was exclusively observed in the cytoplasm, with no detectable nuclear localization Figure 33. This shows that overexpression of GAPVD1 does not affect PER2 localization, which also indicates that the interaction between PER2 and GAPVD1 does not alter the localization of PER2. Figure 33 shows that T1ΔVPS9 seemed to have the same localization pattern as GAPVD1, suggesting that the VPS9 domain does not affect GAPVD1's gross cellular localization. Moreover, PER2-GFP exhibited a persistent nuclear localization indicating that deletion of the VPS9 domain does not affect PER2 localization. These findings collectively demonstrate that the cytosol/nucleus distribution of PER2, GAPVD1, T11ΔVPS9 and M2ΔVPS9 remains unchanged despite their mutual presence. The increased binding of PER2 to VPS9-deletion mutants in the immunoprecipitation experiment is therefore likely to be attributed to a mechanism other than a change in subcellular localization, requiring further investigation to elucidate the underlying mechanism.

In summary, PER2 had a nuclear localization under all conditions, regardless of the overexpressed GAPVD1 mutants. Deletion of the VPS9 domain did not alter GAPVD1's gross cytoplasmic localization. Collectively, these results indicate that the enhanced binding of T1ΔVPS9 and M2ΔVPS9 to PER2 is independent of their respective subcellular localizations.

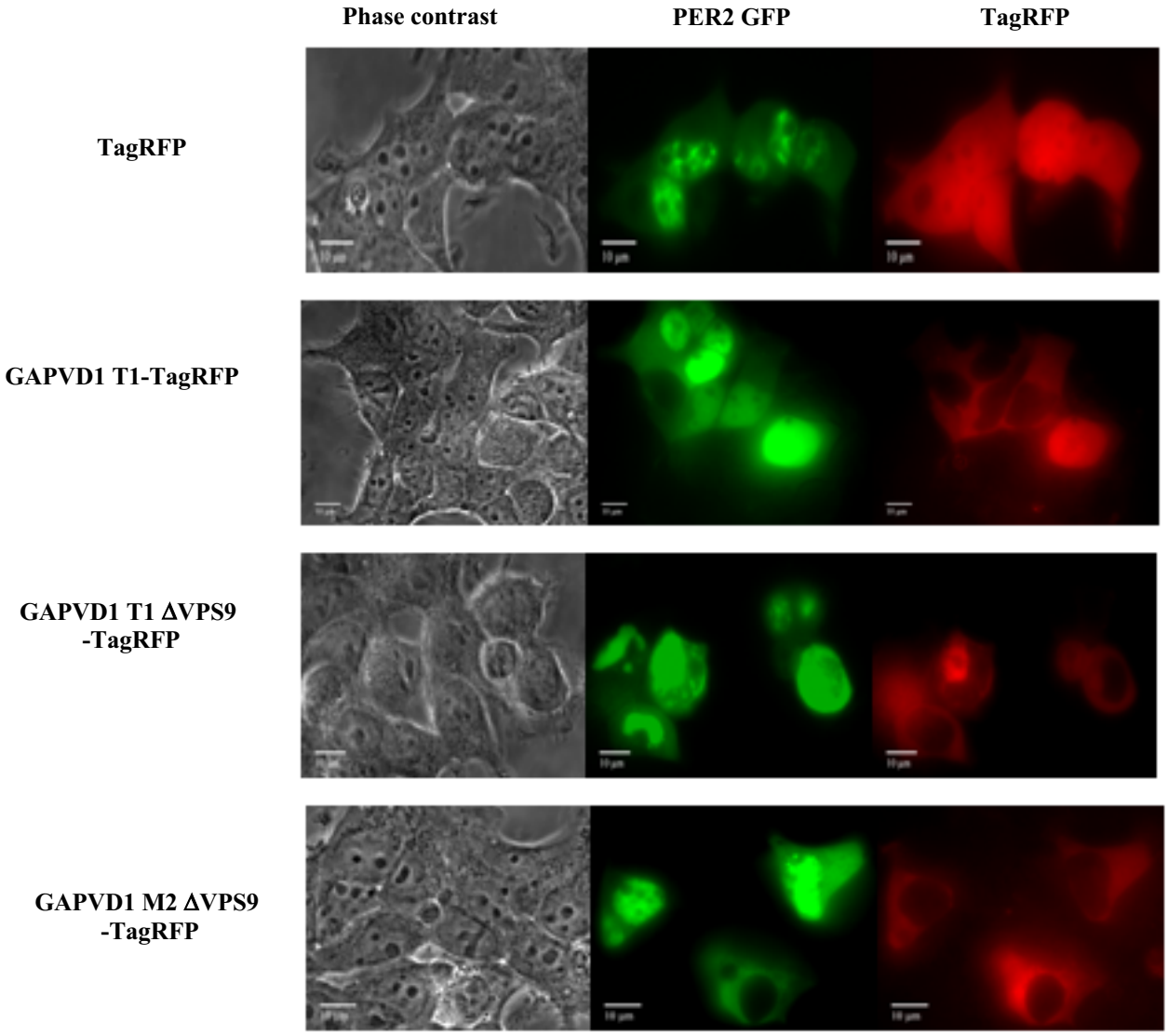

Figure 33. Distribution of PER2-GFP with coexpression of different constructs of GAPVD1. HEK293T cells were transiently transfected with PER2-GFP and either GAPVD1 full length (T1), T1ΔVPS9, M2ΔVPS9 or tagRFP as a control. Selected epifluorescence microscopy images of different cells that express PER2-GFP in green with either TagRFP, T1, T1 Δ VPS9 or M2 Δ VPS9 in red. Shown are representative phase-contrast and fluorescence pictures of PER2-GFP and different constructs of GAPVD1-TagRFP. Bar 10 µm.

5. Discussion

5.1. GAPVD1 is part of the PER complex

The aim of this study was to identify and characterize binding partners of the clock protein PER2 to broaden our comprehension of the cellular function of PER2 beyond its established role as a transcription factor. The affinity enrichment - mass spectrometry (AE-MS) analysis identified several binding proteins of PER2. At their apex are, with the exception of PER3, all PER complex components that were described in mice (Aryal et al., 2017). Most interestingly, the AE-MS and co-immunoprecipitation results also identified GAPVD1 as PER2 binding partner similar to the findings in mouse tissue (Aryal et al., 2017). GAPVD1 stands for GTPase Activating Protein and VPS9 Domains 1 which acts both as a GTPase-activating protein (GAP) and a guanine nucleotide exchange factor (GEF) facilitating its function in processes such as vesicle mediated transport (Guillen et al., 2020). This MS study, which was done on HT1080 cells, is the first study that detected GAPVD1 as PER2 binding protein in human cells. Several studies before that used PER2 as a bait failed to detect GAPVD1. For example, Wu and colleagues successfully identified regulatory-associated protein of mTOR (Raptor), a key component of the mTORC1 complex, as PER2 binding partner after IP of Flag-PER2 in HEK293T cells (Wu et al., 2019). GAPVD1 was not detected in this study. Neither did Gul and his colleagues detect GAPVD1 in a Streptavidin pull-down of biotinylated PER2 from U2OS cells that stably express PER2-13xLinker-BioID2-HA (Gul et al., 2022). Moreover, it has been shown that there is a very close association between GAPVD1 and either CSNK1D or PER2 in situ as demonstrated by proximity ligation assay (PLA) that detects protein associations only if two proteins are spaced at a distance of less than ~30 nm (Ibrahim et al., 2021; Mundorf, 2022). On the other hand, in a LC-MS/MS analysis of HEK293 cells that stably express dually-tagged CSNK1D, GAPVD1 was identified at all circadian time points examined (Kategaya et al., 2012). Likewise, in my experiment with synchronized U2OS cells, GAPVD1 was co-immunoprecipitated with CSNK1D at all circadian time points throughout the day. Taken together, my data along with other studies support the conclusion that GAPVD1 is part of the mammalian PER complex in different organisms and cell lines.

It is unclear why my experiment did not detect the known PER2-binding partner PER3, which stands in contrast to the finding in (Aryal et al., 2017). One possible reason why PER3 was missing is that PER3 has tissue-specific functions in circadian rhythmicity (Pendergast et al., 2012) and might therefore not be expressed at a sufficient quantity in HT1080 cells. Moreover, PER3 and other clock proteins are significantly downregulated in cancer cells such as colorectal cancer (Karantanos et al., 2013; Mazzoccoli et al., 2011; Oshima et al., 2011). It is noteworthy in this context that HT1080 cells are epithelial cells derived from connective tissue from a human patient diagnosed with fibrosarcoma. Moreover, the process of transfection itself may affect PER3 expression levels. For example, stable expression of a non-clock related protein such as hepatitis B virus X protein (HBx) involved in hepatocellular carcinogenesis, can alter the mRNA expression levels of core clock genes and thereby lead to downregulation of PER3 along with BMAL1, CRY1/2 and CSNK1D as well as upregulation of CLOCK and PER1/2 (Yang et al., 2014). Likewise, PER2 overexpression could lead to downregulation of PER3 expression. In addition, it is not uncommon to fail to identify strong binding partners of a protein by mass spectrometry. For example, PER2 and PER3 were not identified as binding partners of HA-PER1 in primary mouse hepatocytes (Wu et al., 2019). The same group did not identify PER1 and PER3 as binding partners of Flag-PER2 in cytoplasmic extracts of HEK293T cells (Wu et al., 2019). Neither PER1 nor PER3 were identified as binding partners of biotinylated PER2 in U2OS cells at two different circadian time points (Gul et al., 2022).

5.2. Beyond GAPVD1: Discovery of novel PER2 binding partners

Arguably, the main discovery of this thesis is the identification of GAPVD1 as a novel PER2 binding protein and the study of their mutual relationship. Beyond GAPVD1, AE-MS has revealed a plethora of additional PER2 binding partners, including proteins involved in transcription, mRNA regulation, chromatin remodeling and vesicular transport. Although our investigation aimed to identify only individual protein binding partners, surprisingly, the findings revealed associations of PER2 with various distinct proteins that form protein complexes. These include the COPI complex, the AP2 complex, the MCM complex, and the SKI complex. These findings suggest that PER2's regulatory network is more intricate and extensive than previously thought.

The identification of these proteins that form complexes might hold significant biological implications. For instance, association of several proteins of the COPI complex with PER2 suggests potential involvement of circadian regulation in intracellular transport processes (Arakel and Schwappach, 2018). Enrichment of AP2 complex proteins may indicate a role of the circadian clock in endocytosis and vesicle trafficking, while proteins of the MCM and SKI complexes could link the clock to DNA replication and transcriptional regulation, respectively (Faini et al., 2013; Kögel et al., 2022; Lei, 2005). Furthermore, mutual functional relationships between the circadian clock and complexes formed by the newly identified proteins have to be considered, as they can often affect each other in unexpected ways. For example, the circadian clock and clathrin-mediated endocytosis might not be independent processes, but they might influence each other in a number of ways. Such mutual relationships are central for the proper functioning of cells. For example, melanopsin, a photopigment expressed in retinal ganglion cells (RGCs) is a circadian photoreceptor (Beaulé et al., 2003) and at the same time it undergoes endocytosis in a clathrin-dependent manner (Valdez-Lopez et al., 2020). Hence, clathrin-mediated endocytosis may also influence the circadian clock. Endocytosis also removes receptors from the plasma membrane, which could disrupt signaling pathways that are involved in circadian rhythm regulation (Xu et al., 2017). On the other hand, the circadian clock regulates the expression of receptors that bind to ligands that promote endocytosis and in this way the circadian clock can influence which molecules are taken up by endocytosis (Akhtar et al., 2002; Yeung et al., 2022). For example, PER2 regulates the diurnal expression of Na+/H+ exchanger regulatory factor-1 (NHERF1) and its scaffolding function (Tsurudome et al., 2018). NHERF1 as a scaffolding protein allows the close proximity and correct conformation of membrane proteins and their associated effectors, facilitating signaling efficiency (Vaquero et al., 2017). In this case PER2 functions as a transcriptional modulator as PER2 binds to p65 protein and prevents p65/p50-mediated transactivation of *NHERF1* (Tsurudome et al., 2018). Our results demonstrated interaction of PER2 with the AP2 complex, and others showed that PER2 works as a scaffolding protein, which recruits TSC1 to the mTORC1 complex (Wu et al., 2019). Therefore, we suggest that a similar mechanism might involve PER2 recruiting the AP2 complex to for example the plasma membrane.

Rhythmic RNA expression is a pertinent phenomenon in the circadian system and is driven either by rhythmic RNA synthesis or rhythmic RNA degradation or a combination of both (Nolte and Staiger, 2015). In addition, *PER2* is among others a clock gene mRNA that exhibits circadian rhythmicity, which is regulated through various mechanisms including mRNA degradation (Lee et al., 2014; Woo et al., 2009). These studies also showed that rhythmic RNA expression is based mostly on transcription factors within the molecular clock. For example, PER2 can regulate its own mRNA levels by inhibiting the activity of the CLOCK-BMAL1 complex (Cao et al., 2021). The SKI complex, cytoplasmic co-factor and regulator of the RNA-degrading exosome (Kögel et al., 2022), has been identified in this study as a PER2 binding

partner. PER2 might be involved in SKI complex assembly, recruitment, or phosphorylation as emerging evidence of a cytoplasmic function of PER2 (Ibrahim et al., 2021; Wu et al., 2019). This would suggest a potential link between PER2 and the modulation of RNA stability or turnover through a PER2-SKI axis. Further experiments, including validation studies and functional assays, are warranted to validate and characterize the regulatory role of PER2 in conjunction with the SKI complex. The identification of the interaction between PER2 and the SKI complex opens avenues for future research. Additionally, understanding the dynamics of the association of the SKI complex with PER2 could provide insights into broader regulatory networks governing mRNA processing in circadian rhythms.

Existing studies revealed limited prior evidence of PER2 forming complexes with COPI, AP2, MCM, or SKI. Our study, therefore, contributes novel insights into the composition and potential functions of these complexes in the context of circadian rhythm regulation. Given that I did not verify these interactions with an alternative approach, it is crucial to recognize the limitations of our study. Affinity enrichment methods may suffer from non-specific interactions with components present in the sample matrix, such as lipids, nucleic acids, or other cellular debris, leading to background noise or interference (Kim et al., 2018). Further investigations such as co-immunoprecipitation and similar validation studies are necessary to enhance the reliability of these results. Building on these discoveries, future research directions may involve exploring the functional implications of these complexes in circadian rhythm regulation. Additionally, an in-depth analysis of additional components within these complexes and the regulatory mechanisms governing their assembly and disassembly would provide a more comprehensive understanding of PER2-associated molecular pathways. The identification of novel PER2 binding partners has opened new avenues for research, offering insights into the molecular mechanisms underlying circadian rhythm regulation. By unraveling the complex interactions of PER2, we can gain a deeper understanding of how the circadian clock maintains homeostasis and orchestrates physiological processes across the organism. Additionally, these findings hold promise for the development of novel therapeutic approaches for circadian rhythm disorders, such as jet lag and sleep disorders.

In summary, mass spectrometry has played a pivotal role in expanding our knowledge of PER2's molecular landscape. The identification of novel PER2 binding partners has provided valuable insights into the intricate network of interactions that regulate circadian rhythms. These findings are paving the way for further research on the molecular basis of circadian rhythms and the development of novel therapeutic strategies for circadian rhythm disorders.

5.3. Phosphorylation of GAPVD1 is regulated by the PER complex

In my thesis GAPVD1 phosphorylation has been revealed to be regulated by the PER complex using different approaches such as protein mobility shift combined with siRNA knockdown or kinase inhibition or mass spectrometry analysis. Treatment of cells with CSNK1D specific siRNA disturbs the normal phosphorylation levels of GAPVD1. This result is in alignment with another study that has demonstrated that CSNK1D phosphorylates GAPVD1 (Guillen et al., 2020). Additional knockdown of CSNK1E, a closely related family member of CSNK1D, only subtly enhanced this effect. This suggests that CSNK1D/E are both involved in GAPVD1 phosphorylation but CSNK1D seems to play the bigger role. My results do not allow me to conclude that CSNK1E alone can phosphorylate GAPVD1; only a knockdown of CSNK1E alone would be able to answer this question. Notably, CSNK1D/E can phosphorylate PER2 in vitro and in cultured cells (Akashi et al., 2002; Camacho et al., 2001; Keesler et al., 2000; Vielhaber et al., 2000). In summary, the results suggest that both kinases phosphorylate

GAPVD1 and that CSNK1D is the default kinase for setting the phosphorylation levels of GAPVD1.

The participation of the PER complex in GAPVD1 phosphorylation had been unknown and has been addressed in this study as well. In the loss of function experiments, the requirement for either PER1 or PER2 in this mechanism suggests that the CSNK1D-mediated phosphorylation of GAPVD1 is indeed influenced by the PER complex. One interesting feature of clock proteins is their redundancy (i.e., CLOCK and NPAS2, PER1 and PER2, CRY1 and CRY2). The PER1 and PER2 proteins share a similar role in regulating CRY1 activity, suggesting some redundancy between the two proteins (Akashi et al., 2014). Despite that, PER1 has also nonredundant roles in the circadian clock (Bae et al., 2001; Zheng et al., 2001), specifically in regulating CRY2 activity (Akashi et al., 2014). PER3 has tissue-specific functions in circadian rhythmicity (Pendergast et al., 2012), and this indicates non-redundant roles of PER3 and PER2. Tissue-specific function is generally common in the circadian system, for example for molecular oscillator function NPAS2 holds greater significance in the brain, while CLOCK is more important in peripheral tissues (DeBruyne et al., 2007a, 2007b). Despite some redundancy in PER1/2 function, their combined action seems to be crucial for specific regulatory steps, such as GAPVD1 phosphorylation. These findings further emphasize the nuanced, partially redundant and partially non-redundant roles of clock proteins within the circadian system. In summary, one crucial function of the PER complex is the regulation of GAPVD1 phosphorylation, and our recent study has indicated that PER2 neutralizes the autoinhibitory function of the C-terminal domain of CSNK1D, which in turn enhances CSNK1D-dependent phosphorylation of GAPVD1 (Ibrahim et al., 2021).

Nonetheless, my findings do not exclude the possibility that phosphorylation of GAPVD1 by CSNK1D may also occur outside of PER complexes. (Batty et al., 2020; Guillen et al., 2020) showed that CSNK1D phosphorylates GAPVD1 in *in vitro* kinase assays with no involvement of PER2. Phosphorylation of GAPVD1 by CSNK1D alone also takes place in human red blood cells, which do not contain PER2 protein, infected with *Plasmodium falciparum* (Batty et al., 2020). The involvement of a potential pfPER2 can not be excluded, however. Consequently, CSNK1D alone can phosphorylate GAPVD1, and PER2 seems to be capable of modulating this phosphorylation.

However, my experiments also showed that phosphorylation of GAPVD1 is not entirely hindered by the specific inhibition of CSNK1D, other kinases may also be involved in GAPVD1 phosphorylation alongside with or independently of CSNK1D. CK1 preferably phosphorylates substrates that are prephosphorylated (primed) at the -3 position (Flotow et al., 1990), for example in the case of phosphorylation of the FASP site in PER2 (Marzoll et al., 2022). Priming phosphorylation of GAPVD1 despite specific inhibition of CSNK1D could be due to other priming kinases that work alongside with CSNK1D. Indeed, GAPVD1 has been shown to be phosphorylated by other kinases, which are listed in Table 32. Phosphorylated amino acids uniquely identified in this thesis are highlighted in red. Kinases that also phosphorylate GAPVD1 are 5' adenosine monophosphate-activated protein kinase (AMPK) (Ducommun et al., 2019), Cyclin-dependent kinase 1 (CDK1) (Blethrow et al., 2008) and Transforming growth factor-β (TGF-β)-activated kinase 1 (TAK1) (Levin et al., 2016).

AMPK is known to phosphorylate CRY1, a PER complex component, at S71 or S280, which leads to its destabilization (Lamia et al., 2009). My results show that S902 and S903 at site 5 are highly responding to PER complex-dependent phosphorylation activity (Ducommun et al.,

2019), and GAPVD1 S902 is a consensus site for AMPK, which itself has a diurnal rhythm (Jordan and Lamia, 2013). Thus, AMPK might be involved in GAPVD1 phosphorylation within the PER complex. In addition, AMPK phosphorylates CSNK1E at S389 which leads to increased kinase activity (Um et al., 2007). Thus, activation of CSNK1E/D by AMPK might also play a role in GAPVD1 phosphorylation. Moreover, CDK1 kinase activity shows temporal rhythmicity in a phosphoproteome analysis (Robles et al., 2017), and is inhibited by Wee1-dependent phosphorylation (Harvey et al., 2005). Notably, Wee1 expression is induced by CLOCK/BMAL1 (Gérard and Goldbeter, 2012; Matsuo et al., 2003), and therefore CDK1-dependent phosphorylation of GAPVD1 could be under circadian control through indirect inhibition by CLOCK/BMAL1.

TAK1, a member of the MAPK kinase kinase (MAPKKK) family, might phosphorylate GAPVD1 at S1012 and T1013 (Levin et al., 2016). In addition, TAK1 is known to regulate the p38 MAPK signaling pathway, which modulates the endogenous oscillator (Goldsmith and Bell-Pedersen, 2013). Although my results do not provide direct evidence for it, GAPVD1 could be involved in any of these pathways since its phosphorylation is not fully blocked by inhibition of CSNK1D/E.

It is tempting to ask if the regulation of GAPVD1 phosphorylation shows similarities to the phosphoswitch model of PER2. The PER2 phosphoswitch is based on two antagonistic phosphorylation sites (Figure 5) (Masuda et al., 2020; Narasimamurthy and Virshup, 2021). Phosphorylation of one site, the so-called FASP site, blocks the phosphorylation of the other site, the so-called Degron site. While phosphorylation of the FASP site leads to the stabilization of PER2, phosphorylation of the Degron site leads to PER2 degradation. In HT1080-CP cells, the phosphorylation of some sites correlated with the overexpression of PER complex components, i.e., site 3 and 5 and to a lesser extent site 7 were highly phosphorylated under this condition. The phosphorylation level of site 6, which is next to site 5, was at its lowest level under identical conditions. Another evidence is that we have found in another study that CSNK1D inhibitor treatment of HT1080 cells, where site 5 is dephosphorylated and site 6 is phosphorylated in my experiment, leads to significantly delayed degradation of GAPVD1 (Ibrahim et al., 2021). Conversely, under conditions in which CSNK1D was highly active, site 5 was highly phosphorylated and site 6 dephosphorylated, and degradation of GAPVD1 was accelerated (Ibrahim et al., 2021). Analyses of degradation kinetics of relevant GAPVD1 point mutations, e.g. in site 3, 5, 6 and 7, might shed more light on this question in the future.

Table 21: Summary of phosphorylation sites found in GAPVD1

Study		This thesis	(Guillen et al., 2020)	(Batty et al., 2020)	(Levin et al., 2016)	(Blethrow et al., 2008)	(Ducommun et al., 2019)
Kinase		CSNK1D			TAK1	CDK1	AMPK
1	T390	X					
	T391			X			
2	S461			X			
	S466	X					
3	T562	X					
	S566	X	X				
	S569	X	X				
4	S757	X					
	S758	X					
	S761	X					
	T762	X					
	S740		X				
	S742		X				
	S746		X				
	S747		X				
5	S902	X	X	X			X
	S903	X	X	X			
	S914			X			
6	S949	X					
	S950	X					
	S972			X			
	987					X	
	S999			X			
7	S1096	X					
	S1104			X			
	S1105	X					
	S1012				X		
	S1013				X		

My results suggest that the PER complex regulates GAPVD1 phosphorylation in a temporal manner. I have demonstrated that GAPVD1 phosphorylation follows a circadian rhythm, with higher levels observed during the day and lower levels at night. Interestingly, it has also been revealed that the same site 5 that seemed to be responsive to PER complex-mediated phosphorylation in my thesis, undergoes rhythmic phosphorylation in mouse tissue (Robles et al., 2017). Therefore, it is plausible that site 5 might be at least in part responsible for the circadian rhythmicity of GAPVD1. This finding aligns with existing knowledge about circadian rhythmicity of other clock proteins. In analogy to the circadian phosphorylation levels of GAPVD1, PER1 and PER2 within the PER complex show likewise rhythmicity in their protein abundance and phosphorylation levels (Lee et al., 2001). In particular, phosphorylation at S693 and S697 is oscillating, and CDK5 phosphorylates PER2 at S394 in a diurnal manner, which promotes its interaction with CRY1 and facilitates their nuclear translocation (Brenna et al., 2019). Moreover, CRY1/2 show rhythmic temporal phosphorylation at CRY1 S588 and CRY2 S557 (Robles et al., 2017). Taken together, this indicates that GAPVD1 phosphorylation by the

PER complex might play a role in circadian clock function, potentially by facilitating the binding of other proteins, promoting subcellular localization changes, and regulating protein stability.

Several factors might contribute to the temporal phosphorylation pattern of GAPVD1 as my findings demonstrate that the binding of GAPVD1 to CSNK1D is also rhythmic, which suggests temporal enzymatic activity of CSNK1D towards GAPVD1. Another factor contributing to the temporal phosphorylation of GAPVD1 might be rhythmic kinase activity exhibited by several kinases known to phosphorylate GAPVD1. Examples include CSNK1D, AMPK, and CDK1, all of which display rhythmic kinase activity (Jordan and Lamia, 2013; Robles et al., 2017).

In summary, GAPVD1 as part of the PER complex exhibits rhythmic phosphorylation levels, which could well be connected to its cellular role. Phosphorylation is considered a cornerstone of clock function with a double role in the molecular clockwork and a central mechanism for the circadian control of metabolism and physiology (Brenna and Albrecht, 2020; Robles et al., 2017). Phosphorylation as part of the post-translational machinery regulates the pace of the clock itself. On other hand, phosphorylation can be an output mechanism of the clock to impose an overt rhythm upon other cellular components.

5.4. GAPVD1 regulation as an output mechanism of the clock

My data showed that GAPVD1 phosphorylation is regulated by the PER complex and also that GAPVD1 phosphorylation exhibits circadian rhythms in synchronized U2OS cells. This implies that GAPVD1 phosphorylation could be part of a circadian output system. GAPVD1 is a regulator of small G proteins such as RAB31, RAB5 and RAS. Small G proteins are a family of proteins that act as molecular switches and play a pivotal role in numerous cellular processes, including cell division, cell growth, and cell signaling (Farshadi et al., 2020), all of which are partly under circadian clock control (Feillet et al., 2015; Shostak, 2017). GAPVD1 has guanine nucleotide exchange factor (GEF) activity for RAB5, RAB31 and GTPase-activating (GAP) activity for RAS (Hunker et al., 2006; Lodhi et al., 2007). Phosphorylation of GAPs/GEFs can either enhance or inhibit their activity, depending on the specific site of phosphorylation and the kinase involved (Bos et al., 2007; Xu et al., 2021). Thus, phosphorylation of GAPVD1 could impact the GAP/GEF functions of these associated proteins.

Indeed, several GEF proteins have been reported to be regulated by phosphorylation. For example, the Non-receptor Tyrosine Kinase (PYK2) phosphorylates Rho guanine nucleotide exchange factor 11 (ARHGEF11), a RhoGEF family member that acts on RhoA GTPase, providing positive regulation of its GEF activity (Ohtsu et al., 2005; Ying et al., 2009). Additionally, it has been demonstrated that FYN, a SRC family kinase positively regulates Leukemia-associated RhoGEF (LARG) activity through tyrosine phosphorylation (Guilluy et al., 2011). GAPVD1 also has GAP activity for RAS (Hunker et al., 2006). A good example that phosphorylation regulates GAP activity is Tuberous sclerosis 2 (TSC2). The GAP activity of TSC2, which together with TSC1 forms the TSC complex that inhibits MTOR (Rehbein et al., 2021), is regulated on different levels. Akt/Protein kinase B kinases such as ERK, PKC, and RSK phosphorylate and inactivate TSC2 (Inoki et al., 2002; Ma et al., 2005; Zhan et al., 2019). Moreover, during low energy states AMPK phosphorylates TSC2 at T1227 and S1345 which increases its GAP activity (Inoki et al., 2003). Furthermore, GSK3 phosphorylates TSC2 at S1337 and S1341, which leads to TSC2 activation, a process that may require AMPK as a priming kinase. (Inoki et al., 2006). It is worth mentioning that PER2 recruits TSC1 to the mTORC1 complex to suppress mTORC1 activity (Wu et al., 2019). In conclusion, these findings highlight the diverse regulatory roles of phosphorylation in GAP/GEF proteins.

Phosphorylation can both activate and inactivate their enzymatic activities, demonstrating the complex and multifaceted control mechanisms within these signaling pathways. Likewise, phosphorylation of GAPVD1 could also potentially affect its GEF or GAP activity, hinting towards a potentially broad role for phosphorylation in regulating GAPVD1 output activity through its GAP/GEF functions. Further investigation into the specific kinases and phosphorylated amino acids responsible for the regulation of GAP/GEF activity might provide a deeper understanding of how these processes influence cellular function and disease development.

The phosphorylation of GAPVD1 might also affect other cellular processes in which GAPVD1 is involved. Indeed, (Guillen et al., 2020) showed that CSNK1D-phosphorylation of GAPVD1 promotes endocytosis, which opens the possibility that the PER complex regulates endocytosis as a circadian output function through the CSNK1D-dependent phosphorylation of GAPVD1. Notably, CSNK1D/E as well as its ortholog Hrr25 in *Saccharomyces cerevisiae* have conserved roles in endocytosis (Peng et al., 2015). The temporal phosphorylation of GAPVD1, which I observed in my experiment, may introduce an additional potential layer of time-dependent regulation for cellular processes related to GAPVD1, such as endocytosis. In addition, the recruitment of GAPVD1 into the PER complex could have implications for its function. GAPVD1 mediates endocytosis through its enzymatic acivity as (Lodhi et al., 2007) showed that upon insulin receptor activation a CIP4/GAPVD1 complex is recruited to the plasma membrane away from RAB31. This leads to a redcution of RAB31 activity that consequently allows Glucose Transporter Type 4 (GLUT4) vesicles to migrate to the cell surface, where they dock and fuse with the plasma membrane, facilitating the transport of glucose into the cell. A similar scenario is possible for formation of a GAPVD1-PER complex, which according to my findings oscillates with a 24h rhythm, and retention of GAPVD1 in the complex may affect its enzymatic activity or other output functions.

Another relevant finding is a specific mutation (Arg910Gln) in GAPVD1 which has been shown to result in steroid-resistant nephrotic syndrome (Hermle et al., 2018). Renal functions such as glomerular filtration rate, renal blood flow, urine production, and electrolyte excretion are well known to exhibit daily oscillations (Stow and Gumz, 2011). Circadian rhythm disruption leads to renal impairment in humans (Firsov and Bonny, 2010). Deleting CLOCK in podocytes, terminally differentiated cells that have a crucial role in maintaining the integrity of the kidney filtration barrier, led to the alteration of 1666 gene transcripts, resulting in the loss of circadian rhythm, including autophagy genes (Wang et al., 2024). This deletion exacerbated podocyte injury and proteinuria in diabetic mice. The GAPVD1 Arg910Gln mutation plays a role for GAPVD1 binding to RAB5 and nephrin, a vital protein in the slit diaphragm of the podocyte, in this process (Hermle et al., 2018) . Importantly the mutation occurs in the immediate vicinity of phosphosite 5, and it has been demonstrated that phosphorylation at a specific site can influence the affinity of protein-protein interactions occurring at or near this site. For example phosphorylation at a site adjacent to a nuclear localization signal (NLS) reduces the binding affinity of the NLS for importin α (Harreman et al., 2004). Likewise, phosphorylation of site 5 may influence the binding of GAPVD1 to RAB5 or Nephrin. Investigating this phenomenon further may strengthen the link between the circadian clock and renal function through GAPVD1. Notably, the benefits of chronotherapy on renal function in patients are well documented (Prkacin et al., 2015; Rahman et al., 2019).

In the same context, suppressor of auxin resistance 1 A and B (SAR1A/B), the required GTPase of the COPII complex, exhibited low-amplitude rhythms (Mauvoisin et al., 2014). In addition, clock-regulated transcription of Puratrophin-1-like (Pura) leads to controlled rhythms in Rho1

activity. Taken together, the circadian clock could exhibit part of its output functions through GAPVD1. Whether or not GAPVD1 GAP or GEF activities are under circadian control remains unclear and needs to be further investigated.

5.5 GAPVD1 as a regulatory protein in the molecular circadian oscillator

The PER protein complex is a pillar of the molecular circadian oscillator, and many studies have examined regulatory mechanisms involving the PER complex and its protein components. It has been observed that knockdown of GAPVD1 prolongs the circadian period of cultured cells, indicating that GAPVD1 likely affects the molecular clockwork (Aryal et al., 2017). In my thesis, I attempted to study the impact of GAPVD1 on the interaction between CSNK1D and PER2.

Analysis of the CSNK1D-PER2 interaction in GAPVD1 knockout and overexpression experiments indicates that GAPVD1 affects the binding of CSNK1D and PER2. Several explanations might account for this observation. First, GAPVD1 could act as scaffold protein in building the PER2-CSNK1D complex, in which GAPVD1 would have the role of a repellent. Although this is apparently in contradiction to the general idea that scaffold proteins provide meeting platforms and facilitate the activation processes of substrates, examples for this mode of regulation exist. A good example is SEC8, a component of the SEC6/8 complex, which is essential for targeting exocytic vesicles to specific docking sites on the plasma membrane (Matern et al., 2001). Knockdown of SEC8 enhances the binding affinity of c-Jun N-terminal kinase (JNK)-interacting protein 4 (JIP4) for mitogen-activated protein kinase kinase 4 (MKK4) and suppresses the phosphorylation of MKK4 and JNK (Tanaka et al., 2014). In analogy to this, GAPVD1 might disturb the binding between CSNK1D and PER2, potentially through blocking interaction surfaces in either protein, which would be sufficient to affect the circadian period length. In support of this hypothesis I identified domains in GAPVD1, e.g. the VPS9 domain that affect the binding of GAPVD1 to PER2 and CSNK1D.

In another scenario binding of GAPVD1 could induce a conformational change in CSNK1D and thereby affect its kinase activity. Several cases are known, in which binding proteins and substrates regulate the activity of kinases. A good example is PER2 itself as binding of PER2 shifts the activity of CSNK1D away from output proteins towards core clock proteins (Qin et al., 2015). In analogy to this finding we found in a different study that PER2 induces CSNK1D-dependent phosphorylation of GAPVD1 by inhibiting the autoinhibitory activity of the CSNK1D C-terminal domain (Ibrahim et al., 2021).

Another explanation for the effect of GAPVD1 on CSNK1D binding to PER2 could be the phosphorylation state of PER2 or CSNK1D. Given that the amounts of CSNK1D and PER2 were quite similar in GAPVD1 overexpression or knockout cells, the cells might for example differ in the ratio of phosphorylated to unphosphorylated PER2, since CSNK1D seems to bind mostly to the phosphorylated form of PER2 (Lee et al., 2001). Therefore, investigating the phosphorylation levels of PER2 in GAPVD1 knockout and overexpressing cells might provide further insight into the observed changes in CSNK1D binding.

Several experiments have demonstrated that GAPVD1 binds to CSNK1D. This interaction could potentially regulate CSNK1D activity. Examples exist in other signaling pathways. For example, in WNT signaling the binding of Dishevelled Homolog (DVL) to CSNK1E is required for phosphorylation of Frizzled 6 (FZD6) (Strakova et al., 2018). Another example is the inhibition of protein kinase CK2α by CRY (Tamaru et al., 2015). In this case CRY inhibits the phosphorylation of BMAL1 at S90 by CK2α via mediating the rhythmic binding of CK2β to BMAL1 (Tamaru et al., 2015). Therefore, further investigating the functional consequences of

GAPVD1 binding to CSNK1D is crucial for a complete understanding of how this interaction might influence cellular processes.

(Aryal et al., 2017) proposed that the PER complex exists as a cytoplasmic precursor complex (0.9 MDa) and a mature PER complex (1.1 MDa). Besides the difference in molecular weight, the composition of the two complexes is also different. The so-called "lower complex" (LC) contains PER1, PER2, CRY1, CRY2 and CSNK1D. The "upper complex" (UC) contains all components of the lower PER complex and in addition GAPVD1 and PER3. The protein ratios in both complexes were calculated based on a PER2 ratio of one in both complexes (Tabel 22) (Aryal et al., 2017). Since in my CSNK1D-PER2 interaction experiments comparable amounts of CSNK1D in the different cell lines were immunoprecipitated, the co-immunoprecipitated PER2 amount was normalized to immunoprecipitated CSNK1D in all samples. Therefore I have recalculated the ratio in (Aryal et al., 2017) to a CSNK1D ration of one in both PER complexes (Tabel 22) in order to compare PER2 levels in both experiments. The ratio of PER2 bound to CSNK1D changed in the presence of GAPVD1 from 1 to 0.7 in (Aryal et al., 2017), which correlates with the reduced interaction of CSNK1D and PER2 in the presence of GAPVD1 in my results (Figure22 B).

Table 22: Proteins of LC and UC and their relative representation in the two complexes determined by quantitative mass spectrometry normalized to CSNK1D or PER2 based on (Aryal et al., 2017).

PER Complex components	UC/LC Ratio Normalized to PER2	UC/LC Ratio normalized to CSNK1D
PER2	1	0.7
PER1	2.34	1.6
CRY1	1.3	0.9
CRY2	1.16	0.8
CSNK1D	1.45	1.0
PER3	10	6.9
GAPVD1	10	6.9

In my experiments, CSNK1D levels were treated as a constant and GAPVD1 and PER2 as variables. Hence, I could exclusively attribute altered PER2-CSNK1D binding to the variable GAPVD1 levels contrary to (Aryal et al., 2017), since their calculation was based on constant PER2 and variable CSNK1D and GAPVD1 levels. The similar ratios I obtained after recalculation of Aryal et al., (2017) and my experiments alone are not conclusive. However, additional support of the conclusion that GAPVD1 alters the PER2-CSNK1D interaction stems from the subsequent experiment in GAPVD1 KO cells. Indeed, there the opposite was observed, namely more PER2 was co-immunoprecipitated with CSNK1D in GAPVD1 KO cells compared to WT.

Several additional questions have arisen. For example, what role, if any, does GAPVD1 play for PER complex formation and the transition between the two complexes. For example, GAPVD1 could potentially inhibit PER2 binding and increase PER3 binding to the complex

thus speeding up the maturation of the lower complex towards the upper complex which leads to nuclear import of the complex. In support of this idea, PER3 was shown to trigger dimerization and nuclear import of PER1 and PER2 (Yagita et al., 2000).

Overall, this suggests that GAPVD1 alters PER complex composition, potentially facilitating the binding of PER3 to the complex. GAPVD1 contains helical coils, which might act as scaffold for protein-protein interactions (Truebestein and Leonard, 2016). For example, the coiled-coil domain of the protein Bicaudal D homolog 2 (BICD2) acts as a scaffold for interaction of the cytoplasmic microtubule motor DYNEIN and its activating cofactor DYNACTIN (Chaaban and Carter, 2022; Urnavicius et al., 2015). Additional experiments would be required to validate this hypothesis and to elucidate a potential regulatory role of GAPVD1 in recruiting PER3 to the PER complex.

Not only do GAPVD1 levels influence PER2-CSNK1D binding, but the total cellular amount of PER2 protein also plays a fundamental role. In cells overexpressing PER2, GAPVD1 appears to have no effect on PER2-CSNK1D binding (Figure 23). These findings indicate that the amount of PER2 available for binding contributes to modulating the effect of GAPVD1 on the PER2-CSNK1D interaction. The cellular availability of PER2 is maximal at CT12-16 (Buhr and Takahashi, 2013). GAPVD1 could therefore affect PER2-CSNK1D binding when PER2 levels are lowest, for example between CT 0 and 6 or between CT 18 and 24 (Aryal et al., 2017). This implies that GAPVD1 has at best a fine-tuning role in PER2-CSNK1D binding, which in turn would explain the small effects of GAPVD1 on circadian period length (Aryal et al., 2017). In conclusion, GAPVD1 might play a role in regulating the activity of the PER complex by controlling the binding levels of the complex's components. Further studies are needed to fully understand the mechanisms by which GAPVD1 functionally interacts with the PER complex.

5.6. Mapping PER2/CSNK1D interaction domains in GAPVD1

An essential element in understanding regulatory mechanisms within the PER complex is to define the domains responsible for protein-protein interactions. The final aim of this study was to elucidate the binding domains of GAPVD1 responsible for its interaction with PER2 and CSNK1D. This is also the first study that investigates binding domains of GAPVD1 based on its 3D structure predicted with AlphaFold (Varadi et al., 2022). My findings reveal that the Bottom helices (aa 1114-1192) and H2 helix (aa 1193-1260) of GAPVD1, collectively referred to as H2B, are sufficient for binding to both PER2 and CSNK1D.

It is noteworthy to mention that the Bottom helices are a three-helix bundle and H2 is a coiled-coil double helix. Hence, a good example for comparison of H2B binding to PER2 is the interaction between Acyl-CoA-binding domain-containing 3 (ACBD3) and palmitoyl-CoA hydrolase using its ACBD domain. In terms of similarity, ACBD3 contains a short helix bundle followed by an alpha helical structure similar to the H2B domain of GAPVD1 (Yue et al., 2019). Moreover, palmitoyl-CoA hydrolase contains small helix bundles adjacent to beta sheets similar to the PASA/B domain in PER2. It seems therefore possible that the PASA/B domain in PER2 is responsible for GAPVD1 binding.

The impact of identifying H2B as the binding domain for PER2 and CSNK1D in GAPVD1 lies in several points. First, the Bottom helices are three-helix bundles, which exhibit in general a diverse range of binding and catalytic functions and at the same time are very selective (Lombardi et al., 1997; Schneider et al., 1998). They can contain small-molecule binding sites or metal-binding sites, thus enabling them to play roles in various biochemical processes, such

as enzymatic reactions, signal transduction, or structural stabilization of proteins (Dieckmann et al., 1997; Gonzalez et al., 1996; Schneider et al., 1998). Second, H2 is a coiled-coil helix in GAPVD1 which might act as a molecular spacer (Truebestein and Leonard, 2016). Indeed, based on Alphafold it separates the Bottom helices from the VPS9 and RasGAP domains. Coiled-coil domains can also serve as scaffolds for large macromolecular complexes (Truebestein and Leonard, 2016), which in the case of H2 may be a function as scaffold for the PER complex. Therefore, identifying H2B as a binding domain in GAPVD1 suggests its potential role as a selective interaction site for diverse partners including PER2 and CSNK1D and also as a scaffold for the PER complex.

Nevertheless, my results show that a GAPVD1 mutant with a deletion of H2B still binds effectively to PER2, which suggests the intriguing possibility that a second binding domain exists. The presence of multiple binding sites in GAPVD1 could allow for diverse parallel functions such as regulation, signaling, and structural stabilization. A good example is the existence of two CSNK1D binding domains in PER2, CK1BD-A and CK1BD-B (Narasimamurthy and Virshup, 2021). I also observed that the IDR region (AA679-1113) does not bind to PER2 or CSNK1D on its own. In addition, the M1 construct (AA1-690) binds very weakly if at all to PER2 and CSNK1D (Buschhaus, 2021). However, a GAPVD1 mutant containing amino acid resuide 1-1113 binds strongly to PER2 and CSNK1D (Figure 34). Furthermore, a structural domain consisting of amino acids 354- 679 is wrapped around the GAP domain (60-353), thereby acting as a physical barrier between amino acid residues 679-1113 and the Ras-GAP domain (Figure 35). Based on these observations I speculate that the second binding domain may reside within the Intrinsically Disordered Region (IDR) (aa 353-1113) of GAPVD1 (Figure 34). Additional GAPVD1 mutants such as one containing amino acids 353-679 representing only the N terminal part of the IDR, or another containing amino acids 353-1113 containing the entire IDR, will have to be tested in co-immunoprecipitation experiments with PER2 to confirm this hypothesis. This speculation is supported by previous studies highlighting the significance of IDRs in facilitating protein-protein interactions by providing flexibility and adaptability to accommodate diverse binding partners (Chakrabarti and Chakravarty, 2022).

Furthermore, the intrinsically disordered region (IDR) of GAPVD1 contains a proline-rich region. Previous studies have demonstrated the importance of proline-rich motifs in protein-protein interactions. For example, Lodhi et al. (2007) showed that the Cdc42-interacting protein 4 (CIP4) binds to mouse GAPVD1 through a proline-rich region (ARPSHPPPDP, residues 827-836). A corresponding region exists in human GAPVD1 (residues 848-857). Interestingly, a GAPVD1 mutant lacking this proline-rich motif exhibited an inability to interact with CIP4 (Lodhi et al., 2007). However, my results indicate that this proline-rich region is not sufficient for binding to PER2 or CSNK1D. This suggests that the interaction between GAPVD1 and these proteins might involve other regions or require specific conformations within the IDR.

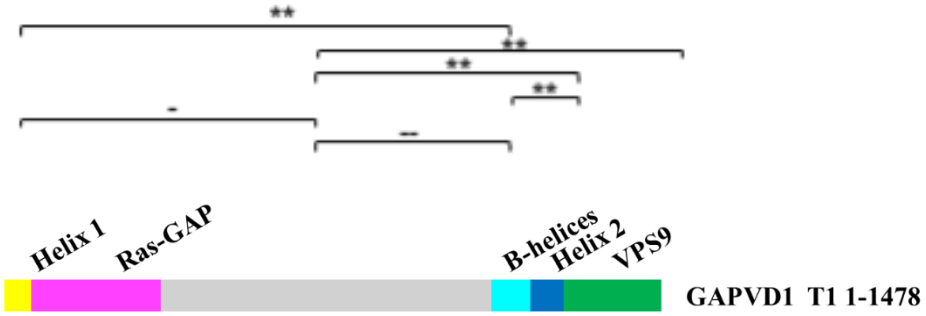

Figure 34. A schematic representation of the binding affintity of PER2 to different GAPVD1 mutants. The symbols indicate the relative binding affinity of each construct to PER2. Two stars (**) denote high-affinity, strong binding, while one dash (-) signifies moderate affinity, and two dashes (--) denote low-affinity, weak binding.

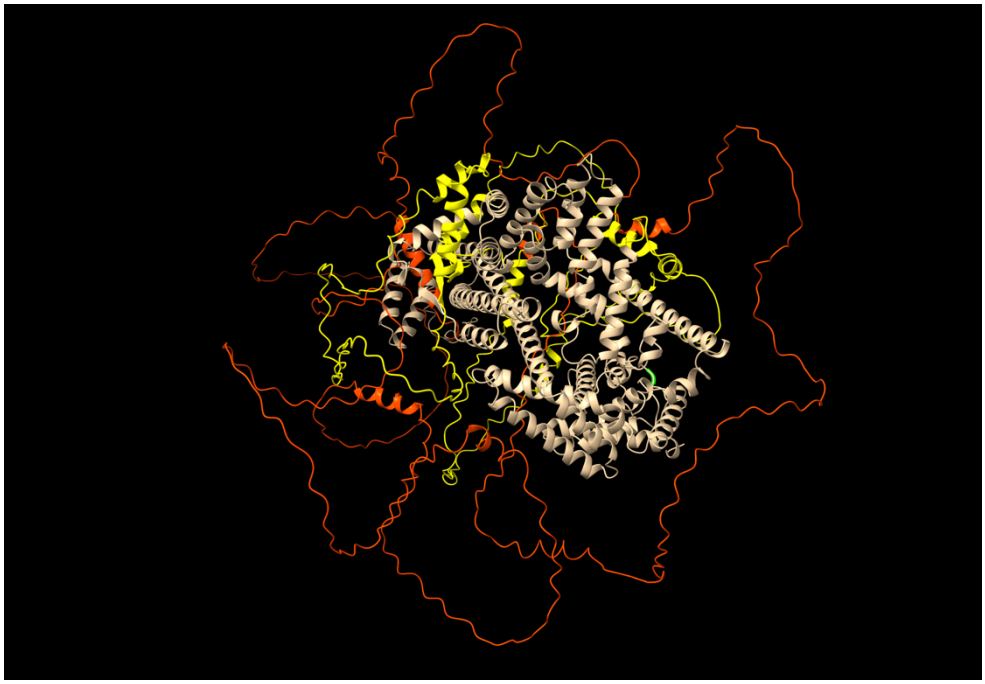

Figure 35. 3D structure of GAPVD1. Overview of its domain structure. GAPVD1 T1 aa 1-1478 is shown with amino acid residues 354- 679 (yellow), GAP domain (AA60-353) (Gray), (AA 679- 1113) (red).

My results also showed that deletion of the VPS9 domain of GAPVD1 increases the binding affinity between GAPVD1 and PER2. This is the first observation of a VPS9 domain modulating the binding of another protein. This result also supports the notion that GAPVD1 provides a repllent scaffold for PER2 and CSNK1D, a conclusion based on other experiments in this thesis. Deletion of the VPS9 domain of GAPVD1 increases the binding affinity between GAPVD1 and PER2, thus full-length GAPVD1 might bring substoichometric amounts of PER2 to the GAPVD1-containing PER complex. Previously, intramolecular regulation of VPS9 domains was reported. The VPS9 domain in *S. cerevisiae* VPS9P interacts with the adjacent CUE domain, a domain that binds mono- and poly-ubiquitin, thus increasing the affinity of the CUE domain for ubiquitin (Kang et al., 2003; Prag et al., 2003; Shih et al., 2003). This example indicates a potential for the VPS9 domain to be involved in intramolecular regulation within GAPVD1 and may hint at yet another regulatory role for the VPS9 domain in the PER complex. In this context, a key question emerges: how would PER2-CSNK1D binding be affected by deletion of the VPS9 domain of GAPVD1? Furthermore, it is noteworthy that deleting the VPS9

domain did not alter the overall localization of PER2 within the cells, suggesting that the VPS9 domain specifically affects the interaction between GAPVD1 and PER2, rather than PER2 localization itself.

In essence, my initial research hypothesis was centered on the existence of (a) specific binding domain(s) within GAPVD1 that interact with PER2, assuming the existence of well-defined interaction domains in both proteins. The identification of the H2B domain as a facilitator of PER2 binding aligns with these initial expectations and provides valuable insights into the molecular basis of this interaction. However, the unexpected finding of the VPS9 domain acting as an inhibitory domain adds a layer of complexity to our understanding of the interaction dynamics between GAPVD1, PER2, and CSNK1D. This complexity suggests a more nuanced regulatory mechanism than initially anticipated. Furthermore, our results point towards the possibility of a second binding domain on GAPVD1 that interacts with PER2 and CSNK1D. Future studies aimed at elucidating the role of this potential second binding site and the interplay between H2B and VPS9 domains will be crucial for comprehensively understanding the regulation of PER2-CSNK1D binding by GAPVD1.

In conclusion, as depicted in Figure 36, this thesis has significantly advanced our understanding of the cytoplasmic role of PER2. By identifying several novel PER2 binding partners, including GAPVD1 as a key component of the PER complex (Figure 36A), new avenues for investigation have opened. This work has also elucidated a new function for the PER complex, namely its participation in the regulation of GAPVD1 phosphorylation. Complementary to this finding, GAPVD1 is being phosphorylated on multiple sites by CSNK1D and this phosphorylation displays rhythmic activity during 24 h. GAPVD1 also regulates the binding between PER2 and CSNK1D, suggesting in summary that GAPVD1 could act as both a regulator and an output of the circadian clock. Domain interaction mapping experiments revealed that the interaction between GAPVD1 and both PER2 and CSNK1D is primarily mediated by the H2B domain (amino acid residues 1114-1260) of GAPVD1. Furthermore, the VPS9 domain seems to play a modulatory role in PER2 binding. Understanding this intricate molecular regulation between PER2 and GAPVD1 is crucial for comprehensively deciphering the role of cytoplasmic PER2 within the PER complex.

Future investigations are necessary to elucidate the functional consequences of the mutual regulation between PER2 and GAPVD1 (Figure 36B). Particularly, it is essential to determine if GAPVD1 also regulates the phosphorylation status of PER2 (Figure 36B, dashed line 1). Additionally, the phosphorylation of GAPVD1 and the potential regulation of GAPVD1's enzymatic activity, specifically its role as a guanine nucleotide exchange factor or GTPase activator, warrants further exploration. This could have significant implications for various output functions of the circadian clock (Figure 36B, dashed line 2). Moreover, understanding how GAPVD1 as a whole, and its VPS9 domain in particular, impacts the circadian clock also remains an important area of investigation (Figure 36B, dashed line 3).

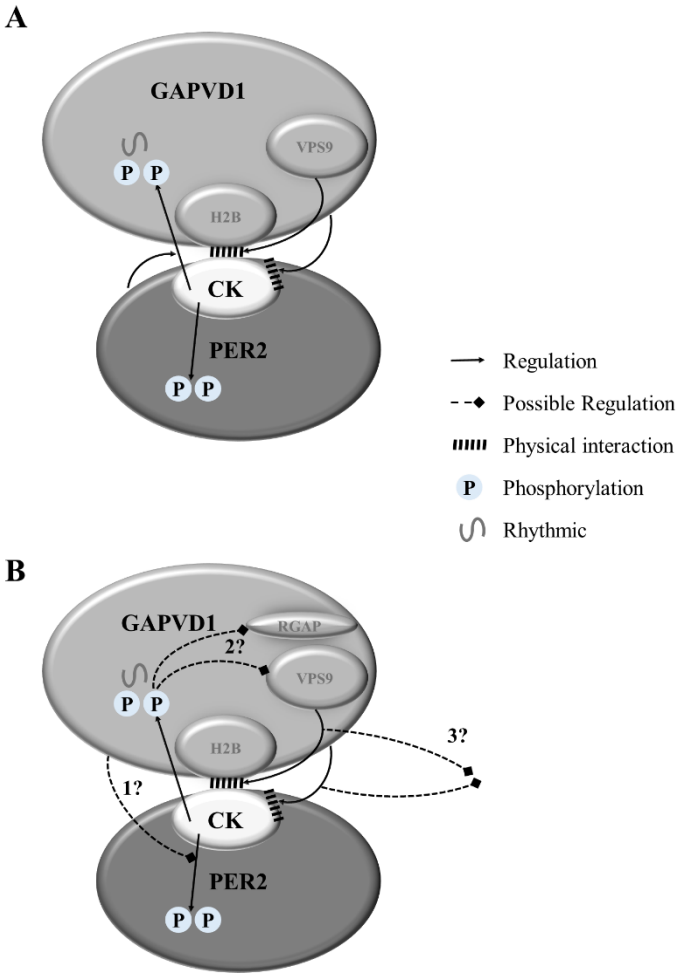

Figure 36. Summary of the work and future perspectives. The findings in this thesis are depicted in A) as solid lines and future questions are depicted in B) as dashed lines. GAPVD1, PER2 and CSNK1D are depicted as circles whose sizes are relative to their molecular weight. Physical interaction between GAPVD1, CSNK1D or PER2 is shown as small black lines. Phosphorylation sites are depicted as small light blue circles (P).

6. References

Akashi, M., Ichise, T., Mamine, T., Takumi, T., 2006. Molecular Mechanism of Cell-autonomous Circadian Gene Expression of Period2, a Crucial Regulator of the Mammalian Circadian Clock. Mol. Biol. Cell 17, 555–565. https://doi.org/10.1091/mbc.E05-05-0396

Akashi, M., Okamoto, A., Tsuchiya, Y., Todo, T., Nishida, E., Node, K., 2014. A Positive Role for PERIOD in Mammalian Circadian Gene Expression. Cell Rep. 7, 1056–1064. https://doi.org/10.1016/j.celrep.2014.03.072

Akashi, M., Tsuchiya, Y., Yoshino, T., Nishida, E., 2002. Control of intracellular dynamics of mammalian period proteins by casein kinase I epsilon (CKIepsilon) and CKIdelta in cultured cells. Mol. Cell. Biol. 22, 1693–1703. https://doi.org/10.1128/MCB.22.6.1693-1703.2002

Akhtar, R.A., Reddy, A.B., Maywood, E.S., Clayton, J.D., King, V.M., Smith, A.G., Gant, T.W., Hastings, M.H., Kyriacou, C.P., 2002. Circadian cycling of the mouse liver transcriptome, as revealed by cDNA microarray, is driven by the suprachiasmatic nucleus. Curr. Biol. CB 12, 540–550. https://doi.org/10.1016/s0960-9822(02)00759-5

Albrecht, U., 2012. Timing to perfection: the biology of central and peripheral circadian clocks. Neuron 74, 246–260. https://doi.org/10.1016/j.neuron.2012.04.006

Albrecht, U., Bordon, A., Schmutz, I., Ripperger, J., 2007. The multiple facets of Per2. Cold Spring Harb. Symp. Quant. Biol. 72, 95–104. https://doi.org/10.1101/sqb.2007.72.001

Albrecht, U., Sun, Z.S., Eichele, G., Lee, C.C., 1997. A differential response of two putative mammalian circadian regulators, mper1 and mper2, to light. Cell 91, 1055–1064. https://doi.org/10.1016/s0092-8674(00)80495-x

An, Y., Yuan, B., Xie, P., Gu, Y., Liu, Z., Wang, T., Li, Z., Xu, Y., Liu, Y., 2022. Decoupling PER phosphorylation, stability and rhythmic expression from circadian clock function by abolishing PER-CK1 interaction. Nat. Commun. 13, 3991. https://doi.org/10.1038/s41467-022-31715-4

Antoun, G., Bouchard-Cannon, P., Cheng, H.-Y.M., 2012. Regulation of MAPK/ERK signaling and photic entrainment of the suprachiasmatic nucleus circadian clock by Raf kinase inhibitor protein. J. Neurosci. Off. J. Soc. Neurosci. 32, 4867–4877. https://doi.org/10.1523/JNEUROSCI.5650-11.2012

Arakel, E.C., Schwappach, B., 2018. Formation of COPI-coated vesicles at a glance. J. Cell Sci. 131, jcs209890. https://doi.org/10.1242/jcs.209890

Aryal, R.P., Kwak, P.B., Tamayo, A.G., Gebert, M., Chiu, P.-L., Walz, T., Weitz, C.J., 2017. Macromolecular Assemblies of the Mammalian Circadian Clock. Mol. Cell 67, 770-782.e6. https://doi.org/10.1016/j.molcel.2017.07.017

Asher, G., Gatfield, D., Stratmann, M., Reinke, H., Dibner, C., Kreppel, F., Mostoslavsky, R., Alt, F.W., Schibler, U., 2008. SIRT1 Regulates Circadian Clock Gene Expression through PER2 Deacetylation. Cell 134, 317–328. https://doi.org/10.1016/j.cell.2008.06.050

Babicki, S., Arndt, D., Marcu, A., Liang, Y., Grant, J.R., Maciejewski, A., Wishart, D.S., 2016. Heatmapper: web-enabled heat mapping for all. Nucleic Acids Res. 44, W147-153. https://doi.org/10.1093/nar/gkw419

Bada, M., Turi, D., McEntire, R., Stevens, R., 2004. Using reasoning to guide annotation with gene ontology terms in GOAT. ACM SIGMOD Rec. 33, 27–32. https://doi.org/10.1145/1024694.1024699

Badura, L., Swanson, T., Adamowicz, W., Adams, J., Cianfrogna, J., Fisher, K., Holland, J., Kleiman, R., Nelson, F., Reynolds, L., Germain, K.S., Schaeffer, E., Tate, B., Sprouse, J., 2007a. An Inhibitor of Casein Kinase Iϵ Induces Phase Delays in Circadian Rhythms under Free-Running and Entrained Conditions. J. Pharmacol. Exp. Ther. 322, 730–738. https://doi.org/10.1124/jpet.107.122846

Badura, L., Swanson, T., Adamowicz, W., Adams, J., Cianfrogna, J., Fisher, K., Holland, J., Kleiman, R., Nelson, F., Reynolds, L., St Germain, K., Schaeffer, E., Tate, B., Sprouse, J., 2007b. An inhibitor of casein kinase I epsilon induces phase delays in circadian rhythms under free-running and entrained conditions. J. Pharmacol. Exp. Ther. 322, 730–738. https://doi.org/10.1124/jpet.107.122846

Bae, K., Jin, X., Maywood, E.S., Hastings, M.H., Reppert, S.M., Weaver, D.R., 2001. Differential functions of mPer1, mPer2, and mPer3 in the SCN circadian clock. Neuron 30, 525–536. https://doi.org/10.1016/s0896-6273(01)00302-6

Batty, M.B., Schittenhelm, R.B., Dorin-Semblat, D., Doerig, C., Garcia-Bustos, J.F., 2020. Interaction of Plasmodium falciparum casein kinase 1 with components of host cell protein trafficking machinery. IUBMB Life 72, 1243–1249. https://doi.org/10.1002/iub.2294

Beaulé, C., Robinson, B., Lamont, E.W., Amir, S., 2003. Melanopsin in the circadian timing system. J. Mol. Neurosci. MN 21, 73–89. https://doi.org/10.1385/JMN:21:1:73

Bender, A., Pringle, J.R., 1991. Use of a screen for synthetic lethal and multicopy suppressee mutants to identify two new genes involved in morphogenesis in Saccharomyces cerevisiae. Mol. Cell. Biol. 11, 1295–1305.

Béthune, J., Wieland, F.T., 2018. Assembly of COPI and COPII Vesicular Coat Proteins on Membranes. Annu. Rev. Biophys. 47, 63–83. https://doi.org/10.1146/annurev-biophys-070317-033259

Bibian, M., Rahaim, R.J., Choi, J.Y., Noguchi, Y., Schürer, S., Chen, W., Nakanishi, S., Licht, K., Rosenberg, L.H., Li, L., Feng, Y., Cameron, M.D., Duckett, D.R., Cleveland, J.L., Roush, W.R., 2013. Development of highly selective casein kinase 1δ/1ε (CK1δ/ε) inhibitors with potent antiproliferative properties. Bioorg. Med. Chem. Lett. 23, 4374–4380. https://doi.org/10.1016/j.bmcl.2013.05.075

Blethrow, J.D., Glavy, J.S., Morgan, D.O., Shokat, K.M., 2008. Covalent capture of kinase-specific phosphopeptides reveals Cdk1-cyclin B substrates. Proc. Natl. Acad. Sci. U. S. A. 105, 1442–1447. https://doi.org/10.1073/pnas.0708966105

Borrmann, H., McKeating, J.A., Zhuang, X., 2021. The Circadian Clock and Viral Infections. J. Biol. Rhythms 36, 9–22. https://doi.org/10.1177/0748730420967768

Bos, J.L., Rehmann, H., Wittinghofer, A., 2007. GEFs and GAPs: Critical Elements in the Control of Small G Proteins. Cell 129, 865–877. https://doi.org/10.1016/j.cell.2007.05.018

Brenna, A., Albrecht, U., 2020. Phosphorylation and Circadian Molecular Timing. Front. Physiol. 11.

Brenna, A., Olejniczak, I., Chavan, R., Ripperger, J.A., Langmesser, S., Cameroni, E., Hu, Z., De Virgilio, C., Dengjel, J., Albrecht, U., 2019. Cyclin-dependent kinase 5 (CDK5) regulates the circadian clock. eLife 8, e50925. https://doi.org/10.7554/eLife.50925

Buhr, E.D., Takahashi, J.S., 2013. Molecular components of the Mammalian circadian clock. Handb. Exp. Pharmacol. 3–27. https://doi.org/10.1007/978-3-642-25950-0_1

Bunger, M.K., Wilsbacher, L.D., Moran, S.M., Clendenin, C., Radcliffe, L.A., Hogenesch, J.B., Simon, M.C., Takahashi, J.S., Bradfield, C.A., 2000. Mop3 is an essential component of the master circadian pacemaker in mammals. Cell 103, 1009–1017. https://doi.org/10.1016/s0092-8674(00)00205-1

Buschhaus, C., 2021. Characterization of the Protein-Protein Interactions between GAPVD1, PER2, and CSNK1D in the Circadian Clock. heinrich heine universität.

Busino, L., Bassermann, F., Maiolica, A., Lee, C., Nolan, P.M., Godinho, S.I.H., Draetta, G.F., Pagano, M., 2007. SCFFbxl3 Controls the Oscillation of the Circadian Clock by Directing the Degradation of Cryptochrome Proteins. Science 316, 900–904. https://doi.org/10.1126/science.1141194

Caesar, L.K., Kvalheim, O.M., Cech, N.B., 2018. Hierarchical cluster analysis of technical replicates to identify interferents in untargeted mass spectrometry metabolomics. Anal. Chim. Acta 1021, 69–77. https://doi.org/10.1016/j.aca.2018.03.013

Callaway, E., 2020. 'It will change everything': DeepMind's AI makes gigantic leap in solving protein structures. Nature 588, 203–204. https://doi.org/10.1038/d41586-020-03348-4

Camacho, F., Cilio, M., Guo, Y., Virshup, D.M., Patel, K., Khorkova, O., Styren, S., Morse, B., Yao, Z., Keesler, G.A., 2001. Human casein kinase Iδ phosphorylation of human circadian clock proteins period 1 and 2. FEBS Lett. 489, 159–165. https://doi.org/10.1016/S0014-5793(00)02434-0

Cao, X., Wang, L., Selby, C.P., Lindsey-Boltz, L.A., Sancar, A., 2023. Analysis of mammalian circadian clock protein complexes over a circadian cycle. J. Biol. Chem. 299, 102929. https://doi.org/10.1016/j.jbc.2023.102929

Cao, X., Yang, Y., Selby, C.P., Liu, Z., Sancar, A., 2021. Molecular mechanism of the repressive phase of the mammalian circadian clock. Proc. Natl. Acad. Sci. U. S. A. 118, e2021174118. https://doi.org/10.1073/pnas.2021174118

Carney, D.S., Davies, B.A., Horazdovsky, B.F., 2006. Vps9 domain-containing proteins: activators of Rab5 GTPases from yeast to neurons. Trends Cell Biol. 16, 27–35. https://doi.org/10.1016/j.tcb.2005.11.001

Carvas, J.M., Vukolic, A., Yepuri, G., Xiong, Y., Popp, K., Schmutz, I., Chappuis, S., Albrecht, U., Ming, X.-F., Montani, J.-P., Yang, Z., 2012. Period2 gene mutant mice show compromised insulin-mediated endothelial nitric oxide release and altered glucose homeostasis. Front. Physiol. 3, 337. https://doi.org/10.3389/fphys.2012.00337

Chaaban, S., Carter, A.P., 2022. Structure of dynein–dynactin on microtubules shows tandem adaptor binding. Nature 610, 212–216. https://doi.org/10.1038/s41586-022-05186-y

Chakrabarti, P., Chakravarty, D., 2022. Intrinsically disordered proteins/regions and insight into their biomolecular interactions. Biophys. Chem. 283, 106769. https://doi.org/10.1016/j.bpc.2022.106769

Chappuis, S., Ripperger, J.A., Schnell, A., Rando, G., Jud, C., Wahli, W., Albrecht, U., 2013. Role of the circadian clock gene Per2 in adaptation to cold temperature. Mol. Metab. 2, 184–193. https://doi.org/10.1016/j.molmet.2013.05.002

Chen, L.-C., Hsieh, Y.-L., Tan, G.Y.T., Kuo, T.-Y., Chou, Y.-C., Hsu, P.-H., Hwang-Verslues, W.W., 2021. Differential effects of SUMO1 and SUMO2 on circadian protein PER2 stability and function. Sci. Rep. 11, 14431. https://doi.org/10.1038/s41598-021-93933-y

Chen, R., Schirmer, A., Lee, Y., Lee, H., Kumar, V., Yoo, S.-H., Takahashi, J.S., Lee, C., 2009. Rhythmic PER abundance defines a critical nodal point for negative feedback within the circadian clock mechanism. Mol. Cell 36, 417–430. https://doi.org/10.1016/j.molcel.2009.10.012

Chen, Z., Yoo, S.-H., Park, Y.-S., Kim, K.-H., Wei, S., Buhr, E., Ye, Z.-Y., Pan, H.-L., Takahashi, J.S., 2012. Identification of diverse modulators of central and peripheral circadian clocks by high-throughput chemical screening. Proc. Natl. Acad. Sci. U. S. A. 109, 101–106. https://doi.org/10.1073/pnas.1118034108

Cheng, H.-Y.M., Papp, J.W., Varlamova, O., Dziema, H., Russell, B., Curfman, J.P., Nakazawa, T., Shimizu, K., Okamura, H., Impey, S., Obrietan, K., 2007. microRNA modulation of circadian clock period and entrainment. Neuron 54, 813–829. https://doi.org/10.1016/j.neuron.2007.05.017

Chico, L.K., Van Eldik, L.J., Watterson, D.M., 2009. Targeting protein kinases in central nervous system disorders. Nat. Rev. Drug Discov. 8, 892–909. https://doi.org/10.1038/nrd2999

Chiou, Y.-Y., Yang, Y., Rashid, N., Ye, R., Selby, C.P., Sancar, A., 2016. Mammalian Period represses and de-represses transcription by displacing CLOCK–BMAL1 from promoters in a Cryptochrome-dependent manner. Proc. Natl. Acad. Sci. 113, E6072–E6079. https://doi.org/10.1073/pnas.1612917113

Christensen, M.O., Barthelmes, H.U., Boege, F., Mielke, C., 2002. The N-terminal domain anchors human topoisomerase I at fibrillar centers of nucleoli and nucleolar organizer regions of mitotic chromosomes. J. Biol. Chem. 277, 35932–35938. https://doi.org/10.1074/jbc.M204738200

Cox, K.H., Takahashi, J.S., 2019. Circadian clock genes and the transcriptional architecture of the clock mechanism. J. Mol. Endocrinol. 63, R93–R102. https://doi.org/10.1530/JME-19-0153

Dang, F., Sun, X., Ma, X., Wu, R., Zhang, D., Chen, Y., Xu, Q., Wu, Y., Liu, Y., 2016. Insulin post-transcriptionally modulates Bmal1 protein to affect the hepatic circadian clock. Nat. Commun. 7, 12696. https://doi.org/10.1038/ncomms12696

Deane, C.M., Salwiński, Ł., Xenarios, I., Eisenberg, D., 2002. Protein interactions: two methods for assessment of the reliability of high throughput observations. Mol. Cell. Proteomics MCP 1, 349–356. https://doi.org/10.1074/mcp.m100037-mcp200

DeBruyne, J.P., Weaver, D.R., Reppert, S.M., 2007a. CLOCK and NPAS2 have overlapping roles in the suprachiasmatic circadian clock. Nat. Neurosci. 10, 543–545. https://doi.org/10.1038/nn1884

DeBruyne, J.P., Weaver, D.R., Reppert, S.M., 2007b. Peripheral circadian oscillators require CLOCK. Curr. Biol. CB 17, R538-539. https://doi.org/10.1016/j.cub.2007.05.067

Dephoure, N., Zhou, C., Villén, J., Beausoleil, S.A., Bakalarski, C.E., Elledge, S.J., Gygi, S.P., 2008. A quantitative atlas of mitotic phosphorylation. Proc. Natl. Acad. Sci. U. S. A. 105, 10762–10767. https://doi.org/10.1073/pnas.0805139105

Dey, J., Carr, A.-J.F., Cagampang, F.R.A., Semikhodskii, A.S., Loudon, A.S.I., Hastings, M.H., Maywood, E.S., 2005. The tau mutation in the Syrian hamster differentially reprograms the circadian clock in the SCN and peripheral tissues. J. Biol. Rhythms 20, 99–110. https://doi.org/10.1177/0748730404274264

Dieckmann, G.R., McRorie, D.K., Tierney, D.L., Utschig, L.M., Singer, C.P., O'Halloran, T.V., Penner-Hahn, J.E., DeGrado, W.F., Pecoraro, V.L., 1997. De Novo Design of Mercury-Binding Two- and Three-Helical Bundles. J. Am. Chem. Soc. 119, 6195–6196. https://doi.org/10.1021/ja964351i

Ducommun, S., Deak, M., Zeigerer, A., Göransson, O., Seitz, S., Collodet, C., Madsen, A.B., Jensen, T.E., Viollet, B., Foretz, M., Gut, P., Sumpton, D., Sakamoto, K., 2019. Chemical genetic screen identifies Gapex-5/GAPVD1 and STBD1 as novel AMPK substrates. Cell. Signal. 57, 45–57. https://doi.org/10.1016/j.cellsig.2019.02.001

Eide, E.J., Woolf, M.F., Kang, H., Woolf, P., Hurst, W., Camacho, F., Vielhaber, E.L., Giovanni, A., Virshup, D.M., 2005. Control of mammalian circadian rhythm by CKIepsilon-regulated proteasome-mediated PER2 degradation. Mol. Cell. Biol. 25, 2795–2807. https://doi.org/10.1128/MCB.25.7.2795-2807.2005

Eng, G.W.L., Edison, Virshup, D.M., 2017. Site-specific phosphorylation of casein kinase 1 δ (CK1δ) regulates its activity towards the circadian regulator PER2. PLoS ONE 12, e0177834. https://doi.org/10.1371/journal.pone.0177834

Etchegaray, J.-P., Machida, K.K., Noton, E., Constance, C.M., Dallmann, R., Di Napoli, M.N., DeBruyne, J.P., Lambert, C.M., Yu, E.A., Reppert, S.M., Weaver, D.R., 2009. Casein kinase 1 delta regulates the pace of the mammalian circadian clock. Mol. Cell. Biol. 29, 3853–3866. https://doi.org/10.1128/MCB.00338-09

Faini, M., Beck, R., Wieland, F.T., Briggs, J.A.G., 2013. Vesicle coats: structure, function, and general principles of assembly. Trends Cell Biol. 23, 279–288. https://doi.org/10.1016/j.tcb.2013.01.005

Fang, L., Yang, Z., Zhou, J., Tung, J.-Y., Hsiao, C.-D., Wang, L., Deng, Y., Wang, P., Wang, J., Lee, M.-H., 2015. Circadian Clock Gene CRY2 Degradation Is Involved in Chemoresistance of Colorectal Cancer. Mol. Cancer Ther. 14, 1476–1487. https://doi.org/10.1158/1535-7163.MCT-15-0030

Farhud, D., Aryan, Z., 2018. Circadian Rhythm, Lifestyle and Health: A Narrative Review. Iran. J. Public Health 47, 1068–1076.

Farshadi, E., van der Horst, G.T.J., Chaves, I., 2020. Molecular Links between the Circadian Clock and the Cell Cycle. J. Mol. Biol., Circadian Regulation: from Molecules to Physiology 432, 3515–3524. https://doi.org/10.1016/j.jmb.2020.04.003

Fealey, M.E., Binder, B.P., Uversky, V.N., Hinderliter, A., Thomas, D.D., 2018. Structural Impact of Phosphorylation and Dielectric Constant Variation on Synaptotagmin's IDR. Biophys. J. 114, 550–561. https://doi.org/10.1016/j.bpj.2017.12.013

Feillet, C., Horst, G.T.J. van der, Levi, F., Rand, D.A., Delaunay, F., 2015. Coupling between the Circadian Clock and Cell Cycle Oscillators: Implication for Healthy Cells and Malignant Growth. Front. Neurol. 6. https://doi.org/10.3389/fneur.2015.00096

Feillet, C., Krusche, P., Tamanini, F., Janssens, R.C., Downey, M.J., Martin, P., Teboul, M., Saito, S., Lévi, F.A., Bretschneider, T., van der Horst, G.T.J., Delaunay, F., Rand, D.A., 2014. Phase locking and multiple oscillating attractors for the coupled mammalian clock and cell cycle. Proc. Natl. Acad. Sci. U. S. A. 111, 9828–9833. https://doi.org/10.1073/pnas.1320474111

Firsov, D., Bonny, O., 2010. Circadian regulation of renal function. Kidney Int. 78, 640–645. https://doi.org/10.1038/ki.2010.227

Fishbein, A.B., Knutson, K.L., Zee, P.C., 2021. Circadian disruption and human health. J. Clin. Invest. 131. https://doi.org/10.1172/JCI148286

Flotow, H., Graves, P.R., Wang, A.Q., Fiol, C.J., Roeske, R.W., Roach, P.J., 1990. Phosphate groups as substrate determinants for casein kinase I action. J. Biol. Chem. 265, 14264–14269.

Frahm, J.L., Li, L.O., Grevengoed, T.J., Coleman, R.A., 2011. Phosphorylation and Acetylation of Acyl-CoA Synthetase- I. J. Proteomics Bioinform. 4, 129–137. https://doi.org/10.4172/jpb.1000180

Fu, L., Pelicano, H., Liu, J., Huang, P., Lee, C., 2002. The circadian gene Period2 plays an important role in tumor suppression and DNA damage response in vivo. Cell 111, 41–50. https://doi.org/10.1016/s0092-8674(02)00961-3

Furuya, E., Yokoyama, M., Uyeda, K., 1982. Regulation of fructose-6-phosphate 2-kinase by phosphorylation and dephosphorylation: possible mechanism for coordinated control of glycolysis and glycogenolysis. Proc. Natl. Acad. Sci. U. S. A. 79, 325–329.

Gao, P., Yoo, S.-H., Lee, K.-J., Rosensweig, C., Takahashi, J.S., Chen, B.P., Green, C.B., 2013. Phosphorylation of the cryptochrome 1 C-terminal tail regulates circadian period length. J. Biol. Chem. 288, 35277–35286. https://doi.org/10.1074/jbc.M113.509604

Gekakis, N., Staknis, D., Nguyen, H.B., Davis, F.C., Wilsbacher, L.D., King, D.P., Takahashi, J.S., Weitz, C.J., 1998. Role of the CLOCK protein in the mammalian circadian mechanism. Science 280, 1564–1569. https://doi.org/10.1126/science.280.5369.1564

Gérard, C., Goldbeter, A., 2012. Entrainment of the mammalian cell cycle by the circadian clock: modeling two coupled cellular rhythms. PLoS Comput. Biol. 8, e1002516. https://doi.org/10.1371/journal.pcbi.1002516

Giguère, S.S.B., Guise, A.J., Jean Beltran, P.M., Joshi, P.M., Greco, T.M., Quach, O.L., Kong, J., Cristea, I.M., 2016. The Proteomic Profile of Deleted in Breast Cancer 1 (DBC1)

Interactions Points to a Multifaceted Regulation of Gene Expression. Mol. Cell. Proteomics MCP 15, 791–809. https://doi.org/10.1074/mcp.M115.054619

Gingras, A.-C., Gstaiger, M., Raught, B., Aebersold, R., 2007. Analysis of protein complexes using mass spectrometry. Nat. Rev. Mol. Cell Biol. 8, 645–654. https://doi.org/10.1038/nrm2208

Giulietti, A., Overbergh, L., Valckx, D., Decallonne, B., Bouillon, R., Mathieu, C., 2001. An Overview of Real-Time Quantitative PCR: Applications to Quantify Cytokine Gene Expression. Methods 25, 386–401. https://doi.org/10.1006/meth.2001.1261

Goldsmith, C.S., Bell-Pedersen, D., 2013. Diverse Roles for MAPK Signaling in Circadian Clocks. Adv. Genet. 84, 1–39. https://doi.org/10.1016/B978-0-12-407703-4.00001-3

Golombek, D.A., Rosenstein, R.E., 2010. Physiology of circadian entrainment. Physiol. Rev. 90, 1063–1102. https://doi.org/10.1152/physrev.00009.2009

Gonçalves, C.F., Meng, Q.-J., 2019. Timing metabolism in cartilage and bone: links between circadian clocks and tissue homeostasis. J. Endocrinol. JOE-19-0256.R1. https://doi.org/10.1530/JOE-19-0256

Gonzalez, L., Plecs, J.J., Alber, T., 1996. An engineered allosteric switch in leucine-zipper oligomerization. Nat. Struct. Biol. 3, 510–515. https://doi.org/10.1038/nsb0696-510

Gooley, J.J., Lu, J., Chou, T.C., Scammell, T.E., Saper, C.B., 2001. Melanopsin in cells of origin of the retinohypothalamic tract. Nat. Neurosci. 4, 1165. https://doi.org/10.1038/nn768

Goriki, A., Hatanaka, F., Myung, J., Kim, J.K., Yoritaka, T., Tanoue, S., Abe, T., Kiyonari, H., Fujimoto, K., Kato, Y., Todo, T., Matsubara, A., Forger, D., Takumi, T., 2014. A novel protein, CHRONO, functions as a core component of the mammalian circadian clock. PLoS Biol. 12, e1001839. https://doi.org/10.1371/journal.pbio.1001839

Gossan, N.C., Zhang, F., Guo, B., Jin, D., Yoshitane, H., Yao, A., Glossop, N., Zhang, Y.Q., Fukada, Y., Meng, Q.-J., 2014. The E3 ubiquitin ligase UBE3A is an integral component of the molecular circadian clock through regulating the BMAL1 transcription factor. Nucleic Acids Res. 42, 5765–5775. https://doi.org/10.1093/nar/gku225

Gotoh, T., Vila-Caballer, M., Santos, C.S., Liu, J., Yang, J., Finkielstein, C.V., 2014. The circadian factor Period 2 modulates p53 stability and transcriptional activity in unstressed cells. Mol. Biol. Cell 25, 3081–3093. https://doi.org/10.1091/mbc.E14-05-0993

Green, C.B., 2018. Circadian Posttranscriptional Regulatory Mechanisms in Mammals. Cold Spring Harb. Perspect. Biol. 10, a030692. https://doi.org/10.1101/cshperspect.a030692

Guillen, R.X., Beckley, J.R., Chen, J.-S., Gould, K.L., 2020. CRISPR-mediated gene targeting of CK1δ/ε leads to enhanced understanding of their role in endocytosis via phosphoregulation of GAPVD1. Sci. Rep. 10, 6797. https://doi.org/10.1038/s41598-020-63669-2

Guilluy, C., Swaminathan, V., Garcia-Mata, R., O'Brien, E.T., Superfine, R., Burridge, K., 2011. The Rho GEFs LARG and GEF-H1 regulate the mechanical response to force on integrins. Nat. Cell Biol. 13, 722–727. https://doi.org/10.1038/ncb2254

Gul, H., Selvi, S., Yilmaz, F., Ozcelik, G., Olfaz-Aslan, S., Yazan, S., Tiryaki, B., Gul, S., Yurtseven, A., Kavakli, I.H., Ozlu, N., Ozturk, N., 2022. Proteome analysis of the circadian clock protein PERIOD2. Proteins Struct. Funct. Bioinforma. 90, 1315–1330. https://doi.org/10.1002/prot.26314

Gupta, N.J., 2019. Lifestyle and Circadian Health: Where the Challenges Lie? Nutr. Metab. Insights 12, 1178638819869024. https://doi.org/10.1177/1178638819869024

Hardin, P.E., Hall, J.C., Rosbash, M., 1990. Feedback of the Drosophila period gene product on circadian cycling of its messenger RNA levels. Nature 343, 536–540. https://doi.org/10.1038/343536a0

Harreman, M.T., Kline, T.M., Milford, H.G., Harben, M.B., Hodel, A.E., Corbett, A.H., 2004. Regulation of nuclear import by phosphorylation adjacent to nuclear localization signals. J. Biol. Chem. 279, 20613–20621. https://doi.org/10.1074/jbc.M401720200

Harvey, S.L., Charlet, A., Haas, W., Gygi, S.P., Kellogg, D.R., 2005. Cdk1-dependent regulation of the mitotic inhibitor Wee1. Cell 122, 407–420. https://doi.org/10.1016/j.cell.2005.05.029

Hermle, T., Schneider, R., Schapiro, D., Braun, D.A., van der Ven, A.T., Warejko, J.K., Daga, A., Widmeier, E., Nakayama, M., Jobst-Schwan, T., Majmundar, A.J., Ashraf, S., Rao, J., Finn, L.S., Tasic, V., Hernandez, J.D., Bagga, A., Jalalah, S.M., El Desoky, S., Kari, J.A., Laricchia, K.M., Lek, M., Rehm, H.L., MacArthur, D.G., Mane, S., Lifton, R.P., Shril, S., Hildebrandt, F., 2018. GAPVD1 and ANKFY1 Mutations Implicate RAB5 Regulation in Nephrotic Syndrome. J. Am. Soc. Nephrol. JASN 29, 2123–2138. https://doi.org/10.1681/ASN.2017121312

Hirayama, J., Sahar, S., Grimaldi, B., Tamaru, T., Takamatsu, K., Nakahata, Y., Sassone-Corsi, P., 2007. CLOCK-mediated acetylation of BMAL1 controls circadian function. Nature 450, 1086–1090. https://doi.org/10.1038/nature06394

Hodge, K., Have, S.T., Hutton, L., Lamond, A.I., 2013. Cleaning up the masses: Exclusion lists to reduce contamination with HPLC-MS/MS. J. Proteomics 88, 92–103. https://doi.org/10.1016/j.jprot.2013.02.023

Honma, S., Kawamoto, T., Takagi, Y., Fujimoto, K., Sato, F., Noshiro, M., Kato, Y., Honma, K., 2002. Dec1 and Dec2 are regulators of the mammalian molecular clock. Nature 419, 841–844. https://doi.org/10.1038/nature01123

Hornbeck, P.V., Kornhauser, J.M., Tkachev, S., Zhang, B., Skrzypek, E., Murray, B., Latham, V., Sullivan, M., 2012. PhosphoSitePlus: a comprehensive resource for investigating the structure and function of experimentally determined post-translational modifications in man and mouse. Nucleic Acids Res. 40, D261-270. https://doi.org/10.1093/nar/gkr1122

Hosaka, M., Hammer, R.E., Südhof, T.C., 1999. A Phospho-Switch Controls the Dynamic Association of Synapsins with Synaptic Vesicles. Neuron 24, 377–387. https://doi.org/10.1016/S0896-6273(00)80851-X

Hua, H., Wang, Y., Wan, C., Liu, Y., Zhu, B., Yang, C., Wang, X., Wang, Z., Cornelissen-Guillaume, G., Halberg, F., 2006. Circadian gene mPer2 overexpression induces cancer cell apoptosis. Cancer Sci. 97, 589–596. https://doi.org/10.1111/j.1349-7006.2006.00225.x

Huang, D.W., Sherman, B.T., Lempicki, R.A., 2009. Systematic and integrative analysis of large gene lists using DAVID bioinformatics resources. Nat. Protoc. 4, 44–57. https://doi.org/10.1038/nprot.2008.211

Huang, Z.J., Edery, I., Rosbash, M., 1993. PAS is a dimerization domain common to Drosophila period and several transcription factors. Nature 364, 259–262. https://doi.org/10.1038/364259a0

Hunker, C.M., Galvis, A., Kruk, I., Giambini, H., Veisaga, M.L., Barbieri, M.A., 2006. Rab5-activating protein 6, a novel endosomal protein with a role in endocytosis. Biochem. Biophys. Res. Commun. 340, 967–975. https://doi.org/10.1016/j.bbrc.2005.12.099

Hurley, J.M., Loros, J.J., Dunlap, J.C., 2016. Circadian Oscillators: Around the Transcription-Translation Feedback Loop and on to Output. Trends Biochem. Sci. 41, 834–846. https://doi.org/10.1016/j.tibs.2016.07.009

Ibrahim, H., Reus, P., Mundorf, A.K., Grothoff, A.-L., Rudenko, V., Buschhaus, C., Stefanski, A., Berleth, N., Stork, B., Stühler, K., Kalfalah, F., Reinke, H., 2021. Phosphorylation of GAPVD1 Is Regulated by the PER Complex and Linked to GAPVD1 Degradation. Int. J. Mol. Sci. 22, 3787. https://doi.org/10.3390/ijms22073787

Iitaka, C., Miyazaki, K., Akaike, T., Ishida, N., 2005. A role for glycogen synthase kinase-3beta in the mammalian circadian clock. J. Biol. Chem. 280, 29397–29402. https://doi.org/10.1074/jbc.M503526200

Inoki, K., Li, Y., Zhu, T., Wu, J., Guan, K.-L., 2002. TSC2 is phosphorylated and inhibited by Akt and suppresses mTOR signalling. Nat. Cell Biol. 4, 648–657. https://doi.org/10.1038/ncb839

Inoki, K., Ouyang, H., Zhu, T., Lindvall, C., Wang, Y., Zhang, X., Yang, Q., Bennett, C., Harada, Y., Stankunas, K., Wang, C.-Y., He, X., MacDougald, O.A., You, M., Williams, B.O., Guan, K.-L., 2006. TSC2 integrates Wnt and energy signals via a coordinated phosphorylation by AMPK and GSK3 to regulate cell growth. Cell 126, 955–968. https://doi.org/10.1016/j.cell.2006.06.055

Inoki, K., Zhu, T., Guan, K.-L., 2003. TSC2 mediates cellular energy response to control cell growth and survival. Cell 115, 577–590. https://doi.org/10.1016/s0092-8674(03)00929-2

Isojima, Y., Nakajima, M., Ukai, H., Fujishima, H., Yamada, R.G., Masumoto, K., Kiuchi, R., Ishida, M., Ukai-Tadenuma, M., Minami, Y., Kito, R., Nakao, K., Kishimoto, W., Yoo, S.-H., Shimomura, K., Takao, T., Takano, A., Kojima, T., Nagai, K., Sakaki, Y., Takahashi, J.S., Ueda, H.R., 2009. CKIepsilon/delta-dependent phosphorylation is a temperature-insensitive, period-determining process in the mammalian circadian clock. Proc. Natl. Acad. Sci. U. S. A. 106, 15744–15749. https://doi.org/10.1073/pnas.0908733106

Ito, T., Chiba, T., Ozawa, R., Yoshida, M., Hattori, M., Sakaki, Y., 2001. A comprehensive two-hybrid analysis to explore the yeast protein interactome. Proc. Natl. Acad. Sci. U. S. A. 98, 4569–4574. https://doi.org/10.1073/pnas.061034498

Iurisci, I., Filipski, E., Reinhardt, J., Bach, S., Gianella-Borradori, A., Iacobelli, S., Meijer, L., Lévi, F., 2006. Improved tumor control through circadian clock induction by Seliciclib, a cyclin-dependent kinase inhibitor. Cancer Res. 66, 10720–10728. https://doi.org/10.1158/0008-5472.CAN-06-2086

Janovska, P., Verner, J., Kohoutek, J., Bryjova, L., Gregorova, M., Dzimkova, M., Skabrahova, H., Radaszkiewicz, T., Ovesna, P., Vondalova Blanarova, O., Nemcova, T., Hoferova, Z., Vasickova, K., Smyckova, L., Egle, A., Pavlova, S., Poppova, L., Plevova, K., Pospisilova, S., Bryja, V., 2018. Casein kinase 1 is a therapeutic target in chronic lymphocytic leukemia. Blood 131, 1206–1218. https://doi.org/10.1182/blood-2017-05-786947

Jeffrey, S., Linda, R., Terri A, S., Michael, E., 2009. Inhibition of casein kinase I epsilon/delta produces phase shifts in the circadian rhythms of Cynomolgus monkeys. Psychopharmacology (Berl.) 204. https://doi.org/10.1007/s00213-009-1503-x

Jetten, A.M., 2009. Retinoid-related orphan receptors (RORs): critical roles in development, immunity, circadian rhythm, and cellular metabolism. Nucl. Recept. Signal. 7, e003. https://doi.org/10.1621/nrs.07003

Jordan, S.D., Lamia, K.A., 2013. AMPK at the crossroads of circadian clocks and metabolism. Mol. Cell. Endocrinol. 366, 163–169. https://doi.org/10.1016/j.mce.2012.06.017

Jumper, J., Evans, R., Pritzel, A., Green, T., Figurnov, M., Ronneberger, O., Tunyasuvunakool, K., Bates, R., Žídek, A., Potapenko, A., Bridgland, A., Meyer, C., Kohl, S.A.A., Ballard, A.J., Cowie, A., Romera-Paredes, B., Nikolov, S., Jain, R., Adler, J., Back, T., Petersen, S., Reiman, D., Clancy, E., Zielinski, M., Steinegger, M., Pacholska, M., Berghammer, T., Bodenstein, S., Silver, D., Vinyals, O., Senior, A.W., Kavukcuoglu, K., Kohli, P., Hassabis, D., 2021. Highly accurate protein structure prediction with AlphaFold. Nature 596, 583–589. https://doi.org/10.1038/s41586-021-03819-2

Kaasik, K., Lee, C.C., 2004. Reciprocal regulation of haem biosynthesis and the circadian clock in mammals. Nature 430, 467–471. https://doi.org/10.1038/nature02724

Kalfalah, F., Janke, L., Schiavi, A., Tigges, J., Ix, A., Ventura, N., Boege, F., Reinke, H., 2016. Crosstalk of clock gene expression and autophagy in aging. Aging 8, 1876–1895. https://doi.org/10.18632/aging.101018

Kang, D.-H., Gho, Y.-S., Suh, M.-K., Kang, C.-H., 2002. Highly Sensitive and Fast Protein Detection with Coomassie Brilliant Blue in Sodium Dodecyl Sulfate-Polyacrylamide Gel Electrophoresis. Bull. Korean Chem. Soc. 23, 1511–1512. https://doi.org/10.5012/bkcs.2002.23.11.1511

Kang, R.S., Daniels, C.M., Francis, S.A., Shih, S.C., Salerno, W.J., Hicke, L., Radhakrishnan, I., 2003. Solution structure of a CUE-ubiquitin complex reveals a conserved mode of ubiquitin binding. Cell 113, 621–630. https://doi.org/10.1016/s0092-8674(03)00362-3

Karantanos, T., Theodoropoulos, G., Gazouli, M., Vaiopoulou, A., Karantanou, C., Lymberi, M., Pektasides, D., 2013. Expression of clock genes in patients with colorectal cancer. Int. J. Biol. Markers 28, 280–285. https://doi.org/10.5301/jbm.5000033

Kategaya, L.S., Hilliard, A., Zhang, L., Asara, J.M., Ptáček, L.J., Fu, Y.-H., 2012. Casein kinase 1 proteomics reveal prohibitin 2 function in molecular clock. PloS One 7, e31987. https://doi.org/10.1371/journal.pone.0031987

Keesler, G.A., Camacho, F., Guo, Y., Virshup, D., Mondadori, C., Yao, Z., 2000. Phosphorylation and destabilization of human period I clock protein by human casein kinase I epsilon. Neuroreport 11, 951–955. https://doi.org/10.1097/00001756-200004070-00011

Keilhauer, E.C., Hein, M.Y., Mann, M., 2015. Accurate protein complex retrieval by affinity enrichment mass spectrometry (AE-MS) rather than affinity purification mass spectrometry (AP-MS). Mol. Cell. Proteomics MCP 14, 120–135. https://doi.org/10.1074/mcp.M114.041012

Kim, B., Araujo, R., Howard, M., Magni, R., Liotta, L., Luchini, A., 2018. Affinity Enrichment for MS: Improving the yield of low abundance biomarkers. Expert Rev. Proteomics 15, 353. https://doi.org/10.1080/14789450.2018.1450631

Kim, E.Y., Jeong, E.H., Park, S., Jeong, H.-J., Edery, I., Cho, J.W., 2012. A role for O-GlcNAcylation in setting circadian clock speed. Genes Dev. 26, 490–502. https://doi.org/10.1101/gad.182378.111

Kögel, A., Keidel, A., Bonneau, F., Schäfer, I.B., Conti, E., 2022. The human SKI complex regulates channeling of ribosome-bound RNA to the exosome via an intrinsic gatekeeping mechanism. Mol. Cell 82, 756-769.e8. https://doi.org/10.1016/j.molcel.2022.01.009

Koike, R., Amano, M., Kaibuchi, K., Ota, M., 2020. Protein kinases phosphorylate long disordered regions in intrinsically disordered proteins. Protein Sci. Publ. Protein Soc. 29, 564–571. https://doi.org/10.1002/pro.3789

Kojima, S., Shingle, D.L., Green, C.B., 2011. Post-transcriptional control of circadian rhythms. J. Cell Sci. 124, 311–320. https://doi.org/10.1242/jcs.065771

Kuhlman, S.J., Craig, L.M., Duffy, J.F., 2018. Introduction to Chronobiology. Cold Spring Harb. Perspect. Biol. 10, a033613. https://doi.org/10.1101/cshperspect.a033613

Kume, K., Zylka, M.J., Sriram, S., Shearman, L.P., Weaver, D.R., Jin, X., Maywood, E.S., Hastings, M.H., Reppert, S.M., 1999. mCRY1 and mCRY2 are essential components of the negative limb of the circadian clock feedback loop. Cell 98, 193–205. https://doi.org/10.1016/s0092-8674(00)81014-4

Kwak, Y., Jeong, J., Lee, S., Park, Y.-U., Lee, S.-A., Han, D.-H., Kim, J.-H., Ohshima, T., Mikoshiba, K., Suh, Y.-H., Cho, S., Park, S.K., 2013. Cyclin-dependent kinase 5 (Cdk5) regulates the function of CLOCK protein by direct phosphorylation. J. Biol. Chem. 288, 36878–36889. https://doi.org/10.1074/jbc.M113.494856

Lamia, K.A., Papp, S.J., Yu, R.T., Barish, G.D., Uhlenhaut, N.H., Jonker, J.W., Downes, M., Evans, R.M., 2011. Cryptochromes mediate rhythmic repression of the glucocorticoid receptor. Nature 480, 552–556. https://doi.org/10.1038/nature10700

Lamia, K.A., Sachdeva, U.M., DiTacchio, L., Williams, E.C., Alvarez, J.G., Egan, D.F., Vasquez, D.S., Juguilon, H., Panda, S., Shaw, R.J., Thompson, C.B., Evans, R.M., 2009. AMPK regulates the circadian clock by cryptochrome phosphorylation and degradation. Science 326, 437–440. https://doi.org/10.1126/science.1172156

Langmesser, S., Tallone, T., Bordon, A., Rusconi, S., Albrecht, U., 2008. Interaction of circadian clock proteins PER2 and CRY with BMAL1 and CLOCK. BMC Mol. Biol. 9, 41. https://doi.org/10.1186/1471-2199-9-41

Lee, C., Etchegaray, J.P., Cagampang, F.R., Loudon, A.S., Reppert, S.M., 2001. Posttranslational mechanisms regulate the mammalian circadian clock. Cell 107, 855–867. https://doi.org/10.1016/s0092-8674(01)00610-9

Lee, C., Weaver, D.R., Reppert, S.M., 2004. Direct association between mouse PERIOD and CKIepsilon is critical for a functioning circadian clock. Mol. Cell. Biol. 24, 584–594. https://doi.org/10.1128/MCB.24.2.584-594.2004

Lee, C.-R., Park, Y.-H., Kim, Y.-R., Peterkofsky, A., Seok, Y.-J., 2013. Phosphorylation-Dependent Mobility Shift of Proteins on SDS-PAGE is Due to Decreased Binding of SDS. Bull. Korean Chem. Soc. 34, 2063–2066. https://doi.org/10.5012/bkcs.2013.34.7.2063

Lee, H., Chen, R., Lee, Y., Yoo, S., Lee, C., 2009. Essential roles of CKIdelta and CKIepsilon in the mammalian circadian clock. Proc. Natl. Acad. Sci. U. S. A. 106, 21359–21364. https://doi.org/10.1073/pnas.0906651106

Lee, J., Lee, S., Chung, S., Park, N., Son, G.H., An, H., Jang, J., Chang, D.-J., Suh, Y.-G., Kim, K., 2016. Identification of a novel circadian clock modulator controlling BMAL1 expression through a ROR/REV-ERB-response element-dependent mechanism. Biochem. Biophys. Res. Commun. 469, 580–586. https://doi.org/10.1016/j.bbrc.2015.12.030

Lee, K.-H., Kim, S.-H., Kim, H.-J., Kim, W., Lee, H.-R., Jung, Y., Choi, J.-H., Hong, K.Y., Jang, S.K., Kim, K.-T., 2014. AUF1 contributes to Cryptochrome1 mRNA degradation and rhythmic translation. Nucleic Acids Res. 42, 3590–3606. https://doi.org/10.1093/nar/gkt1379

Lee, S.-A., Chan, C., Tsai, C.-H., Lai, J.-M., Wang, F.-S., Kao, C.-Y., Huang, C.-Y.F., 2008. Ortholog-based protein-protein interaction prediction and its application to inter-species interactions. BMC Bioinformatics 9, S11. https://doi.org/10.1186/1471-2105-9-S12-S11

Lee, Y., Chun, S.K., Kim, K., 2015. Sumoylation controls CLOCK-BMAL1-mediated clock resetting via CBP recruitment in nuclear transcriptional foci. Biochim. Biophys. Acta BBA - Mol. Cell Res. 1853, 2697–2708. https://doi.org/10.1016/j.bbamcr.2015.07.005

Lei, M., 2005. The MCM complex: its role in DNA replication and implications for cancer therapy. Curr. Cancer Drug Targets 5, 365–380. https://doi.org/10.2174/1568009054629654

Levin, R.S., Hertz, N.T., Burlingame, A.L., Shokat, K.M., Mukherjee, S., 2016. Innate immunity kinase TAK1 phosphorylates Rab1 on a hotspot for posttranslational modifications by host and pathogen. Proc. Natl. Acad. Sci. U. S. A. 113, E4776-4783. https://doi.org/10.1073/pnas.1608355113

Li, H., Xu, L.-X., Yu, J., Tan, L., Miao, P., Yang, X., Tian, Q., Li, M., Feng, C.-X., Yang, Y., Sha, N., Feng, X., Sun, B., Gong, M., Ding, X., 2020. The role of a lncRNA (TCONS_00044595) in regulating pineal CLOCK expression after neonatal hypoxia-ischemia brain injury. Biochem. Biophys. Res. Commun. 528, 1–6. https://doi.org/10.1016/j.bbrc.2020.05.047

Li, M.-D., Ruan, H.-B., Hughes, M.E., Lee, J.-S., Singh, J.P., Jones, S.P., Nitabach, M.N., Yang, X., 2013. O-GlcNAc signaling entrains the circadian clock by inhibiting

BMAL1/CLOCK ubiquitination. Cell Metab. 17, 303–310. https://doi.org/10.1016/j.cmet.2012.12.015

Li, T., Wen, Y., Guo, H., Yang, T., Yang, H., Ji, X., 2022. Molecular Mechanism of SARS-CoVs Orf6 Targeting the Rae1–Nup98 Complex to Compete With mRNA Nuclear Export. Front. Mol. Biosci. 8, 813248. https://doi.org/10.3389/fmolb.2021.813248

Li, Y., 2010. Commonly used tag combinations for tandem affinity purification. Biotechnol. Appl. Biochem. 55, 73–83. https://doi.org/10.1042/BA20090273

Lipton, J.O., Yuan, E.D., Boyle, L.M., Ebrahimi-Fakhari, D., Kwiatkowski, E., Nathan, A., Güttler, T., Davis, F., Asara, J.M., Sahin, M., 2015. The Circadian Protein BMAL1 Regulates Translation in Response to S6K1-Mediated Phosphorylation. Cell 161, 1138–1151. https://doi.org/10.1016/j.cell.2015.04.002

Liu, J., Malkani, G., Shi, X., Meyer, M., Cunningham-Runddles, S., Ma, X., Sun, Z.S., 2006. The circadian clock Period 2 gene regulates gamma interferon production of NK cells in host response to lipopolysaccharide-induced endotoxic shock. Infect. Immun. 74, 4750–4756. https://doi.org/10.1128/IAI.00287-06

Liu, Li, Liu, Lingli, Deng, S., Zou, L., He, Y., Zhu, X., Li, H., Hu, Y., Chu, W., Wang, X., 2024. Circadian Rhythm Alteration of the Core Clock Genes and the Lipid Metabolism Genes Induced by High-Fat Diet (HFD) in the Liver Tissue of the Chinese Soft-Shelled Turtle (Trionyx sinensis). Genes 15. https://doi.org/10.3390/genes15020157

Livak, K.J., Schmittgen, T.D., 2001. Analysis of relative gene expression data using real-time quantitative PCR and the 2(-Delta Delta C(T)) Method. Methods San Diego Calif 25, 402–408. https://doi.org/10.1006/meth.2001.1262

Lodhi, I.J., Chiang, S.-H., Chang, L., Vollenweider, D., Watson, R.T., Inoue, M., Pessin, J.E., Saltiel, A.R., 2007. Gapex-5, a Rab31 guanine nucleotide exchange factor that regulates Glut4 trafficking in adipocytes. Cell Metab. 5, 59–72. https://doi.org/10.1016/j.cmet.2006.12.006

Lombardi, A., Bryson, J.W., Ghirlanda, G., DeGrado, W.F., 1997. Design of a Synthetic Receptor for the Calmodulin-Binding Domain of Calcineurin. J. Am. Chem. Soc. 119, 12378–12379. https://doi.org/10.1021/ja972973d

Lowrey, P.L., Shimomura, K., Antoch, M.P., Yamazaki, S., Zemenides, P.D., Ralph, M.R., Menaker, M., Takahashi, J.S., 2000. Positional syntenic cloning and functional characterization of the mammalian circadian mutation tau. Science 288, 483–492. https://doi.org/10.1126/science.288.5465.483

Ma, D., Hou, L., Xia, H., Li, H., Fan, H., Jia, X., Niu, Z., 2020. PER2 inhibits proliferation and stemness of glioma stem cells via the Wnt/β-catenin signaling pathway. Oncol. Rep. 44, 533–542. https://doi.org/10.3892/or.2020.7624

Ma, L., Chen, Z., Erdjument-Bromage, H., Tempst, P., Pandolfi, P.P., 2005. Phosphorylation and functional inactivation of TSC2 by Erk implications for tuberous sclerosis and cancer pathogenesis. Cell 121, 179–193. https://doi.org/10.1016/j.cell.2005.02.031

Maekawa, F., Shimba, S., Takumi, S., Sano, T., Suzuki, T., Bao, J., Ohwada, M., Ehara, T., Ogawa, Y., Nohara, K., 2012. Diurnal expression of Dnmt3b mRNA in mouse liver is regulated by feeding and hepatic clockwork. Epigenetics 7, 1046–1056. https://doi.org/10.4161/epi.21539

Magni, M., Buscemi, G., Zannini, L., 2018. Cell cycle and apoptosis regulator 2 at the interface between DNA damage response and cell physiology. Mutat. Res. Mutat. Res. 776, 1–9. https://doi.org/10.1016/j.mrrev.2018.03.004

Marin, O., Bustos, V.H., Cesaro, L., Meggio, F., Pagano, M.A., Antonelli, M., Allende, C.C., Pinna, L.A., Allende, J.E., 2003. A noncanonical sequence phosphorylated by casein kinase 1 in beta-catenin may play a role in casein kinase 1 targeting of important signaling

proteins. Proc. Natl. Acad. Sci. U. S. A. 100, 10193–10200. https://doi.org/10.1073/pnas.1733909100

Martins, A., Shuman, S., 2002. The domain order of mammalian capping enzyme can be inverted and baculovirus phosphatase can function in cap formation in vivo. Virology 304, 167–175. https://doi.org/10.1006/viro.2002.1606

Marzoll, D., Serrano, F.E., Shostak, A., Schunke, C., Diernfellner, A.C.R., Brunner, M., 2022. Casein kinase 1 and disordered clock proteins form functionally equivalent, phospho-based circadian modules in fungi and mammals. Proc. Natl. Acad. Sci. U. S. A. 119, e2118286119. https://doi.org/10.1073/pnas.2118286119

Masuda, S., Narasimamurthy, R., Yoshitane, H., Kim, J.K., Fukada, Y., Virshup, D.M., 2020. Mutation of a PER2 phosphodegron perturbs the circadian phosphoswitch. Proc. Natl. Acad. Sci. 117, 10888–10896. https://doi.org/10.1073/pnas.2000266117

Matern, H.T., Yeaman, C., Nelson, W.J., Scheller, R.H., 2001. The Sec6/8 complex in mammalian cells: characterization of mammalian Sec3, subunit interactions, and expression of subunits in polarized cells. Proc. Natl. Acad. Sci. U. S. A. 98, 9648–9653. https://doi.org/10.1073/pnas.171317898

Matsuo, T., Yamaguchi, S., Mitsui, S., Emi, A., Shimoda, F., Okamura, H., 2003. Control mechanism of the circadian clock for timing of cell division in vivo. Science 302, 255–259. https://doi.org/10.1126/science.1086271

Mauvoisin, D., Gachon, F., 2020. Proteomics in Circadian Biology. J. Mol. Biol., Circadian Regulation: from Molecules to Physiology 432, 3565–3577. https://doi.org/10.1016/j.jmb.2019.12.004

Mauvoisin, D., Wang, J., Jouffe, C., Martin, E., Atger, F., Waridel, P., Quadroni, M., Gachon, F., Naef, F., 2014. Circadian clock-dependent and -independent rhythmic proteomes implement distinct diurnal functions in mouse liver. Proc. Natl. Acad. Sci. U. S. A. 111, 167–172. https://doi.org/10.1073/pnas.1314066111

Mazzoccoli, G., Panza, A., Valvano, M.R., Palumbo, O., Carella, M., Pazienza, V., Biscaglia, G., Tavano, F., Di Sebastiano, P., Andriulli, A., Piepoli, A., 2011. Clock gene expression levels and relationship with clinical and pathological features in colorectal cancer patients. Chronobiol. Int. 28, 841–851. https://doi.org/10.3109/07420528.2011.615182

Mehra, A., Baker, C.L., Loros, J.J., Dunlap, J.C., 2009. Post-translational modifications in circadian rhythms. Trends Biochem. Sci. 34, 483–490. https://doi.org/10.1016/j.tibs.2009.06.006

Meng, E.C., Goddard, T.D., Pettersen, E.F., Couch, G.S., Pearson, Z.J., Morris, J.H., Ferrin, T.E., 2023. UCSF ChimeraX: Tools for structure building and analysis. Protein Sci. Publ. Protein Soc. 32, e4792. https://doi.org/10.1002/pro.4792

Meng, Q.-J., Logunova, L., Maywood, E.S., Gallego, M., Lebiecki, J., Brown, T.M., Sládek, M., Semikhodskii, A.S., Glossop, N.R.J., Piggins, H.D., Chesham, J.E., Bechtold, D.A., Yoo, S.-H., Takahashi, J.S., Virshup, D.M., Boot-Handford, R.P., Hastings, M.H., Loudon, A.S.I., 2008. Setting clock speed in mammals: the CK1ε tau mutation in mice accelerates the circadian pacemaker by selectively destabilizing PERIOD proteins. Neuron 58, 78–88. https://doi.org/10.1016/j.neuron.2008.01.019

Mielke, C., Tümmler, M., Schübeler, D., von Hoegen, I., Hauser, H., 2000. Stabilized, long-term expression of heterodimeric proteins from tricistronic mRNA. Gene 254, 1–8. https://doi.org/10.1016/s0378-1119(00)00294-8

Milroy, L.-G., Brunsveld, L., Ottmann, C., 2013. Stabilization and inhibition of protein-protein interactions: the 14-3-3 case study. ACS Chem. Biol. 8, 27–35. https://doi.org/10.1021/cb300599t

Miyazaki, K., Mesaki, M., Ishida, N., 2001. Nuclear entry mechanism of rat PER2 (rPER2): role of rPER2 in nuclear localization of CRY protein. Mol. Cell. Biol. 21, 6651–6659. https://doi.org/10.1128/MCB.21.19.6651-6659.2001

Miyazaki, Koyomi, Mesaki, M., Ishida, N., 2001. Nuclear Entry Mechanism of Rat PER2 (rPER2): Role of rPER2 in Nuclear Localization of CRY Protein. Mol. Cell. Biol. 21, 6651–6659. https://doi.org/10.1128/MCB.21.19.6651-6659.2001

Miyazaki, K., Wakabayashi, M., Chikahisa, S., Sei, H., Ishida, N., 2007. PER2 controls circadian periods through nuclear localization in the suprachiasmatic nucleus. Genes Cells Devoted Mol. Cell. Mech. 12, 1225–1234. https://doi.org/10.1111/j.1365-2443.2007.01129.x

Mohamed, H.M.A., Takahashi, A., Nishijima, S., Adachi, S., Murai, I., Okamura, H., Yamamoto, T., 2022. CNOT1 regulates circadian behaviour through Per2 mRNA decay in a deadenylation-dependent manner. RNA Biol. 19, 703–718. https://doi.org/10.1080/15476286.2022.2071026

Molina, J.R., Adjei, A.A., 2006. The Ras/Raf/MAPK Pathway. J. Thorac. Oncol. 1, 7–9. https://doi.org/10.1016/S1556-0864(15)31506-9

Mosig, R.A., Kojima, S., 2022. Timing without coding: How do long non-coding RNAs regulate circadian rhythms? Semin. Cell Dev. Biol. 126, 79–86. https://doi.org/10.1016/j.semcdb.2021.04.020

Mundorf, A.K., 2022. Überprüfung der Interaktion des Uhrenproteins PER2 mit dem Protein GAPVD1 durch Proximity Ligation Assay. heinrich heine universität.

Nakashima, A., Kawamoto, T., Honda, K.K., Ueshima, T., Noshiro, M., Iwata, T., Fujimoto, K., Kubo, H., Honma, S., Yorioka, N., Kohno, N., Kato, Y., 2008. DEC1 Modulates the Circadian Phase of Clock Gene Expression. Mol. Cell. Biol. 28, 4080–4092. https://doi.org/10.1128/MCB.02168-07

Nam, H.J., Boo, K., Kim, D., Han, D.-H., Choe, H.K., Kim, C.R., Sun, W., Kim, H., Kim, K., Lee, H., Metzger, E., Schuele, R., Yoo, S.-H., Takahashi, J.S., Cho, S., Son, G.H., Baek, S.H., 2014. Phosphorylation of LSD1 by PKCα is crucial for circadian rhythmicity and phase resetting. Mol. Cell 53, 791–805. https://doi.org/10.1016/j.molcel.2014.01.028

Nangle, S.N., Rosensweig, C., Koike, N., Tei, H., Takahashi, J.S., Green, C.B., Zheng, N., 2014. Molecular assembly of the period-cryptochrome circadian transcriptional repressor complex. eLife 3, e03674. https://doi.org/10.7554/eLife.03674

Narasimamurthy, R., Hunt, S.R., Lu, Y., Fustin, J.-M., Okamura, H., Partch, C.L., Forger, D.B., Kim, J.K., Virshup, D.M., 2018. CK1δ/ε protein kinase primes the PER2 circadian phosphoswitch. Proc. Natl. Acad. Sci. 115, 5986–5991. https://doi.org/10.1073/pnas.1721076115

Narasimamurthy, R., Virshup, D.M., 2021. The phosphorylation switch that regulates ticking of the circadian clock. Mol. Cell 81, 1133–1146. https://doi.org/10.1016/j.molcel.2021.01.006

Naumov, V., Balashov, I., Lagutin, V., Borovikov, P., Alexeev, A., 2017. VolcanoR - web service to produce volcano plots and do basic enrichment analysis. https://doi.org/10.1101/165100

Neufeld-Cohen, A., Robles, M.S., Aviram, R., Manella, G., Adamovich, Y., Ladeuix, B., Nir, D., Rousso-Noori, L., Kuperman, Y., Golik, M., Mann, M., Asher, G., 2016. Circadian control of oscillations in mitochondrial rate-limiting enzymes and nutrient utilization by PERIOD proteins. Proc. Natl. Acad. Sci. U. S. A. 113, E1673–E1682. https://doi.org/10.1073/pnas.1519650113

Nolte, C., Staiger, D., 2015. RNA around the clock – regulation at the RNA level in biological timing. Front. Plant Sci. 6, 311. https://doi.org/10.3389/fpls.2015.00311

Nooren, I.M.A., Thornton, J.M., 2003. Diversity of protein-protein interactions. EMBO J. 22, 3486–3492. https://doi.org/10.1093/emboj/cdg359

Ohno, T., Onishi, Y., Ishida, N., 2007. The negative transcription factor E4BP4 is associated with circadian clock protein PERIOD2. Biochem. Biophys. Res. Commun. 354, 1010–1015. https://doi.org/10.1016/j.bbrc.2007.01.084

Ohsaki, K., Oishi, K., Kozono, Y., Nakayama, K., Nakayama, K.I., Ishida, N., 2008. The role of {beta}-TrCP1 and {beta}-TrCP2 in circadian rhythm generation by mediating degradation of clock protein PER2. J. Biochem. (Tokyo) 144, 609–618. https://doi.org/10.1093/jb/mvn112

Ohtsu, H., Mifune, M., Frank, G.D., Saito, S., Inagami, T., Kim-Mitsuyama, S., Takuwa, Y., Sasaki, T., Rothstein, J.D., Suzuki, H., Nakashima, H., Woolfolk, E.A., Motley, E.D., Eguchi, S., 2005. Signal-crosstalk between Rho/ROCK and c-Jun NH2-terminal kinase mediates migration of vascular smooth muscle cells stimulated by angiotensin II. Arterioscler. Thromb. Vasc. Biol. 25, 1831–1836. https://doi.org/10.1161/01.ATV.0000175749.41799.9b

Olsen, J.V., Vermeulen, M., Santamaria, A., Kumar, C., Miller, M.L., Jensen, L.J., Gnad, F., Cox, J., Jensen, T.S., Nigg, E.A., Brunak, S., Mann, M., 2010. Quantitative phosphoproteomics reveals widespread full phosphorylation site occupancy during mitosis. Sci. Signal. 3, ra3. https://doi.org/10.1126/scisignal.2000475

Ooi, S.L., Pan, X., Peyser, B.D., Ye, P., Meluh, P.B., Yuan, D.S., Irizarry, R.A., Bader, J.S., Spencer, F.A., Boeke, J.D., 2006. Global synthetic-lethality analysis and yeast functional profiling. Trends Genet. TIG 22, 56–63. https://doi.org/10.1016/j.tig.2005.11.003

Oshima, T., Takenoshita, S., Akaike, M., Kunisaki, C., Fujii, S., Nozaki, A., Numata, K., Shiozawa, M., Rino, Y., Tanaka, K., Masuda, M., Imada, T., 2011. Expression of circadian genes correlates with liver metastasis and outcomes in colorectal cancer. Oncol. Rep. 25, 1439–1446. https://doi.org/10.3892/or.2011.1207

Oyama, Y., Shuff, S.R., Burns, N., Vohwinkel, C.U., Eckle, T., 2022. Intense light-elicited alveolar type 2-specific circadian PER2 protects from bacterial lung injury via BPIFB1. Am. J. Physiol. Lung Cell. Mol. Physiol. 322, L647–L661. https://doi.org/10.1152/ajplung.00301.2021

Panda, S., Antoch, M.P., Miller, B.H., Su, A.I., Schook, A.B., Straume, M., Schultz, P.G., Kay, S.A., Takahashi, J.S., Hogenesch, J.B., 2002. Coordinated transcription of key pathways in the mouse by the circadian clock. Cell 109, 307–320. https://doi.org/10.1016/s0092-8674(02)00722-5

Paneque, A., Fortus, H., Zheng, J., Werlen, G., Jacinto, E., 2023. The Hexosamine Biosynthesis Pathway: Regulation and Function. Genes 14, 933. https://doi.org/10.3390/genes14040933

Papp, S.J., Huber, A.-L., Jordan, S.D., Kriebs, A., Nguyen, M., Moresco, J.J., Yates, J.R., III, Lamia, K.A., 2015. DNA damage shifts circadian clock time via Hausp-dependent Cry1 stabilization. eLife 4, e04883. https://doi.org/10.7554/eLife.04883

Parico, G.C.G., Partch, C.L., 2020. The tail of cryptochromes: an intrinsically disordered cog within the mammalian circadian clock. Cell Commun. Signal. CCS 18, 182. https://doi.org/10.1186/s12964-020-00665-z

Parico, G.C.G., Perez, I., Fribourgh, J.L., Hernandez, B.N., Lee, H.-W., Partch, C.L., 2020. The human CRY1 tail controls circadian timing by regulating its association with CLOCK:BMAL1. Proc. Natl. Acad. Sci. U. S. A. 117, 27971–27979. https://doi.org/10.1073/pnas.1920653117

Patke, A., Young, M.W., Axelrod, S., 2020. Molecular mechanisms and physiological importance of circadian rhythms. Nat. Rev. Mol. Cell Biol. 21, 67–84. https://doi.org/10.1038/s41580-019-0179-2

Pendergast, J.S., Niswender, K.D., Yamazaki, S., 2012. Tissue-specific function of Period3 in circadian rhythmicity. PloS One 7, e30254. https://doi.org/10.1371/journal.pone.0030254

Peng, Y., Grassart, A., Lu, R., Wong, C.C.L., Yates, J., Barnes, G., Drubin, D.G., 2015. Casein Kinase 1 Promotes Initiation of Clathrin-Mediated Endocytosis. Dev. Cell 32, 231–240. https://doi.org/10.1016/j.devcel.2014.11.014

Philpott, J.M., Narasimamurthy, R., Ricci, C.G., Freeberg, A.M., Hunt, S.R., Yee, L.E., Pelofsky, R.S., Tripathi, S., Virshup, D.M., Partch, C.L., 2020. Casein kinase 1 dynamics underlie substrate selectivity and the PER2 circadian phosphoswitch. eLife 9, e52343. https://doi.org/10.7554/eLife.52343

Pitt, J.J., 2009. Principles and Applications of Liquid Chromatography-Mass Spectrometry in Clinical Biochemistry. Clin. Biochem. Rev. 30, 19–34.

Pomaznoy, M., Ha, B., Peters, B., 2018. GOnet: a tool for interactive Gene Ontology analysis. BMC Bioinformatics 19, 470. https://doi.org/10.1186/s12859-018-2533-3

Ponting, C.P., Aravind, L., 1997. PAS: a multifunctional domain family comes to light. Curr. Biol. CB 7, R674-677. https://doi.org/10.1016/s0960-9822(06)00352-6

Prag, G., Misra, S., Jones, E.A., Ghirlando, R., Davies, B.A., Horazdovsky, B.F., Hurley, J.H., 2003. Mechanism of Ubiquitin Recognition by the CUE Domain of Vps9p. Cell 113, 609–620. https://doi.org/10.1016/S0092-8674(03)00364-7

Preitner, N., Damiola, F., Lopez-Molina, L., Zakany, J., Duboule, D., Albrecht, U., Schibler, U., 2002. The orphan nuclear receptor REV-ERBalpha controls circadian transcription within the positive limb of the mammalian circadian oscillator. Cell 110, 251–260. https://doi.org/10.1016/s0092-8674(02)00825-5

Prkacin, I., Balenovic, D., Djermanovic-Dobrota, V., Lukac, I., Drazic, P., Pranjic, I.-K., 2015. Resistant Hypertension and Chronotherapy. Mater. Socio-Medica 27, 118–121. https://doi.org/10.5455/msm.2015.27.118-121

PubChem, n.d. PF-670462 [WWW Document]. URL https://pubchem.ncbi.nlm.nih.gov/compound/51049607 (accessed 1.1.23).

Qin, X., Mori, T., Zhang, Y., Johnson, C.H., 2015. PER2 Differentially Regulates Clock Phosphorylation versus Transcription by Reciprocal Switching of CK1ε Activity. J. Biol. Rhythms 30, 206–216. https://doi.org/10.1177/0748730415582127

Rahman, A., Hasan, A.U., Kobori, H., 2019. Melatonin in chronic kidney disease: a promising chronotherapy targeting the intrarenal renin-angiotensin system. Hypertens. Res. Off. J. Jpn. Soc. Hypertens. 42, 920–923. https://doi.org/10.1038/s41440-019-0223-9

Ralph, M.R., Menaker, M., 1988. A mutation of the circadian system in golden hamsters. Science 241, 1225–1227. https://doi.org/10.1126/science.3413487

Rao, V.S., Srinivas, K., Sujini, G.N., Kumar, G.N.S., 2014. Protein-Protein Interaction Detection: Methods and Analysis. Int. J. Proteomics 2014, 147648. https://doi.org/10.1155/2014/147648

Raudvere, U., Kolberg, L., Kuzmin, I., Arak, T., Adler, P., Peterson, H., Vilo, J., 2019. g:Profiler: a web server for functional enrichment analysis and conversions of gene lists (2019 update). Nucleic Acids Res. 47, W191–W198. https://doi.org/10.1093/nar/gkz369

Reddy, P., Zehring, W.A., Wheeler, D.A., Pirrotta, V., Hadfield, C., Hall, J.C., Rosbash, M., 1984. Molecular analysis of the period locus in Drosophila melanogaster and identification of a transcript involved in biological rhythms. Cell 38, 701–710. https://doi.org/10.1016/0092-8674(84)90265-4

Regulation of nuclear import by phosphorylation adjacent to nuclear localization signals - PubMed [WWW Document], n.d. URL https://pubmed.ncbi.nlm.nih.gov/14998990/ (accessed 3.29.24).

Rehbein, U., Prentzell, M.T., Cadena Sandoval, M., Heberle, A.M., Henske, E.P., Opitz, C.A., Thedieck, K., 2021. The TSC Complex-mTORC1 Axis: From Lysosomes to Stress Granules and Back. Front. Cell Dev. Biol. 9, 751892. https://doi.org/10.3389/fcell.2021.751892

Reischl, S., Vanselow, K., Westermark, P.O., Thierfelder, N., Maier, B., Herzel, H., Kramer, A., 2007. Beta-TrCP1-mediated degradation of PERIOD2 is essential for circadian dynamics. J. Biol. Rhythms 22, 375–386. https://doi.org/10.1177/0748730407303926

Reus, P., 2020. Gegenseitige Regulation von PER-Komplex- Komponenten: Kontrolle der GAPVD1-Phosphorylierung durch PER2 und CSNK1D. heinrich heine universität.

Richards, J., Greenlee, M.M., Jeffers, L.A., Cheng, K.-Y., Guo, L., Eaton, D.C., Gumz, M.L., 2012. Inhibition of αENaC expression and ENaC activity following blockade of the circadian clock-regulatory kinases CK1δ/ε. Am. J. Physiol. - Ren. Physiol. 303, F918–F927. https://doi.org/10.1152/ajprenal.00678.2011

Rieloff, E., Skepö, M., 2020. Phosphorylation of a Disordered Peptide-Structural Effects and Force Field Inconsistencies. J. Chem. Theory Comput. 16, 1924–1935. https://doi.org/10.1021/acs.jctc.9b01190

Ripperger, J.A., Albrecht, U., 2012. The circadian clock component PERIOD2: from molecular to cerebral functions. Prog. Brain Res. 199, 233–245. https://doi.org/10.1016/B978-0-444-59427-3.00014-9

Ripperger, J.A., Schibler, U., 2006. Rhythmic CLOCK-BMAL1 binding to multiple E-box motifs drives circadian Dbp transcription and chromatin transitions. Nat. Genet. 38, 369–374. https://doi.org/10.1038/ng1738

Robles, M.S., Boyault, C., Knutti, D., Padmanabhan, K., Weitz, C.J., 2010. Identification of RACK1 and protein kinase Calpha as integral components of the mammalian circadian clock. Science 327, 463–466. https://doi.org/10.1126/science.1180067

Robles, M.S., Humphrey, S.J., Mann, M., 2017a. Phosphorylation Is a Central Mechanism for Circadian Control of Metabolism and Physiology. Cell Metab. 25, 118–127. https://doi.org/10.1016/j.cmet.2016.10.004

Robles, M.S., Humphrey, S.J., Mann, M., 2017b. Phosphorylation Is a Central Mechanism for Circadian Control of Metabolism and Physiology. Cell Metab. 25, 118–127. https://doi.org/10.1016/j.cmet.2016.10.004

Robles, M.S., Humphrey, S.J., Mann, M., 2017c. Phosphorylation Is a Central Mechanism for Circadian Control of Metabolism and Physiology. Cell Metab. 25, 118–127. https://doi.org/10.1016/j.cmet.2016.10.004

Robles, M.S., Mann, M., 2013. Proteomic Approaches in Circadian Biology, in: Kramer, A., Merrow, M. (Eds.), Circadian Clocks, Handbook of Experimental Pharmacology. Springer, Berlin, Heidelberg, pp. 389–407. https://doi.org/10.1007/978-3-642-25950-0_17

Rodrigues, R.P., Silva, C.H.T.P. da, 2017. Discovery of potential neurodegenerative inhibitors in Alzheimer's disease by casein kinase 1 structure-based virtual screening. Med. Chem. Res. 26, 3274–3285. https://doi.org/10.1007/s00044-017-2020-9

Rossi Sebastiano, M., Konstantinidou, G., 2019. Targeting Long Chain Acyl-CoA Synthetases for Cancer Therapy. Int. J. Mol. Sci. 20, 3624. https://doi.org/10.3390/ijms20153624

Rossner, M.J., Dörr, J., Gass, P., Schwab, M.H., Nave, K.A., 1997. SHARPs: mammalian enhancer-of-split- and hairy-related proteins coupled to neuronal stimulation. Mol. Cell. Neurosci. 9, 460–475. https://doi.org/10.1006/mcne.1997.0640

Sahar, S., Zocchi, L., Kinoshita, C., Borrelli, E., Sassone-Corsi, P., 2010. Regulation of BMAL1 protein stability and circadian function by GSK3beta-mediated phosphorylation. PloS One 5, e8561. https://doi.org/10.1371/journal.pone.0008561

Sakura, T., Sindikubwabo, F., Oesterlin, L.K., Bousquet, H., Slomianny, C., Hakimi, M.-A., Langsley, G., Tomavo, S., 2016. A Critical Role for Toxoplasma gondii Vacuolar Protein Sorting VPS9 in Secretory Organelle Biogenesis and Host Infection. Sci. Rep. 6, 38842. https://doi.org/10.1038/srep38842

Sanada, K., Harada, Y., Sakai, M., Todo, T., Fukada, Y., 2004. Serine phosphorylation of mCRY1 and mCRY2 by mitogen-activated protein kinase. Genes Cells Devoted Mol. Cell. Mech. 9, 697–708. https://doi.org/10.1111/j.1356-9597.2004.00758.x

Sato, F., Kawamoto, T., Fujimoto, K., Noshiro, M., Honda, K.K., Honma, S., Honma, K., Kato, Y., 2004. Functional analysis of the basic helix-loop-helix transcription factor DEC1 in circadian regulation. Interaction with BMAL1. Eur. J. Biochem. 271, 4409–4419. https://doi.org/10.1111/j.1432-1033.2004.04379.x

Sato, M., Sato, K., Fonarev, P., Huang, C.-J., Liou, W., Grant, B.D., 2005. Caenorhabditis elegans RME-6 is a novel regulator of RAB-5 at the clathrin-coated pit. Nat. Cell Biol. 7, 559–569. https://doi.org/10.1038/ncb1261

Sato, S., Fujita, N., Tsuruo, T., 2000. Modulation of Akt kinase activity by binding to Hsp90. Proc. Natl. Acad. Sci. 97, 10832–10837. https://doi.org/10.1073/pnas.170276797

Sato, T.K., Panda, S., Miraglia, L.J., Reyes, T.M., Rudic, R.D., McNamara, P., Naik, K.A., FitzGerald, G.A., Kay, S.A., Hogenesch, J.B., 2004. A functional genomics strategy reveals Rora as a component of the mammalian circadian clock. Neuron 43, 527–537. https://doi.org/10.1016/j.neuron.2004.07.018

Schibler, U., 2007. The daily timing of gene expression and physiology in mammals. Dialogues Clin. Neurosci. 9, 257–72. https://doi.org/10.31887/DCNS.2007.9.3/uschibler

Schmalen, I., Reischl, S., Wallach, T., Klemz, R., Grudziecki, A., Prabu, J.R., Benda, C., Kramer, A., Wolf, E., 2014. Interaction of circadian clock proteins CRY1 and PER2 is modulated by zinc binding and disulfide bond formation. Cell 157, 1203–1215. https://doi.org/10.1016/j.cell.2014.03.057

Schneider, J.P., Lombardi, A., DeGrado, W.F., 1998. Analysis and design of three-stranded coiled coils and three-helix bundles. Fold. Des. 3, R29–R40. https://doi.org/10.1016/S1359-0278(98)00011-X

Semerdjieva, S., Shortt, B., Maxwell, E., Singh, S., Fonarev, P., Hansen, J., Schiavo, G., Grant, B.D., Smythe, E., 2008. Coordinated regulation of AP2 uncoating from clathrin-coated vesicles by rab5 and hRME-6. J. Cell Biol. 183, 499–511. https://doi.org/10.1083/jcb.200806016

Shearman, L.P., Zylka, M.J., Weaver, D.R., Kolakowski, L.F., Reppert, S.M., 1997. Two period homologs: circadian expression and photic regulation in the suprachiasmatic nuclei. Neuron 19, 1261–1269. https://doi.org/10.1016/s0896-6273(00)80417-1

Shende, V.R., Neuendorff, N., Earnest, D.J., 2013. Role of miR-142-3p in the post-transcriptional regulation of the clock gene Bmal1 in the mouse SCN. PloS One 8, e65300. https://doi.org/10.1371/journal.pone.0065300

Shih, S.C., Prag, G., Francis, S.A., Sutanto, M.A., Hurley, J.H., Hicke, L., 2003. A ubiquitin-binding motif required for intramolecular monoubiquitylation, the CUE domain. EMBO J. 22, 1273–1281. https://doi.org/10.1093/emboj/cdg140

Shirogane, T., Jin, J., Ang, X.L., Harper, J.W., 2005a. SCFbeta-TRCP controls clock-dependent transcription via casein kinase 1-dependent degradation of the mammalian period-1 (Per1) protein. J. Biol. Chem. 280, 26863–26872. https://doi.org/10.1074/jbc.M502862200

Shirogane, T., Jin, J., Ang, X.L., Harper, J.W., 2005b. SCFβ-TRCP Controls Clock-dependent Transcription via Casein Kinase 1-dependent Degradation of the Mammalian Period-1 (Per1) Proteinm*. J. Biol. Chem. 280, 26863–26872. https://doi.org/10.1074/jbc.M502862200

Shostak, A., 2017. Circadian Clock, Cell Division, and Cancer: From Molecules to Organism. Int. J. Mol. Sci. 18, 873. https://doi.org/10.3390/ijms18040873

Smyllie, N.J., Pilorz, V., Boyd, J., Meng, Q.-J., Saer, B., Chesham, J.E., Maywood, E.S., Krogager, T.P., Spiller, D.G., Boot-Handford, R., White, M.R.H., Hastings, M.H., Loudon, A.S.I., 2016. Visualizing and Quantifying Intracellular Behavior and Abundance of the Core Circadian Clock Protein PERIOD2. Curr. Biol. 26, 1880–1886. https://doi.org/10.1016/j.cub.2016.05.018

Spengler, M.L., Kuropatwinski, K.K., Schumer, M., Antoch, M.P., 2009. A serine cluster mediates BMAL1-dependent CLOCK phosphorylation and degradation. Cell Cycle Georget. Tex 8, 4138–4146. https://doi.org/10.4161/cc.8.24.10273

Spoelstra, K., Albrecht, U., van der Horst, G.T.J., Brauer, V., Daan, S., 2004. Phase responses to light pulses in mice lacking functional per or cry genes. J. Biol. Rhythms 19, 518–529. https://doi.org/10.1177/0748730404268122

Sridharan, S., Hernandez-Armendariz, A., Kurzawa, N., Potel, C.M., Memon, D., Beltrao, P., Bantscheff, M., Huber, W., Cuylen-Haering, S., Savitski, M.M., 2022. Systematic discovery of biomolecular condensate-specific protein phosphorylation. Nat. Chem. Biol. 18, 1104–1114. https://doi.org/10.1038/s41589-022-01062-y

Stallcup, M.R., Kim, J.H., Teyssier, C., Lee, Y.-H., Ma, H., Chen, D., 2003. The roles of protein-protein interactions and protein methylation in transcriptional activation by nuclear receptors and their coactivators. J. Steroid Biochem. Mol. Biol. 85, 139–145. https://doi.org/10.1016/s0960-0760(03)00222-x

Stojkovic, K., Wing, S.S., Cermakian, N., 2014. A central role for ubiquitination within a circadian clock protein modification code. Front. Mol. Neurosci. 7, 69. https://doi.org/10.3389/fnmol.2014.00069

Storch, K.-F., Lipan, O., Leykin, I., Viswanathan, N., Davis, F.C., Wong, W.H., Weitz, C.J., 2002. Extensive and divergent circadian gene expression in liver and heart. Nature 417, 78–83. https://doi.org/10.1038/nature744

Stow, L.R., Gumz, M.L., 2011. The circadian clock in the kidney. J. Am. Soc. Nephrol. JASN 22, 598–604. https://doi.org/10.1681/ASN.2010080803

Strakova, K., Kowalski-Jahn, M., Gybel, T., Valnohova, J., Dhople, V.M., Harnos, J., Bernatik, O., Ganji, R.S., Zdrahal, Z., Mulder, J., Lindskog, C., Bryja, V., Schulte, G., 2018. Dishevelled enables casein kinase 1-mediated phosphorylation of Frizzled 6 required for cell membrane localization. J. Biol. Chem. 293, 18477–18493. https://doi.org/10.1074/jbc.RA118.004656

Stratmann, M., Stadler, F., Tamanini, F., van der Horst, G.T.J., Ripperger, J.A., 2010. Flexible phase adjustment of circadian albumin D site-binding protein (Dbp) gene expression by CRYPTOCHROME1. Genes Dev. 24, 1317–1328. https://doi.org/10.1101/gad.578810

Sun, Z.S., Albrecht, U., Zhuchenko, O., Bailey, J., Eichele, G., Lee, C.C., 1997. RIGUI, a putative mammalian ortholog of the Drosophila period gene. Cell 90, 1003–1011. https://doi.org/10.1016/s0092-8674(00)80366-9

Takahashi, J.S., 2017. Transcriptional architecture of the mammalian circadian clock. Nat. Rev. Genet. 18, 164–179. https://doi.org/10.1038/nrg.2016.150

Takeda, Y., Jothi, R., Birault, V., Jetten, A.M., 2012. RORγ directly regulates the circadian expression of clock genes and downstream targets in vivo. Nucleic Acids Res. 40, 8519–8535. https://doi.org/10.1093/nar/gks630

Takumi, T., Taguchi, K., Miyake, S., Sakakida, Y., Takashima, N., Matsubara, C., Maebayashi, Y., Okumura, K., Takekida, S., Yamamoto, S., Yagita, K., Yan, L., Young, M.W., Okamura, H., 1998. A light-independent oscillatory gene mPer3 in mouse SCN and OVLT. EMBO J. 17, 4753–4759. https://doi.org/10.1093/emboj/17.16.4753

Tamaru, T., Hattori, M., Honda, K., Nakahata, Y., Sassone-Corsi, P., van der Horst, G.T.J., Ozawa, T., Takamatsu, K., 2015. CRY Drives Cyclic CK2-Mediated BMAL1 Phosphorylation to Control the Mammalian Circadian Clock. PLoS Biol. 13, e1002293. https://doi.org/10.1371/journal.pbio.1002293

Tamayo, A.G., Duong, H.A., Robles, M.S., Mann, M., Weitz, C.J., 2015. Histone monoubiquitination by Clock-Bmal1 complex marks Per1 and Per2 genes for circadian feedback. Nat. Struct. Mol. Biol. 22, 759–766. https://doi.org/10.1038/nsmb.3076

Tanaka, T., Iino, M., Goto, K., 2014. Knockdown of Sec8 enhances the binding affinity of c-Jun N-terminal kinase (JNK)-interacting protein 4 for mitogen-activated protein kinase kinase 4 (MKK4) and suppresses the phosphorylation of MKK4, p38, and JNK, thereby inhibiting apoptosis. FEBS J. 281, 5237–5250. https://doi.org/10.1111/febs.13063

Thornton, B., Basu, C., 2011. Real-time PCR (qPCR) primer design using free online software. Biochem. Mol. Biol. Educ. Bimon. Publ. Int. Union Biochem. Mol. Biol. 39, 145–154. https://doi.org/10.1002/bmb.20461

Thurley, K., Herbst, C., Wesener, F., Koller, B., Wallach, T., Maier, B., Kramer, A., Westermark, P.O., 2017. Principles for circadian orchestration of metabolic pathways. Proc. Natl. Acad. Sci. 114, 1572–1577. https://doi.org/10.1073/pnas.1613103114

Truebestein, L., Leonard, T.A., 2016. Coiled-coils: The long and short of it. Bioessays 38, 903–916. https://doi.org/10.1002/bies.201600062

Tsuchiya, Y., Akashi, M., Matsuda, M., Goto, K., Miyata, Y., Node, K., Nishida, E., 2009. Involvement of the protein kinase CK2 in the regulation of mammalian circadian rhythms. Sci. Signal. 2, ra26. https://doi.org/10.1126/scisignal.2000305

Tsurudome, Y., Koyanagi, S., Kanemitsu, T., Katamune, C., Oda, M., Kanado, Y., Kato, M., Morita, A., Tahara, Y., Matsunaga, N., Shibata, S., Ohdo, S., 2018. Circadian clock component PERIOD2 regulates diurnal expression of Na+/H+ exchanger regulatory factor-1 and its scaffolding function. Sci. Rep. 8, 9072. https://doi.org/10.1038/s41598-018-27280-w

Um, J.H., Yang, S., Yamazaki, S., Kang, H., Viollet, B., Foretz, M., Chung, J.H., 2007. Activation of 5'-AMP-activated kinase with diabetes drug metformin induces casein kinase Iepsilon (CKIepsilon)-dependent degradation of clock protein mPer2. J. Biol. Chem. 282, 20794–20798. https://doi.org/10.1074/jbc.C700070200

Untergasser, A., Cutcutache, I., Koressaar, T., Ye, J., Faircloth, B.C., Remm, M., Rozen, S.G., 2012. Primer3—new capabilities and interfaces. Nucleic Acids Res. 40, e115. https://doi.org/10.1093/nar/gks596

Urnavicius, L., Zhang, K., Diamant, A.G., Motz, C., Schlager, M.A., Yu, M., Patel, N.A., Robinson, C.V., Carter, A.P., 2015. The structure of the dynactin complex and its interaction with dynein. Science 347, 1441–1446. https://doi.org/10.1126/science.aaa4080

Valdez-Lopez, J.C., Gebreegziabher, M., Bailey, R.J., Flores, J., Awotunde, O., Burnett, T., Robinson, P.R., 2020. Protein Phosphatase 2A and Clathrin-Mediated Endocytosis Facilitate Robust Melanopsin Light Responses and Resensitization. Invest. Ophthalmol. Vis. Sci. 61, 10. https://doi.org/10.1167/iovs.61.12.10

Vanselow, K., Vanselow, J.T., Westermark, P.O., Reischl, S., Maier, B., Korte, T., Herrmann, A., Herzel, H., Schlosser, A., Kramer, A., 2006. Differential effects of PER2 phosphorylation: molecular basis for the human familial advanced sleep phase syndrome (FASPS). Genes Dev. 20, 2660–2672. https://doi.org/10.1101/gad.397006

Vaquero, J., Nguyen Ho-Bouldoires, T.H., Clapéron, A., Fouassier, L., 2017. Role of the PDZ-scaffold protein NHERF1/EBP50 in cancer biology: from signaling regulation to clinical relevance. Oncogene 36, 3067–3079. https://doi.org/10.1038/onc.2016.462

Varadi, M., Anyango, S., Deshpande, M., Nair, S., Natassia, C., Yordanova, G., Yuan, D., Stroe, O., Wood, G., Laydon, A., Žídek, A., Green, T., Tunyasuvunakool, K., Petersen, S.,

Jumper, J., Clancy, E., Green, R., Vora, A., Lutfi, M., Figurnov, M., Cowie, A., Hobbs, N., Kohli, P., Kleywegt, G., Birney, E., Hassabis, D., Velankar, S., 2022. AlphaFold Protein Structure Database: massively expanding the structural coverage of protein-sequence space with high-accuracy models. Nucleic Acids Res. 50, D439–D444. https://doi.org/10.1093/nar/gkab1061

Venerando, A., Ruzzene, M., Pinna, L.A., 2014. Casein kinase: the triple meaning of a misnomer. Biochem. J. 460, 141–156. https://doi.org/10.1042/BJ20140178

Vielhaber, Erica, Eide, E., Rivers, A., Gao, Z.-H., Virshup, D.M., 2000. Nuclear Entry of the Circadian Regulator mPER1 Is Controlled by Mammalian Casein Kinase I ε. Mol. Cell. Biol. 20, 4888–4899.

Vielhaber, E., Eide, E., Rivers, A., Gao, Z.H., Virshup, D.M., 2000. Nuclear entry of the circadian regulator mPER1 is controlled by mammalian casein kinase I epsilon. Mol. Cell. Biol. 20, 4888–4899. https://doi.org/10.1128/MCB.20.13.4888-4899.2000

Virshup, D.M., Eide, E.J., Forger, D.B., Gallego, M., Harnish, E.V., 2007. Reversible protein phosphorylation regulates circadian rhythms. Cold Spring Harb. Symp. Quant. Biol. 72, 413–420. https://doi.org/10.1101/sqb.2007.72.048

Viswambharan, H., Carvas, J.M., Antic, V., Marecic, A., Jud, C., Zaugg, C.E., Ming, X.-F., Montani, J.-P., Albrecht, U., Yang, Z., 2007. Mutation of the circadian clock gene Per2 alters vascular endothelial function. Circulation 115, 2188–2195. https://doi.org/10.1161/CIRCULATIONAHA.106.653303

Vitaterna, M.H., Selby, C.P., Todo, T., Niwa, H., Thompson, C., Fruechte, E.M., Hitomi, K., Thresher, R.J., Ishikawa, T., Miyazaki, J., Takahashi, J.S., Sancar, A., 1999. Differential regulation of mammalian Period genes and circadian rhythmicity by cryptochromes 1 and 2. Proc. Natl. Acad. Sci. 96, 12114–12119. https://doi.org/10.1073/pnas.96.21.12114

Vitaterna, M.H., Takahashi, J.S., Turek, F.W., 2001. Overview of Circadian Rhythms. Alcohol Res. Health 25, 85–93.

Wang, L., Tian, H., Wang, H., Mao, X., Luo, J., He, Q., Wen, P., Cao, H., Fang, L., Zhou, Y., Yang, J., Jiang, L., 2024. Disrupting circadian control of autophagy induces podocyte injury and proteinuria. Kidney Int. S0085-2538(24)00118–2. https://doi.org/10.1016/j.kint.2024.01.035

Wang, R.-H., Zhao, T., Cui, K., Hu, G., Chen, Q., Chen, W., Wang, X.-W., Soto-Gutierrez, A., Zhao, K., Deng, C.-X., 2016. Negative reciprocal regulation between Sirt1 and Per2 modulates the circadian clock and aging. Sci. Rep. 6, 28633. https://doi.org/10.1038/srep28633

Woo, K.-C., Ha, D.-C., Lee, K.-H., Kim, D.-Y., Kim, T.-D., Kim, K.-T., 2010. Circadian amplitude of cryptochrome 1 is modulated by mRNA stability regulation via cytoplasmic hnRNP D oscillation. Mol. Cell. Biol. 30, 197–205. https://doi.org/10.1128/MCB.01154-09

Woo, K.-C., Kim, T.-D., Lee, K.-H., Kim, D.-Y., Kim, W., Lee, K.-Y., Kim, K.-T., 2009. Mouse period 2 mRNA circadian oscillation is modulated by PTB-mediated rhythmic mRNA degradation. Nucleic Acids Res. 37, 26–37. https://doi.org/10.1093/nar/gkn893

Wu, R., Dang, F., Li, P., Wang, P., Xu, Q., Liu, Z., Li, Y., Wu, Y., Chen, Y., Liu, Y., 2019. The Circadian Protein Period2 Suppresses mTORC1 Activity via Recruiting Tsc1 to mTORC1 Complex. Cell Metab. 29, 653-667.e6. https://doi.org/10.1016/j.cmet.2018.11.006

Xu, L., Nagai, Y., Kajihara, Y., Ito, G., Tomita, T., 2021. The Regulation of Rab GTPases by Phosphorylation. Biomolecules 11, 1340. https://doi.org/10.3390/biom11091340

Xu, Y., Liu, S., Xia, J., Stein, S., Ramon, C., Xi, H., Wang, L., Xiong, X., Zhang, L., He, D., Yang, W., Zhao, X., Cheng, X., Yang, X., Wang, H., 2017. Endocytosis and membrane

receptor internalization: implication of F-BAR protein Carom. Front. Biosci. Landmark Ed. 22, 1439–1457.

Xu, Z., Ogawa, H., Vagnarelli, P., Bergmann, J.H., Hudson, D.F., Ruchaud, S., Fukagawa, T., Earnshaw, W.C., Samejima, K., 2009. INCENP–aurora B interactions modulate kinase activity and chromosome passenger complex localization. J. Cell Biol. 187, 637–653. https://doi.org/10.1083/jcb.200906053

Yagita, K., Tamanini, F., Yasuda, M., Hoeijmakers, J.H.J., van der Horst, G.T.J., Okamura, H., 2002. Nucleocytoplasmic shuttling and mCRY-dependent inhibition of ubiquitylation of the mPER2 clock protein. EMBO J. 21, 1301–1314. https://doi.org/10.1093/emboj/21.6.1301

Yagita, K., Yamaguchi, S., Tamanini, F., Horst, G.T.J. van der, Hoeijmakers, J.H.J., Yasui, A., Loros, J.J., Dunlap, J.C., Okamura, H., 2000. Dimerization and nuclear entry of mPER proteins in mammalian cells. Genes Dev. 14, 1353–1363. https://doi.org/10.1101/gad.14.11.1353

Yan, J., Goldbeter, A., 2019. Robust synchronization of the cell cycle and the circadian clock through bidirectional coupling. J. R. Soc. Interface 16, 20190376. https://doi.org/10.1098/rsif.2019.0376

Yang, S.-L., Yu, C., Jiang, J.-X., Liu, L.-P., Fang, X., Wu, C., 2014. Hepatitis B virus X protein disrupts the balance of the expression of circadian rhythm genes in hepatocellular carcinoma. Oncol. Lett. 8, 2715–2720. https://doi.org/10.3892/ol.2014.2570

Ye, R., Selby, C.P., Chiou, Y.-Y., Ozkan-Dagliyan, I., Gaddameedhi, S., Sancar, A., 2014. Dual modes of CLOCK:BMAL1 inhibition mediated by Cryptochrome and Period proteins in the mammalian circadian clock. Genes Dev. 28, 1989–1998. https://doi.org/10.1101/gad.249417.114

Yeung, C.-Y.C., Dondelinger, F., Schoof, E.M., Georg, B., Lu, Y., Zheng, Z., Zhang, J., Hannibal, J., Fahrenkrug, J., Kjaer, M., 2022. Circadian regulation of protein cargo in extracellular vesicles. Sci. Adv. 8, eabc9061. https://doi.org/10.1126/sciadv.abc9061

Yildiz, O., Doi, M., Yujnovsky, I., Cardone, L., Berndt, A., Hennig, S., Schulze, S., Urbanke, C., Sassone-Corsi, P., Wolf, E., 2005. Crystal structure and interactions of the PAS repeat region of the Drosophila clock protein PERIOD. Mol. Cell 17, 69–82. https://doi.org/10.1016/j.molcel.2004.11.022

Yin, L., Joshi, S., Wu, N., Tong, X., Lazar, M.A., 2010. E3 ligases Arf-bp1 and Pam mediate lithium-stimulated degradation of the circadian heme receptor Rev-erbα. Proc. Natl. Acad. Sci. 107, 11614–11619. https://doi.org/10.1073/pnas.1000438107

Ying, Z., Giachini, F.R.C., Tostes, R.C., Webb, R.C., 2009. PYK2/PDZ-RhoGEF links Ca2+ signaling to RhoA. Arterioscler. Thromb. Vasc. Biol. 29, 1657–1663. https://doi.org/10.1161/ATVBAHA.109.190892

Yoo, S.-H., Mohawk, J.A., Siepka, S.M., Shan, Y., Huh, S.K., Hong, H.-K., Kornblum, I., Kumar, V., Koike, N., Xu, M., Nussbaum, J., Liu, X., Chen, Z., Chen, Z.J., Green, C.B., Takahashi, J.S., 2013. Competing E3 Ubiquitin Ligases Determine Circadian Period by Regulated Degradation of CRY in Nucleus and Cytoplasm. Cell 152, 1091–1105. https://doi.org/10.1016/j.cell.2013.01.055

Yoshitane, H., Takao, T., Satomi, Y., Du, N.-H., Okano, T., Fukada, Y., 2009. Roles of CLOCK phosphorylation in suppression of E-box-dependent transcription. Mol. Cell. Biol. 29, 3675–3686. https://doi.org/10.1128/MCB.01864-08

Young, M.D., Wakefield, M.J., Smyth, G.K., Oshlack, A., 2010. Gene ontology analysis for RNA-seq: accounting for selection bias. Genome Biol. 11, R14. https://doi.org/10.1186/gb-2010-11-2-r14

Yue, X., Qian, Y., Gim, B., Lee, I., 2019. Acyl-CoA-Binding Domain-Containing 3 (ACBD3; PAP7; GCP60): A Multi-Functional Membrane Domain Organizer. Int. J. Mol. Sci. 20, 2028. https://doi.org/10.3390/ijms20082028

Zhan, J., Chitta, R.K., Harwood, F.C., Grosveld, G.C., 2019. Phosphorylation of TSC2 by PKC-δ reveals a novel signaling pathway that couples protein synthesis to mTORC1 activity. Mol. Cell. Biochem. 456, 123–134. https://doi.org/10.1007/s11010-019-03498-8

Zhang, E.E., Liu, Y., Dentin, R., Pongsawakul, P.Y., Liu, A.C., Hirota, T., Nusinow, D.A., Sun, X., Landais, S., Kodama, Y., Brenner, D.A., Montminy, M., Kay, S.A., 2010. Cryptochrome mediates circadian regulation of cAMP signaling and hepatic gluconeogenesis. Nat. Med. 16, 1152–1156. https://doi.org/10.1038/nm.2214

Zhang, Y., Duan, C., Yang, J., Chen, S., Liu, Q., Zhou, L., Huang, Z., Xu, Y., Xu, G., 2018. Deubiquitinating enzyme USP9X regulates cellular clock function by modulating the ubiquitination and degradation of a core circadian protein BMAL1. Biochem. J. 475, 1507–1522. https://doi.org/10.1042/BCJ20180005

Zheng, B., Albrecht, U., Kaasik, K., Sage, M., Lu, W., Vaishnav, S., Li, Q., Sun, Z.S., Eichele, G., Bradley, A., Lee, C.C., 2001. Nonredundant roles of the mPer1 and mPer2 genes in the mammalian circadian clock. Cell 105, 683–694. https://doi.org/10.1016/s0092-8674(01)00380-4

Zheng, B., Larkin, D.W., Albrecht, U., Sun, Z.S., Sage, M., Eichele, G., Lee, C.C., Bradley, A., 1999. The mPer2 gene encodes a functional component of the mammalian circadian clock. Nature 400, 169–173. https://doi.org/10.1038/22118

Zheng, X., Zhao, X., Zhang, Y., Tan, H., Qiu, B., Ma, T., Zeng, J., Tao, D., Liu, Y., Lu, Y., Ma, Y., 2019. RAE1 promotes BMAL1 shuttling and regulates degradation and activity of CLOCK: BMAL1 heterodimer. Cell Death Dis. 10, 1–12. https://doi.org/10.1038/s41419-019-1346-2

Zhou, H., Di Palma, S., Preisinger, C., Peng, M., Polat, A.N., Heck, A.J.R., Mohammed, S., 2013. Toward a comprehensive characterization of a human cancer cell phosphoproteome. J. Proteome Res. 12, 260–271. https://doi.org/10.1021/pr300630k

Zhou, M., Kim, J.K., Eng, G.W.L., Forger, D.B., Virshup, D.M., 2015a. A Period2 Phosphoswitch Regulates and Temperature Compensates Circadian Period. Mol. Cell 60, 77–88. https://doi.org/10.1016/j.molcel.2015.08.022

Zhou, M., Kim, J.K., Eng, G.W.L., Forger, D.B., Virshup, D.M., 2015b. A Period2 Phosphoswitch Regulates and Temperature Compensates Circadian Period. Mol. Cell 60, 77–88. https://doi.org/10.1016/j.molcel.2015.08.022

Zhou, X., Su, Z., 2007. EasyGO: Gene Ontology-based annotation and functional enrichment analysis tool for agronomical species. BMC Genomics 8, 246. https://doi.org/10.1186/1471-2164-8-246

Zhuang, X., Rambhatla, S.B., Lai, A.G., McKeating, J.A., 2017. Interplay between circadian clock and viral infection. J. Mol. Med. 95, 1283–1289. https://doi.org/10.1007/s00109-017-1592-7

Zinder, J.C., Lima, C.D., 2017. Targeting RNA for processing or destruction by the eukaryotic RNA exosome and its cofactors. Genes Dev. 31, 88–100. https://doi.org/10.1101/gad.294769.116

Zuker, M., 2003. Mfold web server for nucleic acid folding and hybridization prediction. Nucleic Acids Res. 31, 3406–3415. https://doi.org/10.1093/nar/gkg595

Zylka, M.J., Shearman, L.P., Weaver, D.R., Reppert, S.M., 1998. Three period homologs in mammals: differential light responses in the suprachiasmatic circadian clock and oscillating transcripts outside of brain. Neuron 20, 1103–1110. https://doi.org/10.1016/s0896-6273(00)80492-4

7. Appendix

Table 1 A: List of refined proteins from MS analysis. The List contains 364 co-purified proteins in HT1080-PER2-GFP and HT1080-GFP, which have P-value < 0.05. Proteins which spcificly enriched in the PER2-GFP samples were highlight in green. Exlucded ribosomal, proteasomal and tubulins proteins were highlighted in yellow.

	GFP			PER2-GFP			t-test p value	t-test Difference	Protein names
	#1	#2	#3	#1	#2	#3			
1	16.11	15.91	15.97	28.06	28.30	26.88	1.19E-05	-11.75	Cryptochrome-2
2	17.27	19.12	19.29	29.26	30.03	29.12	0.00010249	-10.91	Cryptochrome-1
3	15.25	16.33	15.35	26.79	26.25	25.46	3.46E-05	-10.52	F-box/WD repeat-containing protein 11
4	20.82	22.08	22.26	31.24	31.06	30.50	5.29E-05	-9.21	Period circadian protein homolog 2
5	15.39	17.33	16.34	25.01	24.32	23.80	0.00026345	-8.02	Period circadian protein homolog 1
6	21.30	21.20	21.32	28.19	28.57	27.46	3.19E-05	-6.80	Casein kinase I isoform delta
7	17.75	17.25	17.35	24.12	24.30	23.02	0.00012072	-6.36	GTPase-activating protein and VPS9 domain-containing protein 1
8	13.66	15.54	16.44	22.34	21.16	20.11	0.00454376	-5.99	AP-2 complex subunit mu
9	14.51	18.67	15.15	20.82	22.60	22.24	0.0146337	-5.78	Acyl-CoA dehydrogenase family member 11
10	15.11	16.79	15.12	21.19	21.65	21.39	0.00057249	-5.73	60S ribosomal protein L21
11	17.53	17.90	18.30	23.56	23.59	21.80	0.00129802	-5.07	Zinc finger protein 618
12	14.59	16.29	17.27	21.34	21.49	19.78	0.00729536	-4.82	Protein FAM83D
13	14.97	15.38	16.37	20.65	20.56	19.78	0.00067667	-4.75	F-box/WD repeat-containing protein 1A
14	15.66	14.71	18.75	21.37	21.49	20.07	0.0240544	-4.61	Hyaluronan mediated motility receptor
15	14.26	14.38	15.73	18.84	19.53	18.83	0.00123448	-4.28	E3 ubiquitin-protein ligase MYCBP2
16	14.60	15.93	15.34	19.15	19.60	19.94	0.00068894	-4.27	Tripeptidyl-peptidase 1
17	15.97	16.42	20.54	21.98	22.01	21.71	0.0432957	-4.26	Golgin subfamily A member 3
18	19.28	18.30	17.62	22.66	22.79	22.52	0.00096136	-4.26	Prolyl 4-hydroxylase subunit alpha-1

Appendix

	GFP			PER2-GFP			t-test p value	t-test Difference	Protein names
	#1	#2	#3	#1	#2	#3			
19	19.03	14.78	18.61	22.23	21.95	20.97	0.0391446	-4.24	AP-2 complex subunit beta
20	15.13	15.81	17.02	20.01	20.42	20.10	0.00176053	-4.20	Cytidine deaminase
21	14.69	15.81	14.21	18.76	18.93	19.53	0.00140822	-4.17	Galectin-3-binding protein
22	16.07	16.21	14.98	20.21	19.75	19.68	0.00062434	-4.13	Torsin-4A
23	16.24	15.49	16.03	21.03	19.92	19.19	0.00206571	-4.13	Cancer testis antigen family 45 member A1/2/3/5/6/7/8/9/10
24	18.27	17.71	15.06	22.47	20.59	20.33	0.0262368	-4.12	AP-2 complex subunit alpha-1
25	15.26	16.38	15.52	20.26	19.84	18.94	0.00152971	-3.96	Striatin
26	19.90	22.50	23.02	25.86	26.18	25.05	0.0189446	-3.89	Casein kinase I isoform epsilon
27	14.36	14.91	15.55	18.63	18.92	18.31	0.00067892	-3.68	Phospholipase D1
28	15.12	15.44	16.34	19.15	19.18	19.58	0.00072096	-3.67	DTW domain-containing protein 2
29	15.34	15.29	14.83	18.43	18.64	19.34	0.00033749	-3.65	Casein kinase I isoform epsilon
30	16.78	16.72	17.12	20.30	21.03	20.11	0.00029877	-3.61	DNA mismatch repair protein Mlh1
31	17.42	15.62	17.19	21.04	20.32	19.44	0.00850804	-3.52	Signal recognition particle 9 kDa protein
32	16.03	15.28	15.38	19.30	19.22	18.45	0.00065436	-3.43	Centrosomal protein of 78 kDa
33	14.81	15.58	16.29	19.06	18.81	18.86	0.00149668	-3.35	Long-chain fatty acid transport protein 4
34	14.93	15.68	15.74	19.17	18.79	18.10	0.00137912	-3.23	Colorectal mutant cancer protein
35	15.77	16.72	15.50	19.12	19.05	19.46	0.00119176	-3.21	Prolyl 4-hydroxylase subunit alpha-2
36	16.88	15.15	16.65	19.25	19.00	19.82	0.00625877	-3.13	Tissue-type plasminogen activator; Tissue-type plasminogen activator chain A; Tissue-type plasminogen activator chain B
37	16.84	16.30	18.14	19.31	20.34	20.96	0.0129716	-3.11	DnaJ homolog subfamily C member 10
38	16.96	18.47	18.03	21.19	20.90	20.63	0.00292221	-3.09	Obscurin-like protein 1

	GFP			PER2-GFP			t-test p value	t-test Difference	Protein names
	#1	#2	#3	#1	#2	#3			
39	15.59	14.44	15.32	18.13	18.41	17.96	0.00117485	-3.05	Monoacylglycerol lipase ABHD12
40	15.09	14.92	15.22	18.33	17.93	18.11	2.98E-05	-3.04	RAF proto-oncogene serine/threonine-protein kinase
41	16.91	15.48	18.03	20.29	20.38	18.70	0.0312063	-2.99	60 kDa SS-A/Ro ribonucleoprotein
42	16.92	16.68	16.88	19.86	19.96	19.56	3.08E-05	-2.97	mRNA-capping enzyme;Polynucleotide 5-triphosphatase; mRNA guanylyltransferase
43	14.88	16.06	16.29	19.08	18.95	17.96	0.00659397	-2.92	Delta(24)-sterol reductase
44	23.34	22.25	22.50	25.51	25.44	25.68	0.00109253	-2.85	Dehydrogenase/reductase SDR family member 2, mitochondrial
45	15.52	17.11	16.70	20.12	19.64	17.99	0.0250279	-2.81	Zinc finger protein 618
46	19.10	18.95	18.39	22.42	22.06	20.05	0.0248029	-2.69	mRNA export factor
47	14.97	15.33	16.52	17.84	18.42	18.58	0.00683282	-2.67	Glutamate-rich WD repeat-containing protein 1
48	15.79	14.90	17.28	18.83	18.27	18.87	0.0207583	-2.67	Alpha-1,6-mannosyl-glycoprotein 2-beta-N-acetylglucosaminyltransferase
49	18.31	18.61	18.58	20.81	21.12	21.56	0.00035816	-2.66	Acyl-coenzyme A thioesterase 8
50	21.24	22.17	22.28	24.17	24.60	24.77	0.00226497	-2.61	Tubulin alpha-1A chain
51	14.91	17.52	16.96	18.89	19.08	19.17	0.0317247	-2.59	Programmed cell death protein 2
52	15.15	16.13	15.33	18.13	18.09	18.15	0.00102711	-2.59	DnaJ homolog subfamily A member 3, mitochondrial
53	14.92	15.52	15.91	17.96	18.07	18.05	0.00088704	-2.58	Aryl hydrocarbon receptor nuclear translocator-like protein 1
54	20.92	20.08	19.53	22.45	22.91	22.69	0.00412204	-2.51	Tubulin beta-3 chain
55	18.01	19.93	18.94	21.25	21.21	21.77	0.0138375	-2.45	Cancer/testis antigen 1
56	15.98	15.62	17.80	19.06	18.62	19.06	0.023876	-2.45	Lethal(2) giant larvae protein homolog 1

Appendix

	GFP			PER2-GFP			t-test p value	t-test Difference	Protein names
	#1	#2	#3	#1	#2	#3			
57	19.18	18.70	19.04	21.02	21.70	21.48	0.00058901	-2.42	60S ribosomal protein L24
58	20.98	20.88	20.24	22.37	23.23	23.74	0.00634497	-2.41	Cathepsin B; Cathepsin B light chain;Cathepsin B heavy chain
59	14.96	15.83	14.98	17.47	18.00	17.52	0.00195577	-2.40	Fibronectin type III domain-containing protein 3B
60	15.06	15.70	14.46	17.85	16.95	17.61	0.00601349	-2.40	U5 small nuclear ribonucleoprotein 200 kDa helicase
61	16.79	18.16	17.14	18.87	19.77	20.58	0.0210371	-2.37	Fibronectin; Anastellin;Ugl-Y1;Ugl-Y2;Ugl-Y3
62	16.41	15.92	16.16	18.32	18.24	19.01	0.00111163	-2.36	Ubiquitin carboxyl-terminal hydrolase 34; Ubiquitin carboxyl-terminal hydrolase
63	14.46	15.23	15.39	17.07	17.54	17.46	0.00196684	-2.33	Neuronal PAS domain-containing protein 2
64	14.95	16.52	17.47	18.83	19.05	17.93	0.0476216	-2.29	WD repeat-containing protein 6
65	15.24	15.06	17.16	18.26	18.23	17.75	0.0309073	-2.26	Tetratricopeptide repeat protein 37
66	15.05	14.77	16.33	16.77	17.72	18.43	0.0291865	-2.26	Long-chain fatty acid transport protein 1
67	21.47	21.80	21.73	23.64	23.88	24.13	0.00021625	-2.22	Tubulin alpha-4A chain
68	15.04	15.83	17.15	17.69	17.95	19.02	0.0405029	-2.21	Lysophospholipid acyltransferase LPCAT4
69	16.70	17.65	17.03	18.43	19.22	20.34	0.0237789	-2.20	Mannosyl-oligosaccharide glucosidase
70	19.58	19.24	18.85	20.92	21.73	21.47	0.00251813	-2.15	Signal recognition particle 14 kDa protein
71	19.83	20.11	20.82	22.09	22.72	22.39	0.0034654	-2.15	ATP-dependent 6-phosphofructokinase, muscle type
72	15.49	16.58	15.89	17.09	18.22	19.08	0.0312913	-2.15	Neuropathy target esterase
73	17.21	17.98	16.73	18.79	19.93	19.51	0.0130457	-2.11	DnaJ homolog subfamily B member 11
74	22.64	22.02	21.62	24.52	24.36	23.69	0.00582786	-2.10	40S ribosomal protein S11
75	16.99	17.05	15.88	18.47	19.29	18.26	0.0145868	-2.04	Lysyl oxidase homolog 2
76	16.58	15.94	15.48	16.93	18.33	18.69	0.0337745	-1.98	Acyl-CoA dehydrogenase family member 9, mitochondrial

	GFP			PER2-GFP			t-test p value	t-test Difference	Protein names
	#1	#2	#3	#1	#2	#3			
77	25.29	25.03	24.64	26.59	27.70	26.57	0.00919016	-1.97	Tubulin beta chain
78	20.54	20.22	20.88	22.62	22.54	22.38	0.00063482	-1.97	Leucine-rich repeat-containing protein 59
79	27.03	26.88	27.05	28.73	29.42	28.70	0.00123171	-1.96	Tubulin alpha-1B chain
80	18.70	18.29	19.74	20.70	21.27	20.62	0.0151398	-1.95	Tubulin beta-2A chain
81	16.70	17.04	16.58	18.49	18.42	19.18	0.0023697	-1.92	60S ribosomal protein L5
82	20.01	19.16	18.99	21.11	21.94	20.69	0.0184698	-1.86	DnaJ homolog subfamily A member 1
83	15.99	15.94	15.13	17.35	17.46	17.82	0.0039894	-1.86	Ubiquitin carboxyl-terminal hydrolase; Ubiquitin carboxyl-terminal hydrolase 11
84	23.11	22.62	21.49	24.36	24.81	23.62	0.0349098	-1.85	40S ribosomal protein S27
85	27.03	26.52	26.27	28.39	28.99	27.96	0.00785898	-1.84	Tubulin beta-4B chain
86	18.05	18.28	18.81	20.06	20.43	20.15	0.00185532	-1.83	60S ribosomal protein L7
87	21.37	21.54	21.32	23.20	23.41	23.08	9.20E-05	-1.82	40S ribosomal protein S23
88	16.37	15.56	15.46	17.69	17.36	17.78	0.00463682	-1.81	Ran-binding protein 10
89	22.63	22.31	22.47	24.38	24.26	24.19	7.08E-05	-1.81	60S ribosomal protein L23
90	17.77	19.08	18.63	20.05	20.28	20.56	0.0119529	-1.80	Tubulin alpha-3C/D chain;Tubulin alpha-3E chain
91	24.67	24.51	24.60	26.14	26.91	26.09	0.00275368	-1.78	ATP-dependent 6-phosphofructokinase, platelet type
92	22.24	22.24	21.81	23.78	24.19	23.63	0.00128211	-1.77	ATP-dependent 6-phosphofructokinase, liver type
93	24.35	23.04	23.81	25.97	25.61	24.93	0.0220933	-1.77	40S ribosomal protein S16
94	21.50	21.51	21.83	22.63	23.89	23.51	0.0113423	-1.73	60S ribosomal protein L4
95	16.33	16.05	15.53	18.01	17.49	17.61	0.0035742	-1.73	Serine palmitoyltransferase 2
96	19.66	19.95	19.99	21.20	22.00	21.57	0.0024204	-1.72	DnaJ homolog subfamily A member 2
97	21.56	20.81	20.70	22.25	23.30	22.64	0.0141655	-1.70	60S ribosomal protein L28

Appendix

	GFP			PER2-GFP			t-test p value	t-test Difference	Protein names
	#1	#2	#3	#1	#2	#3			
98	17.61	16.49	17.93	18.81	19.51	18.80	0.0269268	-1.70	Urokinase-type plasminogen activator; Urokinase-type plasminogen activator long chain A; Urokinase-type plasminogen activator short chain A; Urokinase-type plasminogen activator chain B
99	15.77	16.20	17.40	17.55	18.22	18.40	0.0446239	-1.60	Helicase SKI2W
100	18.39	18.57	18.39	19.92	20.08	20.10	4.13E-05	-1.58	Cell cycle and apoptosis regulator protein 2
101	17.77	16.94	17.88	18.83	19.23	19.27	0.00839991	-1.58	Very-long-chain 3-oxoacyl-CoA reductase
102	25.23	24.15	23.94	26.54	26.14	25.39	0.0388333	-1.58	60S ribosomal protein L11
103	21.84	21.62	21.09	22.99	23.32	22.90	0.00372364	-1.55	40S ribosomal protein S4, X isoform
104	14.80	15.41	15.92	16.97	16.85	16.94	0.0089276	-1.54	Heat shock 70 kDa protein 4
105	17.00	15.80	16.13	18.30	17.74	17.51	0.022928	-1.54	Pre-mRNA-processing-splicing factor 8
106	15.92	16.44	16.70	17.64	17.94	18.04	0.00425336	-1.52	Putative tRNA (cytidine(32)/guanosine(34)-2-O)-methyltransferase
107	19.79	20.26	19.83	21.32	21.40	21.70	0.00130529	-1.51	Deoxynucleoside triphosphate triphosphohydrolase SAMHD1
108	16.98	15.82	15.36	17.44	17.23	18.03	0.0487787	-1.51	Cytoplasmic tRNA 2-thiolation protein 2
109	16.47	15.07	16.32	16.99	17.80	17.52	0.0423322	-1.49	Thyroid adenoma-associated protein
110	24.09	23.72	23.32	25.01	25.42	25.15	0.00430524	-1.48	Glutamine--fructose-6-phosphate aminotransferase [isomerizing] 2
111	20.99	20.59	21.04	22.69	22.03	22.28	0.00364772	-1.46	PDZ and LIM domain protein 7
112	20.44	20.18	19.88	21.80	21.51	21.55	0.00146137	-1.45	ATP synthase subunit alpha, mitochondrial
113	15.38	16.43	16.14	17.38	17.93	16.99	0.025226	-1.45	Glucocorticoid receptor
114	18.58	18.68	18.61	20.23	20.03	19.93	0.00010412	-1.44	Long-chain-fatty-acid--CoA ligase 1

Appendix

	GFP			PER2-GFP			t-test p value	t-test Difference	Protein names
	#1	#2	#3	#1	#2	#3			
115	16.59	16.67	17.16	17.91	18.51	18.26	0.00464075	-1.42	Tubulin gamma-1 chain;Tubulin gamma-2 chain;Tubulin gamma chain
116	16.51	17.61	17.43	18.81	18.77	18.21	0.0229289	-1.41	Proteasome subunit alpha type;Proteasome subunit alpha type-2
117	18.16	18.69	18.80	19.24	20.39	20.21	0.0264268	-1.40	Aspartyl/asparaginyl beta-hydroxylase
118	19.14	18.32	18.70	19.39	20.18	20.78	0.0407561	-1.40	Signal recognition particle receptor subunit alpha
119	15.51	16.31	15.85	17.79	17.12	16.93	0.0163168	-1.39	Neurofilament light polypeptide
120	19.00	19.43	19.55	20.69	21.23	20.22	0.0146246	-1.39	Coatomer subunit alpha;Xenin;Proxenin
121	20.99	20.28	20.15	21.42	22.36	21.75	0.0224182	-1.37	60S ribosomal protein L18a
122	19.17	19.22	19.68	20.39	20.97	20.75	0.00453193	-1.35	Probable ubiquitin carboxyl-terminal hydrolase FAF-X
123	19.86	18.75	19.62	20.68	21.07	20.51	0.0237153	-1.34	Inositol polyphosphate 5-phosphatase K
124	19.78	20.48	20.07	21.24	21.33	21.79	0.00704061	-1.34	Ribonuclease P protein subunit p30
125	17.23	18.41	17.32	18.93	18.68	19.37	0.0352206	-1.34	Coatomer subunit gamma-2
126	22.41	21.80	22.24	23.90	23.61	22.93	0.0176836	-1.33	40S ribosomal protein S2
127	17.17	17.58	17.40	19.23	19.00	17.90	0.0362174	-1.33	26S proteasome non-ATPase regulatory subunit 11
128	17.00	16.63	16.88	18.52	18.08	17.84	0.00446425	-1.31	Kinesin-like protein KIF2A
129	17.06	17.37	17.65	18.01	18.90	19.09	0.0249144	-1.31	Pleckstrin homology domain-containing family A member 2
130	19.16	18.40	19.19	20.25	20.42	19.96	0.0112309	-1.29	40S ribosomal protein S9
131	24.74	24.03	24.14	25.76	25.89	25.07	0.0196683	-1.27	40S ribosomal protein S3
132	21.20	21.17	21.66	22.68	22.55	22.57	0.00150838	-1.26	Long-chain-fatty-acid--CoA ligase 3
133	21.98	22.44	22.26	23.44	23.45	23.55	0.00082068	-1.25	CAD protein;Glutamine-dependent carbamoyl-phosphate synthase;

Appendix

	GFP			PER2-GFP			t-test p value	t-test Difference	Protein names
	#1	#2	#3	#1	#2	#3			
									Aspartate carbamoyltransferase;Dihydroorotase
134	19.27	20.37	20.34	20.83	21.41	21.46	0.0403769	-1.24	Coatomer subunit gamma-1
135	20.93	21.03	20.59	21.58	22.22	22.41	0.0125292	-1.22	40S ribosomal protein S26;Putative 40S ribosomal protein S26-like 1
136	18.97	20.08	19.67	20.46	21.18	20.75	0.0341308	-1.22	Thymidine kinase;Thymidine kinase, cytosolic
137	22.64	22.34	22.31	23.86	23.92	23.10	0.0132586	-1.20	Tubulin beta-6 chain
138	20.63	21.32	21.13	22.17	22.09	22.26	0.00538825	-1.15	DNA replication licensing factor MCM7
139	18.99	18.63	19.42	20.17	20.13	20.18	0.00724387	-1.15	Tyrosine-protein phosphatase non-receptor type 1; Tyrosine-protein phosphatase non-receptor type
140	18.87	18.91	19.15	20.19	19.44	20.70	0.0395966	-1.13	Lysophosphatidylcholine acyltransferase 2
141	18.88	19.78	19.19	20.55	20.57	20.11	0.02037	-1.13	Transcription intermediary factor 1-beta
142	20.31	20.63	20.15	21.31	21.43	21.71	0.00367215	-1.12	Ubiquitin carboxyl-terminal hydrolase 7; Ubiquitin carboxyl-terminal hydrolase
143	19.12	20.22	19.95	21.27	20.84	20.54	0.046699	-1.12	Transferrin receptor protein 1; Transferrin receptor protein 1, serum form
144	21.23	21.69	21.94	22.83	22.63	22.74	0.00671063	-1.11	tRNA (cytosine(34)-C(5))-methyltransferase
145	19.36	19.95	19.86	21.05	21.11	20.34	0.0227121	-1.11	Aurora kinase A
146	18.61	19.34	19.21	20.10	20.49	19.84	0.0208549	-1.09	Sequestosome-1
147	18.90	18.95	18.99	20.04	20.38	19.67	0.0064811	-1.08	DNA mismatch repair protein Msh6
148	21.16	20.46	21.17	22.31	21.90	21.80	0.0189712	-1.08	Heterogeneous nuclear ribonucleoprotein M
149	20.77	20.42	20.78	21.26	21.99	21.94	0.015327	-1.07	40S ribosomal protein S8
150	22.53	23.20	22.63	24.20	23.56	23.77	0.0198346	-1.06	Leucine-rich repeat-containing protein 47
151	16.64	16.12	16.92	17.40	17.79	17.61	0.0158901	-1.04	Proteasome subunit beta type-2

Appendix

	GFP			PER2-GFP			t-test p value	t-test Difference	Protein names
	#1	#2	#3	#1	#2	#3			
152	20.31	20.46	21.15	21.81	22.02	21.21	0.0437533	-1.04	26S protease regulatory subunit 4
153	19.72	19.70	19.87	20.46	21.20	20.73	0.00983193	-1.04	Nicotinamide N-methyltransferase
154	19.02	19.38	18.65	20.16	20.24	19.76	0.0159249	-1.03	Serine/threonine-protein kinase A-Raf
155	19.48	19.76	19.73	21.09	20.69	20.19	0.0217859	-1.00	Proteasome subunit alpha type-7;Proteasome subunit alpha type-7-like
156	20.32	20.77	20.74	21.46	21.90	21.43	0.00925392	-0.99	Cytoplasmic dynein 1 heavy chain 1
157	16.71	17.20	17.07	17.62	17.83	18.47	0.0291104	-0.98	WD repeat-containing protein 61; WD repeat-containing protein 61, N-terminally processed
158	19.30	19.36	19.64	20.39	20.57	20.25	0.0022708	-0.97	26S protease regulatory subunit 7
159	18.56	18.74	18.98	19.52	19.79	19.86	0.0039108	-0.96	60S ribosomal protein L18
160	18.81	19.15	18.66	19.64	20.07	19.61	0.01224	-0.90	60S ribosomal protein L6
161	18.75	19.08	19.00	19.53	20.05	19.93	0.00859543	-0.89	Serine/threonine-protein phosphatase 6 catalytic subunit; Serine/threonine-protein phosphatase 6 catalytic subunit, N-terminally processed
162	23.00	23.09	22.46	23.97	23.91	23.35	0.0322027	-0.89	Keratin, type I cytoskeletal 18
163	16.32	17.04	16.96	17.64	17.46	17.88	0.027018	-0.89	NF-kappa-B essential modulator
164	22.82	22.57	22.20	23.46	23.29	23.42	0.00962544	-0.86	Serine/threonine-protein phosphatase 2A 55 kDa regulatory subunit B alpha isoform
165	18.86	19.07	19.61	20.02	20.01	20.04	0.0195813	-0.84	Schlafen family member 5
166	18.34	18.31	18.38	19.78	18.87	18.89	0.0494231	-0.84	LIM and senescent cell antigen-like-containing domain protein 1
167	21.39	20.53	20.71	21.78	21.74	21.56	0.0397769	-0.81	60S ribosomal protein L10a

Appendix

	GFP			PER2-GFP			t-test p value	t-test Difference	Protein names
	#1	#2	#3	#1	#2	#3			
168	20.76	20.57	20.43	21.53	21.32	21.32	0.00234535	-0.80	40S ribosomal protein S3a
169	18.45	18.73	18.94	19.73	19.63	19.11	0.0305017	-0.78	DNA replication licensing factor MCM4
170	18.26	18.06	17.84	18.97	18.81	18.64	0.00795061	-0.75	Connective tissue growth factor
171	17.17	17.15	17.67	17.96	18.23	18.03	0.0170765	-0.74	Dihydroxyacetone phosphate acyltransferase
172	18.83	19.01	18.51	19.49	19.88	19.15	0.0475273	-0.72	Pyrroline-5-carboxylate reductase;Pyrroline-5-carboxylate reductase 3
173	18.93	19.30	19.74	20.00	19.89	20.22	0.0474268	-0.72	26S protease regulatory subunit 6A
174	17.09	16.92	17.44	17.47	17.90	18.13	0.0499367	-0.68	Nuclear pore complex protein Nup88
175	18.25	18.32	18.74	19.05	18.97	19.24	0.0190104	-0.65	Acyl-coenzyme A thioesterase 9, mitochondrial
176	21.16	21.05	21.21	21.94	22.04	21.37	0.038415	-0.65	Coatomer subunit beta
177	24.84	25.06	25.12	26.00	25.56	25.37	0.0367224	-0.64	Plectin
178	20.89	21.32	20.88	21.62	21.70	21.68	0.011706	-0.64	Cancer-related nucleoside-triphosphatase
179	20.81	21.15	21.22	21.83	21.50	21.49	0.032581	-0.55	DNA damage-binding protein 1
180	18.99	18.84	19.15	19.44	19.41	19.51	0.00858031	-0.46	Cytosolic acyl coenzyme A thioester hydrolase
181	21.51	21.69	21.51	21.79	22.12	22.18	0.0271654	-0.46	Docking protein 1
182	20.22	20.38	20.39	20.56	20.86	20.88	0.0200762	-0.44	Interleukin-1 receptor-associated kinase 1
183	21.13	21.12	21.08	21.28	21.75	21.57	0.0379997	-0.42	Glutamine--fructose-6-phosphate aminotransferase [isomerizing] 1
184	22.73	22.89	22.93	23.23	23.03	23.42	0.0441748	-0.38	40S ribosomal protein S5;40S ribosomal protein S5, N-terminally processed
185	21.52	21.54	21.71	21.25	21.40	21.14	0.0275125	0.33	Histone-arginine methyltransferase CARM1
186	20.32	20.38	20.65	19.93	20.09	20.23	0.0499665	0.37	Oxygen-dependent coproporphyrinogen-III oxidase, mitochondrial
187	20.83	20.97	20.78	20.48	20.47	20.41	0.0029914	0.40	V-type proton ATPase subunit B, brain isoform

Appendix

	GFP			PER2-GFP			t-test p value	t-test Difference	Protein names
	#1	#2	#3	#1	#2	#3			
188	17.82	18.07	17.95	17.26	17.63	17.66	0.042667	0.43	Mevalonate kinase
189	22.42	22.35	22.39	21.87	21.81	22.18	0.0207398	0.44	Programmed cell death 6-interacting protein
190	22.10	22.09	22.38	21.74	21.70	21.78	0.0096522	0.45	Deoxyuridine 5-triphosphate nucleotidohydrolase, mitochondrial
191	18.58	18.73	18.54	18.05	17.99	18.40	0.0289268	0.47	DnaJ homolog subfamily C member 2; DnaJ homolog subfamily C member 2, N-terminally processed
192	18.03	18.12	17.93	17.62	17.54	17.50	0.00203958	0.48	Rho-associated protein kinase 1
193	22.13	21.76	21.79	21.51	21.31	21.44	0.0239573	0.48	Low molecular weight phosphotyrosine protein phosphatase
194	19.81	19.83	19.47	19.16	19.41	19.09	0.0343098	0.48	Integrin-linked kinase-associated serine/threonine phosphatase 2C
195	20.54	20.76	20.54	20.43	19.89	19.97	0.0492986	0.52	Aspartate--tRNA ligase, cytoplasmic
196	22.38	22.85	22.85	22.17	22.25	22.09	0.0330072	0.52	Neuroblast differentiation-associated protein AHNAK
197	22.69	22.89	22.79	22.17	22.31	22.28	0.00179688	0.53	Protein transport protein Sec23A
198	28.78	28.54	28.53	27.96	28.10	28.20	0.00781948	0.53	Annexin A2;Annexin;Putative annexin A2-like protein
199	25.96	25.92	25.58	25.42	25.21	25.20	0.0192027	0.54	Poly(rC)-binding protein 1
200	21.90	22.14	21.93	21.42	21.55	21.36	0.00437197	0.55	Transportin-1
201	24.59	24.34	24.84	24.16	23.92	24.01	0.0254969	0.56	Phenylalanine--tRNA ligase beta subunit
202	18.96	19.26	19.07	18.57	18.59	18.45	0.00443371	0.56	Bifunctional 3-phosphoadenosine 5-phosphosulfate synthase 1; Sulfate adenylyltransferase;Adenylyl-sulfate kinase
203	21.98	22.04	21.77	21.29	21.48	21.32	0.00495661	0.57	Polypyrimidine tract-binding protein 1

Appendix

	GFP			PER2-GFP			t-test p value	t-test Difference	Protein names
	#1	#2	#3	#1	#2	#3			
204	19.19	18.76	18.64	18.12	18.26	18.50	0.0450728	0.57	UPF0600 protein C5orf51
205	21.99	21.77	21.95	21.59	21.34	21.06	0.0270621	0.57	Pachytene checkpoint protein 2 homolog
206	18.22	18.63	18.53	18.12	17.65	17.87	0.0349309	0.58	Ataxin-2
207	21.31	21.50	21.67	20.91	20.83	20.98	0.00606906	0.59	Actin-related protein 2/3 complex subunit 4
208	25.41	25.34	25.15	24.59	24.69	24.84	0.00517154	0.60	Trifunctional purine biosynthetic protein adenosine-3; Phosphoribosylamine--glycine ligase; Phosphoribosylformylglycinamidine cyclo-ligase; Phosphoribosylglycinamide formyltransferase
209	18.95	18.89	19.47	18.57	18.44	18.51	0.032767	0.60	Nuclear-interacting partner of ALK
210	19.50	19.77	19.50	19.09	18.66	19.21	0.0337123	0.60	Ubiquitin carboxyl-terminal hydrolase 15
211	17.75	17.28	17.36	16.77	17.09	16.74	0.030078	0.60	Regulator of chromosome condensation
212	19.98	20.19	20.52	19.40	19.70	19.75	0.033747	0.61	Myosin light chain kinase, smooth muscle; Myosin light chain kinase, smooth muscle, deglutamylated form
213	24.10	23.79	23.73	23.53	23.22	23.04	0.029063	0.61	Elongation factor 1-gamma
214	21.88	21.62	21.57	20.89	21.18	21.11	0.00841743	0.63	Actin-related protein 2/3 complex subunit 2
215	18.94	18.55	18.76	18.23	18.07	18.06	0.00691223	0.63	THO complex subunit 3
216	19.27	19.64	19.72	18.85	18.69	19.15	0.0281293	0.65	Translation initiation factor eIF-2B subunit alpha
217	20.64	20.17	20.52	20.01	19.73	19.65	0.0223799	0.65	Mitogen-activated protein kinase kinase kinase kinase 4; Misshapen-like kinase 1;TRAF2 and NCK-interacting protein kinase
218	17.77	17.92	18.01	17.53	16.94	17.27	0.0239104	0.65	Vinexin

	GFP			PER2-GFP			t-test p value	t-test Difference	Protein names
	#1	#2	#3	#1	#2	#3			
219	21.77	21.10	21.65	20.84	21.01	20.69	0.0430704	0.66	Actin-related protein 2
220	22.79	22.23	22.60	21.85	22.02	21.76	0.0222365	0.66	LanC-like protein 1
221	22.03	22.65	22.43	21.63	21.77	21.69	0.0221791	0.68	Ubiquitin carboxyl-terminal hydrolase 24
222	17.87	18.44	18.62	17.67	17.73	17.48	0.046054	0.68	L-aminoadipate-semialdehyde dehydrogenase-phosphopantetheinyl transferase
223	24.61	24.17	24.26	23.77	23.79	23.43	0.0181512	0.68	Cysteine and glycine-rich protein 2
224	20.04	19.99	20.57	19.60	19.62	19.31	0.030858	0.69	Carbonyl reductase [NADPH] 3
225	22.86	22.84	22.85	22.20	22.24	21.98	0.00100166	0.71	Multifunctional protein ADE2; Phosphoribosylaminoimidazole-succinocarboxamide synthase; Phosphoribosylaminoimidazole carboxylase
226	21.17	21.26	20.91	20.29	20.13	20.79	0.0337952	0.71	Tripartite motif-containing protein 65
227	21.38	21.46	21.55	20.97	20.92	20.35	0.0250111	0.71	Fascin
228	23.88	24.30	24.13	23.38	23.39	23.39	0.00421022	0.72	Filamin-B
229	20.94	20.32	20.78	20.24	19.84	19.81	0.0369434	0.72	Growth factor receptor-bound protein 2
230	20.58	20.33	20.44	19.47	19.65	20.09	0.0218521	0.72	Arfaptin-2
231	19.02	18.63	18.84	17.82	18.56	17.95	0.0474234	0.72	Protein FAM98B
232	23.27	22.90	22.97	22.70	22.10	22.18	0.0301673	0.72	Mitotic checkpoint protein BUB3
233	21.66	21.25	21.51	20.91	20.93	20.39	0.026568	0.73	Inorganic pyrophosphatase
234	23.88	23.64	23.66	23.30	22.69	23.02	0.0199494	0.73	Heterogeneous nuclear ribonucleoprotein K
235	20.72	21.07	20.59	20.32	19.92	19.96	0.0189239	0.73	Kinesin-1 heavy chain
236	19.16	18.58	19.05	18.18	18.45	17.97	0.0314275	0.73	UDP-glucose 6-dehydrogenase
237	26.89	27.03	26.72	26.17	26.17	26.06	0.0014755	0.74	Filamin-A

Appendix

	GFP			PER2-GFP			t-test p value	t-test Difference	Protein names
	#1	#2	#3	#1	#2	#3			
238	20.04	19.56	19.61	18.97	18.95	19.04	0.00852058	0.75	Four and a half LIM domains protein 1
239	19.62	19.81	19.29	18.48	18.90	19.09	0.0342198	0.75	Ubiquitin-like modifier-activating enzyme ATG7
240	18.25	18.16	18.92	17.70	17.60	17.78	0.0376565	0.75	Clustered mitochondria protein homolog
241	21.57	21.58	21.11	21.02	20.56	20.42	0.0332217	0.75	Isocitrate dehydrogenase [NADP] cytoplasmic
242	21.34	21.60	21.43	20.25	20.69	21.14	0.0477219	0.76	Bifunctional coenzyme A synthase; Phosphopantetheine adenylyltransferase; Dephospho-CoA kinase
243	18.38	17.88	17.64	17.04	17.36	17.22	0.0325081	0.76	Cysteine protease ATG4B
244	22.74	22.24	22.46	21.72	21.58	21.85	0.00947311	0.76	ATP-dependent RNA helicase DDX1
245	22.25	21.57	21.54	20.73	21.19	21.14	0.0486552	0.77	Tyrosine-protein phosphatase non-receptor type 11
246	20.16	20.32	20.36	19.44	19.33	19.75	0.00549895	0.77	Ataxin-2-like protein
247	19.63	20.09	19.31	18.67	18.86	19.17	0.0454847	0.77	Transforming growth factor beta-1-induced transcript 1 protein
248	19.12	18.67	19.48	18.12	18.44	18.39	0.0385228	0.77	Mitochondrial peptide methionine sulfoxide reductase
249	25.46	25.06	25.05	24.54	24.47	24.24	0.00883624	0.77	Glutathione reductase, mitochondrial
250	24.09	23.41	23.46	22.60	23.05	22.98	0.041191	0.78	Cysteine--tRNA ligase, cytoplasmic
251	20.06	20.26	19.56	19.30	18.99	19.24	0.0263228	0.79	UPF0585 protein C16orf13
252	18.76	19.47	19.37	18.30	18.30	18.63	0.0331672	0.79	Glycogen phosphorylase, brain form;Glycogen phosphorylase, muscle form
253	19.62	19.04	18.96	18.26	18.60	18.40	0.0262667	0.79	Golgi resident protein GCP60
254	21.52	21.62	21.59	20.59	20.82	20.95	0.00195691	0.79	Protein transport protein Sec23B
255	23.14	22.94	23.29	22.25	22.26	22.48	0.00329668	0.79	Laminin subunit beta-3
256	20.72	20.83	20.85	19.99	20.00	19.97	4.24E-05	0.81	Lipoma-preferred partner

	GFP			PER2-GFP			t-test p value	t-test Difference	Protein names
	#1	#2	#3	#1	#2	#3			
257	21.40	21.32	21.27	20.14	20.53	20.89	0.0208221	0.82	Procollagen-lysine,2-oxoglutarate 5-dioxygenase 2
258	17.58	17.30	17.79	16.84	16.65	16.67	0.00579964	0.83	Isochorismatase domain-containing protein 2, mitochondrial
259	20.70	20.74	20.73	20.13	19.53	20.00	0.00988928	0.84	Calcium/calmodulin-dependent protein kinase type II subunit delta
260	23.96	23.54	24.04	23.10	23.08	22.78	0.00984099	0.86	40S ribosomal protein SA
261	26.18	26.34	26.15	25.32	25.52	25.25	0.00099979	0.86	Fatty acid synthase;[Acyl-carrier-protein] S-acetyltransferase; [Acyl-carrier-protein] S-malonyltransferase;3-oxoacyl-[acyl-carrier-protein] synthase; 3-oxoacyl-[acyl-carrier-protein] reductase; 3-hydroxyacyl-[acyl-carrier-protein] dehydratase; Enoyl-[acyl-carrier-protein] reductase; Oleoyl-[acyl-carrier-protein] hydrolase
262	19.30	18.71	18.98	18.13	18.32	17.92	0.0129108	0.87	Diacylglycerol kinase alpha;Diacylglycerol kinase
263	23.37	23.44	23.06	22.34	22.22	22.65	0.0070866	0.88	ATP-citrate synthase
264	28.99	28.56	28.45	28.00	27.66	27.67	0.0112597	0.89	Peroxiredoxin-1
265	19.44	19.53	19.85	19.09	18.16	18.89	0.0445544	0.89	Laminin subunit gamma-2
266	21.71	21.32	21.90	20.52	20.92	20.75	0.0117618	0.91	Ubiquitin-conjugating enzyme E2 L3
267	21.00	20.24	20.85	19.86	20.06	19.43	0.0369783	0.92	Ubiquitin-conjugating enzyme E2 variant 3
268	20.88	21.45	21.38	20.07	20.35	20.50	0.0133616	0.93	Mixed lineage kinase domain-like protein
269	19.96	19.12	19.86	18.98	18.59	18.55	0.0339729	0.94	Trafficking protein particle complex subunit 1
270	19.49	19.28	19.28	18.47	17.94	18.80	0.0222676	0.94	Ubiquitin-like modifier-activating enzyme 6
271	21.20	21.32	21.33	20.25	19.92	20.83	0.0240668	0.95	Cysteine and histidine-rich domain-containing protein 1

	GFP			PER2-GFP			t-test p value	t-test Difference	Protein names
	#1	#2	#3	#1	#2	#3			
272	20.18	20.12	20.02	19.39	18.89	19.12	0.00297534	0.97	Tyrosine-protein phosphatase non-receptor type 12
273	21.92	21.65	21.90	20.42	21.07	21.03	0.0125222	0.98	Eukaryotic translation initiation factor 4E
274	22.74	22.21	22.15	21.54	21.26	21.35	0.0087355	0.98	Aspartyl aminopeptidase
275	25.23	24.69	25.12	24.17	23.92	23.98	0.00559829	0.99	F-actin-capping protein subunit alpha-1
276	18.85	19.06	18.72	18.12	17.41	18.11	0.0172517	1.00	UPF0692 protein C19orf54
277	18.89	19.34	19.83	18.15	18.77	18.11	0.0427821	1.01	Tripeptidyl-peptidase 2
278	19.61	20.05	20.41	19.09	18.79	19.15	0.0169845	1.01	Copine-3
279	20.33	20.33	20.52	19.01	19.10	20.00	0.0342638	1.02	Hydroxymethylglutaryl-CoA lyase, mitochondrial
280	22.84	22.94	22.74	21.62	21.61	22.23	0.00856875	1.02	D-3-phosphoglycerate dehydrogenase
281	24.13	23.70	23.96	23.22	22.73	22.76	0.00677791	1.02	Serpin B8
282	22.61	22.28	22.09	20.84	21.15	21.92	0.0459851	1.02	Peroxisomal 2,4-dienoyl-CoA reductase
283	20.80	20.89	20.79	19.90	19.51	19.98	0.00234683	1.03	Xaa-Pro dipeptidase
284	16.25	16.29	16.69	15.00	15.88	15.27	0.0254141	1.03	Methyltransferase-like protein 2A;Methyltransferase-like protein 2B
285	19.80	19.55	19.95	18.47	18.88	18.85	0.00430288	1.03	Annexin A11
286	27.42	27.70	27.65	26.47	26.37	26.82	0.00313445	1.03	SHC-transforming protein 1
287	18.53	18.21	18.33	17.39	17.51	17.05	0.00324408	1.04	Phosphatidylinositol-binding clathrin assembly protein
288	18.29	18.81	18.92	17.79	17.32	17.78	0.0135677	1.04	Sorting nexin-5
289	22.69	22.15	21.43	21.04	20.92	21.16	0.0473505	1.05	Nuclear migration protein nudC
290	23.88	23.28	23.29	22.78	22.10	22.41	0.0194398	1.06	Prelamin-A/C;Lamin-A/C
291	19.96	19.64	19.16	18.64	18.18	18.74	0.0214204	1.07	SET and MYND domain-containing protein 5
292	23.57	22.67	22.72	22.15	21.71	21.88	0.0287656	1.07	Nucleoside diphosphate kinase;Nucleoside diphosphate kinase B

Appendix

	GFP			PER2-GFP			t-test p value	t-test Difference	Protein names
	#1	#2	#3	#1	#2	#3			
293	18.76	18.44	19.38	17.89	17.71	17.76	0.0190654	1.07	SUMO-conjugating enzyme UBC9
294	23.82	22.87	23.62	22.04	22.71	22.34	0.0360957	1.08	Exportin-T
295	20.56	20.32	20.32	19.28	19.74	18.93	0.0120111	1.08	Ataxin-10
296	18.65	18.20	18.95	17.03	18.12	17.35	0.0473455	1.10	Peptidase M20 domain-containing protein 2
297	20.80	21.29	21.29	20.01	20.03	20.02	0.00243924	1.10	Phosphatidylinositol transfer protein beta isoform
298	21.42	20.96	21.29	19.97	20.21	20.07	0.0017692	1.14	Aminopeptidase B
299	21.43	21.06	20.64	20.05	19.99	19.67	0.0113791	1.14	Influenza virus NS1A-binding protein
300	21.72	22.06	21.97	20.62	20.53	21.10	0.00461625	1.17	6-phosphogluconolactonase
301	18.99	19.16	19.47	18.15	17.75	18.21	0.00421232	1.17	Programmed cell death protein 4
302	24.68	23.98	24.16	22.85	23.26	23.20	0.00903607	1.17	Tyrosine-protein kinase CSK
303	20.07	19.22	19.51	18.56	18.34	18.38	0.0106084	1.17	3(2),5-bisphosphate nucleotidase 1
304	23.89	23.08	23.37	22.32	22.28	22.22	0.00801351	1.18	Tumor susceptibility gene 101 protein
305	22.51	21.96	22.02	21.06	20.73	21.17	0.0059167	1.18	NEDD8-conjugating enzyme Ubc12
306	20.67	20.25	20.18	19.27	19.15	19.10	0.00177722	1.19	Catenin alpha-1
307	21.53	21.53	21.25	20.32	20.05	20.32	0.0007623	1.20	Cysteine-rich protein 2
308	20.27	20.61	20.02	19.00	19.07	19.18	0.0025064	1.22	Paxillin
309	22.36	22.27	22.60	20.78	21.37	21.30	0.00383573	1.26	Crk-like protein
310	21.32	21.19	21.30	20.15	19.83	20.05	0.00025286	1.26	Sorting nexin-1
311	22.10	21.82	21.50	20.41	20.26	20.89	0.0075968	1.29	Choline-phosphate cytidylyltransferase A; Choline-phosphate cytidylyltransferase B
312	26.55	25.88	25.65	24.88	24.65	24.67	0.0101548	1.29	Peptidyl-prolyl cis-trans isomerase A; Peptidyl-prolyl cis-trans isomerase A, N-terminally processed;

Appendix

	GFP			PER2-GFP			t-test p value	t-test Difference	Protein names
	#1	#2	#3	#1	#2	#3			
									Peptidyl-prolyl cis-trans isomerase
313	23.73	22.98	23.43	21.90	22.42	21.94	0.00944963	1.30	Plastin-3
314	22.22	22.35	21.86	20.34	21.02	21.13	0.0104215	1.31	Cystathionine beta-synthase
315	25.95	25.46	25.32	24.49	24.12	24.14	0.00421755	1.33	Protein deglycase DJ-1
316	23.16	23.51	23.36	21.94	22.12	21.98	0.00032363	1.33	Cystatin-B
317	21.98	21.59	21.22	20.30	20.16	20.32	0.00422747	1.33	Ribonucleoside-diphosphate reductase subunit M2 B
318	20.35	20.20	19.25	18.59	18.74	18.40	0.019279	1.35	V-type proton ATPase subunit E 1
319	21.37	21.06	20.82	19.78	19.91	19.48	0.00263576	1.36	StAR-related lipid transfer protein 7, mitochondrial
320	24.38	24.16	24.15	22.75	22.97	22.87	0.00016226	1.37	Annexin A1;Annexin
321	21.19	21.19	21.69	19.77	19.87	20.29	0.00388933	1.38	Vacuolar protein sorting-associated protein 37B
322	21.26	21.51	21.54	19.88	20.16	20.13	0.00040109	1.38	Cysteine and glycine-rich protein 1
323	20.23	18.75	19.03	17.97	18.21	17.68	0.0449946	1.38	TIP41-like protein
324	17.34	17.32	17.84	16.47	16.06	15.80	0.00569121	1.39	Protein kinase C delta type; Protein kinase C delta type regulatory subunit; Protein kinase C delta type catalytic subunit
325	20.46	20.32	20.12	18.91	18.83	18.94	0.00016888	1.40	Arfaptin-1
326	20.80	20.60	20.86	19.92	19.07	19.05	0.00890038	1.41	Nascent polypeptide-associated complex subunit alpha; Nascent polypeptide-associated complex subunit alpha, muscle-specific form
327	17.56	17.77	17.68	16.08	16.31	16.37	0.00019779	1.41	Dedicator of cytokinesis protein 7
328	19.53	19.66	19.96	18.18	18.68	18.02	0.00387825	1.42	Isochorismatase domain-containing protein 1
329	17.71	18.11	18.08	15.93	16.39	17.25	0.0238775	1.44	Signal transducer and activator of transcription 6

Appendix

	GFP			PER2-GFP			t-test p value	t-test Difference	Protein names
	#1	#2	#3	#1	#2	#3			
330	16.08	16.19	17.13	15.14	15.03	14.84	0.0131437	1.47	Down syndrome critical region protein 3
331	16.81	17.26	17.97	16.02	15.34	16.16	0.0233044	1.51	WD repeat, SAM and U-box domain-containing protein 1
332	17.19	17.51	17.22	15.93	15.94	15.49	0.00106958	1.52	Copine-7
333	21.90	22.01	21.75	20.18	20.52	20.37	0.00025795	1.53	Diphosphomevalonate decarboxylase
334	21.74	20.72	21.19	19.79	19.23	19.95	0.0131755	1.56	Lysophospholipase-like protein 1
335	23.11	22.16	22.44	21.27	21.01	20.74	0.00811451	1.56	Glutathione S-transferase Mu 3
336	22.80	22.67	22.30	21.05	20.96	21.02	0.00049145	1.58	Palladin
337	23.94	23.76	23.19	21.78	21.82	22.54	0.00916026	1.58	Carboxymethylenebutenolidase homolog
338	20.62	20.69	20.86	19.08	19.05	19.27	9.08E-05	1.59	Epidermal growth factor receptor kinase substrate 8-like protein 2
339	16.67	17.40	16.90	15.25	14.68	16.26	0.0349162	1.60	Engulfment and cell motility protein 2
340	22.25	21.31	21.58	20.43	19.76	19.99	0.00837731	1.65	Ubiquitin-conjugating enzyme E2 N; Putative ubiquitin-conjugating enzyme E2 N-like
341	25.18	25.24	24.14	22.90	23.26	23.39	0.0124342	1.67	Destrin
342	20.21	20.00	19.95	19.08	17.68	18.36	0.0151404	1.68	Hematological and neurological expressed 1-like protein
343	18.30	17.82	17.77	16.18	16.71	15.93	0.00409316	1.69	CB1 cannabinoid receptor-interacting protein 1
344	18.64	18.07	17.94	15.68	17.50	16.32	0.0406156	1.72	E3 ubiquitin-protein ligase RNF135
345	21.94	20.85	21.47	19.84	19.98	19.23	0.0111209	1.74	Serpin B5
346	19.84	20.29	20.67	18.65	18.57	18.25	0.00273802	1.78	Inosine triphosphate pyrophosphatase
347	22.63	21.40	21.95	20.58	20.08	20.00	0.011174	1.78	Caldesmon
348	20.12	19.90	20.03	18.02	17.66	18.73	0.00424162	1.88	Nitrilase homolog 1
349	17.05	17.25	18.25	15.15	16.18	15.14	0.0159601	2.03	Eukaryotic translation initiation factor 3 subunit B

Appendix

	GFP			PER2-GFP			t-test p value	t-test Difference	Protein names
	#1	#2	#3	#1	#2	#3			
350	20.07	20.25	19.45	18.12	17.76	17.74	0.00167357	2.05	Endoplasmic reticulum resident protein 44
351	17.68	17.84	17.44	15.83	14.88	16.08	0.00571848	2.05	Sorting nexin-27
352	18.71	17.63	17.71	15.26	17.09	15.52	0.0369137	2.06	Probable ATP-dependent RNA helicase DDX41
353	18.86	17.57	18.09	15.82	15.40	16.97	0.0247282	2.11	Gamma-interferon-inducible protein 16
354	22.01	22.16	22.03	18.94	20.77	19.71	0.013409	2.26	Plastin-2
355	18.97	18.01	17.74	16.24	14.55	16.47	0.0248908	2.49	Endophilin-B1
356	17.37	18.27	18.25	16.14	14.75	15.22	0.00676519	2.59	tRNA (guanine(10)-N2)-methyltransferase homolog
357	17.15	17.43	18.05	15.08	13.76	15.56	0.01026	2.74	Glyoxylate reductase/hydroxypyruvate reductase
358	17.38	18.01	18.13	13.90	14.35	16.19	0.014787	3.03	RING finger protein 214
359	18.58	18.30	18.01	14.72	15.46	15.34	0.0003752	3.13	Protein S100-A16
360	22.29	22.22	23.74	19.40	19.41	19.92	0.00373968	3.18	
361	19.16	19.77	19.49	16.51	14.43	16.48	0.00674853	3.67	Protein phosphatase 1F
362	20.95	20.74	21.30	19.00	14.83	16.61	0.026476	4.18	Filamin-C
363	22.16	21.74	20.73	15.12	15.59	19.56	0.0312499	4.79	26S proteasome non-ATPase regulatory subunit 9
364	23.20	23.38	23.24	15.66	16.97	15.50	0.00010401	7.23	Actin-like protein 8

Tabel A2: List of Gene ontology Terms generated with DAVID analysis.

Category	Term	Count	%	P Value	Genes
GOTERM_BP_DIRECT	GO:0032922~circadian regulation of gene expression	9	0,038262053	1,25E-08	NPAS2, CRY2, CSNK1D, CSNK1E, GFPT1, PER2, PER1, ARNTL, CRY1
	GO:0042752~regulation of circadian rhythm	8	0,034010713	9,29E-08	CRY2, CSNK1D, CSNK1E, BTRC, PER2, PER1, CRY1, CCAR2
	GO:0006002~fructose 6-phosphate metabolic process	5	0,021256696	2,34E-07	PFKL, GFPT1, GFPT2, PFKP, PFKM
	GO:2000323~negative regulation of glucocorticoid receptor signaling pathway	4	0,017005357	8,92E-06	CRY2, PER1, ARNTL, CRY1
	GO:0000086~G2/M transition of mitotic cell cycle	9	0,038262053	1,13E-05	CSNK1D, CSNK1E, BTRC, CEP78, AURKA, DYNC1H1, FBXW11, HMMR, PPP2R2A
	GO:0016055~Wnt signaling pathway	10	0,042513392	1,50E-05	CSNK1D, WDR61, CSNK1E, BTRC, DDB1, STRN, MCC, USP34, FBXW11, CCAR2
	GO:0035338~long-chain fatty-acyl-CoA biosynthetic process	6	0,025508035	1,74E-05	ACOT9, ACOT7, ACSL1, ACOT8, HSD17B12, ACSL3
	GO:0016032~viral process	10	0,042513392	5,35E-04	USP7, MSH6, KRT18, ACOT8, NUP88, RAE1, COPB1, BTRC, DDB1, RNGTT
	GO:0001676~long-chain fatty acid metabolic process	4	0,017005357	5,45E-04	SLC27A1, ACSL1, ACSL3, SLC27A4
	GO:0006891~intra-Golgi vesicle-mediated transport	4	0,017005357	0,001157624	COPA, COPG2, COPB1, GOLGA3
	GO:0044539~long-chain fatty acid import	3	0,012754018	0,001217649	ACSL1, ACSL3, SLC27A4
	GO:0042753~positive regulation of circadian rhythm	3	0,012754018	0,001615305	BTRC, ARNTL, FBXW11

Appendix

Category	Term	Count	%	P Value	Genes
	GO:0045892~negative regulation of transcription, DNA-templated	12	0,05101607	0,001727049	LIMS1, CRY2, INPP5K, BTRC, TRIM28, PER2, PER1, ARNTL, LOXL2, CRY1, FBXW11, CCAR2
	GO:0042754~negative regulation of circadian rhythm	3	0,012754018	0,002066304	CRY2, PER2, CRY1
	GO:0001837~epithelial to mesenchymal transition	4	0,017005357	0,002276649	FAM83D, LIMS1, TRIM28, LOXL2
	GO:0006654~phosphatidic acid biosynthetic process	4	0,017005357	0,002476107	SLC27A1, PLD1, GNPAT, LPCAT4
	GO:0007623~circadian rhythm	5	0,021256696	0,00272713	NPAS2, CRY2, PER2, PER1, ARNTL
	GO:0043066~negative regulation of apoptotic process	11	0,046764731	0,002851375	IRAK1, DHRS2, KRT18, SQSTM1, DDB1, ARAF, DNAJA1, RAF1, AURKA, DNAJA3, DHCR24
	GO:0007018~microtubule-based movement	5	0,021256696	0,003602564	AP2B1, AP2A1, DYNC1H1, AP2M1, KIF2A
	GO:0006890~retrograde vesicle-mediated transport, Golgi to ER	5	0,021256696	0,003764951	COPA, COPG2, COPG1, COPB1, KIF2A
GOTERM_ CC_ DIRECT	GO:0016020~membrane	46	0,195561602	1,30E-10	COPA, SLC27A1, USP9X, DNAJC10, STRN, MLH1, CAD, MYCBP2, HMMR, HNRNPM, LGALS3BP, AP2B1, MCM7, ACSL1, DNAJB11, INPP5K, P4HA1, COPB1, PRPF8, LRRC59, DNAJA1, GNPAT, ASPH, LOXL2, DYNC1H1, ACSL3, GOLGA3, DHCR24, KIF2A, DNAJA2, PLD1, PFKL, NTPCR, PFKP, MOGS, MCM4, LPCAT4, PNPLA6, MGAT2, GAPVD1, TFRC, AP2A1, SNRNP200, ATP5A1, PLEKHA2, SLC27A4

Appendix

Category	Term	Count	%	P Value	Genes
	GO:0005829~cytosol	58	0,246577672	1,40E-10	COPA, SRP14, BTRC, CEP78, AURKA, CAD, AP2B1, ACOT7, MCM7, CTGF, COPB1, CTU2, DYNC1H1, GOLGA3, KIF2A, DHCR24, IRAK1, PFKL, NUP88, PFKP, PFKM, DOK1, COPG2, GAPVD1, COPG1, SRP9, PPP2R2A, USP7, PPP6C, PYCRL, LIMS1, USP9X, TK1, HMMR, NPAS2, INPP5K, SQSTM1, DNAJA1, CDA, HSPA4, USP34, NEFL, FBXW11, DNAJA3, PLEC, AP2M1, DNAJA2, RAF1, CSNK1D, CSNK1E, AP2A1, GFPT1, GFPT2, IKBKG, ARAF, PTPN1, RANBP10, NNMT
	GO:0030126~COPI vesicle coat	4	0,017005357	1,42E-04	COPA, COPG2, COPG1, COPB1
	GO:0055087~Ski complex	3	0,012754018	1,67E-04	WDR61, SKIV2L, TTC37
	GO:0005783~endoplasmic reticulum	17	0,072272766	4,95E-04	SLC27A1, DNAJC10, MOGS, LPCAT2, LPCAT4, PNPLA6, P4HA2, INPP5K, DNAJB11, SQSTM1, P4HA1, LRRC59, ASPH, PTPN1, ACSL3, SLC27A4, DHCR24
	GO:0005789~endoplasmic reticulum membrane	17	0,072272766	7,62E-04	COPA, PLD1, SPTLC2, HSD17B12, MOGS, LPCAT2, LPCAT4, PNPLA6, COPG2, ACSL1, COPG1, COPB1, LRRC59, ASPH, ACSL3, SLC27A4, DHCR24
	GO:0048471~perinuclear region of cytoplasm	14	0,059518748	8,24E-04	PLD1, LIMS1, AURKA, DOK1, KRT18, TFRC, INPP5K, CSNK1D, CTGF, PER2, DNAJA1, OBSL1, CTSB, ACSL3

Appendix

Category	Term	Count	%	P Value	Genes
	GO:0031012~extracellular matrix	9	0,038262053	0,001806979	PLAT, HNRNPM, LGALS3BP, PFKP, ATP5A1, LOXL2, DYNC1H1, PLEC, FN1
	GO:0005634~nucleus	58	0,246577672	0,001949263	SRP14, PDLIM7, BTRC, MLH1, SLFN5, AURKA, CAD, RNGTT, PDCD2, CRY2, MCM7, P4HA2, DNAJB11, GRWD1, RAE1, USP11, CRY1, ACAD9, LOXL2, CCAR2, GOLGA3, KIF2A, DHCR24, IRAK1, DDB1, TTC37, PFKP, ARNTL, MCM4, DOK1, DHRS2, SNRNP200, MCC, USP7, SKIV2L, NR3C1, ZNF618, MYCBP2, NPAS2, TROVE2, INPP5K, PRPF8, DNAJA1, PER2, PER1, NSUN2, FBXW11, DNAJA3, TRIM28, SAMHD1, RAF1, CSNK1D, WDR61, CSNK1E, IKBKG, ACAD11, PLEKHA2, RANBP10
	GO:0036020~endolysosome membrane	3	0,012754018	0,003524463	AP2B1, AP2A1, AP2M1
	GO:0030122~AP-2 adaptor complex	3	0,012754018	0,004144821	AP2B1, AP2A1, AP2M1

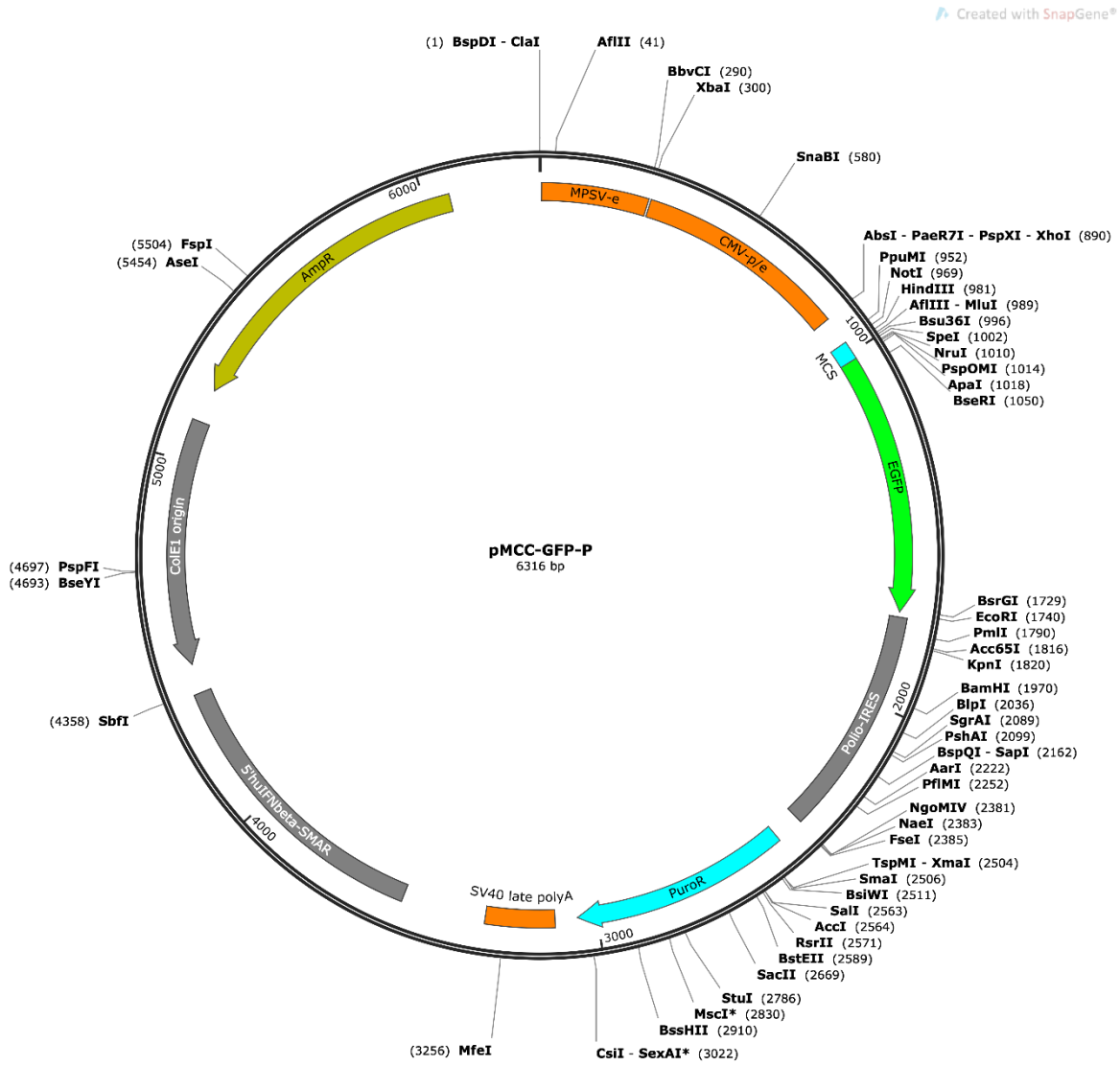

Figure A1. Graphic map of bicistronic expressin plasmid pMCC-GFP-P. The plasmid is 6316 base pair and contains multiple cloning site (MCS), Enhanced GFP (EGFP) and resistance gene puromycine

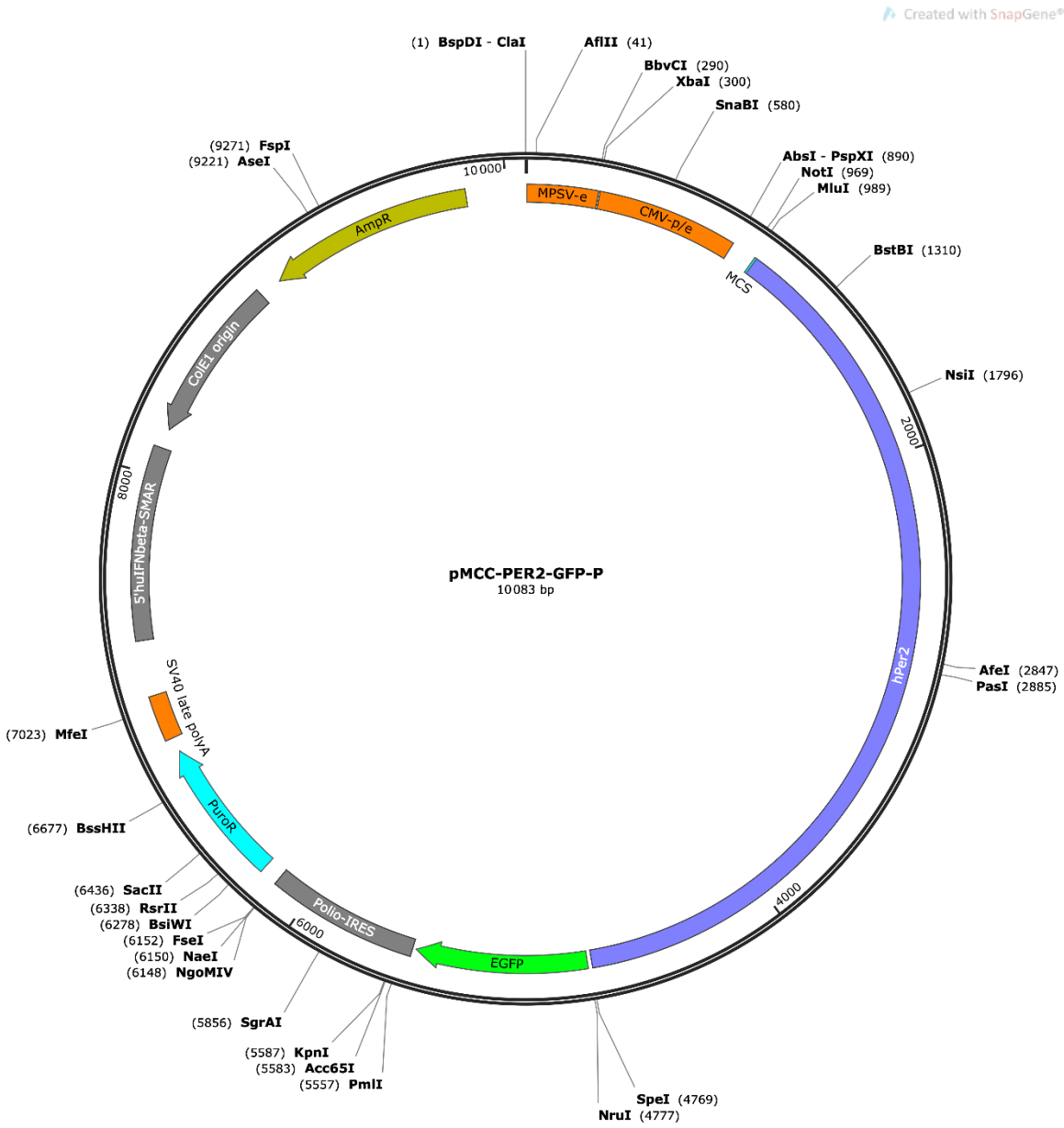

Figure A2. Graphic map of bicistronic expressin plasmid pMCC-PER2-GFP-P. The plasmid is 10083 base pair and contains PER2, Enhanced GFP (EGFP) and resistance gene puromycine

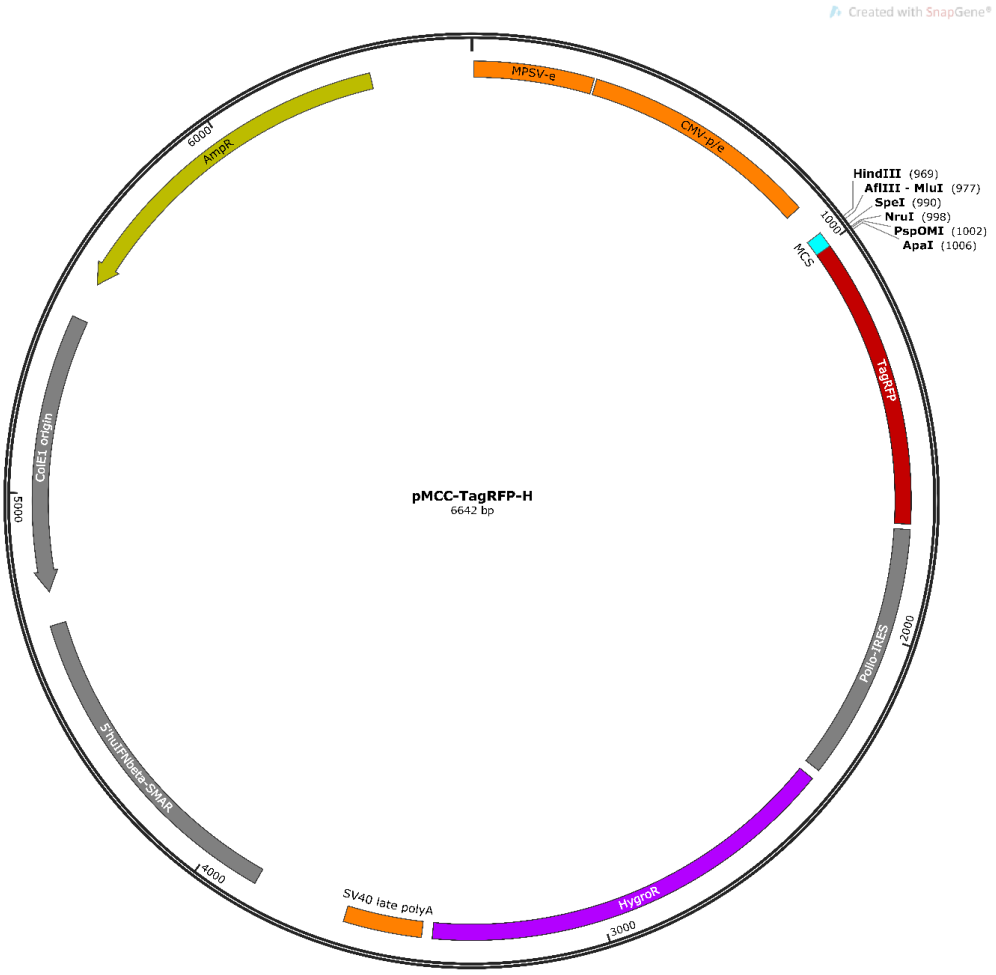

Figure A3. Graphic map of bicistronic expressin plasmid pMCC-TagRFP-H. The plasmid is 6642 base pair and contains multiple cloning site (MCS), Enhanced GFP (EGFP) and resistance gene hygromycine.

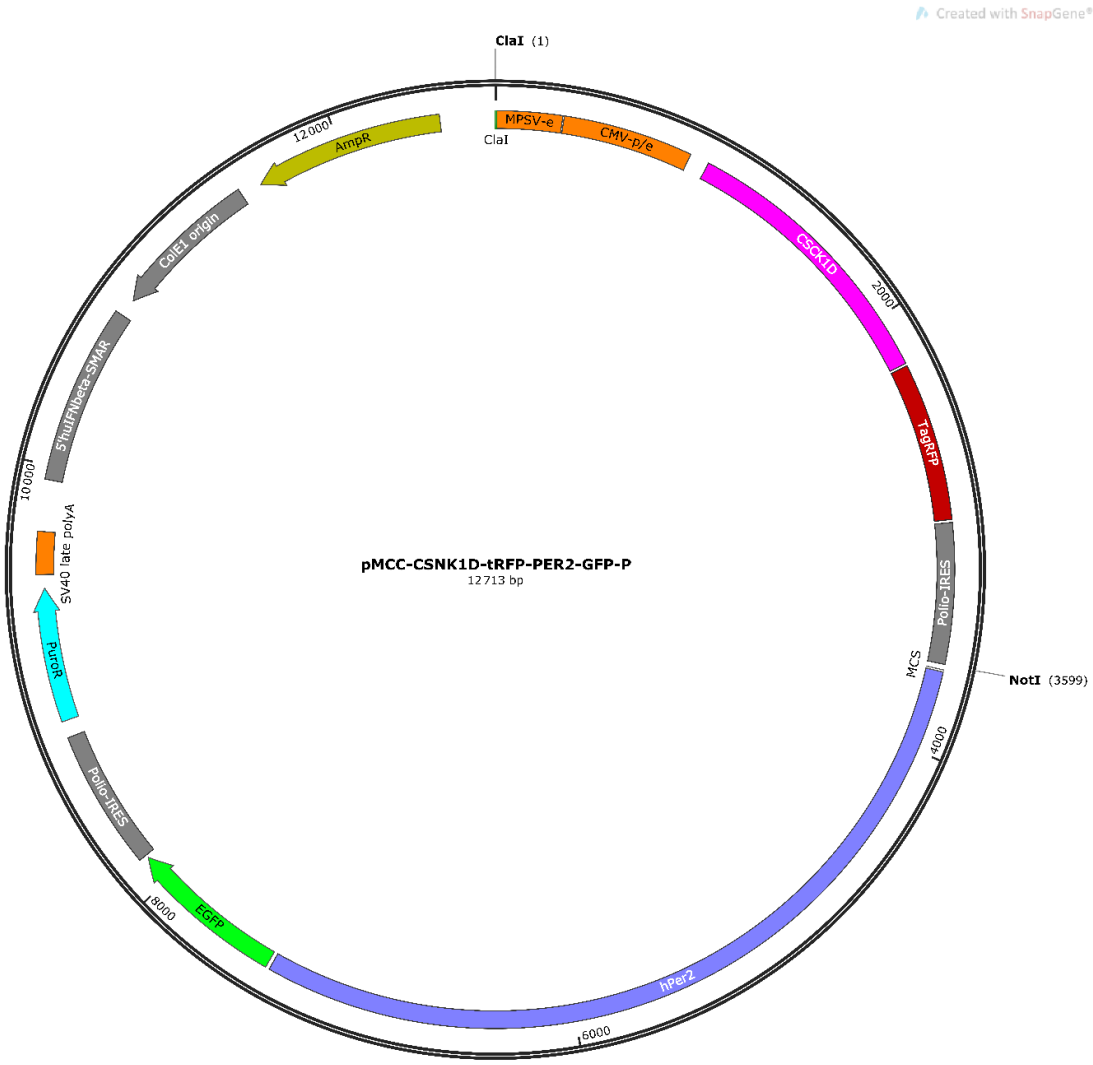

Figure A4. Graphic map of tricistronic expressin plasmid pMCC-CSNK1D-tRFP-PER2-GFP-P. The plasmid is 12713 base pair and CSNK1D tagged with tRFP, PER2 tagged with GFP and resistance gene puromycine.

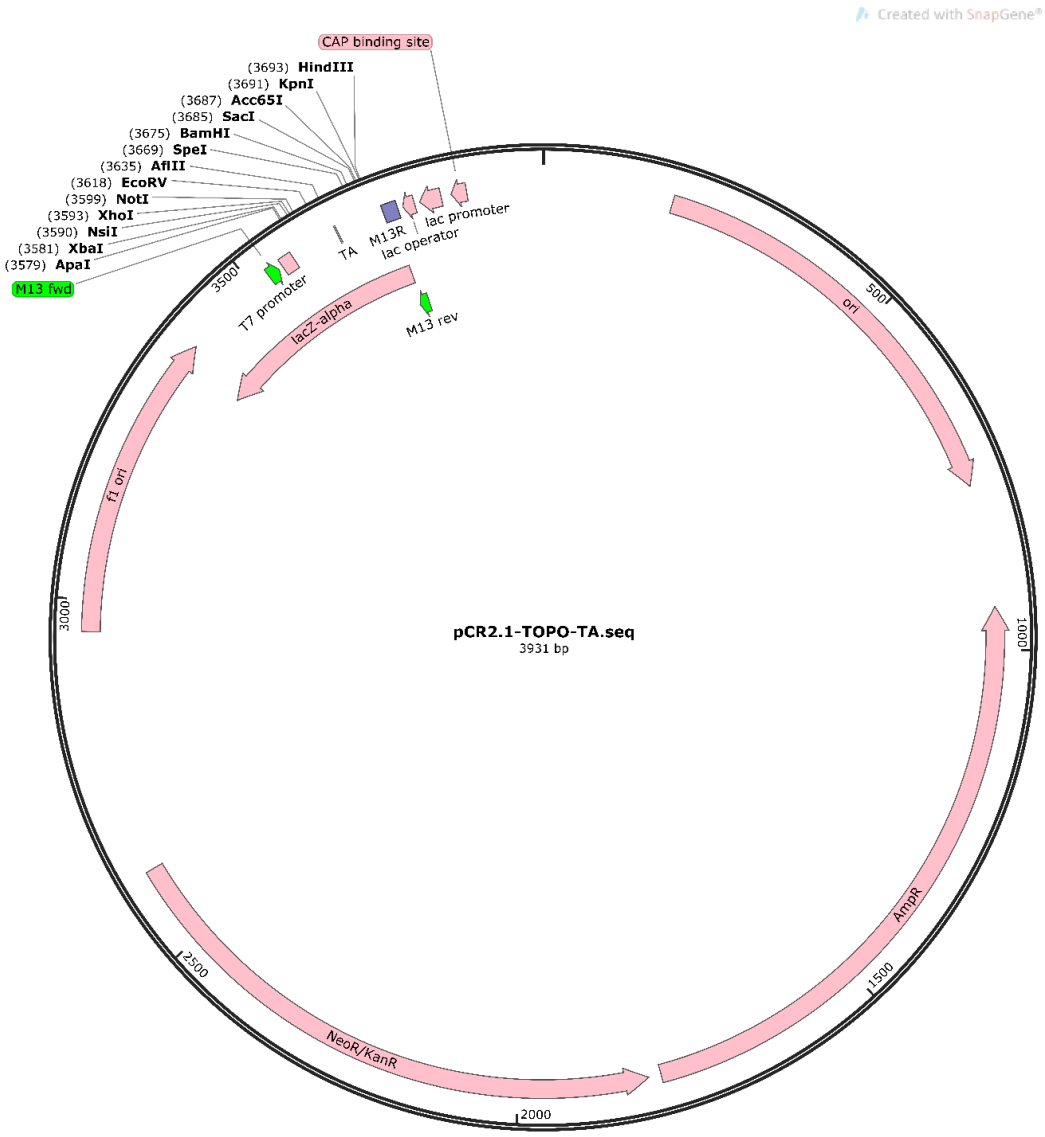

Figure A5. Graphic map of plasmid pCR2.1-TOPO-TA. The plasmid is 3931 base pair cantains the TA ligation site with the target insert.

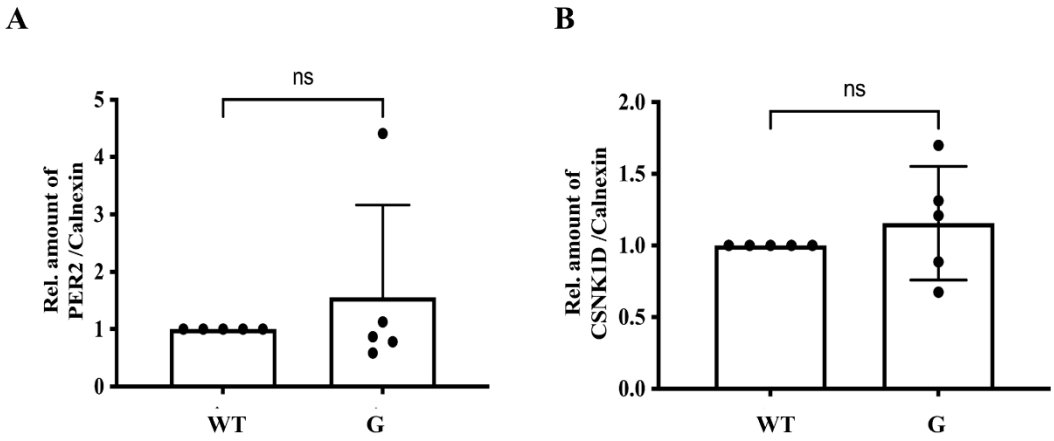

*Figure A6. Related analysis for figure 22 Band intensities for PER2 A and CSNK1D B in HT1080 Wildtype (WT) and GAPVD1 overexpressing HT1080 cells (G) input samples were quantified and plotted as a bar diagram. Single data points are represented by black circles and standard deviations are represented by error bars. * p < 0.05 (t-test).*

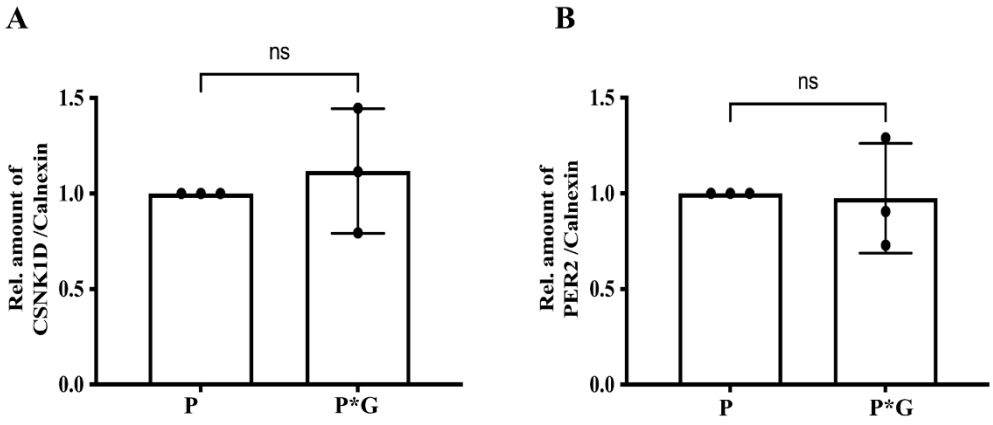

*Figure A7. Related analysis for figure 23 Band intensities for PER2 A and CSNK1D B in HT1080 PER2-GFP (P) and GAPVD1 overexpressing HT1080 PER2-GFP (P*G) input samples were quantified and plotted as a bar diagram. Single data points are represented by black circles and standard deviations are represented by error bars. * p < 0.05 (t-test).*

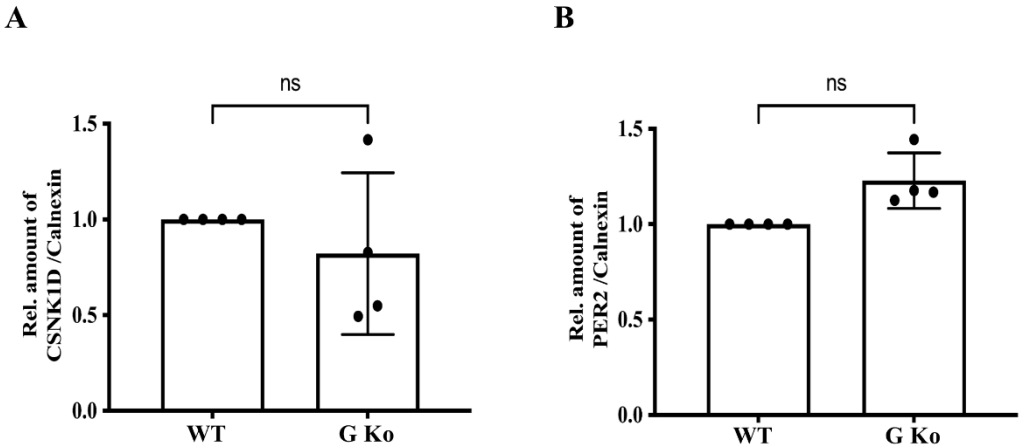

Figure A8. Related analysis for figure 24 Band intensities for PER2 A and CSNK1D B in HeLa wildtype (WT) and GAPVD1 KO HeLa cells (G KO) input samples were quantified and plotted as a bar diagram. Single data points are represented by

Acknowledgments

I would like to take this opportunity to express my sincere gratitude to all those who have contributed to the completion of my Ph.D. thesis.

First and foremost, I extend my heartfelt thanks professor, **Univ.-Prof. Dr. rer. nat. Hans Reinke**, professionally for his guidance, support, dedication, expertise, and invaluable insights throughout my Ph.D. journey. His encouragement, guidance, and unwavering support have been instrumental in shaping my academic pursuits. I would like to express my deepest gratitude to him personally for all of the thoughtful deep conversation, Pizza time, being delightful, and transparency.

I am deeply indebted to **Dr. rer. nat. Faiza Kalfalah** for her critical scientific discussion, technical expertise that indeed shaped my PhD work. I am very grateful to have had the opportunity to learn from her. Your constructive feedback and valuable inputs have been invaluable to my work. Your motto is always there, new week new luck. I'm extremely grateful to **Univ.-Prof. Dr. med. Fritz Boege** for his generous financial support in addition to his scientific advice thought out my Ph.D. thesis. In addition, I would like to extend my sincere thanks to **Dr. rer. nat. Christian Mielke**, discussion, endless technical help in cloning and for the good coffee time.

I'm extremely grateful to **Univ.-Prof. Dr. rer. nat. Björn Stork** for his critical discussion point in my PhD thesis. Many thanks to Dr. rer. nat. **Niklas Berleth**, for his assistance in GFP immunoprecipitation. I would like to extend my sincere thanks to Biologisch-Medizinisches Forschungszentrum der Heinrich-Heine-Universität Düsseldorf mostly to Dr. rer. nat. **Anja Stefanski** for her role in analysis the mass spectrometry data

My sincere thanks also go to the lab staff **Ellen Wannagat, Elke Berg, Birgit Hanzen and Gabi Schoder** for their tireless efforts in facilitating my research work. Your diligence, technical expertise, and attention to detail have been invaluable in ensuring the smooth running of my experiments. I would like to extend my gratitude to my lab mates, whose camaraderie and support have been a constant source of motivation. Your collaborative spirit, and constructive criticism have helped me overcome numerous research challenges. I would express my sincere thanks to **Philipp Reus, Valerie Rudenko, Christina Buschhaus, Eva Effertz, Dr. rer. nat. Stefan Sobek, Dr. med. Anna Katharina Mundorf, Laura Frank and Elonora Croco.** I'd like to recognize **Sandra Szczutkowski, Anna-Lena Grothoff, Mariem Haj Abdelaziz, Vivienne Ogasa, Viviane Zimmer and Verena Schumann,**

I'd like to acknowledge my friends, **Mohammed Abbas, Dr. Mohammed Sahen, Dr. Ahmed Mahmoud, Dr. Hamdy Ali, Dr. rer.med Mohamed Algamal** who have been a constant source of support and throughout my Ph.D. journey.

I would also like to thank family including **my parents, brother Mohamed and my sisters**. for their support. Lastly, I am also deeply grateful to my **Fiancée**, for her unwavering love, support, and patience, scientific discussion during this long and challenging journey. Her encouragement, understanding, and belief in me have been a constant source of strength and inspiration.

Thank you all for your support, encouragement, and contributions to this work.